Relevance of bioaccessibility for the oral bioavailability of poorly water-soluble drugs

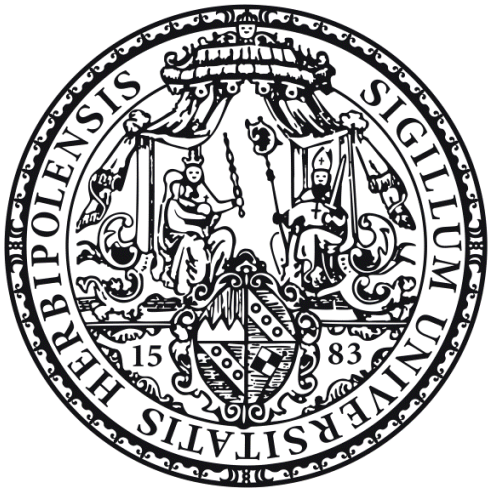

Dissertation zur Erlangung des naturwissenschaftlichen Doktorgrades
an der Fakultät für Chemie und Pharmazie
der Julius-Maximilians-Universität Würzburg

vorgelegt

von

Dominic Pascal Werthmüller

aus **Zürich**, **Schweiz**

Würzburg 2022

Eingereicht bei der Fakultät für Chemie und Pharmazie am

_____

Gutachter der Dissertation

1. Gutachter: _____

2. Gutachter: _____

Prüfer des öffentlichen Promotionskolloquiums

1. Prüfer: _____
2. Prüfer: _____
3. Prüfer: _____

Tag des öffentlichen Promotionskolloquiums

_____

Doktorurkunde ausgehändigt am

_____

It can scarcely be denied that the supreme goal of all theory is to make the irreducible basic elements as simple and as few as possible without having to surrender the adequate representation of a single datum of experience

Albert Einstein – 1933

Rephrased to:

Make everything as simple as possible, but not simpler

Table of Contents

1. List of abbreviations

Abbreviation	Description
ABL:	Aqueous boundary layer (= unstirred water layer, UWL)
ADDF:	Absorption-driven drug formulation (concept)
ADME:	Absorption, distribution, metabolism and elimination
ANOVA:	Analysis of variance (statistical test)
API:	Active pharmaceutical ingredient
ASB:	Acceptor sink buffer
ASD:	Amorphous solid dispersion
ASU:	Asymmetric unit cell (of a crystal lattice)
AUC:	Area-under-the-curve
BCS:	Biopharmaceutical classification system
Caco-2:	Immortalized cell line of human colorectal adenocarcinoma cells
CD:	Cyclodextrin
Cmax:	Maximum concentration of drug observed in the plasma
CMC:	Critical micellar concentration
Cryo-TEM:	Cryogenic-transmissive electron microscopy
DCS:	Developability classification system
DLS:	Dynamic light scattering (= photon correlation spectroscopy, PCS)
DMPK:	Drug metabolism and pharmacokinetics
DMSO:	Dimethyl sulfoxide
EM:	Electron microscopy
EMA:	European Medicines Agency
EPO:	Eudragit EPO (excipient)

FaCS:	Fraction absorbed classification system
FaSSGF:	Fasted-state simulated gastric fluid
FaSSIF:	Fasted-state simulated intestinal fluid
FCT:	Film-coated tablet
FDA:	Food and Drug Administration
FeSSIF:	Fed-state simulated intestinal fluid
FPM:	First-pass metabolism
GIT / GI:	Gastrointestinal tract / gastrointestinal
GIT-PAMPA:	Gastrointestinal tract-Parallel artificial membrane permeability assay
GSE:	General-solubility-equation
HPC:	Hydroxypropylcellulose (excipient)
HPLC:	High performance liquid chromatography
HPMC:	Hydroxypropyl methylcellulose (excipient)
IDR:	Intrinsic dissolution rate
ISO:	International Organization for Standardization
IUPAC:	International Union of Pure and Applied Chemistry
IVIVC:	In vitro-in vivo correlation
Kcps:	Kilo counts per seconds
LBF:	Lipid-based formulation
LC-MS/MS:	Liquid chromatography-tandem mass spectrometry
LC-TEM:	Liquid cell-transmissive electron microscopy
MDCK:	Madin Darby Canine Kidney (cell line)
ME:	Microemulsion
MEPC:	Microemulsion pre-concentrate
NaTC:	Sodium taurocholate (bile salt)

NIBS: Non-invasive backscatter

NMR: Nuclear magnetic resonance (spectroscopy)

NOESY: Nuclear Overhauser effect spectroscopy

OrBiTo: Oral Biopharmaceutics Tools

PBPK: Physiology-based pharmacokinetic (modelling)

PBS: Phosphate-buffered saline

PDA: Photodiode array

PEARRL: Pharmaceutical Education And Research with Regulatory Link

PK: Pharmacokinetics

PTFE: Polytetrafluoroethylene

PVDF: Polyvinylidene fluoride

PWSD: Poorly water-soluble drug

RH40: Kolliphor RH40 (excipient)

RPM: Rotations per minute

SDS: Sodium dodecyl sulfate (= sodium lauryl sulfate, SLS)

SEDDS: Self-emulsifying drug delivery system

SEM: Scanning electron microscopy

SIFs: Simulated intestinal fluids

TKI: Tyrosine kinase inhibitor

Tmax: Time at which the maximum concentration of drug in the blood is observed

UC: Ultracentrifugation

UCFCA: Ultracentrifugation-flux combo assay

UNGAP: Understanding Gastrointestinal Absorption-related Processes

UPLC: Ultra performance liquid chromatography

USA: United States of America

USB:	Unspecific binding
USP:	United States Pharmacopeia
UV/VIS:	Ultraviolett / Visible (light spectroscopy)
UWL:	Unstirred water layer (= aqueous boundary layer, ABL)
VA64:	Kollidon VA64 (excipient)
XRPD:	X-ray powder diffraction

2. Introduction

2.1 Oral drug absorption

For over half a century, scientists have been trying to grasp the fundamentals of the complex oral drug absorption process to understand and predict the rate and extent of absorption (1, 2). How food intake further complicates this endeavor through physiological adaptions of the gastrointestinal tract (GIT) was reviewed already in 1977 by Welling (3) but still continues to puzzle scientists up to the present day. The UNGAP consortium, a multidisciplinary network aiming for understanding gastrointestinal absorption-related processes, provides thorough reviews on oral drug absorption with emphasis on local differences along the GIT (4), gastrointestinal variability (5) and food-drug interactions (6). A review on how to address (some) food-induced changes in absorption (see **Figure 1**) with the drug formulation was published by PEARRL, another European network unifying pharmaceutical industries, academia and regulatory agencies (7). Equally worth mentioning is the collaborative OrBiTo project focusing on the next generation of predictive oral biopharmaceutic tools including both *in vitro* and *in silico* methods and their required synergy (8, 9). The present relevance is further outlined by a new draft guidance from the US Food and Drug Administration (FDA) published in February 2019 on how to assess the effect of food on the systemic availability and associated variability of drugs (10). Requests for changes to this draft document by pharmaceutical industries and the European Medicines Agency (EMA) (11) make evident that there is not (yet) a common agreement on how to approach those still challenging scientific questions.

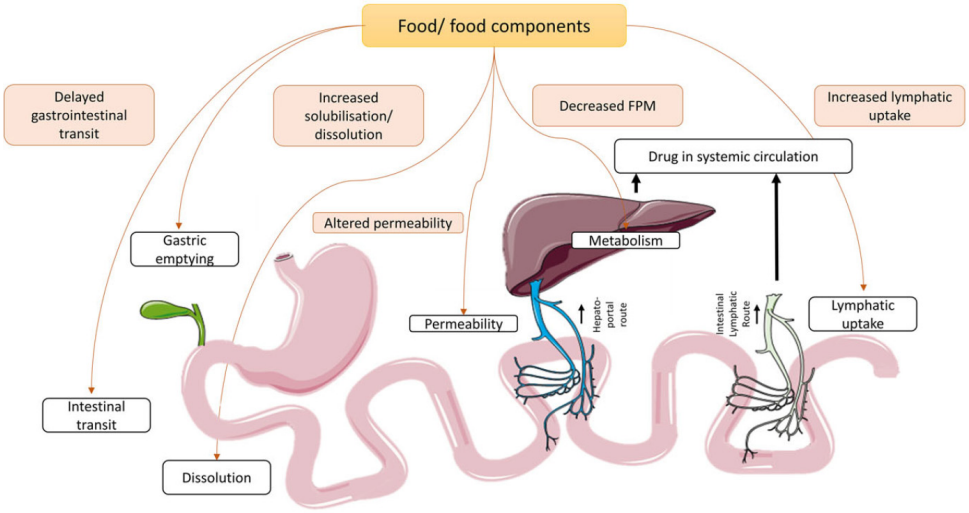

Figure 1: Illustration of food-related impact factors on oral drug absorption along the gastrointestinal tract. FPM stands for first-pass metabolism. Adopted from O'Shea et al, Food for thought: formulating away the food effect – a PEARRL review, Journal of Pharmacy and Pharmacology, 2019, 71, 4, 510-535 (7), by permission of Oxford University Press/ Royal Pharmaceutical society.

The oral route likely remains highly relevant in the future due to its non-invasiveness and ease of administration, improving compliance and subsequently treatment outcomes for patients. The oral route of administration is complex due to various physiological and physicochemical processes occurring in parallel while also sharing the same path with the diet. Furthermore, the gastrointestinal environment and its adaptations to different meal types may vary greatly among different patients, such as geriatric or pediatric populations, but could also depend on their disease-state (12, 13). A review from the UNGAP consortium was published in 2020 involving GI physiology of special populations (14). In scope of patient centricity and drug formulation development, it is essential to achieve systemic drug concentrations within the therapeutic window to ensure treatment efficacy and, equally important, patient safety (15). The therapeutic window can be interpreted as the delta between minimal drug exposure required to result in a therapeutic effect and the highest tolerable exposure exhibiting no toxic effects (16).

There is still a considerable unmet need for tools to better understand and simulate what conditions and factors are affecting the oral absorption process. It is important to aim for mechanistic understanding in order to address them. (17) This would enable more rational formulation development, associated with fewer *in vivo* surprises and more first-time-right decisions, saving money and time during drug development. Ultimately, this also brings us a step closer to reduce the need for extensive animal studies before testing in humans.

This work focused specifically on the journey of poorly water-soluble drugs through the gastrointestinal tract and why it is so difficult to achieve adequate and consistent drug concentrations in the blood within the therapeutic window. Physiological and physicochemical (biopharmaceutical) aspects of the absorption process are presented with special emphasis on what factors might impact and/or limit the rate and extent of oral drug absorption. Additionally, available strategies and concepts are reviewed on how to identify and address those relevant factors while differentiating between what we can influence and what seems out of control from a formulation development perspective. A simple concept and methodology was developed and applied to a single model compound, how to develop mechanistic understanding *in vitro* and how this knowledge can guide formulation development and *in vivo* predictions regarding relative performance of formulations.

2.2 Biopharmaceutical aspects

In a very simplified view, the GIT can be seen as a sequential array of different compartments. Starting within the oral cavity, transitioning via esophagus into the stomach compartment, followed by the small intestine (divided into duodenum, jejunum and ileum) and ending with the large intestine (colon) and rectum (18). Relevant for nutrient uptake, and hence likely also for oral drug absorption, are mainly the upper small intestine (duodenum and jejunum) and secretions from the pancreas (pancreatic juice) and gallbladder (bile). Special attention was paid on the upper small intestine and bile secretions, as considered the relevant environment for absorption of poorly water-soluble drugs (PWSDs). Additionally, the stomach compartment needs to be considered to understand when (gastric emptying time-related) and in which presentation (e.g. dissolved or undissolved) the drug may arrive at the presumed site of absorption. The acidic stomach environment appears especially important for weak bases, related to their ionization, which will be discussed later. More distal regions such as the large intestine were out of scope. The following section provides a brief overview of the gastrointestinal journey of a drug relevant for this work.

2.2.1 The intralumenal environment experienced by a drug product

The gastrointestinal environment is difficult to characterize and depends on the methodology, location of aspiration and time, related to meal or water intake. Several recent review articles from UNGAP and PEARRL are available (4, 5, 19). In the fasted prandial state after oral intake of a medication, the drug product first encounters the acidic stomach environment with a typical pH between 1.5-3.0. The pH of the stomach is elevated to about 3.0-4.0 in the fed state (depending on meal type) but declines back to a pH of about 2.0-3.0 during the course of digestion. After some initial gastric residence time where mixing of food occurs, the stomach contents empty into the small intestine, more specifically into the duodenum where the pH is neutralized to about 6.0-7.0 through pancreatic secretions. Intestinal pH values between fasted and fed prandial state are quite similar compared to the variation in the stomach environment.

The secretion of bile further modifies the lumenal content (18). Bile is constantly produced in the liver and stored in the gall bladder, when not needed. Bile release is considered to be triggered by the presence of food in the GIT but residual levels of bile constituents may also be found in the fasted state. The main components contained in bile are bile salts, cholesterol and lecithin (a mixture of phospholipids). The main function of bile salts is to emulsify lipids, making them accessible to digestive enzymes (pancreatic lipases) through their adsorption and activation on the surface of lipid droplets. Furthermore, they are capable of creating finely dispersed emulsions of poorly water-soluble components (e.g. lipidic digestive products) through their uptake into colloidal structures such as (mixed) micelles and vesicles. Aside from their important natural

function to enable the oral absorption of for example lipid-soluble vitamins A, D, E and K, bile can also have a great impact on the oral absorption of drugs. A publication as early as 1977 has reported evidence of substantially increased exposure (> 2-fold) between a capsule containing only the drug diftalone and a capsule with drug plus additional dry ox bile (20). A more recent study from 2020 evaluated the impact of altered gastrointestinal activity in rats, through co-administered GI-motility modifying agents, on the exposure of nilotinib, a poorly soluble weak base (21). Exposure was found significantly increased with higher intestinal motility (peristaltic movements), however, this change in exposure was absent when bile-duct cannulated rats were used. The observed increased exposure in non-bile cannulated rats were attributed to the combined effects of gastrointestinal activity and the emulsifying properties of bile, relevant for the oral absorption of nilotinib. The exact mechanism how bile components (and resulting mixed colloidal species) can facilitate drug uptake from the intestinal lumen is still unclear. In addition to effects on dissolution rate and apparent solubility (22), it is assumed that colloidal drug species may penetrate the aqueous boundary and eventually mucus layer on the surface of cells and provide an additional transport mechanism (shuttling) parallel to the diffusion of molecularly dissolved drug (23). Whether there is a specific interaction between bile colloids (or individual constituents) and mucus and/or the cellular membrane of enterocytes (intestinal cells) and how this might differ from synthetic surfactants used in drug formulations for example remains largely unknown. Already over 50 years ago, around the same time when the relevance of bile was reported, the beneficial effects of surfactants on oral drug absorption were recognized and reviewed, which supports their wide-spread use in drug formulations (24).

2.2.2 Biorelevant media development

A substantial amount of literature has emerged over the past 20 years characterizing the composition and physicochemical properties of contents in the GIT in presence and absence of drugs. The fluid aspiration technique used at specific time points and locations after oral drug administration has contributed to our overall understanding of the absorption process. A comprehensive review of the history, methodology and application of the aspiration technique was published in 2020 (25). A central conclusion from this review was that intralumenal concentrations of apparently dissolved drug do not allow to directly assess the availability for absorption due to interactions with intralumenal components and resulting formation of colloidal structures such as (mixed) micelles and vesicles. Based on such insights from the aspiration technique, *in vivo* mimicking media compositions were proposed in 1998 by Galia (26) and Dressman (27), nowadays known as biorelevant media, such as fasted- and fed-state simulated intestinal fluids (FaSSIF and FeSSIF). With increasing knowledge about the gastrointestinal fluid composition

(28), updated versions of biorelevant media were proposed over the years with FaSSIF and FeSSIF version 2 in 2008 (29) and FaSSIF-V3 in 2015 (30). In contrast to versions 1 and 2, FaSSIF-V3 is currently not commercially available. For this work, only commercially available biorelevant media versions 1 and 2 were used to represent the fasted- and fed-state intestinal environment plus the so-called fasted-state simulated gastric fluid (FaSSGF). The compositions and rationale for their use are discussed in the materials and methods section.

2.2.3 Fate of drug molecules in the human body

With respect to the upper small intestine, it is important to understand the fate of a drug molecule once it gets transported across the epithelial membrane of enterocytes. When a molecule is taken up from the intestinal lumen, it might get metabolized in the gut wall (or already in the intestinal lumen), and hence chemically altered, for example degraded and inactivated. Drugs with metabolites as active forms (e.g. pro-drugs) are excluded from this view. The unmetabolized fraction leaving the enterocyte is further transported via the portal vein to the liver, where further metabolism usually takes place, widely known as the “liver first-pass effect”. Finally, the remaining fraction of unmetabolized (active) drug that passes the liver and is not distributed in any body tissues will become available to the systemic blood circulation, before eventually being eliminated. The systemic yield of the drug can be denoted as bioavailable fraction, see **Figure 2.**

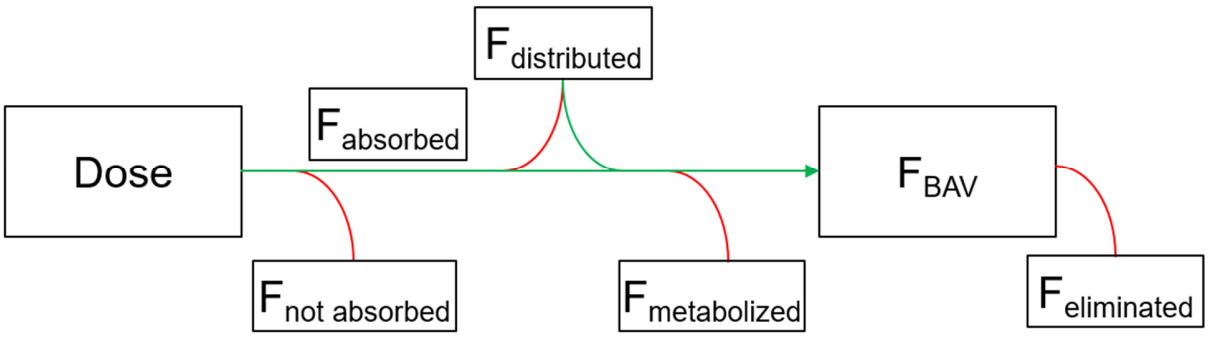

Figure 2: Scheme to illustrate the interplay of physiological processes of drug uptake in the gastrointestinal tract relating the dose as input to the fraction bioavailable (F_{BAV}) typically measured as output from an in vivo study.

The fraction bioavailable refers to the actual amount of drug in the systemic circulation. At the beginning (before administration) and towards “infinity” (long after administration), the fraction bioavailable is zero. In contrast, bioavailability refers to the proportion of an administered dose that passes through the systemic circulation and is typically measured as the area-under-the-curve (AUC) of the plasma concentration-time profile. This is typically referred to as the extent of absorption or exposure to the drug. Absolute bioavailability is measured as the AUC obtained after oral administration divided by the AUC after intravenous administration, assuming 100% fraction

absorbed. Relative bioavailability compares the AUC obtained to the AUC of a reference formulation. For absolute and relative bioavailability, dose needs to be accounted for if the comparison is not done at the same dose level. As long as the absorption process dominates the plasma concentration-time profile, the rate of absorption can be estimated based on its steepest increase over time, neglecting other mechanisms such as distribution, metabolism and elimination. In such a case, a simple way to estimate the rate of absorption could be to divide the maximum concentration observed in the blood (Cmax) by the time required to reach this concentration (Tmax).

For the drug formulation scientist, it is important to understand what can be done to influence the amount of drug in the blood. The fraction bioavailable as a function of time, describing the amount of active drug available in the systemic circulation can be defined as follows:

$$\boldsymbol{Dose}\ x\ \boldsymbol{F_A}(t)\ x\ \left(1-\boldsymbol{F_D}(t)\right)\ x\ \left(1-\boldsymbol{F_M}(t)\right)\ x\ \left(1-\boldsymbol{F_E}(t)\right)=\ \boldsymbol{Dose}\ x\ \boldsymbol{F_{BAV}}(t) \qquad \text{(Equation 1)}$$

$\mathbf{F_A}$: Fraction absorbed across enterocytes from intestinal lumen – relates to **Absorption (A)**

$\mathbf{F_D}$: Fraction distributed within body tissues except the blood – relates to **Distribution (D)**

$\mathbf{F_M}$: Fraction metabolized in the intestinal lumen, gut wall, or liver – relates to **Metabolism (M)**

$\mathbf{F_E}$: Fraction eliminated by clearance mechanisms from the blood – relates to **Elimination (E)**

$\mathbf{F_{BAV}}$: Fraction bioavailable in the systemic circulation - relates to **Pharmacodynamics,** more specifically the **safety and efficacy of a drug (therapeutic window)**

In words, the bioavailable amount is the amount of drug getting absorbed from the GIT, reaching the systemic blood circulation without being distributed in body tissues and not being metabolized presystemically (lumenal/gut wall metablism or liver first-pass) and not yet eliminated. In order to obtain the AUC of the plasma concentration-time profile, **Equation 1** needs to be integrated between the time of administration and the last measured time point. From an oral formulation perspective, mainly the fraction absorbed can be influenced while distribution, intestinal and liver metabolism as well as elimination are considered out of control. An illustrative scheme of a possible drug formulator's focus on the fraction absorbed is depicted in **Figure 3**.

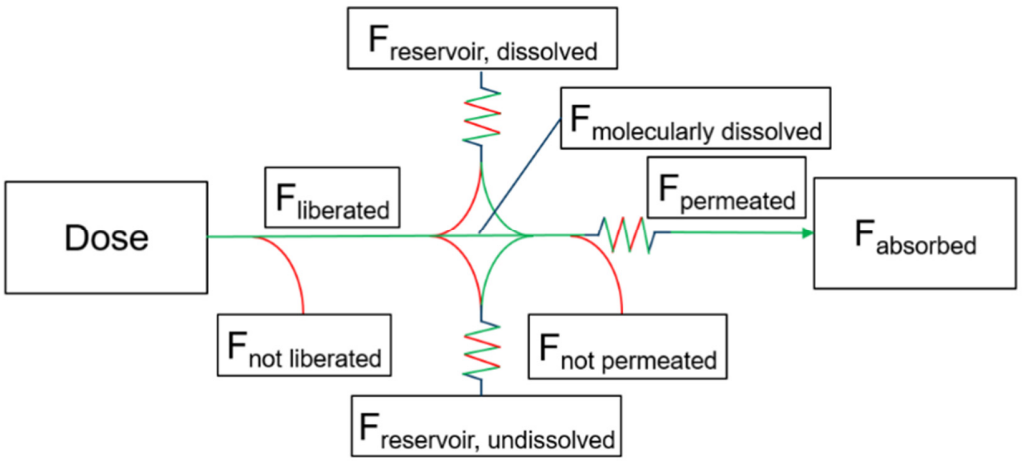

Figure 3: Scheme to illustrate the interplay of physiological processes and drug species in the gastrointestinal tract relating the dose as input to the fraction absorbed from a drug delivery system. The drug reservoirs were differentiated into undissolved drug (solid reservoir) and dissolved/solubilized drug (liquid reservoir). The fraction of molecularly dissolved drug is shown as the main driver of permeation and hence absorption. Both reservoirs and the permeation process are associated with a "resistance", which refers to the resistance for the drug to dissolve (solid reservoir), the release from a solubilized/associated state (liquid reservoir) and the diffusion of those drug species across the unstirred water layer and epithelial membrane of enterocytes.

$$\boldsymbol{Dose}\ x\ \boldsymbol{F_A}(t)\ \approx \boldsymbol{Dose}\ x\ \boldsymbol{F_P}(t) \qquad \text{(Equation 2)}$$

$$\boldsymbol{Dose}\ x\ \frac{\boldsymbol{dF_A}}{\boldsymbol{dt}} = \boldsymbol{J_{\text{absorptive flux}}} * \boldsymbol{A_{\text{absorption}}}\ \approx \boldsymbol{Dose}\ x\ \frac{\boldsymbol{dF_P}}{\boldsymbol{dt}} \qquad \text{(Equation 3)}$$

$$\boldsymbol{J_{\text{absorptive flux}}}(\boldsymbol{t}) \approx \frac{\boldsymbol{Dose}}{\boldsymbol{Volume}}\ x\ \boldsymbol{F_{BAC}}(\boldsymbol{t}) x\ \boldsymbol{P_{\text{effective}}} \qquad \text{(Equation 4)}$$

F_P: Fraction permeated relates to drug entering the epithelial membrane of enterocytes by passive transcellular diffusion. **F_A** corresponds to **F_P** in case absorption would only be based on diffusive uptake and no trapping/degradation/decomposition in the gut wall occurs.

dF_P/dt: The change in fraction permeated over time multiplied with the dose represents the permeation rate and is related to absorptive flux **J** through a permeation area **A**.

$J_{absorptive\ flux}$: Flux defined as mass transfer across a barrier is denoted as **J** and is calculated by a donor concentration (given sink conditions in receiver compartment) times effective permeability. **J** serves as a measure of drug species contribution to permeation, i.e. bioaccessibility.

F_{BAC}: The bioaccessible fraction entails all drug species (dissolved and undissolved) that are effectively contributing to permeation. Liberation of drug from the dosage form is a requirement to become bioaccessible.

$P_{effective}$: Effective permeability describes the permeability of a drug through relevant resistance layers including the unstirred water layer and epithelial membrane, see definition **section 2.3.4.**

Definition: Bioaccessibility describes the sum of drug species contribution to permeation.

Despite knowledge of involved processes, the *in vivo* organism should be considered a "black-box" since in a typical *in vivo* study only the input is known, i.e. dose administered, and the final output is measured, i.e. concentration of drug in the systemic blood circulation. What happens in between remains mostly illusive primarily because we cannot easily measure and differentiate between what has been absorbed from the intestinal lumen, what has been distributed within body tissues and what has been metabolized in the lumen, gut wall or liver. A simplistic approach is to assume the amount distributed, metabolized and eliminated between two formulations or dose levels is proportional to the amount absorbed but this might not always hold true due to possible saturation mechanisms. In addition, as soon as the drug appears in the blood, it will also start to get cleared from the human body. In case of fast clearance, i.e. fast removal of drug from the blood circulation through renal or hepatic/biliary elimination pathways, the absorption will likely be underestimated based on the plasma concentration-time profile of the drug. Deconvoluting various subprocesses that influence the amount of drug in the blood may require an ADME study including administration via intravenous and oral route. Typically, such analysis requires the concomitant use of *in silico* modelling softwares, more specifically so-called physiology-based pharmacokinetic (PBPK) modelling (31). In the frame of early oral drug formulation development, it is questionable how much one can rely on the availability and accuracy of *in silico* models that were trained with more or less rough estimates of parameters. In practice, modelling efforts are mainly tailored to the human situation, associated with regulatory requirements. However, in the screening phase (concept and composition) formulations are typically tested in and optimized based on read outs from preclinical species. One aspect is therefore that model optimization and refinement may be lacking at the stage of animal studies. Guiding early formulation development appears currently not a targeted functionality of available *in silico* software such as GastroPlus® or SimCyp®. As a consequence, no *in silico* modelling tool was employed in this work.

2.2.4 Thesis focus: Bioaccessibility

The concept presented in this work called **"the bioaccessibility concept"**, focuses on what is relevant and controllable with oral formulations related to drug absorption. The concept entails emphasis on how to identify, understand and account for factors impacting rate- and extent of absorption. Ultimately, it allows to estimate and optimize the expected *in vivo* performance by integrating the concept into an *in vitro* guidance. Specifically for early formulation development, it is difficult to decide on suitable formulation approaches from a pure *in vitro* perspective without any *in vivo* confirmation. Furthermore, *in vivo* read outs rarely allow to directly understand further optimization opportunities. Relative exposure comparison of dose levels and formulations are

typically needed, which often translates into the need for more preclinical studies. Focusing on *in vitro* flux across biomimetic membranes as a measure for bioacessibility has the potential to reduce/eliminate the need for at least some *in vivo* studies.

The term “bioaccessibility” originates from the food industry, but increased use can be observed in the pharmaceutical community as well, for example in (9, 25, 32, 33). Various definitions from nutritional and food science can be found and they differ slightly in terms of their translatability into the biopharmaceutical space (34). However, the common baseline is that bioaccessibility is considered a subcategory of bioavailability and can be used as a prediction tool for uptake efficiency from the GIT (35). A very recent publication illustrates how the TIM technology, a physiologically relevant dynamic multi-compartment digestion model originating from food science, can be applied to study the behavior of active pharmaceutical ingredients along the gastrointestinal tract together with food (36). Mainly, bioaccessibility is defined as the extent that a bioactive/nutrient is released from its (food) matrix in the gastrointestinal tract, becoming available for absorption (37, 38). In that sense, the bioaccessible drug would be defined as the fraction released from the drug product, e.g. from a tablet matrix, during a dissolution assay. In contrast, Semple et al. appreciated temporal and spatial constraints and specified a “bioaccessible compound as that which is available to cross an organism’s cellular membrane from the environment, if the organism has access to the chemical” (34). Here, organisms may refer to microbes and accessibility to the chemical may refer to the membrane being permeable to that chemical or whether active uptake mechanisms are available. The definition of bioaccessibility used in this work relates more to the definition from Semple et al. as given in **Equation 4**. Bioaccessibility refers to the contribution of given drug presentations to permeate across the gastrointestinal epithelium and associated resistance layers (e.g. unstirred water layer and mucus). Presentation refers to any physical form such as crystalline or amorphous drug, but also to drug species in solution, for example drug associated with bile colloids. The relative contributions of different drug forms and species towards bioaccessibility is in the scope of this work. A visual representation of the difference between **bioavailability** and **bioaccessibility** (at the intestinal lumen-cell membrane interface) is sketched in **Figure 4. Equation 1** is partially represented in this figure with $\mathbf{F_A}$ on the left and $\mathbf{F_{BAV}}$ on the right.

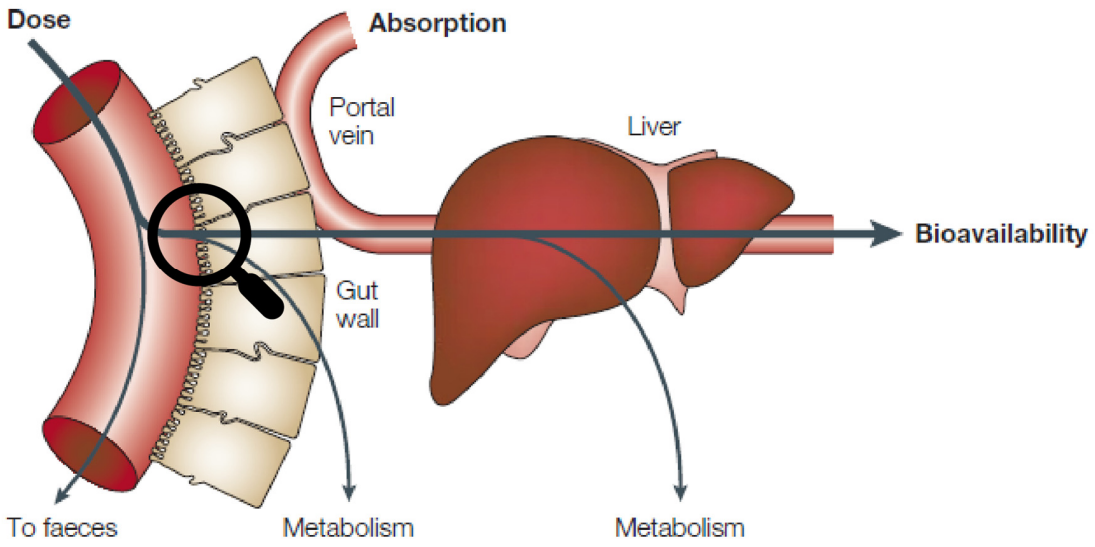

Figure 4: Schematic overview of drug absorption, metabolism and transport into the blood circulation via liver first-pass. Bioaccessibility refers to the process happening at the intestinal lumen-gut wall interface, illustrated with a magnifying glass. Bioavailability refers to drug measured in the blood after liver passage. Adapted by permission from Springer Nature: Nature Reviews Drug Discovery, ADMET in silico modelling: towards prediction paradise? Van de Waterbeemd et al. (39). Copyright 2003 Nature Publishing Group.

A summary of biopharmaceutical aspects, considered as the bridging scientific field between the pharmaceutical technology and therapy can be done according to **ADME**. **A** stands for **Absorption**, **D** for **Distribution**, **M** for **Metabolism** and **E** for **Elimination**, respectively (18). A recommendation for formulation scientists is to extend it by **L** for **Liberation**, related to drug release from the dosage form, and **T** for **Toxicity**, related to the therapeutic window. This yields **LADMET** and covers key areas of biopharmaceutics. For the drug formulator, primarly the liberation and absorption process can be manipulated. The relationship between liberation of drug, dissolution and permeation in the context of absorption was of greatest interest.

Liberation and absorption were main focus areas of this work and have received special attention. Methodologies were explored to understand the mechanistic relationship between those processes. The main physiological impact factors on drug liberation and absorption considered in this work include composition and characteristics of gastric and lumenal contents (e.g. pH and meal/bile components alongside formulation ingredients) and the unstirred water layer (UWL). The mucus layer was out of scope. Passive transcellular diffusion was considered as main absorption mechanism. While different regions of the gastrointestinal tract were outlined above, this work aimed to target specifically the site of absorption, i.e. small intestine, with consideration of important upstream compartments such as the stomach. The understanding of what triggers physiological adaptions of the GIT, for example through vagal innervation, and how the GIT “communicates” across segments, for example related to the gastrointestinal crosstalk between

the intestinal epithelium, the immune systen and endogenous bacteria, was considered out of scope (40, 41). Additional impact factors for oral drug absorption such as the transit time along the GIT (gastric emptying and GI-motility related) and blood flow were not further regarded. An illustration on how *in vivo* absorption was approached via bioaccessibility using *in vitro* flux setups with associated resistances is shown in **Figure 5**.

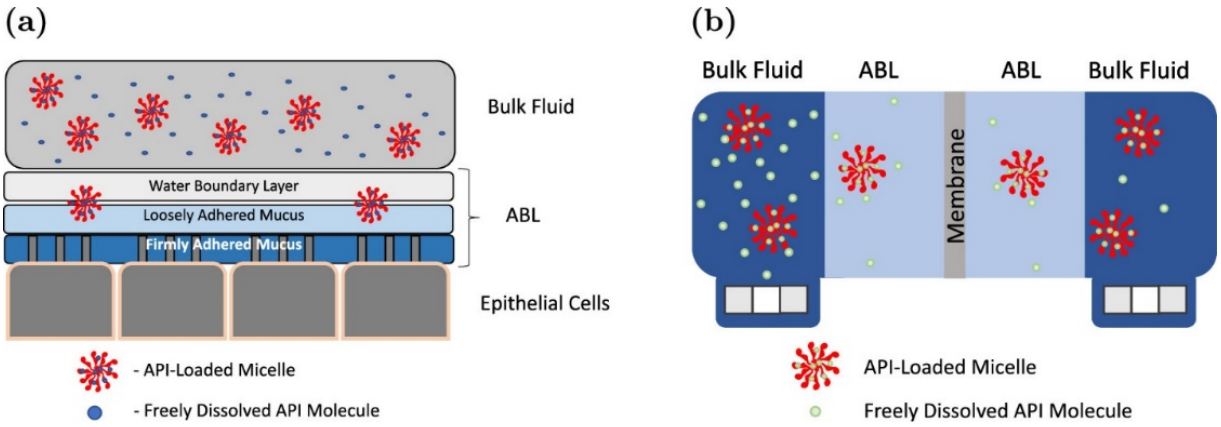

Figure 5: Illustration of a) in vivo and b) in vitro resistances to permeation/absorption based on passive transcellular/transmembrane diffusion. ABL represents the aqueous boundary layer or unstirred water layer (UWL). API stands for active pharmaceutical ingredient. Reprinted with permission from Arce et al. Towards developing discrimating dissolution methods for formulations containing nanoparticulates in solution: the impact of particle drift and drug activity in solution. Molecular pharmaceutics, 17, 11, 4125-4140 (23). Copyright 2020 American Chemical Society.

2.3 Physicochemical basis of the absorption process

Various concepts and mathematical representations of the absorption process have been developed and applied, aiming to reduce a highly complex physiological problem into more simple physicochemical problems relevant to the drug uptake process. It is generally accepted that the physicochemical properties of a drug are main determinants for absorption. It is important to understand that such properties of a drug are dependent on the environment, hence physiological factors from the GIT as well as components from the dosage form (formulation). Key physicochemical principles from a historical perspective are outlined below.

2.3.1 Aqueous solubility

The definition of solubility according to the International Union of Pure and Applied Chemistry (IUPAC) is: The analytical composition of a saturated solution, expressed in terms of the proportion of a designated solute in a designated solvent, is the solubility of that solute (42).

A personal perception for aqueous solubility relating to the solubility of a crystalline drug in aqueous systems is given as follows: Solubility describes the thermodynamic equilibrium between drug molecules in a solid crystal environment and an aqueous environment (e.g. solvated drug molecules). The rate of drug molecules going into solution (dissolution) is then identical with the rate of molecules going out of solution (precipitation). Since the “solubility” of amorphous forms is also relevant in the pharmaceutical field, the following addition is provided. An amorphous drug is theoretically considered a liquid phase (disordered phase) and therefore the term amorphous miscibility referring to the equilibrium between an amorphous phase and the aqueous phase, instead of amorphous “solubility”, would be more appropriate. Nevertheless, amorphous solubility will be used for simplicity. Aside from amorphous drug powder, phase separated drug species of naporafenib (model drug) for example when added via DMSO stock solution to an aqueous system, also appeared as amorphous before eventual conversion to a more stable crystalline form. The phase separation limit where formation of new drug species occurs is also considered the maximum amount of dissolved drug in solution, hence the amorphous solubility (43). Amorphous phases are typically instable, striving to reorganize towards more thermodynamically stable phases. In that sense, amorphous solubility has to be considered a transient equilibrium measure due to likelihood of form conversion from amorphous to crystalline. Independent of the terms used here, every drug presentation in undissolved form, whether crystalline or amorphous, is considered as solid reservoir. Generally, everything that can be removed by conventional filtration is regarded as solid reservoir. Amorphous phase separated drug species that form above the solubility limit are included in the solid reservoir even if they appear as “emulsion or gel-like” phases that might be pushed through the filter sometimes.

It is of general interest to predict the relative solubilities of drug forms, including co-crystals, salts or polymorphisms. Scientists are still working on the precise calculation based on solid-state properties such as crystal energies (packing), release of molecules from the lattice and subsequent solvation (44). A pragmatic but comparably imprecise equation to estimate solubility is the General-solubility-equation (GSE), initially proposed by Jain and Yalkowsky (45, 46):

$$Log\ S = 0.5 - 0.01(Tm - 25) - Log\ P \qquad \text{(Equation 5)}$$

Where S denotes the aqueous solubility (molar) of non-ionized solids, Tm represents the melting point (°C) and Log P the logarithm of the water-octanol partitioning coefficient. This equation reflects two determining factors for solubility, namely the forces between molecules such as in a crystal environment (Tm) and the interaction (or rather avoidance of interaction) with the water molecules (Log P). The melting point is considered a measure for hydrophobicity, while the Log P may function as a measure for lipophilicity. Depending on the underlying root cause for poor aqueous solubility, compounds can be roughly classified into “brick-dust” (hydrophobic) and “grease-ball” (lipophilic) molecules (47, 48). Some guidance is provided on formulation strategies based on this classification (49, 50). Important is that a drug molecule may be both, hydrophobic and lipophilic, and hence cannot be easily classified into one or the other category.

For bases and acids, one important additional aspect regarding solubility is ionization, related to the logarithm of the acid dissociation constant (pKa) of a molecule. This constant describes the relative presence of drug species in ionized and non-ionized form at a given solution pH. According to the Henderson-Hasselbalch equation (51), the solubility can be adjusted based on the pH of the solution and the pKa of the drug molecule to yield

$$S_{\text{total}} = S_{\text{non-ionized}}\left(1 + 10^{(pKa - pH)}\right) \qquad \text{(Equation 6)}$$

S_{total} refers to the total solubility and $S_{non\text{-}ionized}$ to the solubility of the non-ionized form.

In summary, solubility is an intrinsic property and depends on the interaction between molecules within a phase and on interactions with the solvent environment. The intrinsic solubility of a given drug form itself cannot be altered, but the “reference system” can be changed, for example by adding a solubilizer such as cyclodextrins or changing the pH and hence influence ionization of the compound. The commonly encountered phrase “increasing the solubility of a drug” is therefore misleading because either the drug form is changed, e.g. from crystalline to amorphous, or the environment is changed, e.g. by adding a solubilizer. A solubilizer is defined here as a component with the ability to increase the apparent solubility of a drug by providing an additional, typically hydrophobic, environment, while not altering the intrinsic solubility of a molecule. Solubility

therefore always refers to a specific form in a given system. For the purpose of this work, the main differentiation was made between crystalline and amorphous systems. The crystalline system always refers to the monohydrate form of naporafenib, i.e. assumed most stable form in aqueous environment. The amorphous systems include the crystalline tosylate form system due to the salt approaching a concentration cap equivalent to the amorphous solubility before form conversion.

2.3.2 Diffusion

Adolf Fick reported an equation in 1855 about diffusive mass transport, which served as basis for most of the biopharmaceutical concepts we know today (52). Restricted to one spatial dimension, Fick's first law can be stated as:

$$J_{\text{Diffusion}} = -D\frac{d\varphi}{dx} \qquad \text{(Equation 7)}$$

Where J denotes flux by means of diffusion with dimension amount per unit time (s) and area (cm^2). D denotes the diffusion coefficient of a substance in the dimension area per unit time (cm^2/s). φ represents the concentration of diffusing particles for ideal mixtures, and x denotes the position along this spatial dimension. dφ/dx describes the concentration gradient along one dimension and the negative sign indicates that the flux is going from a starting point with high concentration to an endpoint with low concentration. In case the concentration gradient is not constant, one would need to apply Fick's second law, a partial differential equation incorporating the changing concentration gradient over time. For pharmaceutical applications of mass transfer experiments, the differentiation between "finite" and "infinite" dose studies appears important. This may also determine which law to apply, based on either a constant or changing concentration gradient, hence, driving force for diffusion.

The diffusion coefficient contained in Fick's law can be further described by the Stokes-Einstein relationship (53):

$$D = \frac{k_B T}{6\pi\eta R} \qquad \text{(Equation 8)}$$

Where D is the diffusion coefficient (m^2/s), k_B the Boltzmann's constant ($(kg*m^2)/(s^2*K)$), T the absolute temperature (°K), η the dynamic viscosity of the medium (kg/(m*s)) and R the hydrodynamic radius (m) of the diffusing object (assumed to be spherical). Two relevant resistances for diffusion can be derived from this: the larger the hydrodynamic radius of the diffusing object and the larger the viscosity of the medium, the slower the diffusion.

2.3.3 Dissolution rate

In the context of drug dissolution, a personal perception is provided as follows: Dissolution summarizes the kinetic processes from initial contact with water (wetting) up until the release of drug molecules into the solvent environment where they subsequently get surrounded by water molecules (solvated). In practice, dissolution of a tablet incorporates sub-processes such as wetting of the tablet, water uptake and swelling, tablet disintegration into particles, dispersion of particles, and finally dissolution defined as the breakdown of solid-state bonds and solvation of drug molecules by water. (54-56)

The dissolution process defined by IUPAC as “the mixing of two phases with the formation of one new homogeneous phase (i.e. the solution)” (42) mainly refers to particle dissolution and does not incorporate a disintegration and dispersion step. In 1897, Noyes and Whitney described the rate of dissolution of a substance dependent on the concentration in solution relative to the concentration of a saturated solution (solubility of the substance) (57). In 1904, a further modification to this diffusion layer model was proposed by Nernst (58) and Brunner (59), relating back to Fick’s laws of diffusion and yielding the modified Noyes-Whitney equation (also known as Nernst-Brunner equation). The equation states:

$$J_{\text{Dissolution}} = \frac{dm}{dt}\frac{1}{A} = \frac{D}{h}(c_{\text{surface}} - c_{\text{bulk}}) \qquad \text{(Equation 9)}$$

Where dm/dt describes the amount of material (µg) dissolving per unit time (s), A denotes the interfacial surface area (cm^2) between solid and liquid, D the diffusion coefficient (cm^2/s), h the thickness (cm) of the diffusion layer (unstirred water layer, UWL) surrounding the dissolving particle and $c_{surface}$ - c_{bulk} relates back to the concentration gradient (Δ $\mu g/cm^3$) from the Noyes-Whitney equation (and hence Fick’s law). It becomes evident that the dissolution rate can be affected by various means, for example, increasing the available surface area by decreasing particle size (increase in surface-to-volume ratio) or increasing the stirring speed to reduce the thickness of the diffusive layer or extraction of the dissolved material (e.g. sink conditions for c_{bulk}). Drug form design approaches to improve the dissolution rate of poorly water-soluble drugs include the formation of co-crystals, salts or ionic liquids (60, 61).

Essentially, the concepts incorporate diffusion of molecules as the rate-limiting step of the dissolution process. In that sense, drug dissolution is considered a mass transfer process, relating to Fick’s laws. However, it needs to be appreciated that dissolution in a more holistic view may not always be limited by the diffusion itself but could be also limited by other sub-processes such as the wetting of the particle surface, water penetration or the breaking up of molecular bonds in

the crystal environment. Furthermore, one needs to be reminded that **Equation 9** is applicable only with simplifications such as that the particle surface area or unstirred water layer thickness do not change over time.

2.3.4 Flux related to membrane permeability

There are several ways a drug can be taken up from the gastrointestinal lumen while the most important differentiation is between active carrier-mediated transport and passive diffusion (62). While there are other possible uptake mechanisms such as the paracellular route (considered an "aqueous route" between enterocytes), the focus of this work was on passive transcellular diffusion across a membrane ("lipidic route"). This process of drug permeation can be described by:

$$J_{\text{Permeation}} = \frac{dm}{dt}\frac{1}{A} = P_{\text{effective}}\, c_{\text{Donor}} \qquad \text{(Equation 10)}$$

Where J denotes mass transport (dm/dt) of drug molecules (µg) over time (s) perpendicular to a given surface area A (cm^2), $P_{effective}$ stands for effective permeability (cm/s) and c_{Donor} for the concentration in the donor solution ($\mu g/cm^3$), assuming sink conditions in the acceptor compartment related to Fick's Law. Effective permeability instead of membrane permeability is used on purpose because the *in vivo* relevant permeability is not only governed by permeation of drug through the epithelial membrane. Theoretically, this is also associated with a limitation regarding Fick's law and the driving force for permeation. In contrast to a simple concentration gradient Δc over a single layer, the gradients over several resistance layers such as the unstirred water and mucus layer need to be considered additionally. This can be circumvented by assuming sink conditions in the acceptor compartment, and thereby making the permeation only dependent on the donor concentration c_D in case of ideal solutions, as shown in **Equation 10**. The relationship between the permeabilities (cm/s) disregarding mucus can be written in reciprocal form, referring to permeation resistances as follows (adapted from (63)):

$$\frac{1}{P_{\text{effective}}} = \frac{1}{P_{\text{UWL}}} + \frac{1}{P_{\text{neutral}} + P_{\text{ionized}} + P_{\text{paracellular}} + \cdots} \approx \frac{1}{P_{\text{UWL}}} + \frac{1}{P_{\text{Membrane}}} \qquad \text{(Equation 11)}$$

Where P_{UWL} is the permeability of a substance through the unstirred water layer adjacent to the membrane surface, $P_{neutral}$ describes the permeability of non-ionized drug through the membrane, $P_{ionized}$ the permeability of ionized drug and $P_{paracellular}$ the permeability based on the paracellular route. As mentioned above, the paracellular route and others (e.g. "active transport permeability" or "mucus permeability") were disregarded for the purpose of this work. It is generally accepted that the majority of drugs are taken up from the GIT through passive transcellular diffusion (64). Furthermore, since mainly uncharged drug molecules in solution are expected to permeate across

a lipidic membrane, a correction for the membrane permeability based on drug ionization and hence solution pH and pKa of the drug can be found in (63). In general, the intrinsic membrane permeability $P_{membrane}$ of a drug depends on its lipophilicity, molecular size and polarity/ability to form hydrogen bonds and is defined as:

$$P_{\mathrm{Membrane}} = \frac{K_{\mathrm{Membrane}} D_{\mathrm{Membrane}}}{h_{\mathrm{Membrane}}} \qquad \text{(Equation 12)}$$

$K_{Membrane}$ reflects the membrane partitioning coefficient, calculated as the concentration ratio of drug between the membrane environment and the aqueous phase in equilibrium. $D_{Membrane}$ refers to the diffusion coefficient of the drug through the membrane (cm^2/s) and $h_{Membrane}$ is the thickness of the membrane (cm). Typically, membrane permeability of a drug substance is assessed and calculated based on flux measurements using **Equation 10** across cellular membranes such as in Caco-2 or MDCK permeability assays (64, 65). The term apparent permeability is used when values are obtained from *in vitro* experiments. Effective permeability is used when derived from *ex vivo* methods. Typically, permeability across additional resistances such as the unstirred water layer are measured but not corrected for in the reported permeability values. Furthermore, deriving intrinsic membrane permeability usually requires the use of active transport inhibition (inhibitor cocktails) or knock-out cell lines.

2.4 Review of available concepts and methodologies

2.4.1 Absorption rate-limitations (BCS, DCS, FaCS)

Numerous biopharmaceutical concepts have emerged over the last years to understand and address factors limiting oral drug absorption. In 1985, Dressman published the absorption potential concept, illustrating how several key physicochemical properties influencing the absorption process can be summarized into a single equation (66). While it does not incorporate all relevant factors, it showed strong correlation with observed fractions absorbed. Specifically for poorly absorbed compounds, the absorption potential allows to pinpoint critical limiting factors/properties. Ten years later, in 1995, probably the most famous concept was published by Amidon et al. called the biopharmaceutical classification system (BCS) (67). This system classifies compounds according to their solubility and permeability, yielding four classes of drugs. BCS Class I compounds exhibit high solubility and high permeability, BCS II refers to low solubility but high permeability drugs, BCS III contains high solubility but low permeability drugs and the probably most problematic class, the BCS class IV, contains low solubility and low permeability compounds.

Both concepts are based on considerations about oral absorption rate-limitations. To illustrate this, BCS class I and III compound formulations are eligible for biowaivers (oral immediate release dosage forms administered with water), allowing to bypass or reduce the need for an *in vivo* bioequivalence study based on *in vitro* data showing that the dissolution rate between two drug products is similar (within acceptance limits) (68). This is possible with the assumption that the effective permeability can be considered identical comparing two products containing the same drug substance (high for BCS I and low for BCS III) and hence, only equivalence in terms of dissolution rate has to be shown. Furthermore, it should be noted that differences in dissolution rate of BCS class III drugs do not necessarily translate into differences in rate and extent of absorption due to the absorption rate-limitation (permeability-limited). The following two original statements found in (67) summarize the rationale of biowaiver strategies based on dissolution rate: “If two drug products, containing the same drug, have the same concentration-time profile at the intestinal membrane surface then they will have the same rate- and extent of absorption” and “If two drug products have the same *in vivo* dissolution profile under all lumenal conditions, they will have the same rate and extent of drug absorption”. Why such biowaivers based on dissolution rates are hardly possible for poorly water-soluble drugs (BCS class II and IV) is part of the problem statement within this work.

Despite the fact that the BCS is still considered a valid guideline and is used nowadays due to its simplicity, an important revision was provided in 2010 titled the developability classification system (DCS). This revised concept has found its way into the practical industrial setting in the context of developability assessment of new drugs and formulation development (69). In brief, the most important updates made were to incorporate simulated intestinal fluids (SIFs) into the solubility assessment, as well as further differentiating BCS II drugs into dissolution rate-limited (DCS IIa) and solubility-limited (DCS IIb) absorption. This translates into a theoretical advantage for the drug formulation scientists with the ability to assess whether additional solubilizing techniques are required or simpler dissolution rate enhancement may provide sufficient drug exposure. All those classifications allow guiding *in vitro-in vivo* correlation (IVIVC) efforts based on the expected absorption rate-limitation.

Worth mentioning are closely related concepts. First, the absorption-limiting step classification (70), which includes three major processes, namely the dissolution, permeation and transit flow of a drug through the GIT. And secondly, the fraction absorbed equation (Fa equation, (71)) serving as a basis and providing criteria for the fraction absorbed classification system (FaCS, (72, 73)).

By now, it should have become evident that it is all about rate-limitations of mass transfer processes. Mathematical simplifications based on the determining rate-limitation are encountered in both physicochemical and physiological/biopharmaceutical approaches to represent the oral drug absorption process. Consequently, it is key to identify the relevant resistance(s) determining rate and also extent of absorption.

2.4.2 Discovery of absorption resistances with the pH-partitioning hypothesis

Long before the biopharmaceutical classification system has been published, various scientists have attempted to predict absorption in dependency of drug ionization, based on the Hendersson-Hasselbalch equation (51). In 1940, Travell provided a first indication that the gastric mucosa is selectively permeable to non-ionized forms of a molecule (74). An equal dose of alkaloids was observed to be non-toxic under acidic gastric conditions, while at elevated and more basic gastric pH, it was found to be toxic. In the same year, Jacobs extented this observation towards lipidic membranes of cells and investigated permeability of weak electrolytes in dependency of ionization (75). Due to those and many more contributions, the pH-partitioning hypothesis was published around 1957 (76). A historical overview including references is provided in (63). The key assumption is that mainly uncharged drug molecules in solution can be absorbed over a lipidic membrane by passive diffusion. Deviations from the predicted absorption behavior, however, have led to questioning the suitability of the pH-partitioning hypothesis regarding quantitative absorption predictions. In summary, the following insights were gained:

A) The existence of an acidic microclimate on the mucosal surface of enterocytes was hypothesized in 1959 based on apparent “pH-shifts” in the absorption curves (77). *In situ* rat perfusion studies were performed utilizing various pH levels. The amount of drug absorbed was different than predicted from the pKa of the drug and the pH of the perfusate. By direct microelectrode pH measurements, the hypothesis was confirmed in 1975 *in vitro* (78) and 1983 in another *in situ* rat perfusion study *(79).*
B) The acidic microclimate was further linked to a cell-surface adhering mucus layer in 1979, appearing metabolically enriched with protons. This viscous hydrogel-like layer was recognized as additional resistance to oral absorption (80).
C) By means of the segmented flow technique, thickness modification of a “mucosal unstirred water layer” with considerable effect on drug permeation was reported in 1983 (79).
D) In 1991, it was concluded that the pH-partitioning hypothesis is not reliable as quantitative model for absorption predictions (81). While the acidic microclimate is considered the main root cause for this, minor contribution from the unstirred water/mucus layer, passive diffusion of ionized molecules and other absorption routes such as the paracellular

pathway or transporter-mediated uptake were appreciated. Importantly, the unstirred water layer as absorption resistance appeared specifically relevant for lipophilic drugs.

2.4.3 Strategies to address absorption resistances of poorly water-soluble drugs

An extensive review from 2013 is available from Williams et al. titled “strategies to address low drug solubility in discovery and development” (49). Common formulation approaches include particle size reduction (increase in available surface area), the use of co-solvents, surfactants and cyclodextrins (CD), the formation of salts, co-crystals, polymorphs or pro-drugs and more generally, the use of lipid-based formulations (LBF) or amorphous solid dispersions (ASD).

1.4.3.1 The “Spring-Parachute” concept

In order to understand how those strategies may overcome absorption limitations of poorly water-soluble drugs and promote oral absorption and hence bioavailability, a few selected but important concepts are explained in more detail. The first and likely most important is the “spring-parachute” concept, related to drug supersaturation and thereby tackling solubility limitations. The degree of saturation (D_S) as a function of time can be defined as the ratio of dissolved drug or kinetic solubility (c(t) or $S_{kinetic}(t)$) relative to the equilibrium solubility ($c_{equilibrium}$ or S) of the drug (82):

$$D_S(t) = \frac{c(t)}{c_{equilibrium}} = \frac{S_{kinetic}(t)}{S} \qquad \text{(Equation 13)}$$

A $D_s < 1$ indicates a sub-saturated system, where the concentration is below the solubility limit. A $D_s = 1$ indicates a saturated system, at solubility. A $D_s > 1$ reflects supersaturation with concentrations above the thermodynamic solubility of the crystalline drug. Theoretically, the same consideration could be applied to the amorphous system, as approached by (23), expressing the concentration as a fraction of the amorphous solubility. This leads to a degree of saturation with respect to amorphous solubility instead of supersaturation relative to the equilibrium solubility.

Thermodynamically instable drug concentrations in solution (supersaturation) can be generated by using a higher energy form of the drug, such as a salt, co-crystal or amorphous form, compared to the most stable crystalline form. This is referred to as “spring effect”. As outlined in the solubility section, an amorphous form may generate higher drug concentrations (up to the phase separation limit), because it has a higher chemical potential. In turn, to lower this potential the drug strives to crystallize towards the most stable form in aqueous environment, i.e. the one with the lowest chemical potential. Considering the physicochemical basis (Fick’s law), it becomes evident that increased drug concentrations in solution increase the driving force for the absorption process. Since supersaturations are typically not very stable, stabilization of such metastable states are desired, denoted as “parachute effect”. This can be achieved by including precipitation inhibitors,

which are components (e.g. polymers) that can inhibit the drug crystallization process for example through restriction of the drug's molecular mobility required to re-organize molecules into nuclei (dense aggregates) and subsequently, into a crystal lattice. Typically, ASDs incorporate such a "spring and parachute" functionality. A visual representation of a "spring-parachute effect" can be seen in **Figure 6**, adopted from (82):

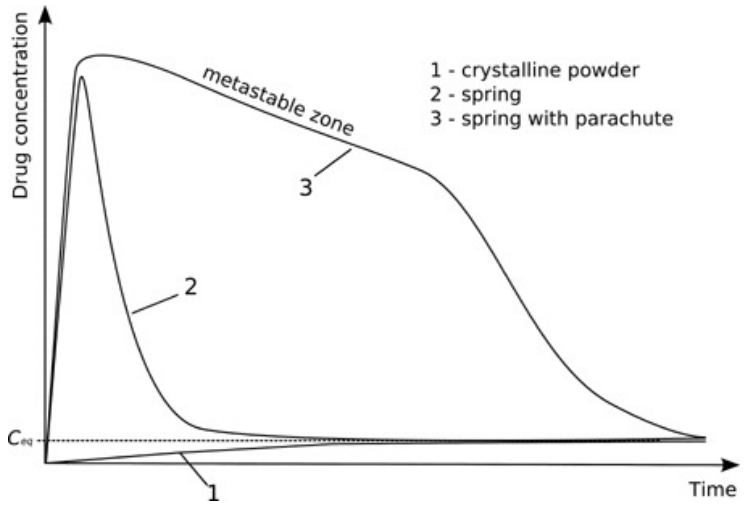

Figure 6: Schematic drug concentration-time profiles of 1) a crystalline powder form, 2) a high energy form exhibiting a spring effect and 3) a high energy form with precipitation inhibitor exhibiting a spring-parachute effect. Reprinted from Journal of Pharmaceutical Sciences, 98, 8, Brouwers et al. Supersaturating drug delivery systems: the answer to solubility-limited oral bioavailability? 2549-2572 (82). Copyright 2008 Wiley Liss, Inc. and the American Pharmacist Association, with permission from Elsevier.

For poorly soluble weak bases, the physiology of the GIT in the fasted prandial state provides a "natural spring effect" which can be harnessed to increase the driving force for absorption. The acidic stomach environment allows a basic drug to dissolve and reach a relatively high concentration through large amounts of ionized drug species. This generates supersaturation after the transition into the small intestine where a higher pH neutralizes the ionic species and reduces the equilibrium solubility to the one of the neutral basic drug.

Similar to the concept above, lipid-based systems may also generate supersaturation through various mechanisms such as dilution/dispersion of the formulation vehicle, intestinal digestion through enzymes of lipidic components, interaction with bile and lipid absorption (83). Those processes can affect (typically reduce) the solubilizing capacity of the formulation/intestinal fluid mixture for the drug and thereby promote drug absorption through generation of supersaturation.The lymphatic pathway of drug absorption may also be promoted through the use of LBF, but is not further discussed here.

1.4.3.2 The "particle-drifting" concept

The unstirred water layer (UWL), as discussed in previous sections, may serve as an additional relevant resistance to oral drug absorption, specifically for lipophilic drug molecules. A more recent strategy has emerged around this resistance called the "particle-drifting concept". To the best of knowledge, K. Sugano was the first to have used this term (84, 85). Since every orally administered drug encounters bile components and therefore (mixed) micelles and vesicles, he additionally simulated how such colloidal structures related to bile may affect the effective permeability of lipophilic drugs (86). Depending on the absorption rate-limitation, he attempted to mechanistically explain food effects by bile micelles, whereas one mechanism is related to the "micellar shuttling" effect based on the "particle-drifting concept" (72).

While the effects of a formulation on the dissolution rate or apparent solubility can be assessed in conventional *in vitro* assays, the assessment of drug permeation and hence a possible "particle-drift" into the unstirred water layer requires the use of *in vitro* flux technology. For educative purposes regarding flux assays and rate-limitations, the reader is referred to a publication provided by Stewart et al. (87). As an application, a positive "particle-drifting" effect based on *in vitro* flux was correlated to increased oral bioavailability in rats, using spray-dried amorphous solid dispersions of itraconazole that generated drug-rich colloids upon dissolution (88). Interestingly, in line with the above concepts, the "particle drifting effect" of the formulation diminished the more micelles/vesicles were present (e.g. by increasing amount of SIF components such as bile salts to a rat-like environment). While currently, one cannot differentiate between media effects on the UWL thickness and effects on assisted drug diffusion ("shuttles"), the observations support that both, the formation of drug-rich colloids as well as the presence of colloidal structures such as (mixed) micelles/vesicles, can positively affect the drug permeation process (effective permeability). This contribution can be expressed through the following equation (88):

$$D_{\mathrm{UWL}} = D_{\mathrm{u}} f_{\mathrm{u}} + D_{\mathrm{m}} f_{\mathrm{m}} + D_{\mathrm{c}} f_{\mathrm{c}} \qquad \text{(Equation 14)}$$

D_{UWL} describes the effective diffusion coefficient through the unstirred water layer as a sum of D_u, D_m and D_c, the diffusion coefficients of the unbound or freely dissolved drug, drug associated to micelles/vesicles (includes all soluble colloids) and drug-rich colloids (such as nanoparticles), respectively. How much each diffusion coefficient contributes to the effective coefficient is determined by the fraction of each species f_u, f_m and f_c, and the hydrodynamic radius of the diffusing species, related to Stokes-Einstein, **Equation 8**. It is important to highlight that both, dissolved drug species (e.g. solubilized in micelles) as well as undissolved drug species (e.g. in the form of drug-rich nanoparticles) may diffuse alongside molecularly dissolved drug through the

unstirred water layer. The overall permeability of a drug in the form of various species through the UWL as contained in **Equation 11** can therefore be written as:

$$P_{\mathrm{UWL}} = \frac{D_{\mathrm{UWL}}}{h_{\mathrm{UWL}}} \qquad \text{(Equation 15)}$$

Where P_{UWL} is the effective permeability coefficient of a drug through the unstirred water layer, D_{UWL} the diffusion coefficient through the UWL and h the thickness of the UWL. Recent efforts incorporating those concepts for oral absorption modelling support the applicability and relevance of the proposed UWL-penetrating mechanisms (89).

2.4.4 Harmonization of concepts by K. Sugano and K. Tereda

Given the plethora of concepts that have evolved, it is important to understand how they differ from each other and what synergies they might share. Considered a “milestone” in that context, K. Sugano and K. Tereda published a work in 2015 about rate- and extent-limiting factors of oral drug absorption where they aimed to harmonize available concepts previously discussed. The contextual relationships of the absorption rate-limitations and hence the FaCS, the BCS, food effect by bile micelles, recommended/proposed formulation technologies as well as underlying considerations for biowaiver strategies are provided in **Figure 7**.

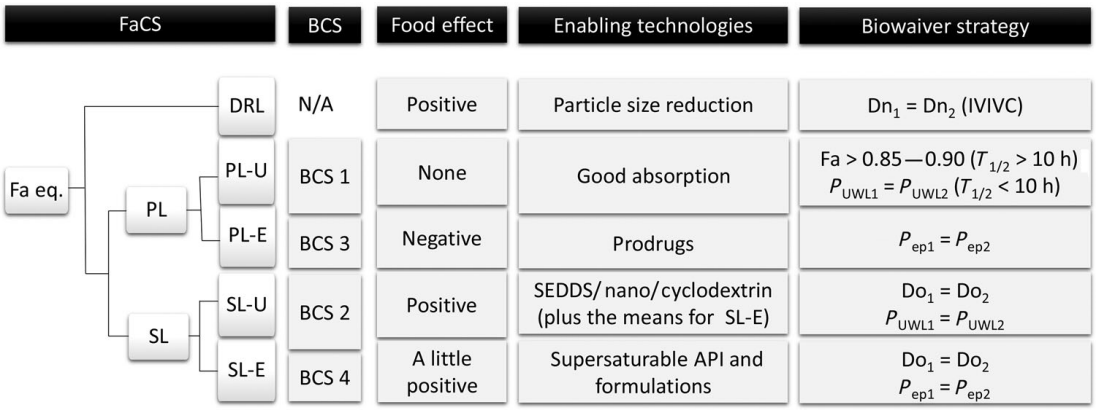

Figure 7: Overview of related concepts regarding oral drug absorption, incorporating the fraction absorbed classification system (FaCS), biopharmaceutical classification system (BCS), food effect by bile micelles, recommended formulation technologies and proposed biowaiver strategies. FaCS incorporates the fraction absorbed equation (Fa eq.) and expected absorption rate-limitations such as dissolution (DRL), permeability (PL) and solubility (SL) with further differentiation into epithelial membrane (-E) or unstirred water layer (-U) limited. SEDDS stands for self-emulsifying drug delivery system and IVIVC for in vitro-in vivo correlation. For more precise definitions of the dissolution number (Dn), dose number (Do), unstirred water layer permeability (P_{UWL}) and epithelial membrane permeability (P_{ep}), refer to (90). Reprinted from Journal of Pharmaceutical Sciences, 104, 9, Sugano, K., Terada, K., Rate- and Extent-limiting factors for oral drug absorption: theory and applications, 2777-2788 (90). Copyright 2015 Wiley Periodicals, Inc. and the American Pharmacist Association, with permission from Elsevier.

Most importantly, all concepts are based on absorption rate-limitations. The classification systems (FaCS and BCS) provide a basis to estimate the dominating oral absorption resistance that needs

to be overcome. The contribution of bile micelles on such resistances are mechanistically linked to food effects. Similarly, the proposed formulation technologies aim to address the relevant absorption resistances. Finally, as previously mentioned, it is possible to reduce/eliminate the need for *in vivo* bioequivalence studies if the oral absorption determining rate-limitation is the same and equal between two drug products. Since BCS II and IV drugs are currently not eligible for a biowaiver, the proposed strategies and associated considerations may at least serve as viable tools to guide IVIVC efforts.

2.5 Risk for absorption predictions: shifts in rate-limitations

The proposed framework will be applied to several case studies, limited to poorly water-soluble drugs (e.g. BCS II and IV drugs). The usefulness and general applicability will be evaluated and discussed, ultimately leading to limitations of the presented concepts and hence, contribute towards the problem statement of this work.

2.5.1 Case: Itraconazole (hydrophobic and lipophilic BCS class II drug)

Itraconazole is a weak base belonging to the BCS class II, low solubility and high permeability drugs. The apparent equilibrium solubility in SIFs is very low at approximately 0.3 µg/mL in FaSSIF-V1 and 0.7 µg/mL in FeSSIF-V1 (91). The melting point is above 160°C and the calculated Log P is above 7, indicating both “brick dust” as well as “grease ball” properties, as mentioned in the solubility section above (91, 92). According to this information, the major absorption resistances for the pure drug substance may be the low solubility potentially paired with poor dissolution behavior. One could expect a positive food effect by bile micelles through an increase in dissolution rate, an increase in apparent solubility and/or assisted diffusion through the unstirred water layer, according to **Figure 7**.

Interestingly, itraconazole formulated as HPMC-based amorphous solid dispersion in capsules (Sporanox capsules®) exhibited a positive food effect at 100 mg dose (93) while formulated as oral solution with Hydroxypropyl-β-cyclodextrin (Sporanox solution®) a negative food effect at a 200 mg dose was observed (94). It is important to note that the oral solution in the fed state still showed higher exposure than the capsule formulation in the fed state. The relative exposures as well as both directions of food effects for the two formulations were correctly predicted by *in vitro* flux (95). Various mechanisms were proposed for this observation related to drug dissolution, precipitation, supersaturation and drug diffusion through the unstirred water layer (95, 96). While it is difficult to prove the determining *in vivo* absorption rate-limitation, it becomes evident that the rate-limitation has shifted between the two formulations, hinting towards limited applicability of the proposed framework (**Figure 7**).

2.5.2 Case: Fenofibrate (lipophilic BCS class II drug)

Fenofibrate is a neutral molecule belonging to the BCS class II, low solubility and high permeability drugs. The apparent equilibrium solubility in SIFs is low at 14 µg/mL in FaSSIF-V1 and 54 µg/mL in FeSSIF-V1 (91). The melting point is around 80°C (97) and the calculated Log P is above 5, indicating mainly "grease ball" properties, as mentioned in the solubility section above (91). According to this information, the major absorption resistance for the pure drug substance may be the low solubility. One could expect a positive food effect by bile micelles through an increase in apparent solubility and/or assisted diffusion through the unstirred water layer, according to **Figure 7**. Interestingly, Fenofibrate formulated as micro particles (Lipanthyl®) exhibited a positive food effect, while formulated as nano particles (Lipanthylnano®) it showed a negative food effect (98). It was possible to illustrate the solubility-permeability interplay in an *in vitro* flux setup as well as using the *in vivo* aspiration technique, providing evidence that increased drug concentrations in solution do not necessarily translate into an increased driving force for absorption and hence, increased exposure (98). The "micellar entrapment" of the drug was suspected to be responsible for this shift in rate-limitation. The hypothesis is that the nanosizing improved the dissolution process and the typically beneficial impact of bile on the dissolution rate turned into a negative contribution on permeation. This directs again towards limited applicability of the proposed framework (**Figure 7**).

2.5.3 Case: Tyrosine kinase inhibitors (BCS class II/IV drugs)

Specifically for oncology drugs such as the tyrosine kinase inhibitor (TKI) family, significant changes in drug exposure related to food effects are of relevance regarding safety and efficacy (99). Anticipating a potential food effect early during drug development can be important for the clinical setting in order to avoid toxicity or efficacy surprises but also for regulatory purposes regarding a required label how the drug should be administered. A large increase in TKI bioavailability if co-administered with food is the rule rather than the exception based on their pharmacology, as stated in (99). To evaluate this, three selected TKI targeting the BCR-ABL protein for the treatment of chronic myeloid leukemia, namely imatinib, nilotinib and asciminib, were evaluated in terms of their observed food effect.

Imatinib mesylate is marketed as Gleevec® and showed high absolute oral bioavailability of 98% irrespective of formulation or dose (100). The BCS class assignment is ambiguous. Below a pH of 5.5, imatinib is stated as freely soluble in water while at physiological pH 7.4, it is considered sparingly soluble with 50 µg/mL (100). Based on the observed bioavailability, imatinib may be considered a high permeability molecule which would result in a BCS class II assignment based on the solubility at intestinal pH. A high-fat breakfast meal did not have a significant impact on the

rate (Cmax reduced by 11%) and extent of absorption (AUC reduced by 7.4%) of a 400 mg dose and was considered clinically irrelevant (100, 101).

Nilotinib hydrochloride monohydrate is marketed as Tasigna® and is classified as either BCS class II or IV compound with low solubility and moderate permeability, depending on the reference (102, 103). The apparent solubility in FaSSIF-V1 and FeSSIF-V1 was reported as 0.3 µg/mL and 3.2 µg/mL, respectively (50). A large positive food effect was observed in healthy volunteers with an increase in AUC of 82% when a 400 mg dose was co-administered with a high-fat meal (104).

Asciminib, just approved by the FDA in 2021 as Scemblix® (105), can be assigned to the BCS class II based on low solubility and medium/high permeability (106, 107). The apparent solubility of the crystalline anhydrous form is reported as 9 µg/mL and 257 µg/mL in FaSSIF-V2 and FeSSIF-V2, respectively (106). The solubility of a solid dispersion (amorphous form) is reported as 260 µg/mL and 625 µg/mL in FaSSIF-V2 and FeSSIF-V2, respectively. Based on solubility and **Figure 7**, a positive food effect by bile micelles would be expected. In contrast, independent of the different formulations tested in humans, all showed a significant negative food effect at a 40 mg dose with about 30% reduction in exposure under low-fat meal condition and over 60% reduction under high-fat meal condition (107, 108). Most interestingly, a crystalline formulation of the free base showed a positive food effect and an equal dose of an amorphous approach resulted in a negative food effect in dogs, indicating a large impact of the drug substance form/formulation on the observed food effect (109).

In conclusion, correlation between BCS class of a drug substance and observed food effect of a given dose and formulation is not always according to **Figure 7**. While it needs to be remembered that food effects may not only be due to the presence of bile micelles, evaluating the impact of bile components and resulting colloidal structures on drug absorption is a good approach to elucidate oral absorption rate-limitations. The main risk for absorption predictions (and hence also formulation development/optimization) is when rate-limitations are shifting between dose levels, drug substance forms, formulations or patient conditions such as prandial state (fasted or fed) or treatment/disease (e.g. use of proton-pump inhibitors). This leads to the following statement: The oral absorption rate-limitation of a drug substance may be affected by the dose, the formulation and the gastrointestinal environment. A limitation of the framework proposed by Sugano and Tereda is therefore that after the drug substance is formulated (e.g. by the proposed technologies in **Figure 7**) the absorption rate-limitation needs to be re-assessed while considering the relevant *in vivo* environment and dose levels. This appears crucial for formulation development but also prediction of bioperformance of a drug formulation/product and was exemplified within this work.

3. Thesis scope

The key problem tackled in this work was to understand and rationally overcome oral absorption limitations for poorly water-soluble drugs. This can be essential to provide a safe and efficaous treatment for patients. Mechanistic understanding is required to transition from an empirical drug development process towards more targeted and rational formulation development. The ultimate goal is "to confirm *in vivo*" rather than to "learn from *in vivo*", enabling to reduce the amount of required preclinical and clinical studies. The problem statement will be explained from different perspectives, illustrating its complexity. Subsequently, the bioaccessibility concept and associated development of an *in vitro* methodology will be introduced. The practical application on a selected model drug (poorly soluble weak base) will then guide the reader throughout this work.

3.1 Problem statement from a pharmaceutical development perspective

It was estimated that around 40% of marketed drugs show poor aqueous solubility, while this number may be even higher in industrial development pipelines (91, 110). The initial BCS/DCS classification is typically performed on the drug substance itself. Apparent equilibrium solubilities are usually determined in various media including the physiological pH range and biorelevant media. Apparent permeabilities are typically assessed using cell-based assays involving Caco2 or MDCK cells. Initial formulation efforts are then tailored around this initial assessment of the expected oral absorption rate-limitation (for example solubility-, dissolution rate- or permeability-limited absorption). For poorly water-soluble drugs (BCS class II and IV drugs), the assumption appears valid that dissolution rate and/or solubility may be primarly limiting the rate and extent of absorption of the unformulated drug substance. This partially justifies the traditional focus of pharmaceutical development on dissolution rate and solubility assays. Knowledge of the estimated/required dose is of help here to further support this assumption. The dissolution rate and solubility are typically assessed multiple times for various formulation principles including enabling formulations (e.g. ASD or LBF) and conventional approaches. In practice, for example for PBPK modelling, the obtained apparently dissolved drug concentrations from those assays are then paired with the intrinsic permeability value of the drug substance. There are some limitations to evaluate cell permeabilities at pharmaceutically relevant dose levels or in presence of certain excipients/formulation components. This leads to an apparent disconnect between solubility and permeability assessed under non-identical condtions and with that "invalidates" the use of frameworks such as the BCS or DCS. The typical increase in apparent solubility and associated decrease in apparent permeability when a drug is for example solubilized by micelles is known for a long time, reported by Amidon already in 1982 (111). However, this awareness appears lacking in current drug formulation development. An important goal of this work was to re-connect solubility

with permeability by looking into passive diffusion of drug across a barrier *in vitro* under pharmaceutically relevant conditions within the same assay.

3.2 Problem statement from a physicochemical perspective

The detrimental impact of the solubility-permeability disconnect mentioned above can be attributed to the inability of apparently dissolved drug concentrations to adequately reflect a driving force for permeation, as stated by experts in the field (24). This is also supported by a proposed change in paradigm regarding pharmaceutical research strategies by Boyd, Bergstörm, Vinarov, Brouwers, Augustijns and many more in 2019 (112). Essentially, they recommended to include biorelevant components for solubility and permeability assessments while emphasizing the concept of freely dissolved drug molecules as key driver for absorption. Differentiating various drug species such as ionized and non-ionized drug molecules as well as drug solubilized in colloids such as (mixed) micelles and vesicles is typically not performed but appears crucial to understand oral drug absorption. The importance of this aspect is outlined by efforts in the scientific community to understand the true driving force for permeation/absorption in complex systems such as drug supersaturation in biorelevant media (113, 114). Such work also supports limited applicability of Fick's laws based on apparent concentrations to understand the oral absorption process because those systems should be considered non-ideal mixtures/solutions. A good illustration of an enabling formulation (involvement of amorphous drug) in a biorelevant absorption context is provided in **Figure 8.**

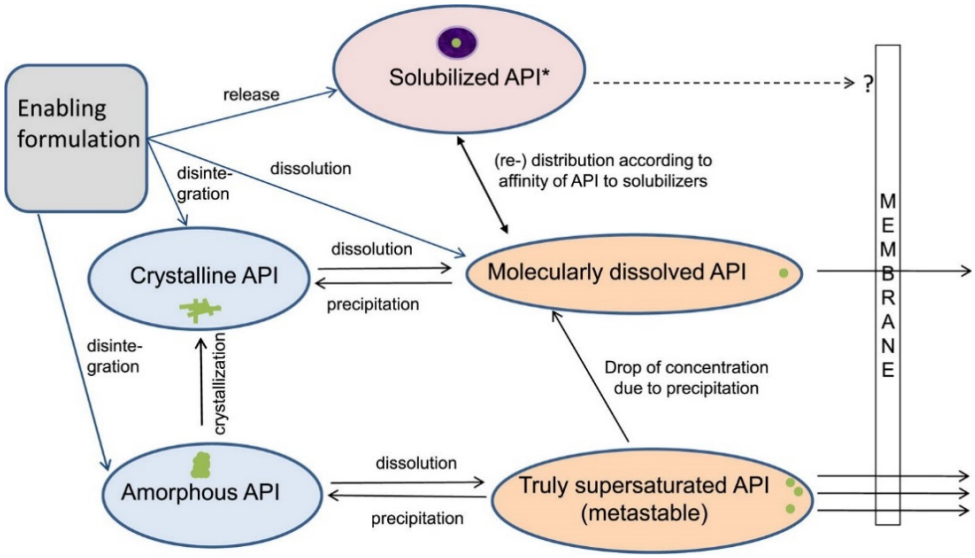

Figure 8: Illustration of various drug species and their interplay resulting from an enabling formulation (involvement of amorphous drug form) added to a biorelevant system with absorption context. API stands for active pharmaceutical ingredient. Reprinted from European Journal of Pharmaceutical Sciences, 50, 1, Buckley et al., Biopharmaceutical classification of poorly soluble drugs with respect to "enabling formulations", 8-16 (115). Copyright 2013 Elsevier B.V., with permission from Elsevier.

3.3 Problem statement from a physiological/biopharmaceutical perspective

As previously mentioned, it is well known that the physicochemical properties of a drug such as pKa, solubility and permeability are important for the drug absorption process. But it needs to be understood that they have to be interpreted in a biopharmaceutical context, that means as a function of the gastrointestinal environment. Such environments are unfortunately not constant and may change between healthy volunteers and patients, disease-states, co-medications, food intake etc. Furthermore, early formulation development is typically accompanied with studies in preclinical species rather than in humans. Essentially formulations are developed and refined based on read outs from preclinical species such as rats or dogs but are intented to work in humans later. Correlation between animal and human bioavailability can be shockingly poor (116). The approach developed within this work aimed for a systematic understanding of individual components (such as bile salts) and factors (such as pH), rather than trying to mimic specific real life conditions (such as fasted and fed state) where multiple factors are changed at the same time. A glimpse of how challenging this endevaour can be, illustrated for the human situation, is shown in **Figure 9.**

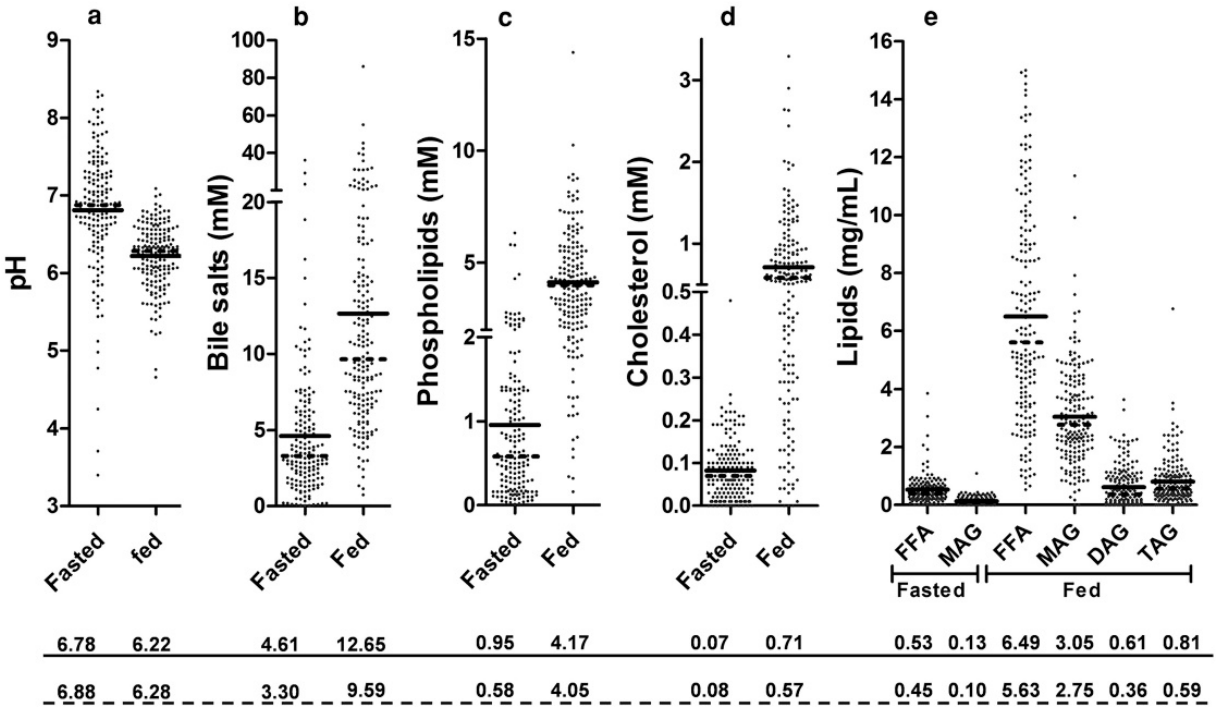

Figure 9: Compositional variability of aspirated human intestinal fluids from 20 healthy human volunteers in the fasted and fed state. Individual data points are presented with mean (solid line) and median (dashed line) provided below in the same unit as above. Reprinted from Journal of Pharmaceutical Sciences, 105, 2, Riethorst et al., Characterization of human duodenal fluids in fasted and fed state conditions, 673-681 (117). Copyright 2016 American Pharmacist Association, with permission from Elsevier.

3.4 Thesis structure

In essence, the key challenge for formulation development of a poorly water-soluble drug is to reach consistent concentrations in the systemic circulation of a patient within the therapeutic window. The problem is linked to the physiological variability, the effects of this variability on physicochemical properties of a drug along the GIT and the lack of mechanistic understanding of the driving forces and resistances (absorption rate-limitations) for permeation in complex systems.

The bioaccessibility concept developed within this work is a proposed simplification of **Figure 8**, illustrating the three key drug species that need to be differentiated. The approach pursued was two-fold, firstly the understanding and differentiation of drug species in dependency of dose, formulation, and (GI) environment and secondly, linking the individual drug species to the driving force for absorption. Inspired from the work of Maria Vertzoni et al. (118) ultracentrifugation (UC) was used to explore the possibility to separate drug associated with biorelevant colloids from freely dissolved drug, during a supersaturated state. Dynamic light scattering (DLS) was used to evaluate the separation efficiency. Combining drug species differentiation and bioaccessibility measurements using *in vitro* flux (permeation) across artificial biomimetic membranes under various conditions led to a novel exploratory assay type, the “ultracentrifugation-flux combo assay” (UCFCA). Applying such mechanistic approach may help to rationally address transport limitations during drug formulation development. The bioaccessibility concept in its simplest form can be seen in **Figure 10.**

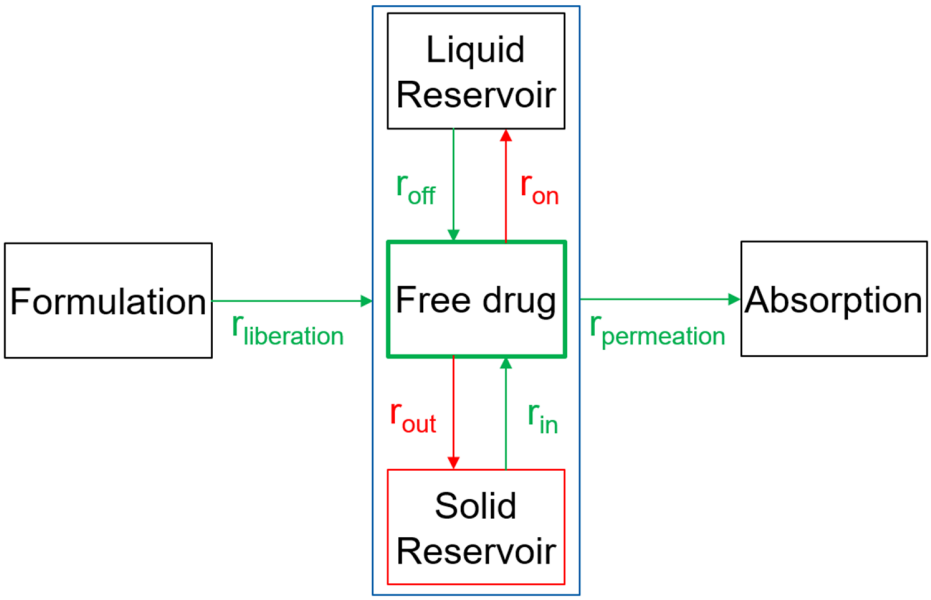

Figure 10: Illustration of the bioaccessibility concept related to drug mass transport processes such as oral absorption based on passive diffusion. The concept incorporates the release of drug from the formulation, the resulting formation of three key drug species upon dispersion/dissolution, their interplay and contribution towards permeation/absorption.

Once a formulation (or related drug substance presentation) is added to an aqueous system, a kinetic process denoted as $r_{liberation}$ takes place, incorporating sub-processes from wetting, water uptake and swelling, disintegration (specifically in case of tablets or capsules) and finally dispersion of drug particles. For some formulations there might already be some dissolved drug (e.g. suspensions or emulsions) while for others (e.g. tablets), liberation and dissolution might happen in parallel. The resulting dynamic equilibrium between the solid reservoir (undissolved drug), freely dissolved drug and the liquid reservoir is shown in the blue box. Solid reservoir refers to undissolved drug material either in crystalline or amorphous form (including phase separated drug species). A potential form conversion and/or co-existence of solid reservoir species is possible. The kinetic processes r_{in} and r_{out} relate to drug dissolution and precipitation, respectively. The liquid reservoir refers to any dissolved drug species, for example, drug solubilized in colloidal aggegrates like mixed micelles. Several liquid reservoir species may also co-exist and/or interact with each other. The kinetic processes r_{on} and r_{off} relate to molecular drug interactions excluding water interactions (solvation) but include partitioning into and out of soluble drug-rich phases. Finally, from the dynamic species equilibrium (blue box), $r_{permeation}$ describes the collective contribution of individual species towards passive permeation in form of a mass transfer rate. This rate incorporates previously introduced principles such as unstirred water layer diffusion and membrane partitioning and permeation via effective permeability (**Equation 10 and 11**). The considerations from **Figure 3** and **Equations 2-4** are included in the concept and the bioaccessible fraction is referring to drug species depicted in the blue box and bioaccessibility to the sum of their contribution towards permeation ($r_{permeation}$). The key principle of this concept is to combine drug species characterization with drug mass transport (flux) evaluation. From the bioaccessibility concept, an *in vitro* guidance was derived in the form of 5 questions to assist in the development of poorly water-soluble drug candidates. The methodology was applied to a single model compound in this work and exemplifies the potential use on other poorly soluble drug candidates. For orientation, each question was dedicated a section of results and at the end of each section, the context to the bioaccessibility concept is briefly discussed.

- ➔ **Question 1:** Which drug form (any presentation such as free form, salts, polymorphs, co-crystals, ionic liquid, amorphous...) to select for formulation development?
- ➔ **Question 2:** What factors influence bioaccessibility?
- ➔ **Question 3**: How can excipients/formulation principles manipulate bioaccessibility?
- ➔ **Question 4**: How does *in vitro* bioaccessibility translate into *in vivo* exposures?
- ➔ **Question 5**: How to address identified oral absorption risks/limitations by rational formulation development?

4. Materials and methods

4.1 Materials

The various drug forms of naporafenib were kindly provided by Novartis Pharma AG (Basel, Switzerland). Sodium hydroxide pellets, sodium chloride and sodium dihydrogen phosphate monohydrate (EMSURE® grade) used for buffer preparation were obtained from Merck KGaA (Darmstadt, Germany) or alternatively from Sigma-Aldrich (Schnelldorf, Germany). In case pH adjustments were required, 1 N sodium hydroxide (NaOH) solution and 1 N hydrochloric acid (HCl), both Titripur® from Merck KGaA were used (alternatively, 2 N HCl/NaOH from same supplier was used). Biorelevant media ready-to-use powders, namely fasted- / fed-state simulated intestinal fluids / fasted-state simulated gastric fluids version 1 (FaSSIF/FeSSIF/FaSSGF), FaSSIF-V2 and FeSSIF-V2 were purchased from Biorelevant.com Ltd. (London, United Kingdom). Dimethyl sulfoxide (DMSO, ≥ 99,9%) for drug stock solutions was acquired from Honeywell International Inc. (Charlotte, North Carolina, USA). Isopropanol (EMSURE® grade) for sample stabilization and reference solution preparation was obtained from Merck KGaA. Hydroxypropyl cellulose (HPC) 300-600 cps (Klucel™ EXF Pharm) was obtained from Ashland Specialty Ingredients (Hopewell, Virginia, USA). Eudragit® E PO (EPO) was provided by Evonik Industries AG (Darmstadt, Germany). Kolliphor® RH40 (RH40) was purchased from Merck KGaA. Sodium taurocholate hydrate (96%, Alfa Aesar) was obtained from ThermoFisher (Kandel) GmbH (Kandel, Germany). Acceptor sink buffer (ASB, P/N 110139) and GIT-0 lipid solution (P/N 110669) are proprietary products and were purchased directly from Pion Inc. Ltd. (Forest Row, United Kingdom). Deionized water was used from local supply, conductivity < 1.0 µS/cm and total organic carbon content < 1 parts per billion or alternatively from an in-house Millipore purification system from Merck KGaA. For NMR, deuterated water (D_2O, 99.9% D) was obtained from Deutero GmbH (Kastellaun, Germany), hexadeuteriodimethyl sulfoxide (DMSO-d6, 99.8% D) from Euriso-top (Saarbrücken, Germany) and deuterated water containing 0.05% (w/v) 3-(trimethylsilyl)propionic-2,2,3,3-d4 sodium salt (TSP-d4), 40% sodium deuteroxide in deuterated water (NaOD, 99% D) and 35% deuterium chloride in deuterated water (DCl, 99% D) were purchased from Sigma-Aldrich. Coaxial insert tubes and NMR tubes (5 mm, clear glass) were obtained from Norell (Landisville, Pennsylvania, USA). For mobile phase preparation, water (HPLC plus), isopropanol and formic acid were obtained from Merck KGaA and ammonium acetate was obtained from SERVA Electrophoresis GmbH (Heidelberg, Germany). All other standard chemicals and laboratory consumables, if not stated otherwise, were purchased from either VWR International GmbH (Ismaning, Germany) or Sigma-Aldrich.

4.2 Methods

4.2.1 Biorelevant media preparation

All biorelevant media were prepared with a common buffer baseline, which deviates from the manufacturers recommendation and general scientific community practice. Modified phosphate buffered saline (PBS) with a pH of 6.5, proposed for the preparation of FaSSIF-V1, was selected for all media due to the established two-step dissolution protocol from OrBiTo (119). The preparation was performed according to biorelevant.com (supplier). In brief, for 1 liter of PBS, dissolve 0.42 g sodium hydroxide pellets (NaOH), 3.954 g sodium dihydrogen phosphate monohydrate (NaH_2PO_4-H_2O) and 6.186 g sodium chloride (NaCl) in about 95% of final volume of deionized water, adjust pH to 6.5 using 1 M NaOH or 1 M HCl if necessary and fill up to 1 liter. As previously mentioned, only commercially available SIF powders were used plus additional pure sodium taurocholate (NaTC, bile salt) to complement the media landscape. The same level of bile salt was deployed as contained in the official media, with 3 mM NaTC corresponding to fasted- and 15 mM NaTC corresponding to the fed-state, respectively. The bile salt level of FeSSIF-V2$_{PBS}$ was increased by 50% to 15 mM NaTC in order to align with FeSSIF-V1$_{PBS}$, denoted as FeSSIF-V2*$_{PBS}$. All prepared media were equilibrated before use based on the recommendation of biorelevant.com. FaSSIF-V1$_{PBS}$ was equilibrated for 2 hours, FaSSIF-V2$_{PBS}$ was equillibrated for 1 hour and FeSSIF-V1$_{PBS}$ and FeSSIF-V2*$_{PBS}$ were considered ready-to-use without equilibration time. Generally, DLS was used on each prepared media to assess equillibration state and consistency in colloidal appearance (particle size distribution and intensity of light scattered). In line with a publication from 2019 (120), it was discovered that FaSSIF-V2$_{PBS}$ theoretically requires about 24 hours equilibration time based on DLS measurements (data not shown). Using only 1 hour equilibration time for FaSSIF-V2$_{PBS}$ may have caused some variability. All prepared media were used at 25°C within 48 hours (~ 48 hours for the drug partitioning analysis using ultracentrifugation).

The systematic design of the biorelevant media landscape was tailored to the rationale of this work, namely to identify relevant components and factors expected to impact oral absorption. The effect of pH was assessed separately by using FaSSGF with a pH of 1.6 (or alternatively 0.01 N HCl with pH about 2) and comparing it to PBS pH 6.5. The effect of media components was assessed primarly at pH 6.5 referencing to the buffer baseline. Comparing FaSSIF-V1$_{PBS}$ to FaSSIF-V2$_{PBS}$, the impact of 0.55 mM Lecithin can be evaluated. Comparing FaSSIF-V1$_{PBS}$ to FeSSIF-V1$_{PBS}$, the effect of a 5-fold increase in bile salts and lecithin can be assessed. Comparing FeSSIF-V1$_{PBS}$ to FeSSIF-V2*$_{PBS}$, the impact of digestive lipidic components (glycerol monooleate and sodium oleate) can be investigated. The 3 and 15 mM NaTC media were added to separate

effects of bile salts and lecithin by comparing to the commercial media compositions. An overview of the composition and nomenclature of the biorelevant media used within this work is given in **Table 1**.

Table 1: Overview of biorelevant media landscape including compositions and nomenclature.

Media name (abbreviation)	**FaSSIF-V1$_{PBS}$ (Fa-V1$_{PBS}$)**	**FaSSIF-V2$_{PBS}$ (Fa-V2$_{PBS}$)**	**FeSSIF-V1$_{PBS}$ (Fe-V1$_{PBS}$)**	**FeSSIF-V2*$_{PBS}$ (Fe-V2*$_{PBS}$)**	**3 & 15 mM TC$_{PBS}$**
Bile salt (NaTC)	3 mM	3 mM	15 mM	15 mM	3 / 15 mM
Lecithin (Phospholipids)	0.75 mM	0.2 mM	3.75 mM	3 mM	-
Digestive lipidic components	-	-	-	5.8 mM	-
Amount of SIF powder to PBS	2.24 mg/mL SIF-V1	1.79 mg/mL FaSSIF-V2	11.2 mg/mL SIF-V1	14.64 mg/mL FeSSIF-V2	-

In addition to the biorelevant media landscape in **Table 1**, FaSSGF and double-concentrated FaSSIF-V1$_{PBS}$ (2xFaSSIF-V1) were used to perform the two-step dissolution assay and the two-step flux assay. The preparation was performed according to the protocol established by OrBiTo (119). In brief, FaSSGF is an unbuffered solution with pH 1.6, where 1 liter contains 1.999 g of NaCl and 0.06 mg/mL SIF-V1 powder. 1 liter of 2xFaSSIF-V1 contains double-concentrated PBS and 4.48 mg/mL SIF-V1 powder with a pH of 7.5. The pH is adjusted with 1 N HCl and 1 N NaOH (exceptionally with 2 N HCl and 2 N NaOH). Both media were considered ready-to-use without equilibration time.

4.2.2 Chromatographic methods

Ultra performance liquid chromatography – photo diode array detector (UV/VIS) – single quadrupole mass spectrum detector (UPLC-PDA-SQD MS) was used for drug quantification. The main analytical equipment were Waters Classic Acquity LC systems (Waters Corporation, Milford, Massachusetts, USA) equipped with a sample manager with sample organizer, a column manager, a binary solvent manager (binary pump), a photo diode array detector (Waters) and an acquity QDa mass detector (Waters). The mobile phase A consisted of water (HPLC plus) with 4.76% (v/v) isopropanol, 0.05% (v/v) formic acid and with 3.75 mM ammonium acetate. Mobile phase B consisted of isopropanol with 0.05% (v/v) formic acid. A 2 minute method using a gradient from initial 1% mobile phase B to 50% B in 1.4 min, followed by 50% to 98% B in 0.3 min with a final hold on 98% B for 0.1 min with flow rate of 1.0 mL/min was used. The systems were equipped

with a CORTECS C18+, 2.1 x 50 mm Column, 2.7 µm (Waters). The injection volume was 2 or 5 µL, depending on the expected sample concentration. The injection mode was partial loop with needle overfill. In addition, mass spectra were acquired over a mass range from 100 m/z to 1200 m/z using electrospray ionization with positive/negative ion-switching and used to verify the presence/absence of the drug according to the monoisotopic mass in the peaks. Auto-integration was performed with MassLynx 4.2 - ApexTrack Peak Integration and automatic noise measurement. The model drug naporafenib was quantified at λ = 250 nm wavelength using logarithmic calibration curves to cover a wide range of concentrations (lowest was 0.1 µg/mL up to a maximum of 300-500 µg/mL), depending on the expected concentrations in the studied systems. Reference solutions were prepared in identical composition to the samples (including media components, excipients and organic solvent) and were injected multiple times (at least 4) throughout the same run. Concentration calculations were performed using a bracketing approach with the closest references UV areas (within 2-fold) and averaging if applicable. While the overall linearity of the regression was high ($R^2 > 0.99$), deviations from linearity were observed specifically for the lower concentrations, however, could be accounted for by the bracketing approach.

An alternative high performance liquid chromatography (HPLC) method for drug quantification was deployed for the phase separation limit assessments (**section 4.2.3.2**), intrinsic dissolution rate experiments (**section 4.2.4.1)** and dialysis flux studies (**section 4.2.5.1**) performed at the university of Würzburg by J. Schlauersbach. The analytical equipment was an Agilent 1260 infinity II HPLC (Agilent Technologies Inc., Waldbronn, Germany) equipped with a Syngergi™ 4 µm Hydro-RP18 80 Å 150 x 4.6 mm LC column (Phenomenex Ltd, Aschaffenburg, Germany), a variable wavelength detector (G7114A, Agilent), an automatic vial sampler (G7129C, Agilent), flexible pump (G7104C, Agilent) and multicolumn oven (G7116A, Agilent). Mobile phase A contained 0.1% (v/v) trifluoracetic acid (TFA) in purified water. Mobile Phase B consistent of acetonitrile with 0.1% (v/v) TFA. The flow was set to 1 mL/min, injection volume was 50 µL and detector wavelength was set to λ = 304 nm. The gradient started at 20% B, increased to 100% within 6 minutes, was held for 4 minutes and decreased back to 20% B within 1 minute with another hold for 4 minutes. Analysis were performed using calibration curves and Agilent OpenLAB CDS ChemStation Software (Agilent).

4.2.3 Solubility methods

Alongside drug quantification by chromatography, X-ray powder diffraction (XRPD) and selectively dynamic light scattering (DLS) measurements were performed which are briefly explained in **section 4.2.9** and **section 4.2.6**, respectively. Final media pH were also verified. Due to the kinetic nature of (some) samples, it was decided to perform all experiments at 25°C, to reduce the

likelihood of precipitation when samples cool down from e.g. 37°C towards 25°C while transferring samples to a next analysis equipment. Generally, all samples analyzed for drug concentration by chromatography were stabilized with organic solvent.

4.2.3.1 Drug equilibration monitored over time

Initially, drug equilibration in various media was performed at 5-10 mg/mL but based on first readouts, it was concluded that 1 mg/mL is sufficient to maintain excess drug conditions for further experiments. This appeared valid even for drug forms reaching higher apparent concentrations than the most stable crystalline (monohydrate) form. Generally, drug equilibration was performed in 20-22 mL volume scale at 1 mg/mL pure drug equivalent over a time frame of 24 hours. For the solution form, a 100 mg/mL DMSO stock solution was used resulting in a final amount of DMSO ≤ 1% (v/v). To maintain a stable temperature, experiments were performed on a heating/stirring device (RET basic, IKA®-Werke GmbH & Co. KG, Staufen, Germany) at 25°C using magnetic stirrers at 300 rpm. At predefined time points (e.g. after 5, 15, 30, 45, 60, 120, 180, 1440 min) 2 mL aliquots were withdrawn, entered into disposable syringe filters (Chromafil® Xtra PTFE-45/25, Macherey-Nagel, Germany) from the back, the first milliliter was discarded and the second mililiter was collected (regardless of likely insufficient filter saturation). From this filtrate, 100 µL was stabilized with 100 µL isopropanol in small glass vials and stored at ambient conditions for analysis. Experiments were performed in at least triplicates (n=3-4). After the experiment, pH was measured and compared to the media pH without drug, at least once for each system (media and drug forms). Remaining solids were collected by several methods, depending on the sedimentation behavior and visual appearance (crystalline or amorphous). Inserting glass microfiber (1.2 µm, Whatman®, England) filter material into the syringe for the filtration procedure of the last measurement point and subsequent XRPD analysis of the material did rarely provide sufficient signals. It was suspected that the low amounts of solids (max. 4 mg total in 4 mL suspension) adhered poorly to the support. Better results were obtained by sedimentation, removal of supernatant and transferring the concentrated suspension directly on XRPD holders. The goal was to measure the suspension in original wet state but some drying on the holder could not be excluded. In case there was little to no sedimentation (mostly in case of amorphous phase separation), short ultracentrifugation for 10-15 minutes at 10’000 g was used to obtain a concentrated pellet of the material which could then be resuspended with minimal volume and transferred on the XRPD holder.

4.2.3.2 Detection of phase separation limits

The phase separation limits, representing liquid-liquid or liquid-glass like phase separation (43) were determined by UV titration and recording at non-absorbing wavelength (121) using a Sirius T3 instrument (Pion Inc., Forest Row, United Kingdom) at the university of Würzburg by J. Schlauersbach. Media with or without excipients were shaken on an orbital shaker Reax 20 (Heidolph GmbH, Schwabach, Germany) for 2 hours at room temperature. 20 mL of media was filled into glass vessels. Suitable naporafenib stock solutions were generated in DMSO depending on the media used and were gradually added. Recording of light scattering at 401 nm was performed with a built-in UV-dip probe. Stirring speed was set to 4800 rpm and experiments were conducted at room temperature in triplicates. Every 20 seconds, a UV spectrum was recorded and additional 10 µL of stock solution was added. Each run consisted of 20 data points. The phase separation limit was determined by the tangent intersection point method using the respective intensity baseline at 401 nm.

4.2.3.3 Drug partitioning analysis using ultracentrifugation

Separation of biorelevant media colloids using ultracentrifugation was explored to separate solubilized drug from molecularly dissolved drug. Various conditions such as rotation speed (541'000 g and 1'019'000 g) and spin time (15, 30, 60, 180 min) were evaluated using several biorelevant media. In a first phase, dynamic light scattering (DLS) measurements were used to evaluate the absence of colloidal species after ultracentrifugation in selected media. In a second phase, drug concentrations were measured alongside DLS before and after ultracentrifugation to support the evaluation of separation efficiency. Relevant feasibility tests and selected DLS data are presented in the results section. The protocol which was developed and found suitable is described below.

Drug partitioning analysis was performed in FaSSIF-V1$_{PBS}$ and FaSSIF-V2$_{PBS}$ after addition of drug via DMSO stock solution. Stock solutions with varying concentrations were prepared in order to result in always 1% (v/v) of DMSO in the final system. The target concentrations were 20, 40, 80, 90, 100, 110, 130, 200, 500, and 1000 µg/mL for FaSSIF-V1$_{PBS}$ and 5, 10, 20, 30, 40, 50, 70, 90, 110, and 130 µg/mL for FaSSIF-V2$_{PBS}$, respectively. The target concentrations were based around the phase separation limit of drug in the respective media. The experiments were carried out in 15-20 mL scale on a heating/stirring device (RET basic) at 25°C using magnetic stirrers at 300 rpm. After addition of the drug and 15-30 minutes equilibration time, DLS samples were retrieved and subsequently a solid-liquid separation was performed through disposable syringe filters (Chromafil® Xtra PTFE-45/25, Macherey-Nagel, Germany). The first 3 mL were discarded and the next 3 mL were collected. From the filtrates, two times 100 µL were stabilized with 100 µL

isopropanol directly in glass vials and stored until analysis (averaged data of technical replicates is reported). Each of the filtrates from each target concentration was also used for ultracentrifugation analysis. The suspension vials were then further equilibrated for 36-48 hours to await amorphous to crystalline phase transition (incomplete crystallization was considered a worse bias than biorelevant media stability). The same procedure was applied for all concentration levels, yielding filtrates for direct quantification and ultracentrifugation analysis.

The analyses were performed using an Optima™ MAX-XP Ultracentrifuge (Beckman Coulter, Nyon, Switzerland). For each sample, 1 mL filtrate was transferred into 1.5 mL polystyrene vials (Beckman Coulter) and inserted into the MLA-130 rotor (S/N 19U1589) at opposite positions for balancing. The vacuum was then pulled for about 45-60 minutes to achieve an internal pressure below 10 micron (1.34 Pascal). The run would be automatically stopped in case of insufficient vacuum (above 31.5 micron for > 5 minutes). Ultracentrifugation was performed at 25°C for 1 hour at 1'019'000 g. Directly after finishing the run, vacuum was released and vials were carefully taken out from the rotor. Using pipette tips for 20-200 µL volume, 120 µL was withdrawn from the location furthest away from the pellet, considering the rotation angle and stored in a glass vial. This sample was denoted top fraction. Another 120 µL were withdrawn from directly under the liquid meniscus, denoted as sub fraction. From those samples, 50 µL was stabilized with 50 µL isopropanol in glass vials and stored for analysis. The other 70 µL were used for DLS analysis to evaluate the colloid separation efficiency. Due to time constraints and amount of samples, the top fraction had priority for DLS analysis and for each sample, at least the top fraction was analyzed on the same day. In case the top fraction did not show any colloids in DLS and the drug concentrations were similar between the two fractions, the data was averaged (technical replicates) and reported as mean, if not stated elsewise. Drug partitioning analysis in FaSSIF-V1$_{PBS}$ and FaSSIF-V2$_{PBS}$ was performed in triplicates for the amorphous (after 15-30 minutes) and crystalline (36-48 hours) system, for each target concentration. For other experiments such as the ultracentrifugation-flux combo assay, an n=2 could be derived from the n=4 flux due to the experimental setup and protocol (see **section 4.2.5.3.**) Individual measurements are presented in case less of less than three replicates.

4.2.4 Dissolution rate methods

4.2.4.1 Intrinsic dissolution rate

Experiments were executed by J. Schlauersbach at the university of Würzburg. Dissolution rates were measured with a Sirius T3 instrument (Pion Inc., Forest Row, United Kingdom) in 20 mL volume and subsequently normalized to a defined surface area of 0.07 cm^2 to obtain intrinsic dissolution rates (122). Tablet discs of naporafenib forms were generated by compression of 3-10 mg sample under a weight of 1.8 tons for 5 min with a manual hydraulic tablet press (Paul Weber,

Stuttgart, Germany). Using a stirring speed of 4800 rpm, the release rates (dissolution rates) were determined photometrically at room temperature following manufacturer's instructions. Dissolved amount of drug was derived using Lambert Beer's law with the spectroscopic data collected by a fiber optic dip probe connected to a diode array detector. The linear part of the relase profile was used to calculate the amount substance dissolved per time and surface area. Experiments were carried out in triplicates.

4.2.4.2 Single-step and two-step dissolution

Both, single-step and two-step dissolution assays were performed on conventional USP II setups at 75 rpm stirring speed (paddle) and 37°C. Biorelevant media were prepared according to the supplier instructions but instead of manual preparation, some commercially available pre-concentrates may have been used (e.g. FaSSGF for the two-step dissolution assay). Media were heated to 37°C before use. Generally, the protocol was adopted from OrBiTo (119) and the quantification method used was the Novartis internal method as developed by the analytical research and development team. The filter material used for both dissolution assays were Millipore Multigrade 0.45 µm PVDF (Merck KGaA).

The single-step dissolution of an amorphous solid dispersion (ASD) powder (milled hot-melt extrudate) in FaSSIF-V1$_{PBS}$ and the tosylate salt form in FaSSIF-V1$_{PBS}$ containing 0.1% (w/v) pre-dissolved HPC was executed up to 60-75 minutes in triplicates. The target concentration of drug was 0.5 mg/mL pure drug equivalent for both systems in 500 mL, correcting for the drug content in the ASD powder and salt factor for the tosylate form. At the selected time points of 5, 10, 15, 20, 30, 45, 60 min, and 75 min = "infinity" (150 rpm stirring speed between 60-75 min) 5 mL volume was withdrawn, filter saturation was performed with 4 mL (back into the vessel) and 1 mL of sample was collected for analysis. The filtrates were stabilized 1:1 (v/v) with isopropanol. The volumes withdrawn were not replaced in the dissolution vessels but were respected in the calculations.

The two-step dissolution assay was performed with a 30 minutes gastric phase at low pH (FaSSGF), followed by 90-105 minutes intestinal phase at neutral pH of 6.5 (FaSSIF-V1$_{PBS}$). The assay was performed targeting a pure drug concentration of 1 mg/mL in the gastric phase and 0.5 mg/mL in the intestinal phase (due to the dilution step). The volume of the assay needed to be adjusted for ASD film-coated tablets (FCT) of 300 mg strength to 300 mL FaSSGF, followed by 300 mL double-concentrated FaSSIF-V1$_{PBS}$. This was kept the same for the Microemulsion (ME) analysis, which was of the same composition as for the *in vivo* dog PK study. For the analysis of the tosylate salt form in absence and presence of 0.1% (w/v) pre-dissolved excipients as well as for the ASD powder (milled hot-melt extrudates), the volume was kept according to the OrBiTo

protocol (final volume of 500 mL). The ASD powder and tosylate form two-step dissolutions were performed in duplicates with sampling points at 5, 10, 20 and 30 min for the gastric phase and 35, 45, 60, 75, 90, 120 min, and 135 min = “infinity” (150 rpm stirring speed between 120-135 min) for the intestinal phase. The ASD FCT and ME assays were performed in triplicates with the same sampling points for the gastric phase but at 35, 40, 50, 60, 75, 90, 120 min, and 135 min = “infinity” (150 rpm stirring speed between 120-135 min) for the intestinal phase. The filtration procedure and sample stabilization was identical to the single-step dissolution assay. Volumes were also not replaced but respected in the calculations.

The single-step dissolution assay was performed by L. Toelle, the two-step dissolution assay was performed by N. Stehle for the ASD FCT, by P. Halbeisen for the ME and by S. Juanes for the tosylate salt +/- excipients and ASD HME. All are members of the analytical research and development team, Novartis Basel.

4.2.5 Flux methods

4.2.5.1 Dialysis flux

Drug mass transports (flux) through dialysis (size-exclusion) membranes were assessed with a side-by-side diffusion cell (PermeGear Inc., Hellertown, USA) setup as described earlier (123) and were performed by J. Schlauersbach at the university of Würzburg. In brief, donor and acceptor compartments contained 10 mL liquid volume and were separated by a regenerated cellulose membrane, PermeaPlain (innoME GmbH, Espelkamp, Germany). The membrane surface area was 1.77 cm^2. Media containing excipients were equilibrated for at least two hours on an orbital shaker at room temperature before use. The acceptor compartment was filled with $Buffer_{PBS}$ containing 2 mg/mL (0.2%) Vitamin E TPGS to establish sink conditions (drug apparent equillibrium solubility about 16 µg/mL). Temperature was kept at room temperature by a Haake Fisons C1 water circulator (Thermo Fisher Scientific Inc., Karlsruhe, Germany) with a DLK 1002 cooling unit (FRYKA GmbH, Esslingen, Germany). A stirring speed of 500 rpm was controlled by an H9-CB-02 stirring apparatus (SES GmbH, Bechenheim, Germany). Flux experiments were initiated by addition of respective amounts of naporafenib stock solutions in DMSO to target the nominal donor concentrations. The concentration of the stock solutions were adjusted to never exceed 1% DMSO (v/v). After predefined time points of 15, 30, 45, 60, 75 or 90, 120, 180, and 240 min, 100 µL aliquots were withdrawn from the acceptor and replaced with fresh media. In cases where the flux rapidly declined, a narrower sampling schedule (every 10 min) was deployed to provide at least four data points for linear regression of the flux. Samples were diluted with 25 µL acetonitrile containing 0.1% (v/v) trifluoracetic acid, subsequently vortexed for at least 30 seconds (VTX-3000L, LMSCO. Ltd., Tokyo, Japan) and centrifuged with a MiniSpin centrifuge

(Eppendorf AG, Hamburg, Germany). The supernatant was then used for drug quantification by HPLC-UV/VIS. Experiments were performed in triplicates. The flux was derived based on linear regression of the slope of cumulative acceptor concentrations using Origin Pro 2020 (OriginLab Corporation, Northhampton, Massachussets, USA) and subsequent normalization to the available surface area for permeation and accounting for liquid volumes to yield absolute mass transport per area per unit time.

4.2.5.2 Lipidic flux (or biomimetic flux)

Drug mass transport (flux) experiments through artificial biomimetic membranes (GIT-PAMPA) were carried out on a μFlux™ from Pion Inc. Ltd. (Forest Row, United Kingdom). Manual sampling with subsequent filtration and analysis of drug concentrations by UPLC-PDA-SQD-MS was performed. The acceptor compartment was filled with acceptor sink buffer, a proprietary product from Pion, with an apparent equilibrium solubility of naporafenib of about 400 μg/mL. Generally, supplier recommendations were followed with some slight exceptions, outlined below. Experiments were performed at 25°C and all chemicals used for the experiments were equilibrated to room temperature before use (acceptor sink buffer was stored in the fridge, GIT-0 lipid solution was stored in the freezer). Donor solutions/suspensions were prepared and equilibrated in separate containers before introducing into the donor compartment to reduce bias from the equilibration process. In brief, biorelevant media were prepared and equilibrated according to suppliers recommendation and excipients were pre-dissolved until clear solutions were obtained. The media for the donor compartments were prepared by adding drug via DMSO stock solution to the media or by adding media to pre-weighted powders to start the experiment, followed by 30 minutes equilibration at 25°C with stirring on a heating/stirring device (RET basic, IKA®-Werke GmbH & Co. KG, Staufen, Germany) using magnetic stirrers at 300 rpm. After 15 minutes equilibration, the setup of the μFlux™ was prepared. First, 50 μL of GIT-0 lipid solution was added to hydrophobic PVDF support membranes (provided by Pion). Special attention was paid that all of the membrane surface appeared transparent after lipid impregnation. Excess lipid solution was wiped off using tissues in order to avoid residual organic solvent (n-dodecane) or phospholipids in the donor or acceptor compartment. The membrane holder was assembled, pre-wetted and inserted between donor and acceptor glass vial. The effective membrane area for permeation is 1.54 cm^2 according to the manufacturer. After finishing the setup for two glass pairs, 22 mL (instead of the recommended 16-20 mL) of acceptor sink buffer was added to the acceptor sides (each) to minimize risk of drying of the membrane through one-sided wetting. The procedure was repeated for the other two pairs. Once all glass pairs were separated by a lipid-impregnated membrane and contained acceptor sink buffer in the receiver compartment, 22 mL of the donor

solutions/suspensions were added. Stirring at 100 rpm (exceptionally 400 rpm) was immediately initiated, denoting the start of the flux experiment (i.e. t=0). Stirring was controlled by the AuPro™ Software 5.1.7.0. (Pion Inc. Ltd.). No other functionality of the software was used. After time intervals of 15, 30, 45, 60, 90, 120, 180, 240, 300, 360, 1320, and 1440 min, 150 µL of each compartment was withdrawn. The acceptor samples were directly inserted into small glass vials and stabilized with 150 µL isopropanol. The donor samples were pipetted into 0.45 µm PVDF centrifugal filters (Ultrafree®-MC-HV, Durapore®, Merck Millipore Ltd., Irland) and spun at 13.4k rpm for 1 minute on a MiniSpin® tabletop centrifuge (Eppendorf AG, Hamburg, Germany). Spin time was extented to 2-4 minutes for samples containing excipients (e.g. Kolliphor RH40) where 1 minute was considered insufficient to obtain enough filtered supernatant. 100 µL of it were withdrawn and stabilized with 100 µL isopropanol into glass vials. The vials were stored at room temperature until analysis. The volume withdrawn from the donor and acceptor compartments was not replaced with fresh media, primarly due to the inability to reproduce the donor media at specific time points. The volume reduction was considered minor (< 10%) over the 24 hours time frame and the concentration-time profiles were not corrected for it. To minimize liquid evaporation, the vessels were sealed with foil (Parafilm® M, Heathrow Scientific®, Illinios, USA) between the 6 hour and 22 hour time point. A visual representation of the µFlux™ equipment is shown below in **Figure 11.**

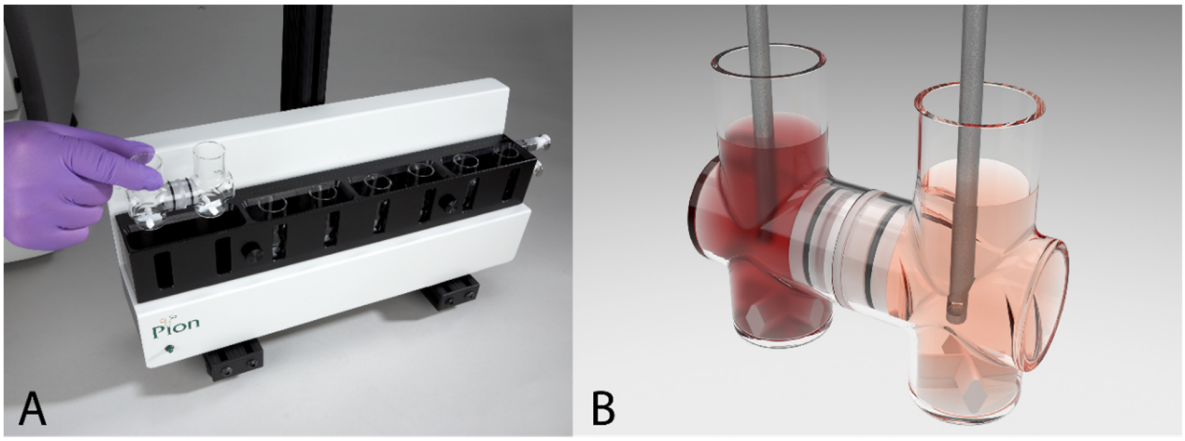

Figure 11: µFlux™ setup shown as A) heating/stirring apparatus and B) donor/acceptor compartments with a mounted artificial biomimetic membrane inbetween. UV fiber optic probes were not used. Images courtesy of Pion Inc. Ltd.

Experiments were performed in quadruplicates with typically an n=2 each on two separate days. Data is reported as mean +/- standard deviation as donor and acceptor concentration-time profiles. The time range for generating the concentration slope for flux was derived based on the donor profile instead of the best fit (R^2 value) from the acceptor profile. It was presumed that up until precipitation occurs in the donor, the driving force for flux remains roughly constant and

therefore the flux should be constant (linear concentration increase in acceptor). A reduction in the donor concentrations of 20% or more was attributed to drug precipitation (mainly relevant for experiments in absence of excess drug). Potential outliers were identified by skipping a data point to check whether the next data point was again within 20% of the previous donor concentration. The last time point in the donor before precipitation occured dictated up to which time point the cumulative acceptor concentrations were used for linearization. Each replicate was analyzed individually and may have used different amount of time points. The flux was derived using linear regression with GraphPad Prism Version 9.3.1 (GraphPad Software, Inc., San Diego, California, USA). Slopes were subsequently normalized to the available surface area for permeation and liquid volumes were accounted for to yield absolute mass transport per area per unit time.

4.2.5.3 Ultracentrifugation-flux combo assay

A novel assay type was developed by combining a membrane transport experiment with drug species characterization, using ultracentrifugation (UC) and dynamic light scattering (DLS). The flux assay was performed as described above plus some additional samples. Around t=0 and at t=1h, t=3h and t=24h, a filtration through disposable syringe filters (Chromafil® Xtra PTFE-45/25, Macherey-Nagel, Germany) was performed. For the t=0 sample, the donor solutions/suspensions were typically used for filtration before the donor compartments were loaded. Exceptionally, for system where filtration was considered tricky (e.g. Kolliphor RH40), filtration was performed between start of the stirring and the first sampling time point at 15 minutes. Filtration was executed by taking 10 mL volume, collecting the first 2.5 mL (unsaturated) directly in a glass vial, discarding the next ~4 mL and collecting the last 3 mL again (~ saturated). From both samples before and after filter saturation, 100 µL was taken and stabillized using 100 µL isopropanol in glass vials and stored until analysis. Those two samples allowed to estimate the impact of syringe filter saturation. In addition, 2.5 mL from the last 3 mL were re-filtered to calculate the unspecific binding loss to the 0.45 µm PTFE syringe filters. Only this binding loss is reported in this work. For the time points t=1h and t=3h, 2.5 mL were withdrawn from the donor compartment of a single replicate (e.g. at t=1h from donor 1 and t=3h from donor 2). It was not possible to take more volume from a single donor as the reduction in liquid volume would cause the membrane to be partially uncovered by fluid. Withdrawing 2.5 mL volume once was considered acceptable, being the reason for increasing the initial donor volume from default 20 mL to 22 mL. At t=24h (end point), the same filtration procedure was performed using more volume to saturate the filter (> 4 mL). From each of the filtrates, 100 µL were taken and stabilized with 100 µL isopropanol, mostly with 2 technical replicates (exception in case of filtration issues). The filtrates generated at the mentioned time points were used for the ultracentrifugation analysis as described in **section 4.2.3.3**.

To additionally account for the unspecific binding loss of drug to the centrifugal filters used for the donor samples, each filtrate generated using the syringe filters (at t=0, t=1h, t=3h and t=24h) was subjected to an identical filtration procedure, namely 150 µL of the filtrates were refiltrated with the centrifugal filters. Comparing the concentration before and after allows to estimate the unspecific binding loss. For each time point, two technical replicates were generated and reported as average. The investigation was required as the centrifugal filters could not be saturated with adequate volumes from the donor compartment of the flux setup. Furthermore, it was of great interest to understand unspecific binding loss to filter materials when supersaturated drug in biorelevant media were used.

4.2.6 Dynamic light scattering (DLS)

Dynamic light scattering is a non-invasive technique to derive a hydrodynamic diameter (nm) of diffusing objects within liquids. The fluctuating intensity of scattered light is measured over time and auto-correlated. The processed signals allow to determine a translational diffusion coefficient (D or D_T), which can be linked to the hydrodynamic radius (R or R_H) by the Stokes-Einstein equation (**Equation 8**). The smaller the particle and its hydrodynamic radius, the faster it will diffuse which results in a faster decay in the autocorrelation function. For more information, the reader is referred to the ISO 22412 (124).

Dynamic light scattering was measured on a Zetasizer Nano ZS (Malvern Panalytical, Malvern, United Kingdom). Measurements were performed at 25°C in triplicates using disposable polystyrene cuvettes with sample volumes about 1 mL (Sarstedt, Nümbrecht, Germany) or sample volumes as low as 70 µL (Brand GmbH & Co KG, Wertheim, Germany). Attenuation selection, run duration and number of subruns were determined automatically from the Zetasizer Software (Version 8.02). For some poorly scattering samples, the attenuator was fixed (fully opened) due to issues with automatic attenuation selection. Light scattering was measured in non-invasive backscatter (NIBS) mode at 173°. For exploratory purposes, forward scattering at 13° or dual mode with detection at 173° and 13° were used to increase sensitivity to detect larger particles. As standard practice, all samples were measured in the center of the cuvette to make the intensity of scattered light (derived count rate in kilo counts per second) comparable between samples. A potential bias from multiple scattering (in case of turbid samples) was appreciated. The measurements were performed with viscosity (0.8872 cP) and refractive index (1.330) for water. For analysis, primarly the raw correlation data were used, alongside the particle size distribution by intensity, the intensity of light scattered and the signal-to-noise ratio. The signal-to-noise ratio is a parameter reported in the DLS software reflecting the amount of correlatable signal. For example, a low ratio is indicative of low correlatable signal. The signal-to-noise ratio is calculated

as follows, as received through private communication from Malvern Panalytical (Grovewood road, Enigma Science Park, Malvern, Worcestershire WR14 1XZ, United Kingdom).

$$Signal\ to\ noise\ ratio = \frac{(Measured\ intercept + 1)}{(Measured\ size\ baseline + 1)} - 1 \qquad \text{(Equation 16)}$$

The measured intercept is determined by extrapolating the correlation coefficients contained in the correlation function to time zero. The measured size baseline is a time-independent constant proportional to the square of the time-averaged scattered intensity, see (125) for more information. Individual peak size of the derived hydrodynamic diameter were considered more meaningful than the Z-average (cumulative size over the whole particle size distribution), due to the colloidal complexity/multimodality observed in some samples/biorelevant media. Due to a lack of understanding of the precise composition, density and architecture of the colloidal objects (material properties), no transformation into number- or volume-based particle size distributions could be performed. Application of DLS to evaluate the absence of colloids after ultracentrifugation is reported in the results section.

Another useful application of DLS was to confirm presence of phase separated drug species, in case the filtration procedure did not yield a clear filtrate. This was quite commonly encountered (specifically in fed biorelevant media and/or when the tosylate salt or solution form was used). However, it was not possible to measure DLS for every filtrate due to the experimental sampling schedule and DLS measurement duration. In addition, some samples may have contained only minor amounts of phase separated drug, which was not easy to detect by eye. Generally, concentration data was reported as measured after sample stabilization with isopropanol as it was not possible to identify all potentially biased samples with DLS, nor was it possible to refilter all turbid filtrates due to volume constraints. Illustrative DLS results of clear samples compared to samples suspected to contain phase separated drug species or samples that have precipitated in the DLS cuvette can be seen in **Figure 12**. Noteworthy, this phenomena was observed for various experiments, not limited to apparent solubility studies. Wherever possible (sufficient volume), refiltration was performed.

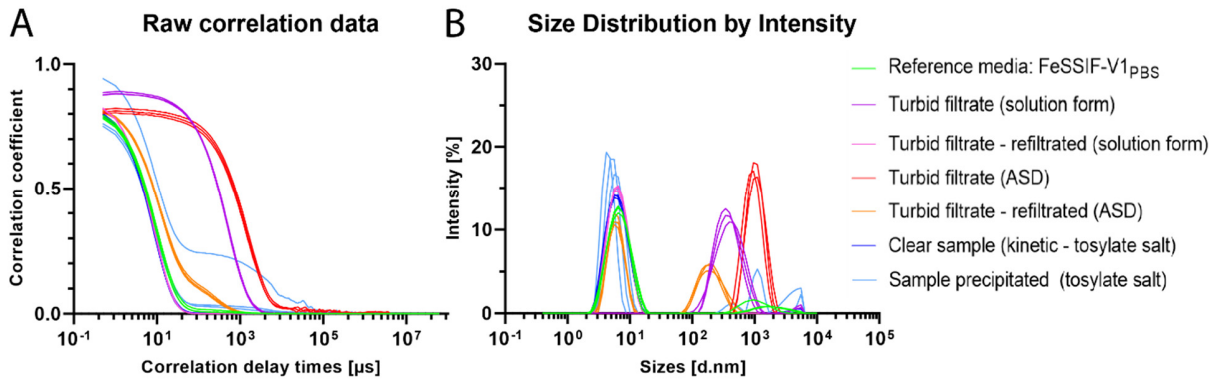

Figure 12: DLS results with A) raw correlation data and B) size distribution based on intensity of scattered light of selected samples (all based on FeSSIF-V1$_{PBS}$) to illustrate potential bias for drug quantification due to the presence of additional species, shown as individual replicates of triplicate measurements.

4.2.7 Nuclear magnetic resonance spectroscopy (^{1}H-NMR and ^{1}H-^{1}H-NOESY)

Nuclear magnetic resonance spectroscopy (NMR) experiments were executed by J. Schlauersbach at the university of Würzburg as described earlier (123). In brief, naporafenib was added to deuterated media with or without excipients via DMSO-d6 stock solution, never exceeding 1% DMSO (v/v). The mixtures were subsequently shaken for two hours at room temperature at 750 rpm on a Thermomixer F1.5 (Eppendorf AG, Hamburg, Germany). ^{1}H-NMR spectra were recorded on a Bruker Avance 400 MHz spectrometer (Bruker BioSpin GmbH, Karlsruhe, Germany) operating at 400.13 MHz and at room temperature (~ 27°C). Acquisition parameters were set as reported earlier (126). Chemical shifts were referenced to an external standard of 0.05% (w/v) 3-(trimethylsilyl) propionic-2,2,3,3-d4 sodium salt (TSP-d4) in D_2O filled in coaxial insert tubes. ^{1}H-^{1}H-NOESY data was recorded on a Bruker Avance III HD spectrometer (Bruker BioSpin) operating at 600.13 MHz. The temperature control unit was set to room temperature (~ 27°C). Before and after the NOESY experiment, ^{1}H-NMR spectra were recorded to verify sample integrity. Two dimensional ^{1}H-^{1}H-NOESY spectra were acquired and signal assignement was performed as described earlier (126, 127). All NMR data was processed using TopSpin 4.0.6 (Bruker BioSpin).

4.2.8 Electron microscopy (SEM, cryo-TEM, LC-TEM)

Scanning electron microscopy (SEM) was performed in collaboration with M. Dehlinger from the Analytical Material Sciences Team, Novartis, Basel. SEM was used to evaluate particle scale, morphology and surface characteristics of relevant drug forms. Samples for SEM analysis were mounted onto standard adhesive carbon-tappet aluminium stubs (13 mm diameter) and chemically modified by gold sputtering (~ 8 nm layer thickness) using a Sputter Coater Leica EM ACE600 (Leica Microsystems GmbH, Wien, Austria). SEM examination was performed using a

Zeiss Supra 40 microscope (Carl Zeiss GmbH, Oberkochen, Germany, distributed by Gloor Intruments AG, Kloten ZH, Switzerland). Beam current use took place between 3-5 keV depending on the magnification used to balance resolution and coverage (3 keV at higher magnification). A secondary electron detector with 31 µm standard aperture was used. Sample overview images were collected typically at 50x, 100x, 250x and 500x magnifications while surface and specific structure evaluations were performed at higher magnifications of 1000-2000x or higher, depending on the sample. A few selected and representative images were provided in this work.

Cryogenic transmissive electron microscopy (cryo-TEM) was performed in collaboration with C. Be from the Novartis Institute for BioMedical Research (NIBR), Basel. Cryo-TEM was used to study objects in frozen liquid environment. Samples were plunge-frozen on either untreated or plasma-cleaned 300 mesh copper Lacey carbon grids (Ted Pella 01895-F, Ted Pella Inc., California, USA). Plasma cleaning was performed for 30 seconds with a H_2O_2 combination using a Solarus Plasma Cleaner 950 (Gatan Inc., California, USA) right before grid preparation. From the sample of interest, 4 µL was applied to the grid for 10-30 seconds, blotted for 3-4 seconds and plunge-frozen into liquid ethane (cooled by liquid nitrogen) using a Vitrobot MarkIV (Thermo Fisher Scientific Inc., Texas, USA) set at ambient temperature and 50-90% humidity. Various conditions were explored (plasma-treatment and blotting parameters) and no conditions were found suitable for all samples. A key parameter identified was the blotting at room temperature which led to higher success rates with biorelevant media compared to blotting at 4°C. Prepared cryo-grids were stored in liquid nitrogen containers until analysis. Inspection of the samples was performed on a Tecnai Spirit microscope (Thermo Fisher Scientific Inc.) operated at 120 kV. Images were recorded using a Veleta CCD camera at nominal magnifications of typically x68'000 and x150'000. Defocus values were between -1.5 and -2.5 µm. The electron beam exposure was kept as low as possible, ideally below 1 electron/Å^2/second, as the samples appeared extremely beam sensitive. Optimal imaging parameters were specific to each sample and required to balance contrast, resolution and beam exposure for each case individually.

Liquid cell-transmissive electron microscopy (LC-TEM) was performed in collaboration with NanoMEGAS SPRL (Brussels, Belgium). Images were collected on either a Tecnai G20 TEM (Thermo Fisher Scientific Inc., NanoPort, Eindhoven, Netherlands) operated at 200 kV with a LaB6 source at NanoMEGAS Brussels laboratory or alternatively on a Talos TEM (Thermo Fisher Scientific Inc.) operated at 200 kV in Getafe, Madrid, Spain. Samples were prepared together with Dr. A. Gomez-Perez and J. González-Casablanca at the sample preparation labs according to preparation instructions by K-Kit manufacturers (Bio Materials Analysis Technology Inc., Hsinchu, Taiwan). For feasibility tests, samples were prepared at Novartis and shipped to the site of

investigation. Dr. S. Nicolopoulos, Dr. P. Pratim Das and Dr. A. Galanis additionally supported the work. Several liquid cells (LC) K-Kit microchips (Bio Materials Analysis Technology Inc.) were prepared with samples of interest according to patent US 9384942 B2 (specimen preparation for transmission electron microscopy, 2016) and pre-checked in vacuum chamber prior to insertion into the TEM for examination. The selection of LC K-Kit with specific spacers (i.e. distance between two electron transparent amorphous silicon nitride windows) of 2 µm or 200 nm allowed observation of objects in liquid. Generally, electron irradiation effects were kept to a minimum using a total cumulated electron beam dose in the range of (or below) 6 $e^-/Å^2$. The liquid (sample of interest) in the cells was visible through two identical superimposed membranes separated by a characteristic distance called gap. It is important to notice that the membranes have certain flexibility and due to the pressure of the liquid and the vacuum in the column of the microscope, they tend to expand (bending), allowing to observe objects of bigger size than the gap spacer. The volume the liquid occupies inside the chip is a cavity of about 25x300 µm with the third dimension being the spacer gap of 200 nm for example without taking into account bending effect of the membranes. For this particular reason, objects can disappear from the field of view during analysis. Images were processed using Digital Micrograph® (v 3.43.3213.0, Gatan Inc.) and Image-J (v.1.53e, National Institute of Health, USA). The use of LC-TEM for imaging biorelevant media systems is novel (exploratory) and has not been reported to date. The goal was to complement insights gained from cryo-TEM, to elucidate whether cryo-preparation alters sample appearance, and to complement dynamic light scattering with two orthogonal electron microscopy approaches. More information regarding the use and associated challenges with this technique is provided in (128, 129).

4.2.9 X-ray powder diffraction (XRPD)

X-ray powder diffraction was measured in transmission mode on Expert from Panalytical or Empyrean from Malvern Panalytical (Worcestershire, United Kingdom), respectively, fully automated multipurpose diffractometers. During the course of this work, the Expert machine was replaced with the newer generation Empyrean. The old detector was an X'Celerator and the new detector was a Pixcel 1D, which is slightly more sensitive, enabling shorter measurement durations. Both detectors are silicium-based. Data was analyzed using Panalytical data viewer software versions 1.5a (old device) and 1.9a (new device). The generator was set to 40 kV and 40 mA for the measurements. The scan axis was 2Theta-Omega with a range of 2.0010-40.0000° and step size of 0.0131° for the new machine and a range of 4.000-39.9961° with step size of 0.0084° with the old machine.

4.2.10 Pharmacokinetic study in dogs (study design)

A cross-over pharmacokinetic (PK) study in male beagle dogs was conducted by Covance and sponsored by Novartis AG. Five different formulations were tested at the same dose level, i.e. 30 mg/kg (referring to free base). Study arm I to III involved administration via oral gavage of crystalline tosylate salt suspensions with 1% (w/v) excipient in phosphate citrate buffer of pH 2.6. The excipients involved were Eudragit® E PO for arm I, Hydroxypropylcellulose for arm II and Kolliphor® RH40 for arm III, respectively. For each dog, the suspension formulation was prepared separately and administered within 15-30 minutes after preparation. Formulation administration was done to conscious dogs at 3 mL/kg, 10 mg/mL drug content, with a subsequent water flush at 2 mL/kg. Related total volume administered was 5 mL/kg and nominal dose was 30 mg/kg. Arm IV was an oral administration to conscious dogs of a 300 mg amorphous solid dispersion tablet, followed by 3 mL/kg of the pH 2.6 phosphate citrate buffer and 2 mL/kg water flush. Related total volume administered was 5 mL/kg and targeted nominal dose was 30 mg/kg (actual 32.4 +/- 6.4 mg/kg). Arm V was performed by oral gavage administration of 1 mL/kg microemulsion (ME) with 30 mg/mL drug concentration, followed by 3 mL/kg pH 2.6 buffer and 1 mL/kg water flush, 5 mL/kg total volume, 30 mg/kg nominal dose. The microemulsion was prepared by mixing 0.3 mL/kg of a microemulsion pre-concentrate (MEPC) at 100 mg/mL drug concentration with 0.7 mL/kg purified water and administered to conscious dogs within 15-30 minutes. The MEPC contained 10% Ethanol (v/v), 27% PEG400 (v/v), 18% Maisine CC (v/v) and 45% Kolliphor RH40 (v/v) (130). On treatment days, dogs were fasted overnight and offered food 4 hours post-dose. On the remaining days, dogs were fed following blood collection. Blood samples were collected at 0.25, 0.5, 1, 2, 4, 7, 24, 48, 72, and 96 hours and analyzed by LC-MS/MS with lower limit of quantification at 1.00 ng/mL. All materials and formulations were provided by Novartis AG. The plasma concentration-time profiles and PK parameters were provided and used without further modification (DMPK R2001111).

5. Results & Discussion

5.1 Drug form assessment in view of biopharmacy

The drug substance, also known as active pharmaceutical ingredient (API), is the key component of a drug product and responsible for its therapeutic effect. Its physical form selection is of fundamental importance for formulation development (2, 61) and was considered the starting point, once a drug candidate with poor aqueous solubility is selected for development (see **section 3.4, question 1**). Several aspects such as stability and processability need to be considered (131), but were out of scope for this work. Instead, drug substance forms were evaluated regarding bioperformance, meaning which form appears most suitable for drug delivery to achieve adequate exposures (bioavailability) *in vivo*. Naporafenib, a poorly water-soluble weak base with moderate-to-high permeability, was selected as model compound (132). Relevant physical forms could be identified through their single crystal structures and X-ray powder diffractograms. The forms were differentiated by apparent solubility in aqueous environments. Phase separation limits were assessed in various biorelevant media using a UV titration approach at a non-absorbing wavelength. Intrinsic dissolution rate (IDR) was evaluated for selected forms. Nuclear magnetic resonance (NMR) spectroscopy complemented the observations with insights into molecular interactions between the drug and biorelevant media components. The overall aim was to provide a rational decision basis for form selection to the formulation scientist. The major concern for *in vivo* drug delivery of this molecule at this stage was the low intrinsic aqueous solubility based on published data from its discovery, assigning it to the BCS class II of drugs (132).

5.1.1 Overview of relevant drug forms

The physical forms were identified by single crystal structures (only crystalline forms) and compared to each other regarding the micro/nanoscopic material apperance using scanning electron microscopy (**Figure 13** and **Figure 14**). Crystalline naporafenib anhydrate (modification A) contains two drug molecules in the asymmetric unit cell (ASU) of the crystal lattice while the ASU of crystalline naporafenib monohydrate is defined by only one drug molecule and a water molecule. Furthermore, the tosylate salt form of naporafenib includes one drug molecule and one tosylic acid in the ASU. The crystalline drug forms had different material appearances under the electron microscope. Anhydrate appeared as needles, hydrate as cubes, and the tosylate salt as aggregated tiles, respectively. X-ray powder diffractograms were used as reference to analyze residual solids and verify the form at the end of *in vitro* experiments (**Figure 15**). Crystallographic parameters are not provided here due to intellectual property constraints.

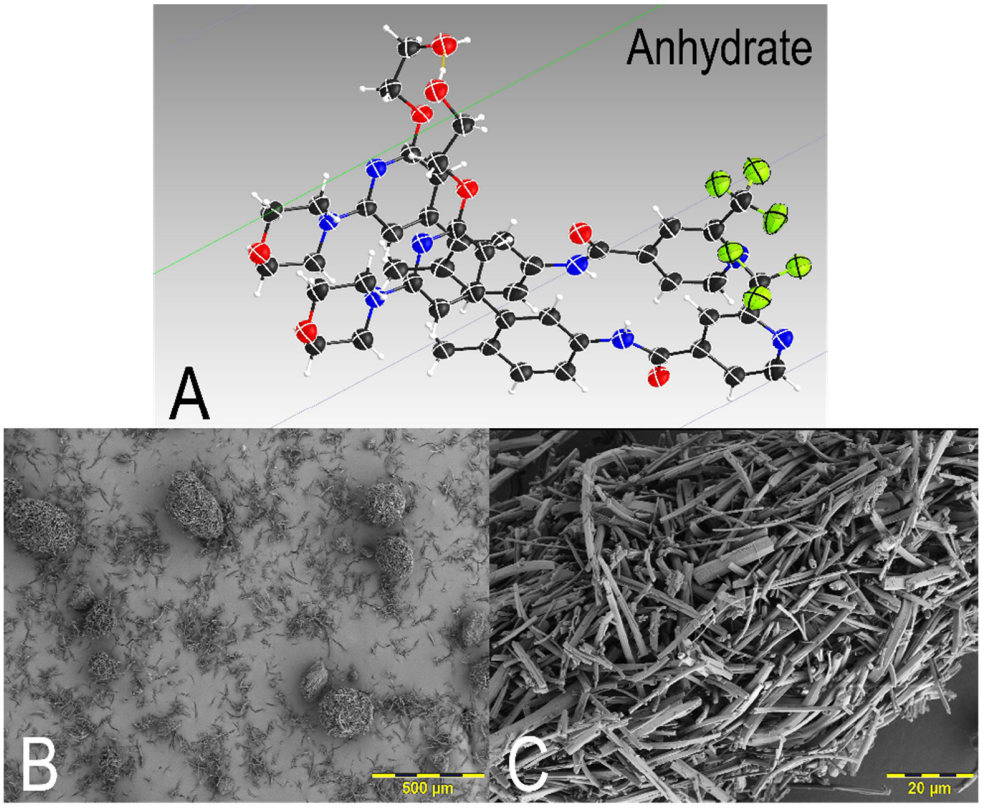
Anhydrate
A
B
500 µm
C
20 µm
Hydrate
D
E
500 µm
F
20 µm

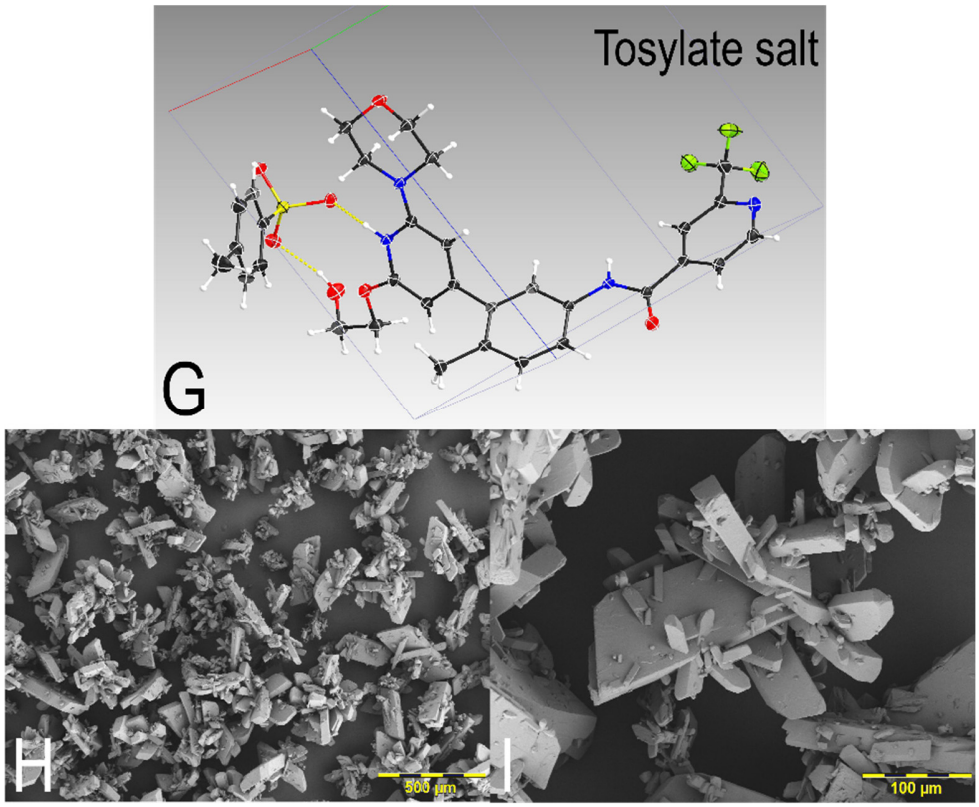

Figure 13: Overview of relevant crystalline forms of naporafenib using crystal structures for identification (A, D, G) and scanning electron microscopy for material appearance (B, C, E, F, H, I). The anhydrate form is shown in A-C, the monohydrate form in D-F and the tosylate salt form in G-I, respectively. Carbon atoms are shown in black, oxygen in red, nitrogen in blue, hydrogen in white, fluor in green and sulfur in yellow. The crystals were measured at the Synchrotron, Paul-Scherrer Institute, Villigen, Switzerland (anhydrate and tosylate salt form) or at Novartis, Basel, Switzerland (monohydrate form), refined/visualized using SHELX/ShelXle (133, 134) and analyzed using the XPREP program which is part of the Bruker APEX software package (135). Single crystal structure illustrations were provided by Dr. B. Dittrich. Scanning electron microscopy images were provided by M. Dehlinger.

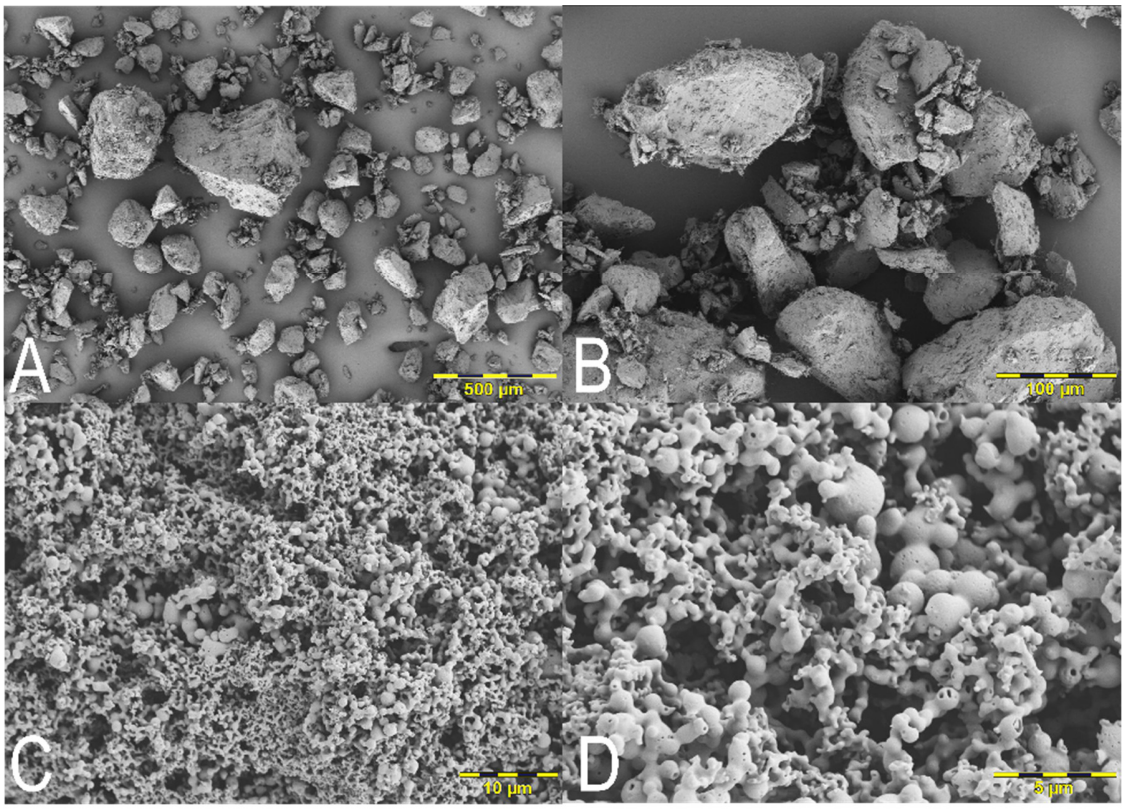

Figure 14: Overview of relevant amorphous forms of naporafenib using scanning electron microscopy, prepared by hot-melt extrusion (A, B) and recovered phase separated amorphous naporafenib generated via addition of the solution form (DMSO) to Buffer$_{PBS}$ (C, D). Obviously, no crystal structure can be provided for amorphous forms. Scanning electron microscopy images were provided by M. Dehlinger.

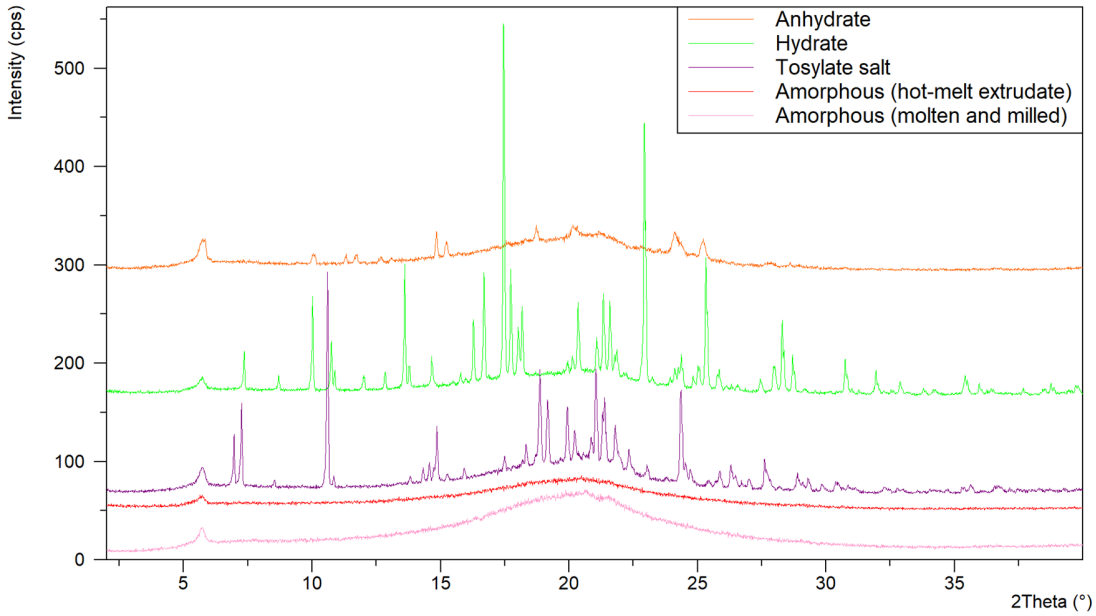

Figure 15: X-ray powder diffractograms of solid naporafenib forms as reference. An arbitrary Y-offset was selected to facilitate visual interpretation. Peak intensities may reflect varying amounts of drug on the sample holder alongside variations in crystallinity.

It is hardly possible to select suitable drug forms solely based on those provided solid-state insights. It would be desirable to link solid-state properties (e.g. crystal packing information) to solution behavior (e.g. dissolution or precipitation) to assist in drug form selection. Computational pharmaceutics, however, is considered to be in its early days and might not provide sufficient confidence without experimental confirmation (136). Furthermore, consideration of physicochemical parameters and application to the general solubility equation (see **section 2.3.1**) to estimate aqueous solubility of relevant naporafenib forms rapidly faced limitations (45, 46). The Log P (partitioning coefficient of drug molecules between an octanol and an aqueous phase) as molecular property should be assumed to be identical (solid form in dependent). In addition, the melting point may not be useful for salts due to potential form conversion and might not be accessible for all forms since for example dehydration of the hydrate form was observed before the melting event (data not shown). Further *In vitro* experiments are obviously required for drug substance form selection.

5.1.2 Form differentiation by apparent solubility

A biopharmaceutical form assessment was established by equilibrating relevant drug forms in selected media over 24 hours and accounting for possible form conversions, supported by XRPD measurements. Commonly encountered low intrinsic aqueous solubility is linked to poor confidence due to analytical quantification limitations and experimental variability. To improve form differentiation, biorelevant media containing bile salt and phospholipids were deployed, as increased apparent solubility facilitates quantification of drug in solution. **Figure 16** summarizes the concentration-time profiles obtained by monitoring drug form equilibration in FaSSIF-V1$_{PBS}$.

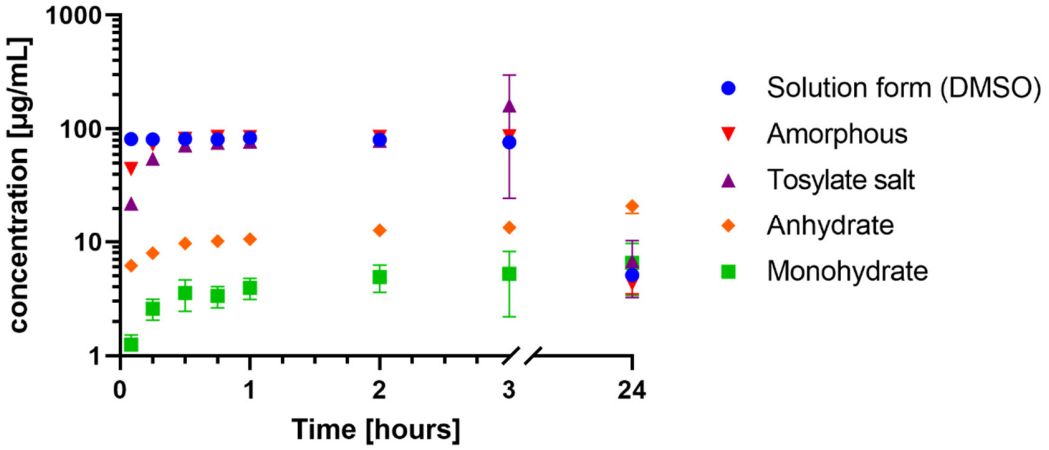

Figure 16: Equilibration monitored over time of relevant naporafenib forms in FaSSIF-V1$_{PBS}$. Concentration data referring to pure drug in solution are presented as mean of at least triplicates +/- standard deviation in semi-log plot. Error bars are in most cases smaller than symbols.

The data reveals overall concentration differences above one order of magnitude, justifying the visualization in logarithmic scale. Three forms, namely the solution form (DMSO), the tosylate salt form and the amorphous drug achieved the same kinetic concentration level. Interestingly, all those forms ended up on a similar level as the crystalline monohydrate after 24 hours. The only exception to this was the anhydrate form which remained anhydrate. It was confirmed by XRPD that all drug forms, except the anhydrate, converted into the monohydrate (see **Table 2**). Accordingly, similar apparent concentration levels after 24 hours can be expected for all, with exception of the anhydrate form (**Figure 16**). Noteworthy, the three hour data points showed the highest variability. It was suspected that phase separated drug species were pushed through the filter, as confirmed by DLS measurements for some samples (refer to **Figure 12**).

This data set served as decision basis to further evaluate the concentration-time profiles of the crystalline monohydrate as reference (suspected most stable form in aqueous environment) and of the amorphous and tosylate salt form as delivery candidates. In addition, the solution form (drug pre-dissolved in DMSO) was included for experimental purposes (upper limit case). The anhydrate form was excluded at this point as more favorable forms, reaching higher aqueous concentrations, were identified (see also **section 5.1.6**). The selected individual forms were subsequently equilibrated in a biorelevant media landscape including the pure phosphate buffer baseline, see **Figure 17**. The aim was to evaluate the universality of the kinetic concentration plateau achieved with high energy forms of the drug and the form conversion to the crystalline monohydrate. An additional purpose was to deconvolute the impact of selected biorelevant media components (e.g. digestive components contained in FeSSIF-V2*$_{PBS}$) on the height and duration of the kinetic concentration plateau.

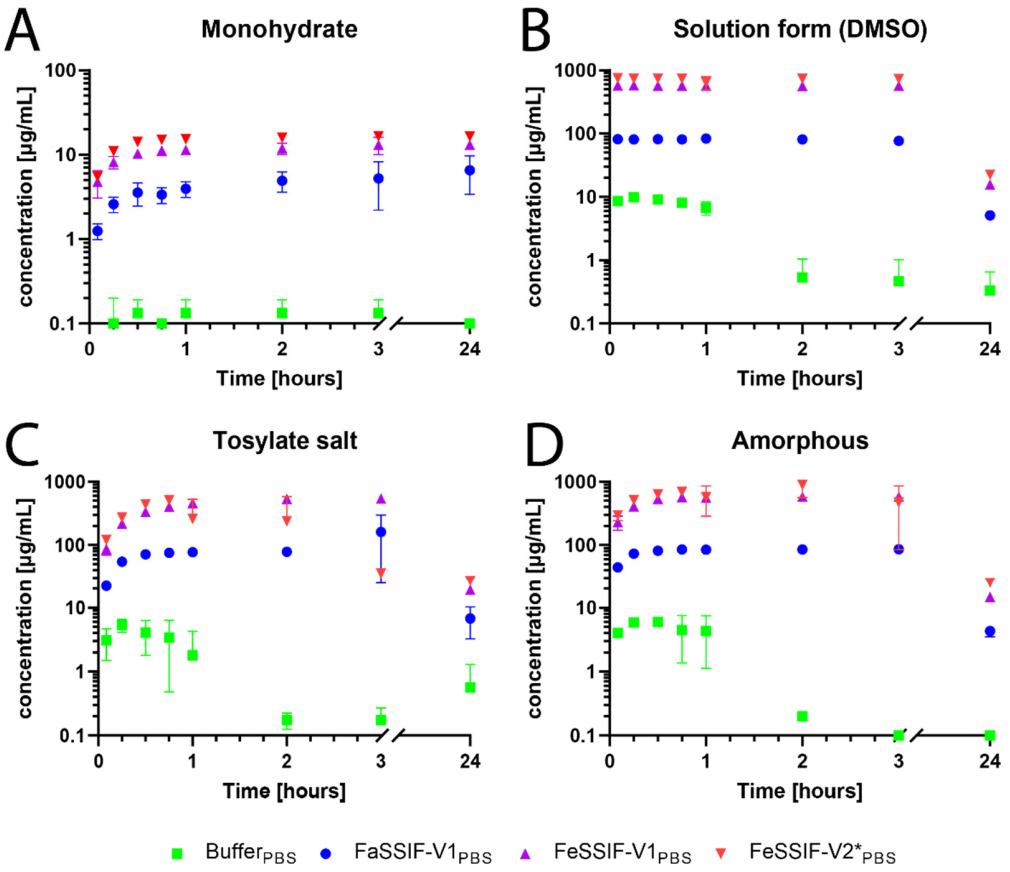

Figure 17: Equilibration monitored over time of selected naporafenib forms in phosphate buffer pH 6.5 (Buffer$_{PBS}$) and biorelevant media (FaSSIF-V1$_{PBS}$, FeSSIF-V1$_{PBS}$ and FeSSIF-V2$_{PBS}$). Concentration data referring to pure drug in solution are presented as mean of at least triplicates +/- standard deviation. All data are shown in semi-log scale. Error bars are in some cases smaller than symbols. Error bars reaching into negative cannot be depicted in log scale. Data in FaSSIF-V1$_{PBS}$ already presented in **Figure 16**.*

Consistent for all forms, including the hydrate form, an impact (orders of magnitude) from biorelevant media components on the concentration-time profiles was observed (profile height). Beyond this rather thermodynamic feature, also kinetic aspects were affected. This can be derived by comparing the hydrate profiles, which are relatively stable, to any other profile. All three other (higher energy) drug forms maintained a high kinetic concentration plateau only for a certain period before a decline in apparent concentrations was observed. As the kinetic concentration plateau was form (amorphous drug, tosylate salt, solution form) independent, universality can be assumed for the amorphous solubility limit of naporafenib, meaning that the same phase separation limit can be achieved from all those forms. **Table 2** summarizes kinetic concentration levels achieved after 30 minutes, approximated crystalline equilibrium levels measured after 24 hours and identified solid form at the end of the experiment by XRPD. Noteworthy, the XRPD read out is only qualitative and does not quantify relative amounts of amorphous and crystalline drug. In addition, due to the low residual amount of solids (estimated 4 mg) in those experiments, some XRPD

results showed primarly amorphous drug but aqueous concentration indicated the presence of crystalline monohydrate.

*Table 2: Overview of (pure) drug concentrations in solution at apparent amorphous solubility limit $C_{(0.5h)}$ [µg/mL], approaching apparent crystalline monohydrate equilibrium solubility $C_{(24h)}$ [µg/mL] and form identification after 24 hours by XRPD. Concentrations are derived from **Figure 17** (except anhydrate form) and are provided as mean of at least triplicates with standard deviation in brackets. Additionally, the anhydrate data in pure phosphate buffer were added while the fed state media equilibration was not performed. XRPD analysis based on references provided in **Figure 15.***

		Monohydrate	**Anhydrate**	**Tosylate salt**	**Amorphous**	**Solution form**
PBS pH 6.5	$C_{(0.5h)}$	0.1 (0.1)	0.6 (0.2)	4.1 (2.2)	6.0 (0.6)	9.1 (1.4)
	$C_{(24h)}$	0.1 (0.0)	1.1 (1.4)	0.6 (0.7)	0.1 (0.0)	0.3 (0.3)
	$Form_{(24h)}$	Monohydrate	Anhydrate	Amorphous/ Monohydrate	Amorphous/ monohydrate	Amorphous/ Monohydrate
Fa-V1 in PBS	$C_{(0.5h)}$	3.6 (1.1)	9.7 (0.5)	71.9 (0.6)	81.8 (6.9)	81.8 (3.9)
	$C_{(24h)}$	6.6 (3.2)	21.1 (2.9)	6.8 (3.5)	4.3 (0.8)	5.1 (0.3)
	$Form_{(24h)}$	Monohydrate	Anhydrate	Amorphous/ Monohydrate	Amorphous/ monohydrate	Amorphous/ monohydrate
Fe-V1 in PBS	$C_{(0.5h)}$	10.2 (1.0)		335.3 (5.0)	533.2 (24.8)	567.9 (48.2)
	$C_{(24h)}$	13.1 (0.3)		19.2 (2.8)	14.8 (0.5)	15.7 (1.5)
	$Form_{(24h)}$	Monohydrate		Amorphous/ Monohydrate	Amorphous/ monohydrate	Amorphous/ monohydrate
Fe-V2* in PBS	$C_{(0.5h)}$	14.2 (0.3)		442.7 (17.3)	635.1 (62.7)	738.7 (18.7)
	$C_{(24h)}$	16.5 (0.6)		26.8 (2.9)	25.0 (1.6)	22.5 (0.5)
	$Form_{(24h)}$	Monohydrate		Amorphous/ Monohydrate	Amorphous/ monohydrate	Amorphous/ monohydrate

5.1.3 Detection of phase separation limits

Media impact on temporary elevated drug concentrations in solution are of great interest for achieving adequate *in vivo* exposures of naporafenib due to a potential solubility-limited absorption. An orthogonal method to the drug form equilibration was used to expand the media landscape. Presuming that above the aqueous miscibility limit phase separation of amorphous drug occurs, amorphous solubility can be estimated through e.g. stepwise addition of drug from a DMSO stock solution and determination of phase separation onset by UV scattering at a non-absorbing wavelength (43, 121). This titration technique was considered a simple methodology to estimate the apparent amorphous solubility altered through SIF components, i.e. biorelevant media landscape and pH. The pH impact was captured by using a 0.01 M HCl solution (pH about 2) as surrogate for the gastric environment and as alternative to FaSSGF (pH about 1.6, containing minor amounts of bile salts and phospholipids).

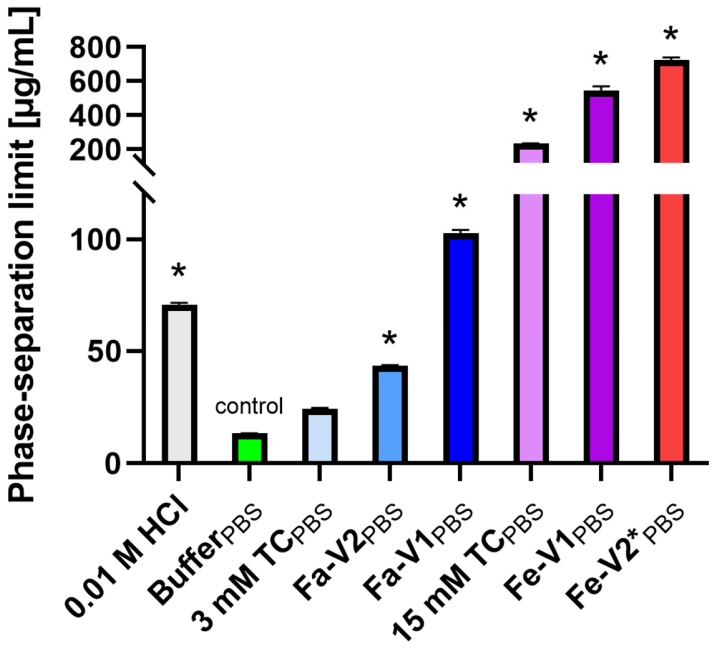

Figure 18: Detection of apparent phase separation limits of naporafenib solution form (DMSO) in a biorelevant media landscape. PBS stands for pH 6.5 phosphate buffered saline and served as baseline for all biorelevant media. TC stands for sodium taurocholate, the representative bile salt contained in all biorelevant media versions. Detailed composition can be found in the material & methods section. Data presented as mean +/- standard deviation of triplicates. Statistical significance (α = 0.05) compared to Buffer$_{PBS}$ as control is indicated by an asterisk (*) and was assessed using one-way ANOVA with post-hoc Dunnet's test for multiple comparison to the control. Analysis was performed with statistics tools in GraphPad Prism Version 9.3.1. Data was provided by J. Schlauersbach.

Figure 18 illustrates how various biorelevant media components and pH affect the maximum concentration of drug in solution that can be achieved before phase separation (formation of a new drug species) occurs. The lowest limit was observed in simple aqueous phosphate buffer at pH 6.5 (baseline). As expected for a poorly water-soluble weak base, this limit was increased by changing the pH to a lower value (representing gastric environment). All biorelevant media, except 3 mM sodium taurocholate, significantly elevated the maximum amount of drug in solution compared to the aqueous buffer baseline. The values (see also **Table 3**) are in reasonable agreement with **Figure 17** and **Table 2**. The impact of bile salt, lecithin (mixture of phospholipids) and lipidic digestive products (glycerol monooleate and sodium oleate) appears roughly additive. At 3 mM NaTC the increasing phase separation limit can be clearly attributed to increasing amounts of lecithin in FaSSIF-V2$_{PBS}$ and FaSSIF-V1$_{PBS}$. This is confirmed at 15 mM NaTC where lecithin in FeSSIF-V1$_{PBS}$ again increases the concentration limit and, furthermore, the addition of lipidic digestive products in FeSSIF-V2*$_{PBS}$ marks the top concentration of drug in solution. In this way also the sensitivity of a drug like naporafenib towards SIF components can be quantified in terms of their effects on apparent solubility.

*Table 3: Overview of orthogonal methods used to determine the phase separation limit (apparent amorphous solubility limit) of naporafenib in selected media: A) using the UV titration method (data from **Figure 18**), B) using a precipitation assay from a DMSO stock solution with subsequent filtration of phase separated species after 30 minutes (data from **Figure 17**/**Table 2**) and C) using dynamic light scattering. Values are provided as mean of at least triplicates with standard deviation in brackets (except for DLS where the highest concentration without observed phase separation is provided).*

Media	A: UV titration	B: Precipitation filtrate	C: Dynamic light scattering
Phosphate buffer pH 6.5	13.3 (0.1) µg/mL	9.1 (1.4) µg/mL	
FaSSIF-V1$_{PBS}$	102.8 (1.3) µg/mL	81.8 (3.9) µg/mL	> 90 µg/mL
FaSSIF-V2$_{PBS}$	43.3 (0.4) µg/mL		> 40 µg/mL
FeSSIF-V1$_{PBS}$	545.4 (24.4) µg/mL	567.9 (48.2) µg/mL	
FeSSIF-V2*$_{PBS}$	726.0 (12.9) µg/mL	738.7 (18.7) µg/mL	

Table 3 provides an overview of three orthogonal methods to measure phase separation limits, resulting in comparable values for the apparent solubility limit of amorphous naporafenib in selected media. The dynamic light scattering approach detects the formation of new colloidal drug species based on a sudden increase in light scattering intensity, similar to the UV titration approach. The onset determined by DLS is provided as the last concentration measured before phase separation occured, deviating from the linear increase in light scattering at lower (previous) concentrations. The precipitation assay on the other hand aims to remove all phase separated (solid-like) drug species by filtration, approaching the maximum amount of drug that can be dissolved under given conditions. It was discovered that all methods provided comparable data, supporting the universality of miscibility or phase separation limit and associated amorphous solubility (121).

5.1.4 Intrinsic dissolution rate

Dissolution rate investigations were performed because not only the maximum amount of drug in solution may matter but also how fast this concentration can be attained. Assuming undissolved drug solids at the site of absorption, the impact of media components at pH 6.5 on the dissolution rate of relevant forms was evaluated. Intrinsic dissolution rate (IDR) measurements on standard USP setups were not successful mainly due to the low aqueous solubility (< 0.2 mg/mL) and drug-surface-to-liquid-volume ratios (data not shown). The decision was taken to evaluate a different setup using smaller volumes and enhanced hydrodynamics. Additional use of biorelevant media instead of simple aqueous buffers elevated the apparent concentration levels to facilitate quantification and hence, form differentation. **Figure 19** compares the surface-normalized

dissolution rate of the tosylate salt with amorphous naporafenib, without drug content correction (salt factor 1.334). The crystalline monohydrate form was barely detectable in any media other than FeSSIF-V1$_{PBS}$ and was included for rather illustrative purposes, but not considered for statistical analysis. A general trend was observed of increasing intrinsic dissolution rate with increasing biorelevant media components, in line with **Figure 17** (form equilibration over time) and **Figure 18** (phase separation limits). One may suspect that the amorphous form dissolves slightly faster, however, if the available disc surface area for dissolution would be corrected for drug content, the IDR of the tosylate form may become indistinguishable from the amorphous form. From a theoretical perspective, this would be further supported by **Equation 9**, when assuming that the tosylate salt and amorphous drug form reach identical concentration levels, dictacted by the phase separation limit in a given media.

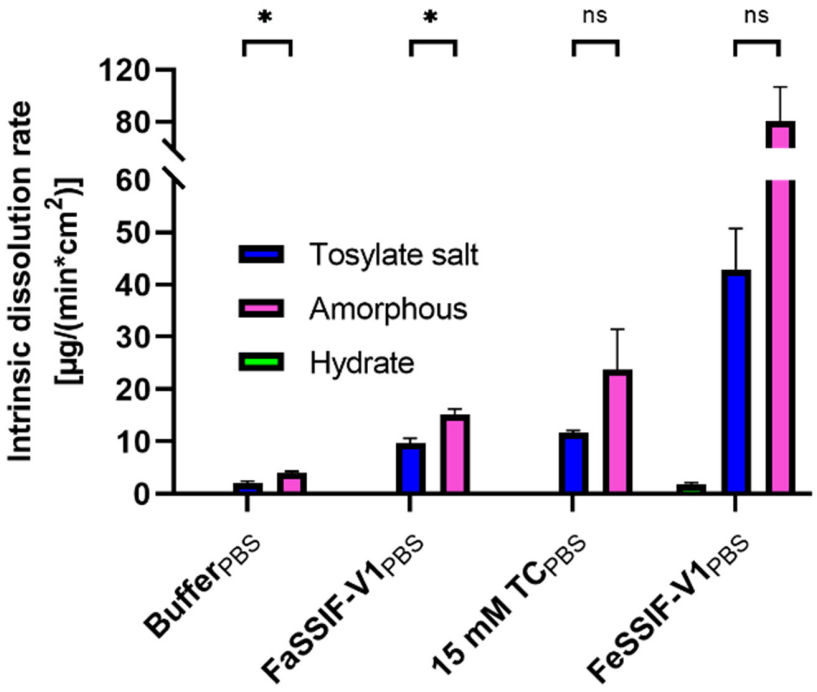

Figure 19: Surface-normalized intrinsic dissolution rates of the tosylate salt and amorphous naporafenib form in selected media. The monohydrate form in FeSSIF-V1$_{PBS}$ was included for illustration. Data is presented as mean of triplicates +/- standard deviation. Statistical significance (α = 0.05) comparing the tosylate salt to the amorphous form within the same media was assessed with multiple t tests and is indicated by an asterisk (*) or labelled as not significant (ns). Analysis was performed with statistics tools in GraphPad Prism Version 9.3.1. Data was provided by J. Schlauersbach.

The results (**Figure 17**, **Figure 18** and **Figure 19**) complement the evidence that biorelevant media components do affect the apparent solubility of the crystalline monohydrate of naporafenib, the maximum achievable concentration in solution (apparent amorphous solubility limit) and associated dissolution kinetics (and possibly also precipitation rate).

5.1.5 Nuclear magnetic resonance spectroscopy

Further insights were provided through proton nuclear magnetic resonance (^{1}H-NMR) spectroscopy with the attempt to detail the molecular interactions between the drug and biorelevant media components. **Figure 20** shows the aromatic drug proton signals in a selected media landscape. The signal intensities varied greatly among the media, especially between fasted and fed prandial state levels of bile components. The weak drug signals in phosphate buffer reflected the poor intrinsic aqueous solubility. The addition of 3 mM bile salt (TC) did not substantially change the signals obtained. Further addition of either 0.2 mM Lecithin (via FaSSIF-V2$_{PBS}$) or 0.75 mM Lecithin (via FaSSIF-V1$_{PBS}$) mainly broadened the signals observed but did barely modify the signal intensities. Relatively sharp signals were recorded at 15 mM bile salt +/- additives (15 mM TC$_{PBS}$, FeSSIF-V1$_{PBS}$, FeSSIF-V2*$_{PBS}$). Intensities in fed media increased with increasing lipidic components. Some aromatic drug proton signals were slightly shifted among the fed media but it was not possible to conclude on its root-cause and further relevance of those shifts. Primarly, the signal intensities correlated with the amount of apparently dissolved drug, based on **Figure 17** and **Figure 18**.

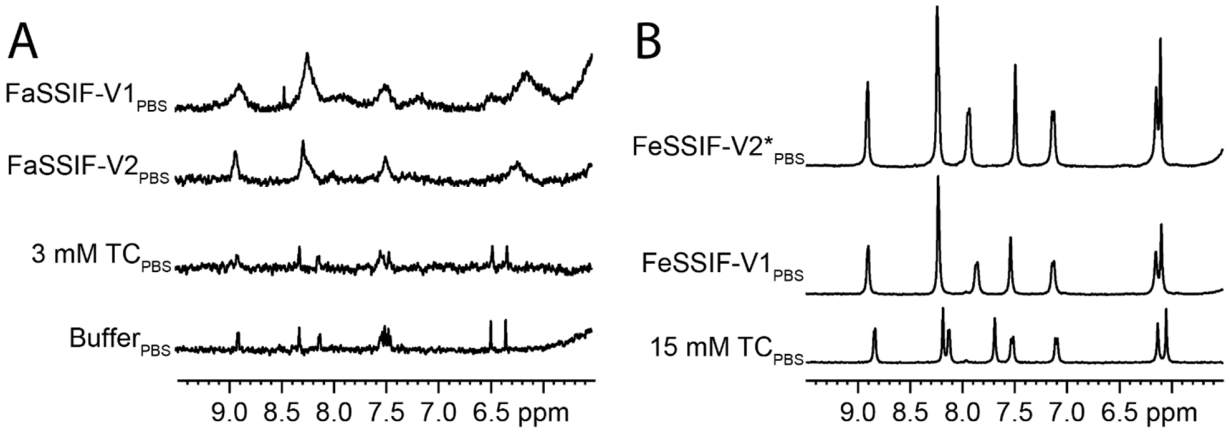

Figure 20: Aromatic proton region of the ^{1}H-NMR spectra of naporafenib in selected media under excess drug condition (above phase separation limit) added via DMSO stock solution: A) buffer baseline and fasted prandial state levels of bile salt and B) fed prandial state levels of bile salt. The scale was adjusted for A) for better visualization of drug signals. Figure was provided by J. Schlauersbach.

Biorelevant media and human intestinal fluids compromise various components and cannot be considered simple aqueous mixtures or ideal solutions. Some ingredients are capable of forming colloidal structures (supramolecular aggregates) with themselves but also other components (mixed colloidal aggregates) including drug molecules. Due to the poor signals observed in simple buffer or 3 mM bile salt media (3 mM TC$_{PBS}$, Fa-V1$_{PBS}$ and Fa-V2$_{PBS}$), further mechanistic investigations in those systems was impeded. More complex systems such as the fed state media

were required to obtain sufficient signals for more sophisticated analysis. To shine light on the molecular interactions governing the effects encountered, a two-dimensional NMR study in FeSSIF-V1$_{PBS}$ was executed. **Figure 21** presents a nuclear Overhauser effect spectroscopy (NOESY) plot of naporafenib. It was derived that naporafenib associated with the hydrophobic side of taurocholate and also the hydrophobic fatty acid residues of lecithin. No interaction with the hydrophilic side of lecithin was observed. Also, no interaction of the aromatic protons of naporafenib with the taurocholate side chains were detected. Hence both bile components were found to interact with the drug in solution. In addition, naporafenib was also interacting with itself or was in molecular proximity of itself. The key question now is how such molecular interactions and/or uptake into supramolecular aggregates may affect a drug's ability to permeate across a barrier and consequently the oral drug absorption process?

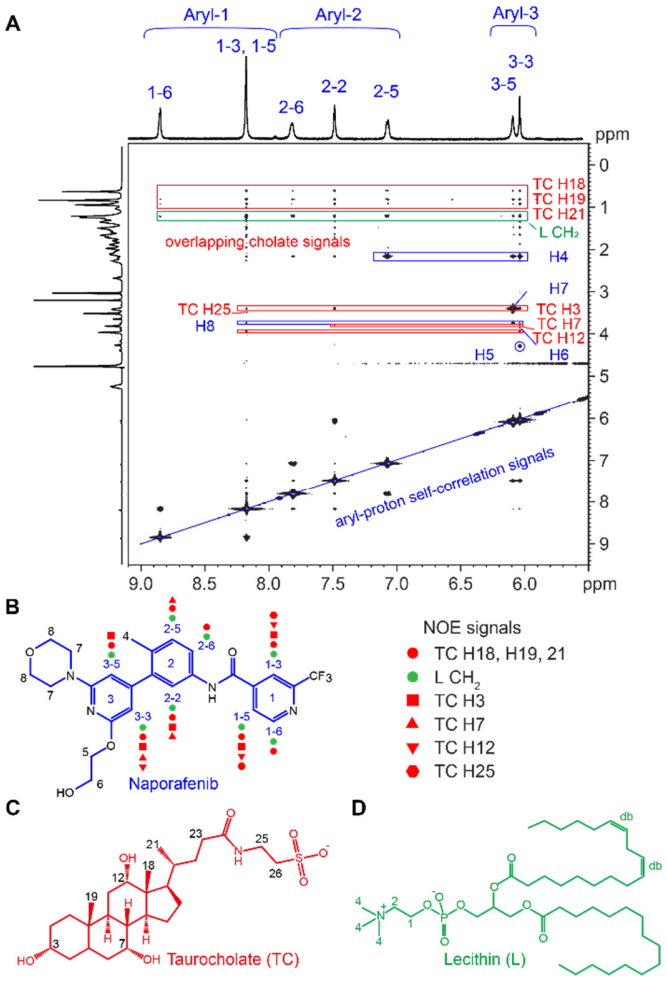

Figure 21: NMR spectroscopy: A) Two dimensional ^{1}H-^{1}H-NOESY plot of naporafenib at 90% of the phase separation limit in FeSSIF-V1$_{PBS}$ including signal assignments according to the molecular structures B) naporafenib, C) sodium taurocholate (bile salt) and D) lecithin (mixture of phospholipids) molecular structures. Proton groups showing an nuclear Overhauser effect are depicted with symbols in the respective colors on the molecular structure of naporafenib. Figure was provided by J. Schlauersbach.

5.1.6 Context to the bioaccessibility concept

Once a poorly water-soluble drug candidate was identified for development, drug substance form selection was the first important step (see **section 3.4**). Naporafenib drug forms were identified using single crystal structures (gold standard) and X-ray powder diffractograms. These forms were evaluated as suitable candidates for formulation development based on *in vitro* data such as apparent crystalline solubility, amorphous solubility and intrinsic dissolution rate. Relating to the bioaccessibility concept, the equilibrium between the solid reservoir and apparently dissolved drug, consisting of freely dissolved drug and a liquid reservoir, was investigated without further differentation of drug species. The liquid reservoir may primarly consist of colloidal structures formed by media components while phase separated drug species belong to the solid reservoir. The tosylate salt form, the amorphous form and the solution form (via DMSO) achieved temporarly higher dissolved drug concentrations compared to crystalline hydrate and anhydrate form. The hydrate was considered the most stable form in aqueous environment, based on observed form conversions. The relevant solid reservoir of naporafenib consists either of an amorphous phase, residual tosylate or crystalline monohydrate phases. The tosylate salt and the amorphous form are potential candidates for *in vivo* delivery based on the aqueous concentration levels achieved. The monohydrate form was considered the relevant reference and the solution form was found suitable for experimental purposes. The anhydrate form was not further considered as *in vivo* delivery candidate based on *in vitro* findings.

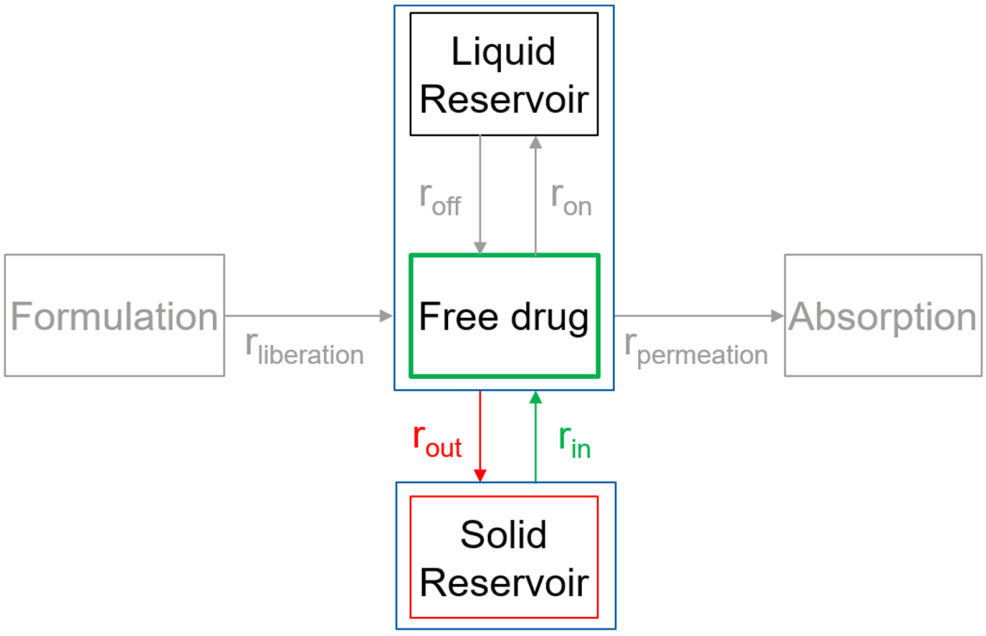

Figure 22: Illustration of the bioaccesibility concept in the context of classical drug form assessments in view of biopharmacy with the upper blue box representing apparently dissolved drug (containing freely dissolved and associated drug) and the lower blue box representing undissolved drug in either amorphous or crystalline form.

5.2 Methods and concepts to evaluate bioaccessibility

The drug form evaluation led to the important finding that biorelevant media components had pronounced effects on apparently dissolved drug concentrations. Assuming that those effects can be primarly attributed to the formation of colloidal species such as (mixed) micelles and vesicles, it was of great interest to identify how much drug is associated to such structures. The primary goal was to understand whether such molecular interactions/associations impact the drug's ability to permeate across a membrane, relating to bioaccessibility (see **section 3.4, question 2**)

Fundamental insights into biorelevant media colloids were gained through electron microscopy (EM) and dynamic light scattering (DLS). An exploratory method was developed to separate colloids from (some) biorelevant media through ultracentrifugation. DLS was used to evaluate the separation efficiency based on a signal-to-noise ratio rather than using derived count rates as measure for the intensity of light scattered, which was considered more biased through potential presence of dust particles for example. The signal-to-noise ratio is able to account for this, at least to some degree by differentiating signal from noise. At equal noise as the signal, the signal-to-noise ratio becomes zero (refer to **Equation 16**). Combining drug quantification with colloid separation allowed to differentiate drug species in solution, both in amorphous and crystalline (presence of monohydrate) systems. Dose-dependent formation of drug species was subsequently linked to flux, either through dialysis or biomimetic membranes. Mechanistic insights into driving and inhibiting factors for permeation were gained. Finally, limitations of *in vitro* drug mass transport were illustrated, e.g. based on the effect of stirring on the unstirrred water layer resistance using two selected biorelevant media with distinct colloidal species.

5.2.1 Feasibility tests to separate biorelevant media colloids

First, a basic understanding of the biorelevant media colloidal landscape was essential. Two selected relations between electron microscopy (cryogenic- and liquid cell-transmissive EM) and DLS obtained in this work are presented in **Figure 23** and **Figure 24**. DLS raw correlation data of FaSSIF-V1$_{PBS}$ decayed slower than for FeSSIF-V1$_{PBS}$, resulting in a larger derived hydrodynamic diameter of around 70-90 nm for FaSSIF-V1$_{PBS}$ compared to about 6 nm for FeSSIF-V1$_{PBS}$. Electron microscopy generally confirmed the size range derived from DLS but indicated potential multimodality in both cases. It was assumed that the larger FaSSIF-V1$_{PBS}$ colloids may have masked the light scattering of smaller species, e.g. elongated objects seen in EM. In contrast, the small species in FeSSIF-V1$_{PBS}$ scattered only little light while the presence of additional phases was indicated based on DLS, and further supported by EM images. This hypothesis was based on >25-fold higher amount of scattered light (derived count rates) observed in FaSSIF-V1$_{PBS}$ compared to FeSSIF-V1$_{PBS}$.

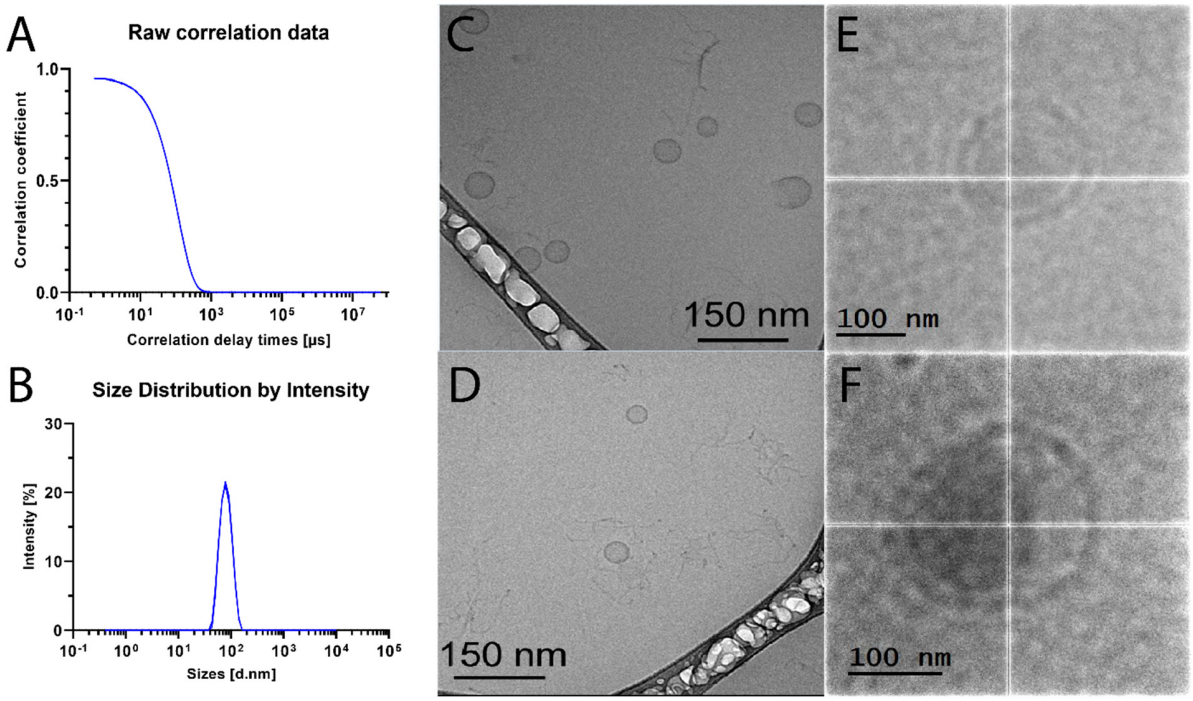

Figure 23: Relation between DLS (A, B), cryo-TEM (C, D) and LC-TEM (E, F) of FaSSIF-V1$_{PBS}$. DLS data provided as triplicates of A) raw correlation data and B) size distribution based on intensity (B). Cryo-TEM images were provided by C. Be. LC-TEM images were recorded on Tecnai G20 TEM, 200 kV and provided by Dr. A. Gomez-Perez.

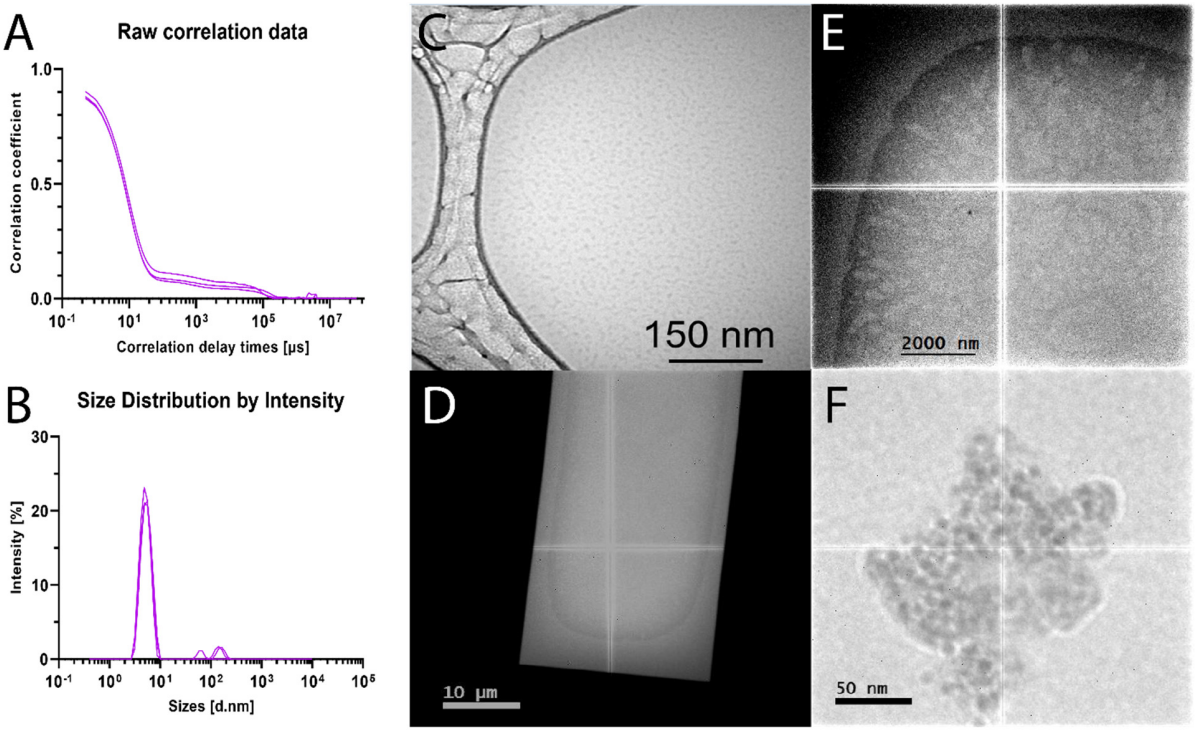

Figure 24: Relation between DLS (A, B), cryo-TEM (C) and LC-TEM (D, E, F) of FeSSIF-V1$_{PBS}$. DLS data provided as triplicates of A) raw correlation data and B) size distribution based on intensity. Cryo-TEM image was provided by C. Be. LC-TEM images were recorded on Tecnai G20 TEM, 200 kV and provided by Dr. A. Gomez-Perez.

Second, parameters for DLS evaluation needed to be established in order to judge the presence or absence of colloidal structures after ultracentrifugation. A dilution series of SIF-V1$_{PBS}$ was considered most suitable due to the reproducible colloidal appearance of this composition once equilibrated. The concentration range referring to bile salt concentration was covered from 0.1 µM to 3 mM sodium taurocholate using logarithmic steps (0.1, 0.3, 1, 3, 10, 30, 100, 300, 1000 and 3000 µM). From each dilution, DLS was measured in triplicates and the derived count rate (amount of light scattered), the signal-to-noise ratio and the mean peak size based on the particle size distribution by intensity (of light scattered) were analyzed.

Such dilution series were performed multiple times in the feasibility phase for various media, at least two times with FaSSIF-V1$_{PBS}$ without drug, once after equilibration with crystalline monohydrate (**Figure 25**) and once for FaSSIF-V2$_{PBS}$ and TC$_{PBS}$, each in absence and presence of crystalline drug (data not shown). The cut-off values for DLS parameters were derived from the most robust media investigation (SIF-V1$_{PBS}$) but were found suitable for other investigated media as well. The concentrations always refer to the bile salt concentration but other media components (such as lecithin/phospholipids) need to be considered as well.

A) The derived count rate is a measure of the amount of light scattered and was around 200-300 kilo counts per second (kcps) for 3 µM bile salt and below, which was comparable to unfiltered buffer systems. At 10 µM bile salt, over 500 kcps were observed and further increased with increasing concentration. It is important to note that some dust (e.g. in buffer, pipettes or cuvettes) may increase the count rate drastically (500-1000 kcps and above) and therefore the count rate was considered a weak indication/measure for the absence of colloids. As reference, FaSSIF-V1$_{PBS}$ typically yields above 40'000 kcps with about 70-90 nm objects and FeSSIF-V1$_{PBS}$ with roughly 6 nm objects only results in 1000-1500 kcps, despite 5-fold concentration of bile components.
B) The main peak size from the particle size distribution was found constant above 100 µM bile salt and reflected a hydrodynamic radius of FaSSIF-V1$_{PBS}$ objects between 70-90 nm. Due to the uncertainy of dilution-induced colloidal changes, the derived hydrodynamic diameter was found not suitable to judge the presence/absence of colloids.
C) The signal-to-noise ratio was provided by the DLS software automatically and reflects the amount of correlatable signal relative to the baseline noise (refer to **section 4.2.6**, **Equation 16**). At equal noise as the signal, the ratio becomes zero. For the SIF-V1$_{PBS}$ dilution series, the signal-to-noise ratio was already above 0.5 at 1 µM bile. At 10 µM bile salt, the ratio was above 0.9 and did not increase much further up to 3 mM.

D) The apparent solubility of crystalline monohydrate in the dilution series was determined as stated in the materials and methods section. Apparent solubility was found constant below 100 µM bile salt at about 0.2 µg/mL (n=1 for each bile salt concentration in each media, FaSSIF-V1$_{PBS}$, FaSSIF-V2$_{PBS}$ and TC$_{PBS}$ respectively). At and above 100 µM bile salt, the apparent solubility started to increase up to a value of about 3.5 µg/mL with 3 mM bile salt (= FaSSIF-V1$_{PBS}$). Noteworthy, excess solids used for drug equilibration may have reduced the effective bile salt concentration in solution due to surface adhesion.

The above discussed signal-to-noise ratio (C) and apparent solubility of crystalline monohydrate (D) was connected as shown in **Figure 25**. Due to reasons mentioned above, the derived count rate was considered not suitable. Interestingly, the increase in signal-to-noise ratio occured 1-2 log units earlier than the apparent solubility increase. This is in line with a publication about the critical micellar concentration (CMC) of sodium taurocholate (TC) based on fluorescence (137). It was claimed that aggregates may also form below the CMC but might not provide sufficient hydrophobic interior for the uptake of a fluorescent compound, which is considered comparable to the solubilization mechanism of poorly water-soluble drugs. Generally the CMC of TC is complex and is significantly affected by the presence of other components such as lecithin (138), therefore likely also poorly soluble drugs. An arbitrary cut-off for the signal-to-noise ratio was selected at 0.5, the estimated inflection point. Below that cut-off, it is claimed that no relevant biorelevant media colloidal species are present affecting aqueous concentrations of naporafenib.

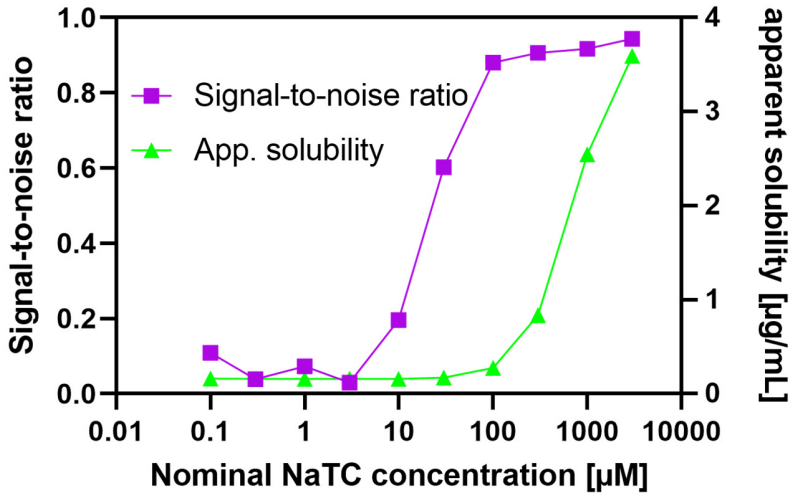

Figure 25: Simulated intestinal fluid version 1 (SIF-V1$_{PBS}$) dilution series after equilibration with crystalline monohydrate of naporafenib with measured signal-to-noise ratio based on DLS (left axis) and apparent solubility (right axis). Data presented as n=1 and no further replication was performed due to consistency with FaSSIF-V2$_{PBS}$ and TC$_{PBS}$ (data not shown). X-axis reflects nominal bile salt concentrations contained in the media.

Based on such baseline knowledge, a biorelevant media landscape was subjected to ultracentrifugation treatment to conclude on the feasibility to separate biorelevant media colloids and to derive an experimental protocol. The investigation was split into three phases. The first phase dealt with media only. The second phase involved equilibration of crystalline monohydrate in selected media. The third phase included dynamic assessment in amorphous systems after drug addition either via solution form (DMSO) or equilibration of an amorphous solid dispersion powder (containing a "parachute functionality" with HPMC). In case the kinetic system would be too instable (likelihood of precipitation due to supersaturation/form conversion), large deviations were expected between the addition via DMSO and addition as ASD powder. Using unfiltered suspension or filtrates appeared both feasible but the decision was made to always analyze filtrates going forward because they were considered more robust. The ultracentrifugation parameters optimized within those three phases included spin time and rotation speed. Having started with 15 minutes and 3 hour spin time as extreme conditions, 1 hour was found suitable in the end considering the risk of precipitation from such instable (supersaturated) systems. The rotation speed was dependent on the rotor, and hence also related to sample volumes. For volumes up to 2-3 mL, a maximum acceleration of 541'000 g was possible. For up to 1 mL, an impressive acceleration of 1'019'000 g was achieved. Referencing to the inspiring work from Vertzoni et al. 2012 (118), an ultracentrifugation acceleration of 410'174 g was used to split aspirated human intestinal fluids into several phases such as a coarse lipid phase, an interphace, a primarly micellar phase and a pellet. In contrast, the complete separation of micelles/vesicles from an aqueous system was targeted within this work.

For testing purposes, three fractions were analyzed after the ultracentrifugation while for the actual experiments, only two fractions were used (see **section 4.2.3.3**). The top fraction was sampled from the point furthest away from the pellet, considering the geometry of the rotor. The sub fraction was retrieved directly below the liquid meniscus. The middle fraction (only used for testing) was taken from the middle of the vial. In case of insufficient separation, a gradient was observed with the top fraction containing the least amount of objects and the middle fraction more or less resembling the untreated media based on DLS.

Selected DLS results from such feasibility investigation involving drug addition via DMSO and subsequent solid-liquid separations are shown for FaSSIF-V1$_{PBS}$ (**Figure 26**) and FeSSIF-V1$_{PBS}$ (**Figure 27**), referencing to the colloidal appearance seen in **Figure 23** and **Figure 24.** The 0.02 µm pore size filters (Anotop®, Whatman®, Sigma-Aldrich) were used for exploratory purpose as reference.

FaSSIF-V1$_{PBS}$ reference media showed a count rate about 40’000 kcps before drug addition. After drug was added via DMSO stock solution, followed by filtration through 0.45 µm pore size, the counts were slightly increased to about 52’000 kcps. The 0.02 µm pore size filtration reduced the counts to about 47’500 kcps. The signal-to-noise ratio was above 0.95 for those 3 systems. The top fraction (shown in **Figure 26**) after ultracentrifugation showed a count rate of 101 kcps and a signal-to-noise ratio of 0.11. The drug concentrations (n=1) were according to expectations based on DLS with 89 µg/mL (0.45 µm filtration), 82 µg/mL (0.02 µm filtration) and 14 µg/mL (top fraction after ultracentrifugation), respectively. The sub fraction provided similar concentration, derived count rate and signal-to-noise ratio (15 µg/mL, 98 kcps and 0.12, respectively), indicating successful separation. The mid fraction contained only slightly more counts (163 kcps), with a slightly larger signal to noise ratio (0.28) and drug concentration (17 µg/mL). Consistent data was obtained using the ASD powder as with the solution form. It was concluded that the ultracentrifugation treatment (top and sub sampling) is feasible with FaSSIF-V1$_{PBS}$. The same conclusions were reached for FaSSIF-V2$_{PBS}$ (feasibility data not presented).

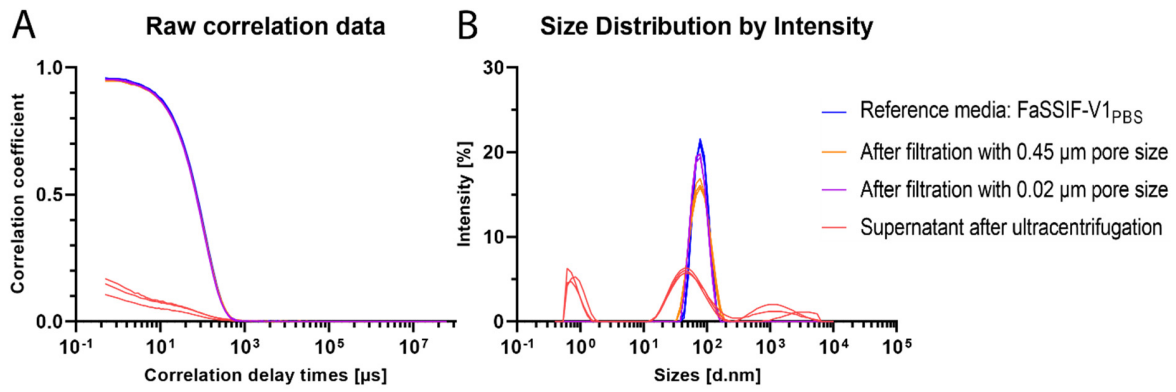

*Figure 26: DLS results from the feasibility investigation for the reference media FaSSIF-V1$_{PBS}$ and media after excess naporafenib addition (solution form) and subsequent analysis by filtration through 0.45 µm, filtration through 0.02 µm and ultracentrifugation treatment. Data provided as individual replicates of A) raw correlation data and B) size distribution by intensity, measured in triplicates. The DLS data for the reference media is identical to **Figure 23**.*

FeSSIF-V1$_{PBS}$ reference media showed a count rate of about 1’200 kcps before drug addition. After drug addition via DMSO stock solution and subsequent filtration through 0.45 µm pore size, a surprising 10’000 kcps were observed, likely associated with the additional peak seen in DLS in **Figure 27** (suspected to be either a phase separated drug species or an emulsion-like phase that formed in presence of biorelevant components and was pushed through the filter, **Figure 28**). The 0.02 µm pore size filtration resulted in 1400 kcps. The signal-to-noise ratio was above 0.8 for those 3 systems. The DLS results appeared more complex compared to the FaSSIF-V1$_{PBS}$ system especially in terms of multimodality. The top fraction after ultracentrifugation showed a count rate

of 293 kcps and a signal-to-noise ratio of 0.16. The drug concentrations (n=1) were 598 µg/mL (0.45 µm filtration), 587 µg/mL (0.02 µm filtration) and 53 µg/mL (top fraction after ultracentrifugation), respectively. The sub fraction showed 78 µg/mL with a signal-to-noise ratio of 0.38 and the middle fraction 348 µg/mL of dissolved drug with a signal-to-noise ratio of 0.74. This manifests rather a gradient instead of complete separation by ultracentrifugation both for the drug concentrations measured as well as the signal-to-noise ratios obtained. The ASD powder approach resulted in the same findings. Consequently, FeSSIF-V1$_{PBS}$ was not considered feasible for ultracentrifugation separation based on the observed gradients. Nonetheless, the final ultracentrifugation protocol was applied to FeSSIF-V1$_{PBS}$ to confirm this, see **section 5.2.5**

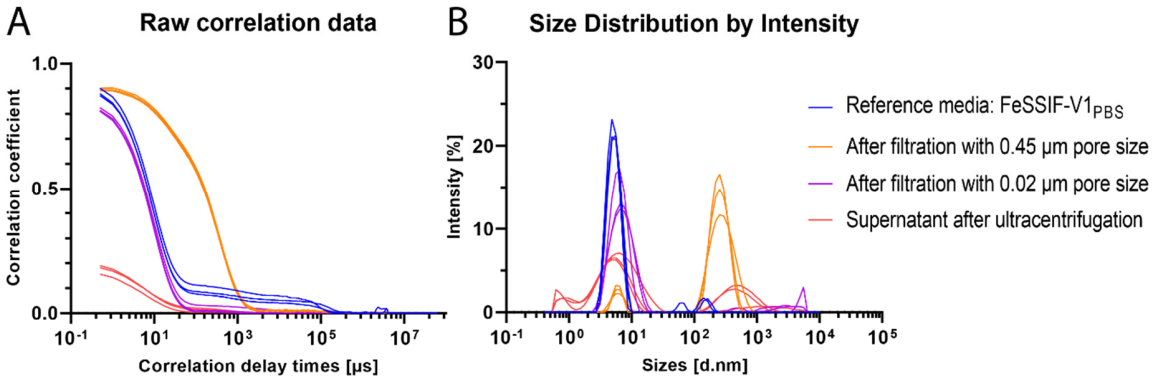

*Figure 27: DLS results from the feasibility investigation for the reference media FeSSIF-V1$_{PBS}$ and media after excess naporafenib addition (solution form) and subsequent analysis by filtration through 0.45 µm, filtration through 0.02 µm and ultracentrifugation treatment. Data provided as individual replicates of A) raw correlation data and B) size distribution by intensity, measured in triplicates. The DLS data for the reference media is identical to **Figure 24**.*

DLS and EM images of pure FeSSIF-V1$_{PBS}$ (**Figure 24**) show that multiple species may be present in that media, which was also observed after drug addition (via DMSO stock solution) and subsequent filtration step (**Figure 27**). It was not possible to conclude on what those species represent but some impressions were gained through Cryo-TEM images, see **Figure 28**. One may speculate about the dynamics of those objects based on material appearance in the sequential images and this supports the hypothesis that such phases might be pushed through a filter. No differentiation between pure phase separated drug (e.g. amorphous nanodroplets) and drug solubilized/emulsified by bile components was possible. In addition, the images illustrate how electron beam sensitive such phases are as they were extensively modified during image acquisition. Some further impressions from LC-TEM are provided in **Figure 29** and **Figure 30** to illustrate the complex solution behavior of naporafenib in presence of biorelevant media. It was attempted to image metastable drug-biorelevant media systems starting from the solution form, followed by equilibration for almost 2 days and compare the appearance to the system where the most stable form (crystalline monohydrate) was equilibrated in the same biorelevant media.

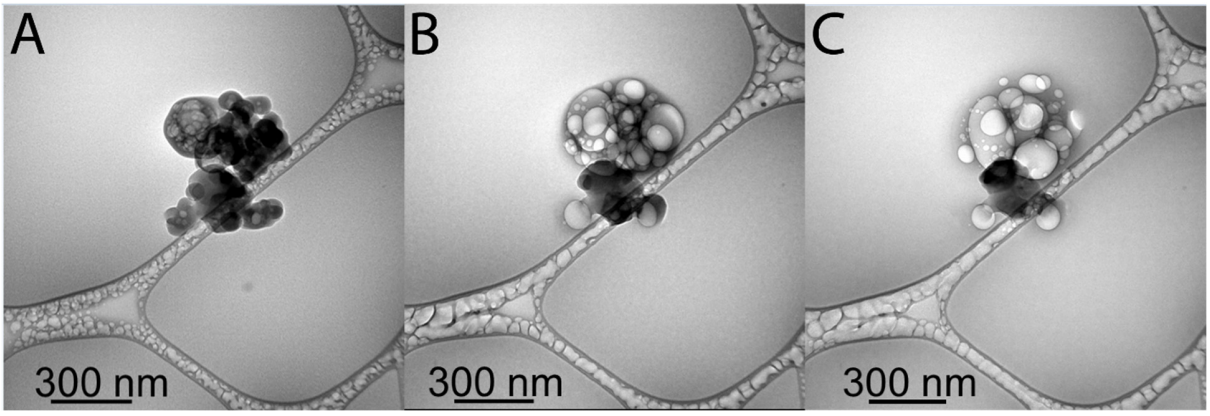

Figure 28: Cryo-TEM images of FeSSIF-V1$_{PBS}$ equilibrated with excess crystalline naporafenib monohydrate for 24 hours with subsequent filtration through 0.45 µm pore size. A) to C) represent sequential images taken a few seconds apart under low dose conditions. Cryo-TEM images were provided by C. Be.

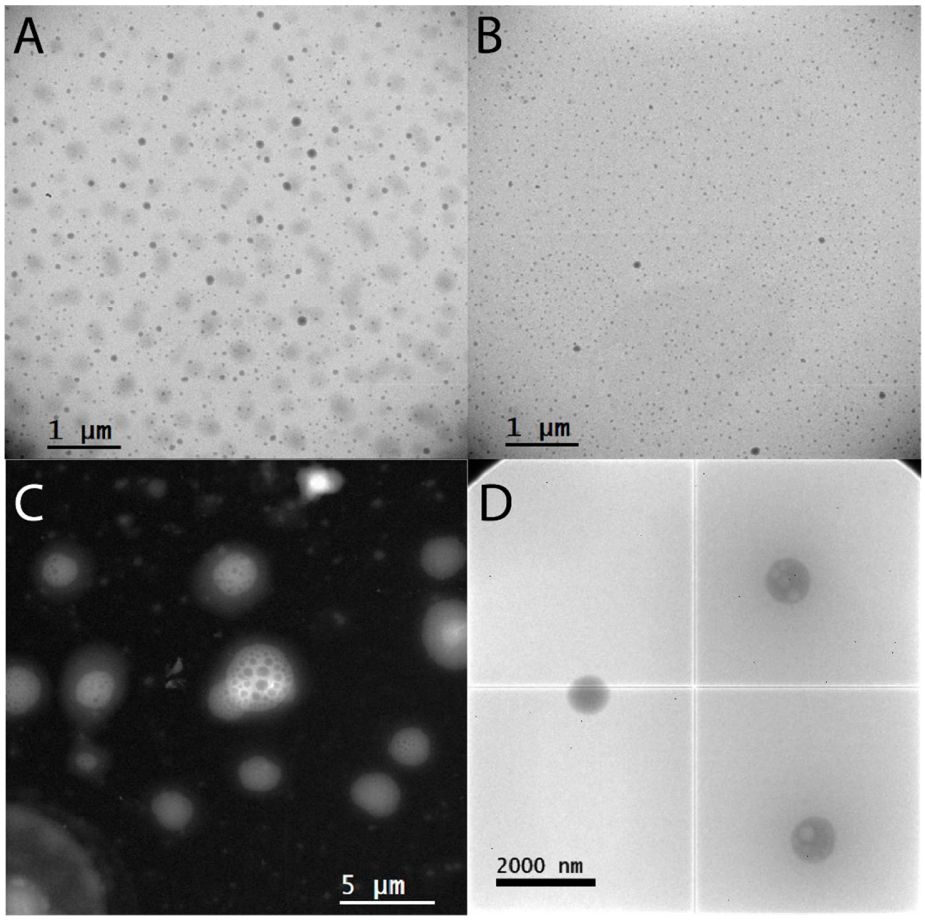

Figure 29: LC-TEM images of a filtrate from crystalline naporafenib monohydrate equilibrated in FaSSIF-V1$_{PBS}$, acquired using a 2 µm spacer liquid-cell. The sample was shipped to the site of investigation (A-C, Talos TEM, 200 kV) and compared to a fresh preparation on site (D, Tecnai G20 TEM, 200 kV) due to uncertainty regarding stability (storage condition and time). C) is reported in high-angle annular dark-field mode for improved contrast. LC-TEM images were provided by Dr. A. Gomez-Perez.

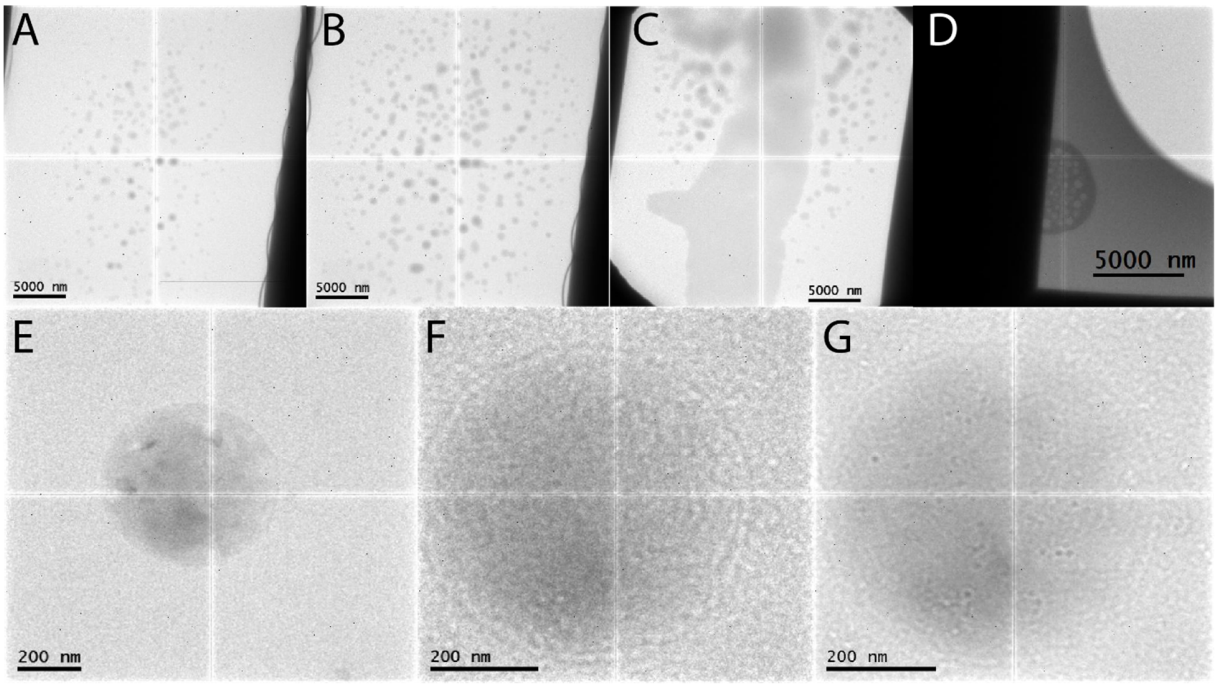

Figure 30: LC-TEM images of naporafenib solution form in FaSSIF-V1$_{PBS}$ after roughly 1 hour (A-D, 200 nm spacer) and after equilibration for about 2 days (E-G, 2 µm spacer). A) to C) represent images taken a few minutes apart. E) to G) represent images from the same object at different magnification and contrast settings. All samples were prepared freshly on site and analyzed with Tecnai G20 TEM, 200 kV. LC-TEM images were provided by Dr. A. Gomez-Perez.

The white appearing background in the top row of **Figure 30** possibly represents a phase separation of naporafenib but is purely speculative. Electron irradiations effects and nano-confinement of such systems needs to be further investigated. No clear differentiation between dry phases, oily phases or aqueous phases was possible. The objects appeared to coalescence over time and could reflect particles recovered from liquid and imaged by SEM in **Figure 14**.

In conclusion, the biorelevant media-drug systems appeared far more complex than anticipated from dynamic light scattering. While DLS indicated that FeSSIF-V1$_{PBS}$ contains multipe co-existing species (**Figure 27**) in contrast to a monomodal appearance for the fasted media (**Figure 26**), a similar degree of complexity was oberved for FaSSIF-V1$_{PBS}$ using electron microscopy, especially in presence of naporafenib. The aim was therefore to remove all colloidal objects through ultracentrifugation rather than targeting selective separation of specific species. This includes drug contained in biorelevant media colloids as well as phase separated drug species. It was assumed that in most cases, phase separated drug species should be removed by filtration and solubilized drug (e.g. in biorelevant media colloids) should pass through the filter. However, based on the observations made during this work, removal of large biorelevant media colloids containing drug (liquid reservoir) by filtration as well pushing phase separated drug species (solid resevoir) through the filter could not be exluded.

5.2.2 Differentation of drug species in solution

The feasibility investigation provided a justification to focus on fasted state biorelevant media such as FaSSIF-V1$_{PBS}$ and FaSSIF-V2$_{PBS}$ for the differentation of drug species in solution. For simplicity, the terms moleculary dissolved drug or freely dissolved drug will be used interchangeable throughout this work, referring to the fraction of drug measured in the supernatant after ultracentrifugation treatment. The possibility of small molecular associates or residual colloidal objects in this phase needs to appreciated. The term liquid reservoir will be used to refer to any other drug species in solution such as drug associated to biorelevant media colloids (e.g. micelles, vesicles, mixed colloids). **Figure 31** shows the amount of apparently dissolved drug as sum of drug in liquid reservoir and freely dissolved drug in dependency of varying nominal drug input via solution form (DMSO). A slight deviation from ideality was observed suspected to be due to unspecific binding to the filter material. An impact of experimental handling error could not be excluded. The saturation of apparently dissolved drug was different for FaSSIF-V1$_{PBS}$ and FaSSIF-V2$_{PBS}$, in good agreement with the determined phase separation onset in **Figure 18**. Noteworthy, the few concentrations in FaSSIF-V2$_{PBS}$ slightly above the phase separation limit (i.e. hump between 70 and 110 µg/mL drug input) were likely biased through quantification of some undissolved phase separated drug species (solid reservoir) alongside apparently dissolved drug. This was suspected based on visual observations and may have contributed to the profile obtained in **Figure 31**.

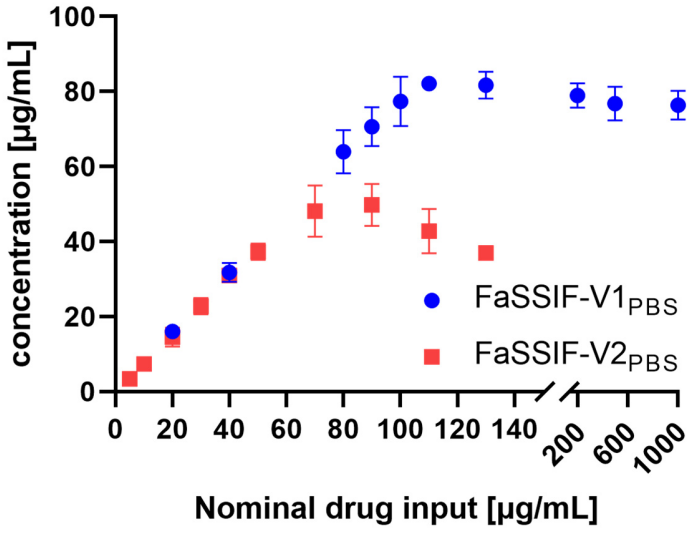

*Figure 31: Saturation of apparently dissolved drug concentrations of pure naporafenib via solution form (DMSO) in FaSSIF-V1$_{PBS}$ and FaSSIF-V2$_{PBS}$. Nominal drug input concentrations were selected based on **Figure 18/Table 3** and apparently dissolved drug concentrations are presented as mean +/- standard deviation of triplicates. Error bars are in some cases smaller than symbols.*

The ultracentrifugation treatment was performed with the exact same filtrates from which apparently dissolved drug was quantified and findings are presented in **Figure 32**. The results show that the saturation of molecularly dissolved drug occurs roughly at saturation of apparently dissolved drug. This saturation point was distinct between FaSSIF-V1$_{PBS}$ (about 100 µg/mL) and FaSSIF-V2$_{PBS}$ (about 40 µg/mL). Before phase separation occurs, freely dissolved drug is in quite linear relationship with total amount of drug added to the system. At the phase separation limit, freely dissolved drug reached saturation and did not further increase with more drug added to the system. Most importantly, the amount of freely dissolved drug above the phase separation limit was found similar, around 10 µg/mL, between FaSSIF-V1$_{PBS}$ and FaSSIF-V2$_{PBS}$ even if the amount of apparently dissolved drug was different. The difference was attributed to the type of liquid reservoir formed by the biorelevant media components.

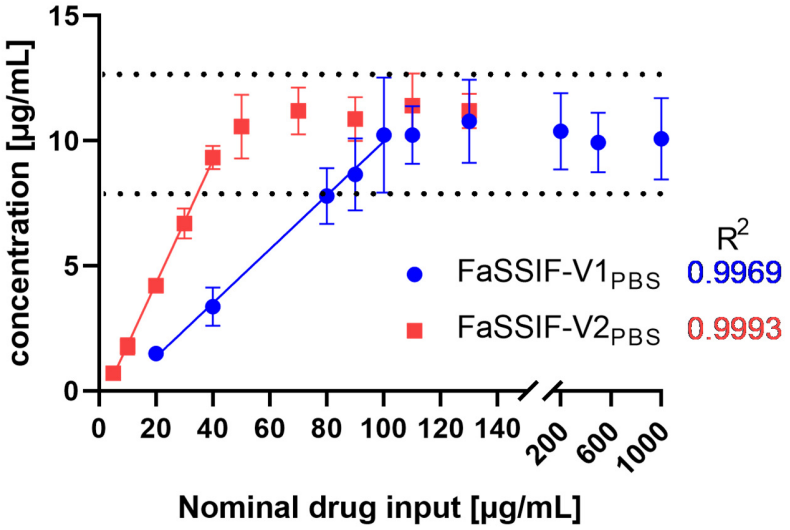

*Figure 32: Saturation of molecularly dissolved drug concentrations of pure naporafenib via solution form (DMSO) in FaSSIF-V1$_{PBS}$ and FaSSIF-V2$_{PBS}$. Data was obtained after ultracentrifugation treatment and subsequent drug quantification of the measured filtrates contained in **Figure 31**. Molecularly dissolved drug concentrations are presented as mean +/- standard deviation of triplicates. Error bars are in some cases smaller than symbols. Linear regression was performed in GraphPad Prism Version 9.3.1.*

The analyses above were executed with kinetically instable samples, relating to the presence of amorphous drug (above phase separation limit) or no drug present (below phase separation limit). Dissolved drug concentrations were above the apparent crystalline monohydrate solubility, i.e. supersaturated (**Equation 13**). On purpose, the exact same systems were equilibrated for another 36-48 hours to allow for form conversion from amorphous phase separated drug to crystalline monohydrate. An identical analysis was performed with those crystalline systems, differentiating apparently dissolved drug measured after filtration from molecularly dissolved drug measured

after ultracentrifugation. The results are shown in **Figure 33**. Consistent with findings in the amorphous systems, the amount of apparently dissolved drug was found different between FaSSIF-V1$_{PBS}$ and FaSSIF-V2$_{PBS}$ but moleculary dissolved drug was similar in both media, and independent of the nominal drug input concentration. The lowest concentration added to both media was above the respective apparent monohydrate solubility. Below the apparent crystalline solubility, a similar behavior would be expected in terms of free drug and apparently dissolved drug as for the amorphous system. Due to experimental sensitivity and analytical constraints in this concentration range, it was not approached in this work. Noteworthy, the lowest concentration tested in FaSSIF-V2$_{PBS}$ was likely insufficient to trigger form conversion as this system showed basically no solids even after equilibration for 36-48 hours.

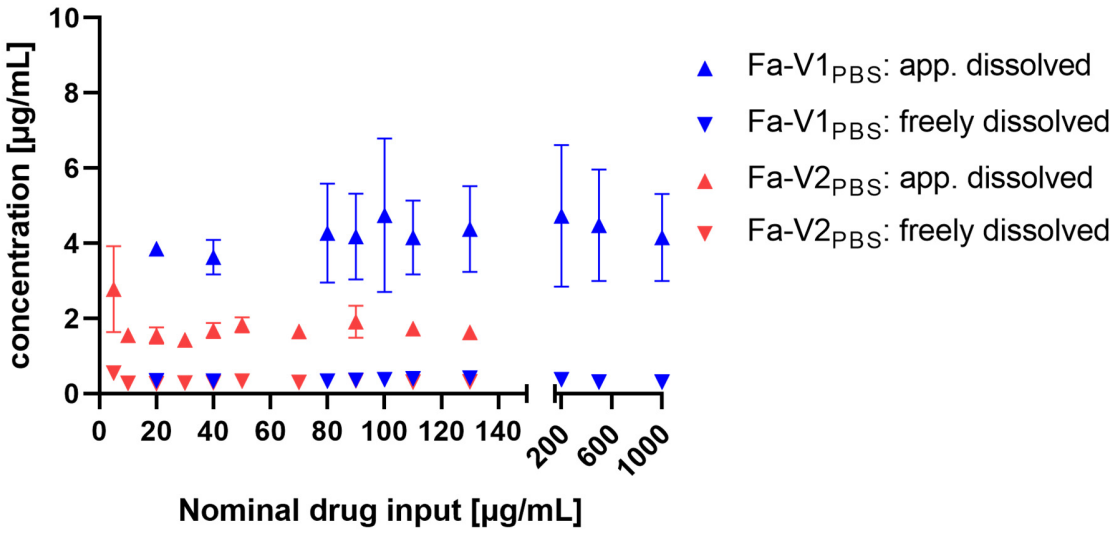

*Figure 33: Evolved systems from **Figure 31/Figure 32** for 36-48 hours to allow for form conversion from amorphous to crystalline drug, differentiated into apparently dissolved (by filtration) and molecularly dissolved (by ultracentrifugation treatment) pure naporafenib in FaSSIF-V1$_{PBS}$ and FaSSIF-V2$_{PBS}$. Dissolved drug concentrations presented as mean +/- standard deviation of triplicates. Error bars are in some cases smaller than symbols.*

The results obtained were further used to calculate a free fraction, defined as the amount of freely dissolved drug relative to the total amount apparently dissolved. An alternative treatment would be to convert the free fraction into a partitioning coefficient to quantify the distribution of drug between the aqueous phase (free drug) and the solubilizing colloids (liquid reservoir). This analysis was performed based on the linear slope below the phase separation limit shown in **Figure 32** or by calculation for the system with no solid reservoir (below phase separation limit), with amorphous solid reservoir (above phase separation limit) and with the crystalline solid reservoir (after 36-48 hours). An overview of the respective results is provided in **Table 4**.

*Table 4: Overview of free drug fractions based on the slope of linearization below phase separation limit (referring to nominal drug input, **Figure 32**) or calculated as freely dissolved divided by total apparently dissolved naporafenib in FaSSIF-V1$_{PBS}$ and FaSSIF-V2$_{PBS}$ in absence of any solids, in presence of amorphous phase separated drug and in presence of crystalline monohydrate after form conversion (36-48 hours). Values are provided as mean with standard deviation and number of data points in brackets. Statistical significance (α = 0.05) comparing the two media under identical (reservoir) conditions was evaluated using multiple t-tests and is indicated by an asterisk (*). The slopes were compared using linear regression. Analyses were performed with statistics tools in GraphPad Prism Version 9.3.1.*

Free fraction (free / total)	FaSSIF-V1$_{PBS}$	FaSSIF-V2$_{PBS}$
Linearization slope	0.1077* (0.004, R^2 = 0.9969)	0.2469* (0.004, R^2 = 0.9993)
No solid reservoir	0.11* (0.02, n=15)	0.27* (0.04, n=15)
Amorphous reservoir	0.13* (0.01, n=15)	0.26* (0.04, n=15)
Crystalline solid reservoir	0.08* (0.01, n=30)	0.18* (0.02, n=30)

A significant difference was found between the free fractions in FaSSIF-V1$_{PBS}$ and FaSSIF-V2$_{PBS}$ which can be attributed to the liquid reservoir compositional differences. For a given medium the fraction of molecularly dissolved drug remained similar above and below the amorphous saturation, respectively. In presence of crystalline solids a slight reduction of the free fraction could be derived. This may indicate that the partitioning mechanism of the drug into the liquid reservoir could be concentration dependent. A different impact of solubilizing additives depending on crystalline or amorphous concentration levels of drug was previously reported (139). Furthermore, such concentration dependent differences in interaction with bile colloids are available in literature (140). Another hypothesis is related to an incomplete micellar loading mechanism involving ionic surfactant systems (141). More investigations would be required to further discuss. Unfortunately, it was not successful to grasp differences in terms of molecular interactions at low (crystalline) and high (amorphous) concentrations using NMR, primarly due to the low amount of dissolved drug in the crystalline systems causing low drug proton signals.

To evaluate the colloid separation efficiency from FaSSIF-V1$_{PBS}$ and FaSSIF-V2$_{PBS}$ using ultracentrifugation, a DLS scatter plot was generated summarizing the signal-to-noise ratios obtained for the reference media (without drug) and the filtrates (measured apparently dissolved drug), and compared to the signal-to-noise ratios of the supernatants after ultracentrifugation. The amorphous and crystalline systems were differentiated but showed identical results. At a minimum, the top fraction was measured with DLS for each separation. The sub fraction was considered as technical replicate with respect to consistency in terms of drug concentration with the top fraction. Not every sub fraction was analyzed by DLS due to time constraints. Overall, the statement is made that with high confidence, no residual colloidal structures were present in the supernatants affecting drug concentrations based on the lack of correlatable signal (signal-to-noise ratio).

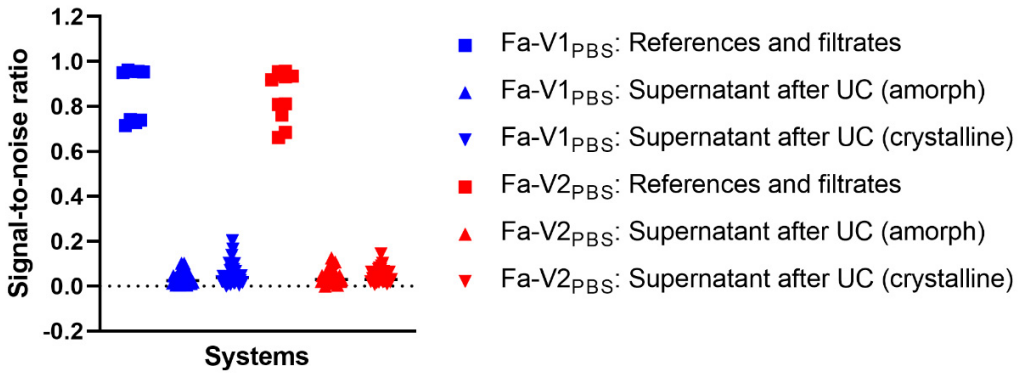

Figure 34: DLS scatter plot of signal-to-noise ratios of naporafenib in FaSSIF-V1$_{PBS}$ and FaSSIF-V2$_{PBS}$, divided into references and filtrates before ultracentrifugation (media before drug addition and filtrates after drug addition) and supernatants measured after ultracentrifugation treatment for both, the amorphous and crystalline systems. Data presented as individual measurements.

5.2.3 Concentration/saturation-dependent dialysis flux

Dialysis flux was used to verify the impact of colloidal partitioning (solubilization) of naporafenib on resulting drug mass transport across a regenerated cellulose (size-exclusion) barrier. A direct comparison between the Buffer$_{PBS}$ and FaSSIF-V1$_{PBS}$ system is shown in **Figure 35**. At low concentration, e.g. below the phase separation limit of Naporafenib in FaSSIF-V1$_{PBS}$, the derived flux was higher in the buffer system compared to the biorelevant medium. At higher concentration, e.g. above the phase separation limit in FaSSIF-V1$_{PBS}$, the flux was found to plateau and was similar between the two systems, in line with the findings presented in **Figure 32** related to the saturation of molecularly dissolved drug.

This was further explored by extension to the biorelevant media landscape. When plotting the flux over drug input as percentage of media saturation, i.e. percentage of the phase separation limit, great linearity was observed from 25% to 100% media saturation, while 200% media saturation did not further cause a substantial increase in flux, see **Figure 36**. Among the media tested at equal/above saturation, the flux showed rather small differences which may be attributed to media effects on for example the unstirred water layer or drug re-supply kinetics from the liquid and solid reservoirs (replenish permeated freely dissolved drug molecules). The data would support that only free drug but neither solid nor liquid reservoir drug were able to permeate in this setup. In that sense, the dialysis membrane functioned as a size-exclusion membrane by only allowing freely dissolved drug molecules to cross the barrier.

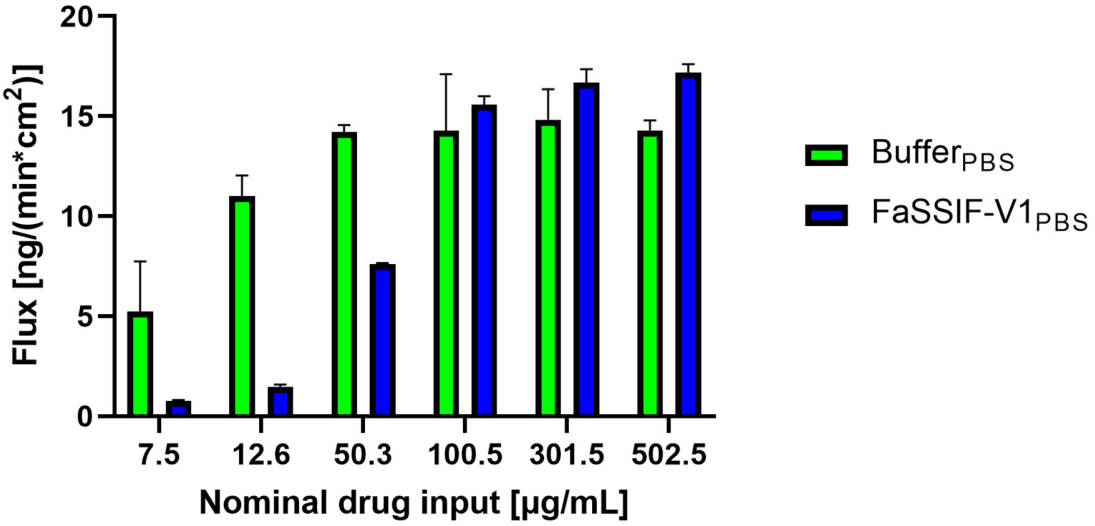

Figure 35: Concentration-dependent flux of naporafenib solution form (DMSO) through regenerated cellulose size-exclusion (dialysis) membrane in Buffer$_{PBS}$ and FaSSIF-V1$_{PBS}$. Nominal drug input was transformed from molar units into µg/mL. Derived flux slopes presented as mean +/- standard deviation of triplicates. Data was provided by J. Schlauersbach.

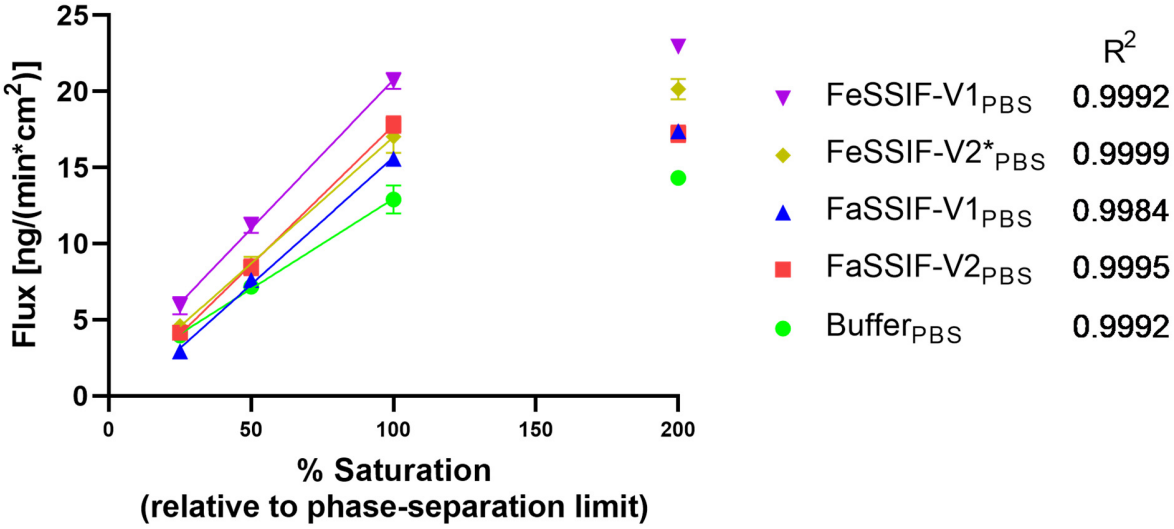

Figure 36: Saturation-dependent flux of naporafenib solution form (DMSO) through regenerated cellulose size-exclusion (dialysis) membrane in Buffer$_{PBS}$, FaSSIF-V2$_{PBS}$, FaSSIF-V1$_{PBS}$, FeSSIF-V2$_{PBS}$ and FeSSIF-V1$_{PBS}$. Drug input shown as percent media saturation relative to the phase separation limit derived from **Figure 18/Table 3**. Linearization between 25% and 100% saturation was performed using a built-in linear regression tool of GraphPad Prism Version 9.3.1. Derived flux slope presented as mean +/- standard deviation of triplicates. Error bars are in some cases smaller than symbols. Data was provided by J. Schlauersbach.*

5.2.4 Dose-dependency of bioaccessibility

With the concept of freely dissolved drug as key driver for permeation, it was of great interest to combine drug species differentiation with a more biomimetic permeation setup that contains a lipidic barrier rather than a size-exclusion barrier. An exploratory ultracentrifugation-flux combo assay was developed using the μFlux™ apparatus from Pion Inc. Ltd., which involved a phospholipid impregnated PVDF support as biomimetic barrier, also known as GIT-PAMPA membrane. Various dose levels below, at and above the phase separation limit were explored to investigate the effect of drug species on resulting membrane flux. The donor and acceptor profiles under excess amount of naporafenib added via DMSO stock solution for FaSSIF-V1$_{PBS}$ and FaSSIF-V2$_{PBS}$ are shown in **Figure 37**. The donor concentration-time profiles showed a stable kinetic concentration plateau until 6 hours, and very low dissolved concentrations at 22 and 24 hours. As a result, the cumulative acceptor concentrations showed a rather linear increase up to 6 hours, while the 22 and 24 hour concentrations indicate that the flux was not maintained between the 6 hour and 22 hour compared to before. The later flux decay is considered a result of concentration drop after 6 hours, likely caused by occurence of the monohydrate form (conversion of solid reservoir) and associated desupersaturation. The onset of form conversion and desupersaturation is a rather stochastic process and may be reflected in the replicate variability observed for the latest time points. Those results nicely illustrate the limitation of using Fick's law as is (given in **Equation 10** for ideal solutions). Obviously, apparent concentrations in such systems do not always allow correlation with the mass transfer observed. But, if drug species are differentiated, one may use Fick's law to relate the concentration of freely dissolved drug with the observed flux. It is, however, important to remind that the mass transfer process measured here is not purely a diffusion processes through a simple single layer. Partitioning processes might play a role, e.g. drug partitioning into the membrane or colloidal structures, and there might be differences in penetration mechanism (depending on layer type). Such processes need to be considered as well when applying Fick's law to permeation experiments, specifically in case of complex systems involving supersaturation and solubilization mechanisms, as will be discussed later.

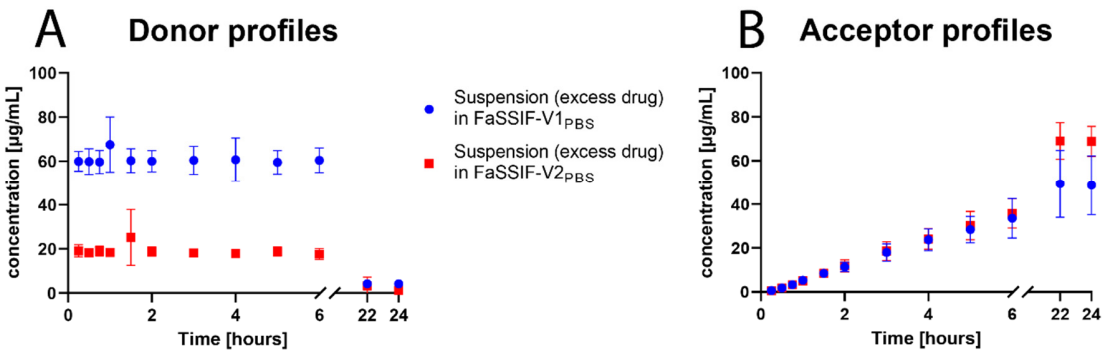

Figure 37: Concentration-time profiles of naporafenib in A) FaSSIF-V1$_{PBS}$ and FaSSIF-V2$_{PBS}$ in the donor and B) resulting mass transport as cumulative concentrations in acceptor sink buffer in the acceptor compartment. Nominal donor input was 1 mg/mL drug via solution form (DMSO) considered excess drug conditions. Data provided as mean +/- standard deviation of quadruplicates. Error bars are in some cases smaller than symbols.

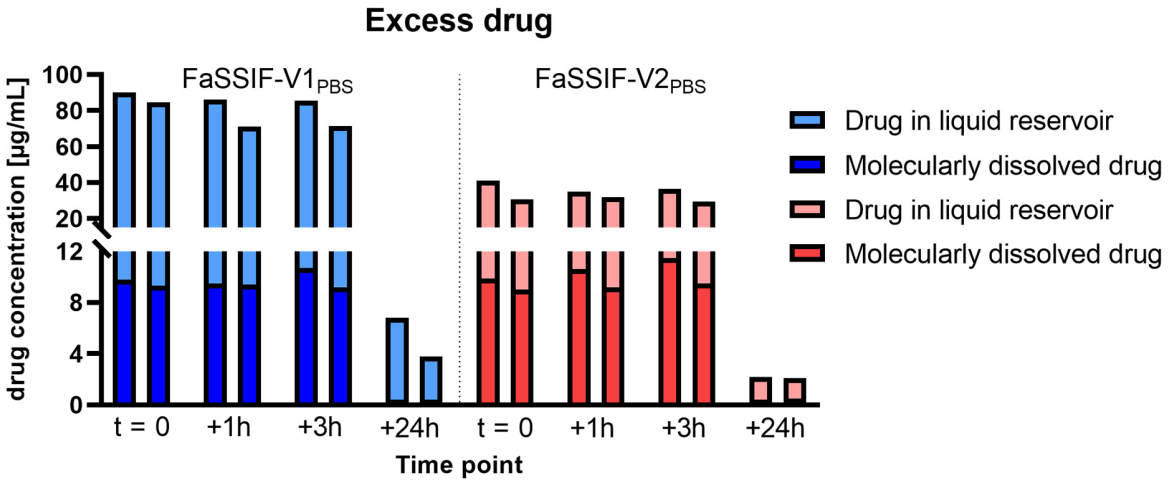

*Figure 38: Ultracentrifugation-flux combo data for excess naporafenib in FaSSIF-V1$_{PBS}$ and FaSSIF-V2$_{PBS}$ presented as bar plots over time (relative to the flux experiment, **Figure 37**), differentiating between molecularly dissolved drug and drug in liquid reservoir. Liquid reservoir calculated from total apparently dissolved drug measured after filtration minus molecularly dissolved drug estimated by ultracentrifugation. Data presented as individual replicates.*

To support the interpretations made, **Figure 38** shows differentiated drug species from the donor compartments as a function over time. The findings are in line with determined freely dissolved drug amount in **section 5.2.2** for both the amorphous (t=0, +1 h and +3 h) and crystalline systems (t=24 h). Potential discrepancies between apparently dissolved amount based on centrifugal filters (Donor, **Figure 37**) and syringe filters (**Figure 38**) are discussed towards the end of this section.

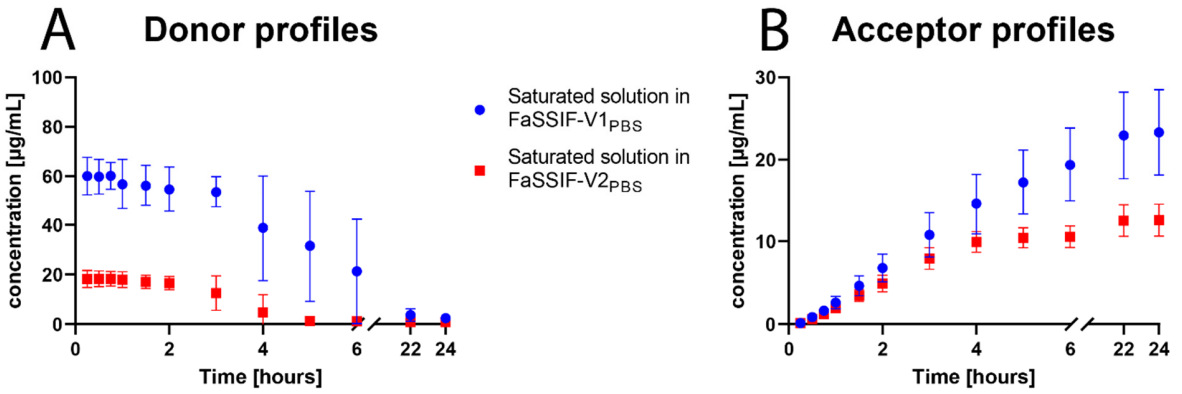

Figure 39: Concentration-time profiles of naporafenib in A) FaSSIF-V1$_{PBS}$ and FaSSIF-V2$_{PBS}$ in the donor and B) resulting mass transport as cumulative concentrations in acceptor sink buffer in the acceptor compartment. Nominal donor input was 1 mg/mL drug via solution form (DMSO) with subsequent removal of undissolved drug by filtration, considered saturated solution conditions relative to the phase separation limit. Data provided as mean +/- standard deviation of quadruplicates. Error bars are in some cases smaller than symbols.

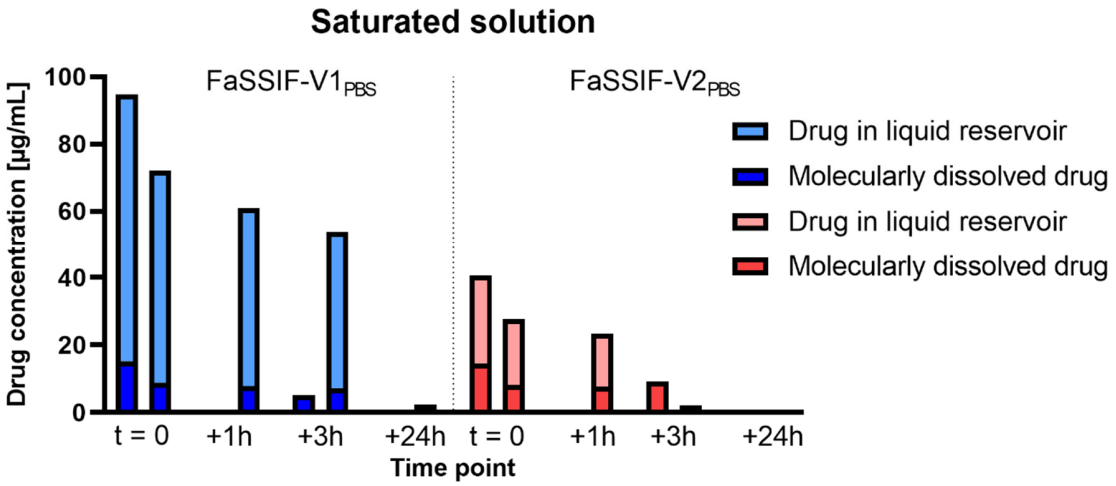

*Figure 40: Ultracentrifugation-flux combo data for FaSSIF-V1$_{PBS}$ and FaSSIF-V2$_{PBS}$ saturated with naporafenib presented as bar plots over time (relative to the flux experiment, **Figure 39**), differentiating between molecularly dissolved drug and drug in liquid reservoir. Liquid reservoir calculated from total apparently dissolved drug measured after filtration minus molecularly dissolved drug estimated by ultracentrifugation. Data presented as individual replicates. Missing replicates/data related to evolution of methodology. Bar plots at 24 hours hardly visible due to very low values.*

Since no differences in flux were observed between FaSSIF-V1$_{PBS}$ and FaSSIF-V2$_{PBS}$ in presence of phase separated drug (excess drug added via solution form), the respective saturated solutions were tested to understand the impact of excess drug material on the observed mass transport. As previously, excess drug was added via solution form (DMSO) but then undissolved drug material was removed by filtration before inserting into the donor compartments. **Figure 39** shows the donor and acceptor profile under such conditions. As expected, the donor concentrations were not constant and the flux was lower compared to excess drug conditions. The decline in donor concentrations was interpreted as the combined effect from drug loss due to permeation (transfer

mass balance) and desupersaturation (drug precipitation / form conversion). The reduction in donor concentration (reduction in driving force for permeation), can be linked to precipitation and desupersaturation and is reflected in the acceptor compartment by a decline in flux slope. Once the system has converted, minimal mass transport resulted, which can be judged based on the difference between acceptor concentrations at 6 hours and 22/24 hours.

Due to differences in absolute donor concentrations between the two media, it was difficult to conclude on the underlying cause for the early flux differences (refer to **Figure 43**). The starting conditions were designed such that both systems were initially identical in terms of free drug concentration, i.e. saturated. It was attempted to monitor the change in free drug over time, as shown in **Figure 40**. As a consequence of method development and protocol optimization, unfortunately not all data points can be provided for this experiment and interpretations have to be made with caution. Some systems were found to have converted from amorphous to crystalline within 3 hours, making a direct comparison of free drug between the two media at some timepoints impossible.

The final condition explored in this series of experiments was using sub-saturated solutions relative to their phase separation limit. An equal drug input of 30 µg/mL was added via solution form to FaSSIF-V1$_{PBS}$ and FaSSIF-V2$_{PBS}$ which corresponds to about 30% and 70% media saturation, respectively. In addition, 70 µg/mL was added to FaSSIF-V1$_{PBS}$ to match the media saturation of about 70%, similar to 30 µg/mL in FaSSIF-V2$_{PBS}$. The donor and acceptor concentration-time profiles are shown in **Figure 41**. 30 µg/mL drug input resulted in almost comparable donor concentrations but lower flux in the case of FaSSIF-V1$_{PBS}$ was observed. This is conceptually in line with observations from dialysis flux (**Figure 35**) where a drug input below the phase separation limit of FaSSIF-V1$_{PBS}$ resulted in lower flux compared to the aqueous buffer system, where the phase separation limit was already exceeded at the same drug input. At about 70% relative media saturation and therefore assumed equal amount of free drug in the beginning, about the same initial flux would be expected in both biorelevant media. Supporting this mechanistic interpretation, a lower free drug was observed in FaSSIF-V1$_{PBS}$ compared to FaSSIF-V2$_{PBS}$ at equal drug input while a similar amount of free drug was measured at equal media saturation, see **Figure 42**. In reality, that was difficult to judge during the course of flux as form conversion and desupersaturation could overrule, for example observed for FaSSIF-V2$_{PBS}$ after approximately 1 hour.

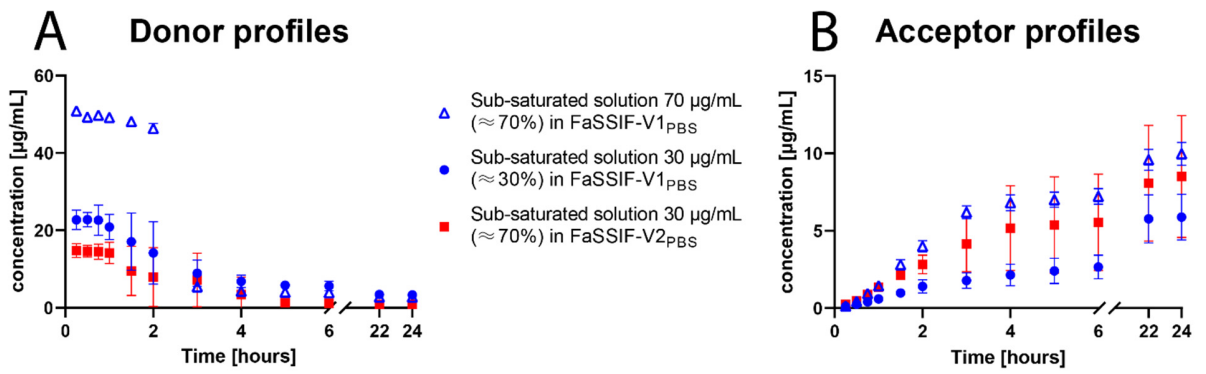

Figure 41: Concentration-time profiles of naporafenib in A) FaSSIF-V1$_{PBS}$ and FaSSIF-V2$_{PBS}$ in the donor and B) resulting mass transport as cumulative concentrations in acceptor sink buffer in the acceptor compartment. Nominal donor input was 30 or 70 µg/mL drug via solution form (DMSO), considered sub-saturated solution conditions relative to the phase separation limit. Data provided as mean +/- standard deviation of quadruplicates. Error bars are in some cases smaller than symbols.

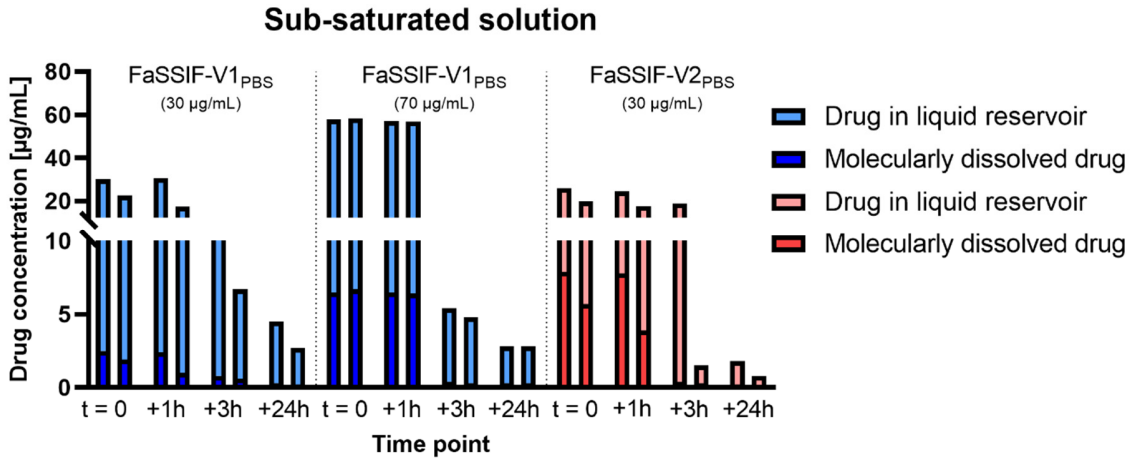

*Figure 42: Ultracentrifugation-flux combo data for FaSSIF-V1$_{PBS}$ and FaSSIF-V2$_{PBS}$ sub-saturated with naporafenib presented as bar plots over time (relative to the flux experiment, **Figure 41**), differentiating between molecularly dissolved drug and drug in liquid reservoir. Liquid reservoir calculated from total apparently dissolved drug measured after filtration minus molecularly dissolved drug estimated by ultracentrifugation. Data presented as individual replicates.*

The first replicate of the 3 hour data point in FaSSIF-V2$_{PBS}$ is an example where the apparently dissolved drug concentration was determined still on the kinetic concentration plateau whereas molecularly dissolved drug was quantified after form conversion and desupersaturation. It was suspected that the sample has evolved and therefore precipitated during the ultracentrifugation treatment. The second replicate of the same time point showed much lower apparent concentrations, supporting the understanding of a stochastic problem related to form conversion and desupersaturation.

Evaluation of relative drug mass transports across dose levels tested in the two media was derived from the slope of cumulative acceptor concentrations, up until the donor compartment indicated form conversion and subsequent normalization, see **section 4.2.5.2**. A summary of surface-normalized flux values is provided in **Figure 43** and **Table 5**. A significant difference between flux in FaSSIF-V1$_{PBS}$ and FaSSIF-V2$_{PBS}$ was observed at equal drug input (i.e. 30 µg/mL) but not at equal media saturation (ca. 70%). Similar flux was also observed under excess drug conditions in both media, despite >2-fold differences in the amount of apparently dissolved drug in the donor compartment. Therefore, a dose above the phase separation limit of naporafenib (solution form) resulted in equal bioaccessibility in FaSSIF-V1$_{PBS}$ as in FaSSIF-V2$_{PBS}$. Doses tested in media below their phase separation limit show reduced bioaccessibility, primarly due to partitioning of drug into colloidal structures contained in biorelevant media, causing a reduction of freely dissolved drug available for permeation. For the saturated solution case, the assumption would be to start from equal free drug in FaSSIF-V1$_{PBS}$ and FaSSIF-V2$_{PBS}$. However, statistical comparison indicates a significant difference in (early) flux. This unexpected outcome could be a result of a slightly different starting point due to unspecific binding loss with the initial filtration step simply different absolute amount of drug in liquid reservoir (colloids contributing to UWL diffusion). Such observations would suggest a benefit from SIF components in terms of solubilization for enhancing drug permeation and therefore absorption.

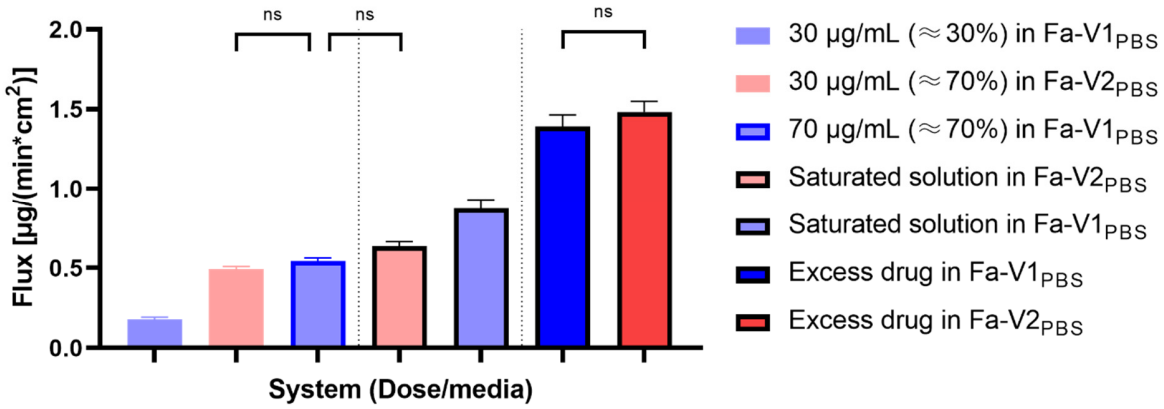

*Figure 43: Overview of surface-normalized flux of naporafenib in FaSSIF-V1$_{PBS}$ and FaSSIF-V2$_{PBS}$ under various dose conditions: excess drug, saturated solution and sub-saturated solution. Slopes were derived from **Figure 37**, **Figure 39** and **Figure 41** using linear regression. Data provided as mean +/- standard deviation of quadruplicates. Statistical significance (α = 0.05) was evaluated using a one-way ANOVA with post-hoc Tuckey's test for multiple comparison. Exceptionally, only not signifcant (ns) comparisons are marked to facilitate interpretation. Analysis performed with GraphPad Prism Version 9.3.1.*

The dose-dependency of lipidic flux, as shown in **Figure 43** or **Table 5**, is in line with findings from the dialysis flux setup. A linear relationship was observed in FaSSIF-V1$_{PBS}$ between flux and media saturation (30%, 70% and 100%) with an R^2 value of 0.9976. More saturations levels in FaSSIF-

$V2_{PBS}$ but also FaSSIF-$V1_{PBS}$ and other media would be required to allow better comparison with the dialysis setup findings. Nevertheless, both setups were able to show reduced flux in the situation of less saturation, i.e. less free drug or more "capacity" left to solubilize drug. As soon as the media saturation was adjusted similar flux was observed.

*Table 5: Table format of **Figure 43** including R^2 values for the linear fit of the cumulative acceptor concentrations based on the donor profiles. Flux slope provided as mean with standard deviation in brackets of quadruplicates.*

System (Media, dose/saturation, stirring speed)	Flux slope [µg/(min*cm²)]	R^2
Fa-$V1_{PBS}$: 30 µg/mL (~ 30% saturation), 100 rpm	0.17 (0.01)	0.9022
Fa-$V2_{PBS}$: 30 µg/mL (~ 70% saturation), 100 rpm	0.49 (0.02)	0.9737
Fa-$V1_{PBS}$: 70 µg/mL (~ 70% saturation), 100 rpm	0.54 (0.02)	0.9700
Fa-$V2_{PBS}$: ~ Saturated (no solids), 100 rpm	0.64 (0.03)	0.9468
Fa-$V1_{PBS}$: ~ Saturated (no solids), 100 rpm	0.87 (0.06)	0.8834
Fa-$V1_{PBS}$: Saturated (excess drug), 100 rpm	1.39 (0.07)	0.9057
Fa-$V2_{PBS}$: Saturated (excess drug), 100 rpm	1.48 (0.07)	0.9304

Dealing with poorly water-soluble drug substances may have big consequences for the practical lab work methodology. One of them may be caused by the natural affinity of hydrophobic/lipophilic molecules towards surfaces. Also, biorelevant media components, specifically bile salts and phospholipids, are considered to have some surface affinity. Working with a poorly water-soluble substance such as naporafenib in biorelevant media, specifically during supersaturated states, it was of great concern that much drug would be lost to filter and other equipment surfaces when they could not sufficiently be saturated (particularly at low sample volumes). **Table 6** provides an overview on the loss of drug during solid-liquid separation (filtration) through so-called unspecific binding. The syringe filters showed lower unspecific binding loss compared to the centrifugal filters, probably related to liquid volumes (2.5 mL for syringe filters and 150 µL for centrifugal filters). The centrifugal filters showed a substantial loss of drug material with up to about 30% in FaSSIF-$V1_{PBS}$ and up to 50% in FaSSIF-$V2_{PBS}$. This may explain absolute differences between the donor concentration-time profiles and the apparently dissolved drug amounts from the ultracentrifugation-flux combo data. Furthermore, the overall loss due to unspecific binding to filters etc. is suspected to have impaired any mass balance analysis from initially targeted systems in absence of excess drug. It could be difficult to reproduce those results if the unspecific binding loss is variable with other materials or even from batch-to-batch variations. It is therefore generally recommended to evaluate the loss to the specific materials used as good practice.

*Table 6: Overview of the unspecific binding loss determined during the ultracentrifugation-flux combo experiment by re-filtering a filtrate of known concentration through either 0.45 µm PTFE syringe filters or 0.45 µm PVDF centrifugal filters using identical volumes to the initial filtration. Loss of drug concentration required to substantiate discrepancies between donor concentration-time profiles (**Figure 37, Figure 39** and **Figure 41**) and apparently dissolved drug levels from the ultracentrifugation-flux combo data (**Figure 38, Figure 40** and **Figure 42**). Unspecific binding loss presented as individual replicates in percentage of the initial drug concentration in the filtrate.*

Unspecific binding loss	**FaSSIF-V1$_{PBS}$ (3 mM taurocholate, 0.75 mM Lecithin)**				**FaSSIF-V2$_{PBS}$ (3 mM taurocholate, 0.2 mM Lecithin)**		
	Excess	**Saturated**	**Sub-sat.**	**Sub-sat. II**	**Excess**	**Saturated**	**Sub-Sat.**
Syringe filter, t=0	- 18.1%	- 7.2%	5.9% 5.1%	-0.7%[b] 0.6%	- 18.7%	- 9.8%	16.7% 10.1%
Centrifugal filter, t=0	24.3%[a] 36.6%	30.5% 23.5%	10.6% 14.1%	17.2% 17.6%	48.0%[a] 48.5%	49.4% 42.6%	40.2% 32.6%
Centrifugal filter, t=1h	- 24.3%	- 28.2%	9.9% 10.2%	17.2% 17.3%	- 47.3%	- 39.8%	39.1% 29.7%
Centrifugal filter, t=3h	- 24.7%	- 25.0%	9.7% 12.3%	9.1% 8.9%	- 44.7%	- 27.4%	46.4% 30.1%
Centrifugal filter, t=24h	-0.4%[b] 12.0/11.6%	- 4.5/12.3%	10.0% 37.8/9.1%	11.7/13.0% 11.4/12.7%	48.7%[a] 27.6/41.0%	- 16.1/23.5%	52.2% 25.6/32.7%

[a]: inconsistency between technical replicates (some data excluded for calculation)

[b]: unexpected result due to higher concentration observed after filtration test

The obtained free drug fractions from the ultracentrifugation-flux combo setups are summarized in **Table 7**, to compare with free fractions determined in **section 5.2.2.** Overall, the values support the previously observed difference between the free fractions in FaSSIF-V1$_{PBS}$ compared to FaSSIF-V2$_{PBS}$. No differentiation between amorphous and crystalline systems was performed due to uncertainties of complete form conversion in this experimental time frame. A trend of lower free fractions at the 24 hour time point compared to other time points was observed for most cases. It has to be noted that those calculated ratios are very sensitive to changes in free drug concentrations. For example, a free fraction determined at t=24h can vary by a factor of 2 when the amount of free drug varies from 0.15 to 0.30 µg/mL while the amount apparently dissolved stays constant. Importantly, this ratio is independent of absolute values and an identical ratio may still contain absolute differences of one order of magnitude or above.

*Table 7: Overview of the free fraction calculated as molecularly dissolved drug measured in the supernatant after ultracentrifugation divided by apparently dissolved drug measured after filtration. The ratio is visually reflected in **Figure 38**, **Figure 40** and **Figure 42**. Data provided as individual replicates.*

Free fraction (free/total)	FaSSIF-V1$_{PBS}$ (3 mM taurocholate, 0.75 mM Lecithin)				FaSSIF-V2$_{PBS}$ (3 mM taurocholate, 0.2 mM Lecithin)		
	Excess	**Saturated**	**Sub-sat.**	**Sub-sat. II**	**Excess**	**Saturated**	**Sub-Sat.**
t=0	0.11 0.11	0.16 0.12	0.08 0.08	0.11 0.11	0.24 0.29	0.37 0.29	0.30 0.29
t=1h	0.11 0.13	- 0.13	0.08 0.06	0.11 0.11	0.30 0.29	- 0.33	0.32 0.22
t=3h	0.13 0.13	- 0.13	0.07 0.09	0.07 0.07	0.32 0.32	- 0.22	~~0.02~~[a] 0.18
t=24h	0.06 0.09/0.09	- 0.09/0.08	0.07 0.07/0.07	0.10/0.10 0.11/0.11	0.19 0.23/0.26	- 0.21/0.25	0.14 0.16/0.13

[a]: system precipitated between filtration and ultracentrifugation treatment

The question may be raised whether such observations appear generally valid also for other systems such as fed state simulating intestinal fluid media? And what are the mass transport rate-limitations in the tested *in vitro* setups? Strikingly, the mass transport through the dialysis membrane was almost 100-fold lower compared to the lipidic membrane setup. In order to attribute those differences to the resistance created by the barrier and not the experimental setup, the same dialysis membrane was tested in the µFlux™ setup and confirmed flux values about 100-fold lower than with the GIT-PAMPA membrane (data not shown). The general validity of findings for other biorelevant media such as FeSSIF-V1$_{PBS}$ as well as investigating flux rate-limitations of the lipidic flux setup were tackled in the next section about *in vitro* rate-limitations of mass transport.

5.2.5 Limitations of *in vitro* drug mass transport

The observation under excess drug conditions with quite equal flux in FaSSIF-V1$_{PBS}$ and FaSSIF-V2$_{PBS}$ in the previous sections formed a hypothesis. In case the only true driving force for permeation in this setup would be the amount of freely dissolved drug and the amount of free drug would be equal in fed state media as in fasted media above saturation, equal flux should be observed with FeSSIF-V1$_{PBS}$ as with the fasted media. Considering the relevance of an unstirred water layer in typical *in vitro* permeation setups, the experiment was performed under two different stirring speeds to challenge the hypothesis. **Figure 44** shows donor and acceptor profiles for FaSSIF-V1$_{PBS}$ and FeSSIF-V1$_{PBS}$ under excess drug condition at 100 and 400 rpm stirring speed. Donor concentrations were equal for the same media but about 5-fold different between fasted

and fed media. In contrast and as expected, the flux observed in the acceptor compartments differed by relatively little amounts whereas the 400 rpm condition resulted in slightly higher flux compared to the 100 rpm condition for both media. The cumulative amount in the acceptor after 24 hours was not substantially different between the two stirring conditions, indicating little to no impact of stirring on the desupersaturation / form conversion kinetics.

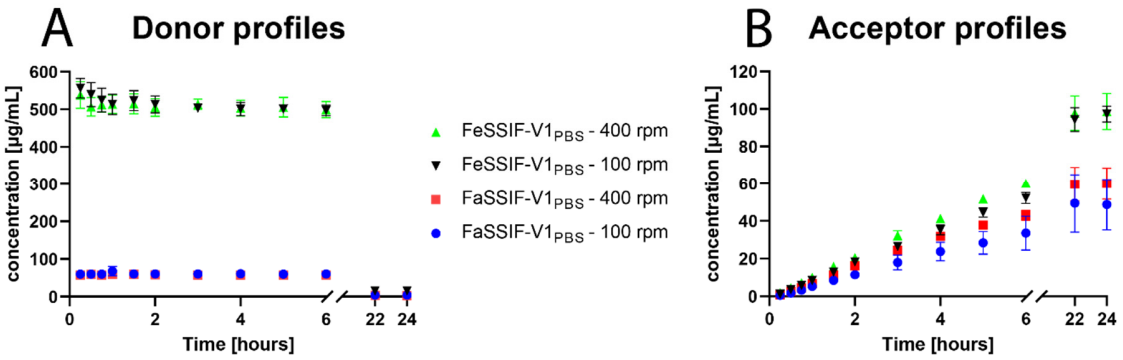

*Figure 44: Concentration-time profiles of naporafenib in A) FaSSIF-V1$_{PBS}$ and FeSSIF-V1$_{PBS}$ in the donor and B) resulting mass transport as cumulative concentrations in acceptor sink buffer in the acceptor compartment. Nominal donor input was 1 mg/mL drug via solution form (DMSO) considered excess drug conditions. Data provided as mean +/- standard deviation of quadruplicates. Data for FaSSIF-V1$_{PBS}$ at 100 rpm already presented in **Figure 37** and included for reference. Error bars are in some cases smaller than symbols.*

Despite difficulties for complete colloidal separation in FeSSIF-V1$_{PBS}$ media based on the feasibility investigation, it was still decided to test the final ultracentrifugation protocol with that media for confirmation. The ultracentrifugation-flux combo data is presented in **Figure 45**. Grey bars reflect issues with the ultracentrifgation procedure (e.g. vacuum issues) and values should not be interpreted. Apparently dissolved drug concentrations are provided for those cases for consistency. The filtrate for FaSSIF-V1$_{PBS}$ at 400 rpm at 24 hours contained phase separated drug and is marked in grey as well.

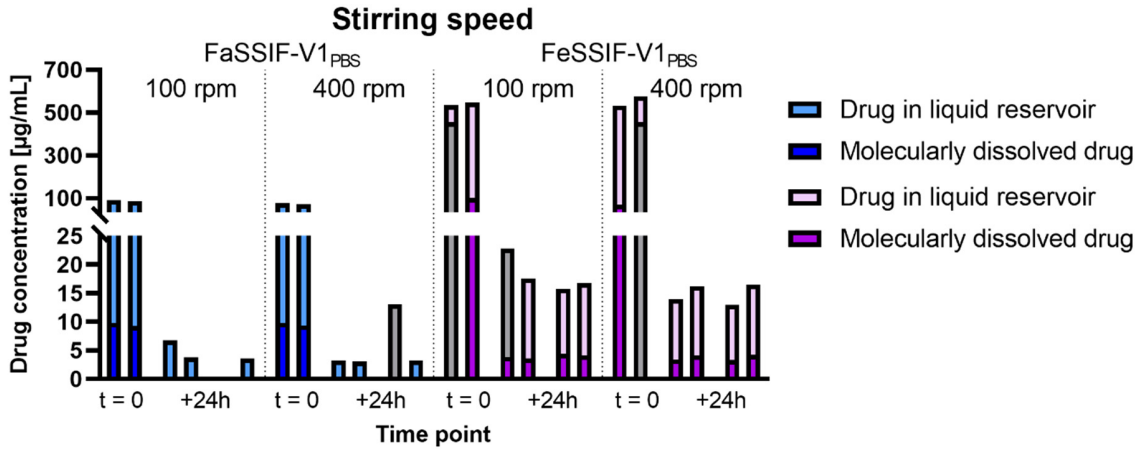

*Figure 45: Ultracentrifugation-flux combo data for excess naporafenib in FaSSIF-V1$_{PBS}$ and FeSSIF-V1$_{PBS}$ presented as bar plots over time (relative to the flux experiment, **Figure 44**), differentiating between molecularly dissolved drug and drug in liquid reservoir. Liquid reservoir calculated from total apparently dissolved drug measured after filtration minus molecularly dissolved drug estimated by ultracentrifugation. Data presented as individual replicates. Grey bars indicate issues with the experimental protocol. Ultracentrifugation data from FeSSIF-V1$_{PBS}$ system should be interpreted with caution due to impaired confidence in separation efficiency.*

The amount of drug measured after ultracentrifugation in the supernatants of FeSSIF-V1$_{PBS}$ were inconsistent between the different fractions, as observed previously, primarly for the t=0 time point. Nevertheless, the values obtained in the top and sub fraction were averaged for graphing purposes. Surprisingly, the eight replicates for the 24 hour time points in FeSSIF-V1$_{PBS}$ all showed a similar range of drug concentrations around 4 µg/mL. This may hint towards selective separation of some colloidal phases, but still, no complete removal of drug contained in the liquid reservoir can be presumed.

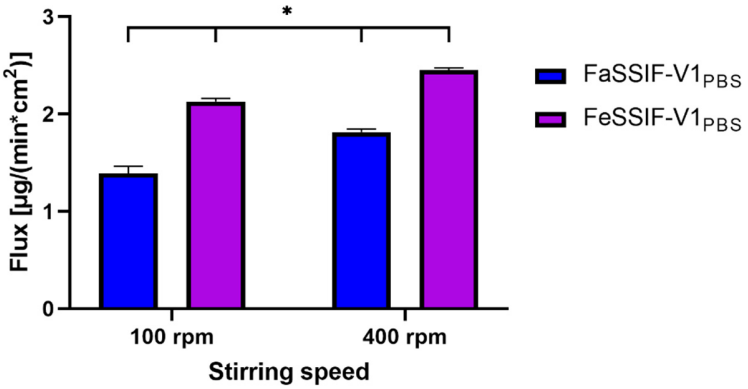

*Figure 46: Overview of surface-normalized flux of excess naporafenib in FaSSIF-V1$_{PBS}$ and FeSSIF-V1$_{PBS}$ under 100 and 400 rpm stirring speed conditions. Slopes were derived from **Figure 44** using linear regression. Data for FaSSIF-V1$_{PBS}$ at 100 rpm already presented in **Figure 43** and included for reference. Data provided as mean +/- standard deviation of quadruplicates. Statistical significance (α = 0.05) was evaluated using a one-way ANOVA with post-hoc Tuckey's test for multiple comparison and is indicated by an asterisk (*). Analysis performed with GraphPad Prism Version 9.3.1.*

The surface-normalized flux in FaSSIF-V1$_{PBS}$ and FeSSIF-V1$_{PBS}$ at 100 and 400 rpm stirring speed is shown in **Figure 46** and **Table 8**. Flux increased by about 30% in FaSSIF-V1$_{PBS}$ from 100 to 400 rpm. Only about 15% increase in flux was observed for FeSSIF-V1$_{PBS}$ when going from 100 rpm to 400 rpm. The difference between the two media was reduced from about 50% at 100 rpm to about 35% at 400 rpm. Importantly, the flux in FeSSIF-V1$_{PBS}$ at 100 rpm was still higher than from FaSSIF-V1$_{PBS}$ at 400 rpm.

*Table 8: Table format of **Figure 46** including R^2 values for the linear fit of the cumulative acceptor concentrations based on the donor profiles. Data for FaSSIF-V1$_{PBS}$ at 100 rpm already presented in **Figure 43**/**Table 5** and included for reference. Flux slope provided as mean with standard deviation in brackets of quadruplicates.*

System (Media, dose/saturation, stirring speed)	Flux slope [µg/(min*cm^2)]	R^2
Fa-V1$_{PBS}$: Saturated (excess drug), 100 rpm	1.39 (0.07)	0.9057
Fa-V1$_{PBS}$: Saturated (excess drug), 400 rpm	1.81 (0.03)	0.9880
Fe-V1$_{PBS}$: Saturated (excess drug), 100 rpm	2.13 (0.03)	0.9922
Fe-V1$_{PBS}$: Saturated (excess drug), 400 rpm	2.45 (0.03)	0.9960

The data supports the hypothesis that the unstirred water layer thickness can be reduced by increasing the hydrodynamics, i.e. flux increases at higher stirring speed. The difference observed between the two media at equal stirring speed and in excess of drug (above phase separation limit) may support the “particle-drifting” concept outlined in the introduction (**Equation 14**). In brief, due to differences in hydrodynamic radius of the colloidal objects between FaSSIF-V1$_{PBS}$ (**Figure 23**) and FeSSIF-V1$_{PBS}$ (**Figure 24**), the diffusion coefficient in the unstirred water layer is different and can be described by the Stokes-Einstein relationship (**Equation 8**). However the difference in flux (35-50%) is smaller than the difference between the diffusion coefficient of the biorelevant media colloids (up to 10 fold based on hydrodynamic diameters of around 70-90 nm for FaSSIF-V1$_{PBS}$ and around 6 nm for FeSSIF-V1$_{PBS}$). The resulting contribution to permeation, hence bioaccessibility, under excess drug condition is therefore also dependent on how much drug is associated to colloidal structures and how much colloids are present. Overall, the contribution of freely disolved drug can still be considered to dominate over the colloidal species impact on diffusive mass transport, simply because of the much larger molecular diffusivity. Further considerable would be for example, effects of the media itself on the unstirred water layer thickness or penetration depth of colloids or the diffusivity of drug in aqueous vs. lipidic environment. To be precise, bioaccessibility highly depends on the rate-limitation. For example, in a system where the membrane permeability is the dominating resistance (BCS III drug), no impact of colloids on flux via unstirred water layer diffusion would be expected.

DLS signal-noise-ratios are shown in **Figure 47**, clearly supporting that the separation efficiency was impaired in FeSSIF-V1$_{PBS}$ compared to both FaSSIF-V1$_{PBS}$ and FaSSIF-V2$_{PBS}$. Apart from a few outliers in FaSSIF-V1$_{PBS}$ showing higher signal-to-noise ratios compared to the majority of supernatants, the data is in great agreement with **Figure 34**. The mentioned outliers contained very low count rates (low amount of light scattered) and poor correlation, even when the reported signal-to-noise ratio was slightly elevated. For FeSSIF-V1$_{PBS}$, an increased variability was detected already for the reference media and filtrates containing drug, but even more pronounced for the fractions measured after ultracentrifugation. Values affected by vacuum issues with the ultracentrifugation were excluded. Those findings support the conclusion that colloidal separation is not feasible in FeSSIF-V1$_{PBS}$ media. Whether selective separation of some phases occurs would require further investigations.

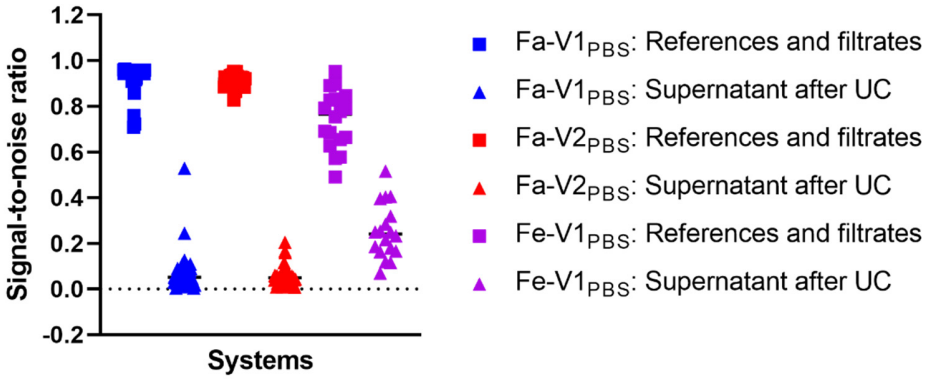

Figure 47: DLS scatter plot of signal-to-noise ratios of naporafenib in FaSSIF-V1$_{PBS}$, FaSSIF-V2$_{PBS}$ and FeSSIF-V1$_{PBS}$, divided into references and filtrates before ultracentrifugation (media before drug addition and filtrates after drug addition) and supernatants after ultracentrifugation treatment for both, the amorphous and crystalline systems (not differentiated). Data presented as individual measurements.

This series of experiments was also subjected to unspecific binding loss determination of drug to filter material, see **Table 9**. Only the centrifugal filters relevant to the donor concentration-time profile were analyzed here. The relative binding loss determined in FeSSIF-V1$_{PBS}$ was considered low compared to the fasted state media. However absolute loss may still be quite substantial using that medium and needs to be considered for judging the values.

*Table 9: Overview of the unspecific binding loss determined during the ultracentrifugation-flux combo experiment by re-filtering a filtrate of known concentration through 0.45 µm PVDF centrifugal filters using identical volumes to the initial filtration. Loss of drug concentration required to substantiate discrepancies between donor concentration-time profiles (**Figure 44**) and apparently dissolved drug levels from the ultracentrifugation-flux combo data (**Figure 45**). Data for FaSSIF-V1$_{PBS}$ at 100 rpm already presented in **Table 6** and included for reference. Unspecific binding loss presented as individual replicates in percentage of the initial drug concentration in the filtrate.*

Unspecific binding loss	FaSSIF-V1$_{PBS}$		FeSSIF-V1$_{PBS}$	
	100 rpm	400 rpm	100 rpm	400 rpm
Centrifugal filter, t=0	24.3%[a] 36.6%	24.4% 24.3%	3.8% 8.3%	8.5% 11.4%
Centrifugal filter, t=24h	-0.4%[b] 12.0/11.6%	13.3/~~78.5%~~[c] 13.9/13.5%	~~30.8~~[c]/-0.6%[b] 8.0/4.9%	6.0/10.0% 5.0/4.0%

[a]: inconsistency between technical replicates (some data excluded for calculation)

[b]: unexpected result due to higher concentration observed after filtration test

[c]: Turbid filtrate contained phase separated drug species

For consistency, the calculated free fractions for this experiment are reported in **Table 10**. The values for FaSSIF-V1$_{PBS}$ at 400 rpm are in range with the values at 100 rpm (t=0). The ratios for the FeSSIF-V1$_{PBS}$ media should not be interpreted as the separation efficiency was not considered sufficient, as discussed above.

*Table 10: Overview of the free fraction calculated as molecularly dissolved drug measured in the supernatant after ultracentrifugation divided by apparently dissolved drug measured after filtration. The ratio is visually reflected in **Figure 45**. Data for FaSSIF-V1$_{PBS}$ at 100 rpm already presented in **Table 7** and included for reference. Data provided as individual replicates.*

Free fraction (free/total)	FaSSIF-V1$_{PBS}$ At 100 and 400 rpm		FeSSIF-V1$_{PBS}$ At 100 and 400 rpm	
t=0	0.12 0.11	0.13 0.13	~~0.85~~[a] 0.18	0.13 ~~0.79~~[a]
t=24h	0.06 0.09/0.09	0.12/~~0.03~~[b] 0.13/0.13	~~0.17~~[b]/0.28 0.21/0.25	0.25/0.25 0.26/0.25

[a]: vacuum issues with ultracentrifugation

[b]: Turbid filtrate contained phase separated drug species

5.2.6 Context to the bioaccessibility concept

In order to assess factors that potentially influence naporafenib's bioaccessibility (see **section 3.4**), it was necessary to get a basic understanding of colloidal structures formed in biorelevant media. This was achieved through electron microscopy and dynamic light scattering (DLS). Since they are part of the solution phase, such structures were attributed to the liquid reservoir in the bioaccessibility concept. The possibility to separate colloidal structures through ultracentrifugation was explored and separation efficiency was evaluated based on DLS. Fasted state biorelevant media were selected to apply the separation protocol to amorphous and crystalline systems. The solid reservoir, independent whether amorphous or crystalline solids were present, did not impair the separation process. Insights into dose-dependent presence of drug species were subsequently linked to mass transport (flux) using dialysis and lipidic membranes. Flux increased linearly with media saturation. It was possible to show that below (amorphous) phase separation limit, the dissolved drug partitions between the aqueous phase and colloidal objects, thereby controlling the amount of free drug and its overall bioaccessibility. Only at saturation, both the amount of freely dissolved drug and drug in liquid reservoir are saturated. Adding more drug beyond this point triggers phase separation of naporafenib and solid reservoir forms. The saturation of freely dissolved drug was at the same level in FaSSIF-V1$_{PBS}$ and FaSSIF-V2$_{PBS}$ and is in agreement with the amorphous phase separation limit determined in blank buffer system (**Figure 18** and **Table 3**).

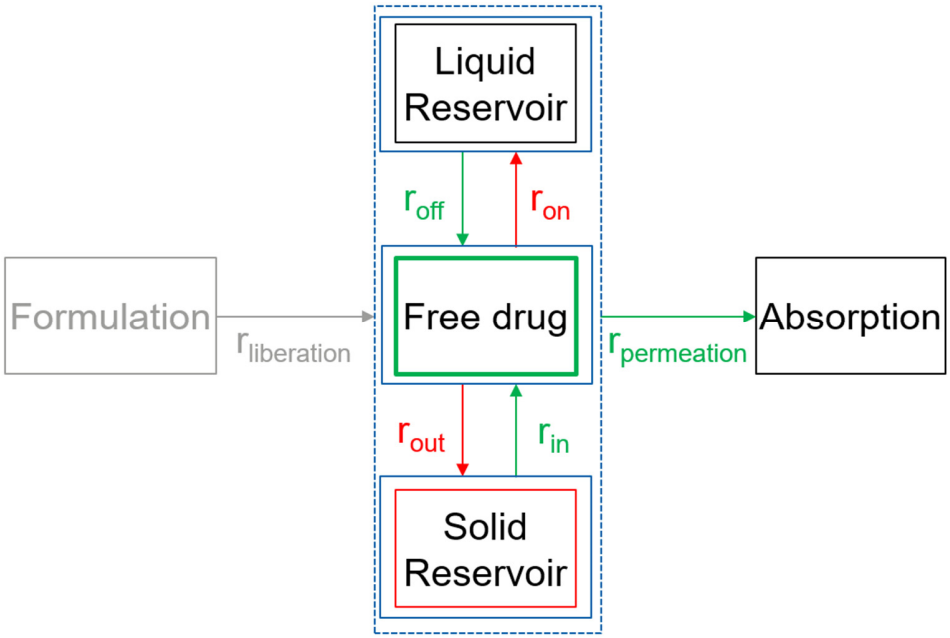

Figure 48: Illustration of the bioaccessibility concept in the context of methods to evaluate bioaccessibility with the dashed blue box representing a dynamic equilibrium between apparently dissolved drug (containing freely dissolved and drug in liquid reservoir) and undissolved drug in either amorphous or crystalline form.

Driving and inhibiting factors for membrane flux were identified. Adding more drug to the system up to the phase separation limit increased flux linearly and could be mainly related to the amount of freely dissolved drug based on Fick's law. At the phase separation limit, drug in liquid reservoir and freely dissolved drug appear saturated and flux is close to its maximum. To be precise, concentrations slightly above the phase separation limit are required in order to observe maximum flux. There has to be enough drug in form of a solid reservoir to replenish permeated amount of drug and keep the driving force for permeation (e.g. free drug) sufficiently long at saturation. Only under such conditions, linear and maximum flux in the acceptor compartment can be measured. Alongside this mechanism, phase separated drug species (solid reservoir) may also diffuse through the unstirred water layer (UWL) alongside freely dissolved and solubilized drug (liquid reservoir). The complexity of various processes running in parallel make quantitative interpretations difficult. Adding drug via solution form eliminates the relevance of the liberation rate ($r_{liberation}$) in the bioaccessibility concept and an equilibrium between the key drug species is formed practically immediately. Under excess drug conditions, freely dissolved drug was saturated (limited by aqueous solubility), drug in liquid reservoir was saturated (limited by media composition/colloidal structures) and the rest precipitated as phase separated amorphous solids (solid reservoir). During the course of flux, it was assumed that only free drug can permeate across the lipid layer barrier in this setup. Permeated drug was replenished by either liquid or solid reservoir, depending on the rate of release (r_{off}) or rate of dissolution (r_{in}), respectively, in the bioaccessibility concept. Both, r_{off} and r_{in} are considered drivers for permeation ($r_{permeation}$) while the rate of uptake into colloidal structures (r_{on}) and rate of precipitation/desupersaturation (r_{out}) are seen as inhibitors. As an example, under saturated and sub-saturated solution conditions, no solid reservoir was present and hence primarly r_{out} related to form conversion but not r_{in} related to dissolution contributed to flux. The kinetic processes r_{on} and r_{off} related to colloidal partitioning and release (liquid reservoir) impacted the flux below phase separation, alongside contribution of the diffusion processes of free drug and liquid reservoir. Finally, the *in vitro* rate-limitation for the lipidic membrane setup was investigated using two biorelevant media with different colloidal species at two different stirring speeds (hydrodynamic conditions). Despite the fact that both media were saturated, i.e. assuming equal free drug, and excess drug was present as amorphous solid reservoir, the observed flux between the two media was different and further increased by increasing the stirring speed. Changes by stirring were attributed to modification of the unstirred water layer thickness, supporting the hypothesis that the membrane flux of naporafenib in this setup is rate-limited by unstirred water layer diffusion. This was futher corroborated considering that the larger amount of small colloidal species in FeSSIF-V1$_{PBS}$ potentially contribute more to UWL diffusive transport compared to bigger but less colloids in FaSSIF-V1$_{PBS}$. As a main

determinant, the amount of freely dissolved drug is considered to drive the flux while its level is dictated by the solubility of the drug substance form as solid reservoir in equilibrium with the liquid phase. The maximum molecularly dissolved drug concentrations were already associated to the amorphous form (or tosylate salt) and possibly cannot be further increased.

5.3 Relevance of bioaccessibility for bioavailability

The factors influencing the bioaccessibility of naporafenib in the studied lipidic membrane flux setup were identified as amount of molecularly dissolved drug, diffusion of drug species through the unstirred water layer towards the membrane, and kinetic processes to replenish permeated drug from the solid and liquid reservoir. Depending on the relative speed of those processes (such as r_{off} or r_{in} relative to $r_{permeation}$), no impact on flux may be observed depending on the *in vitro* setup. Generally, the amount of molecularly dissolved drug is capped by the aqueous solubility of the respective drug form. In this section, it was explored how excipients can manipulate bioaccessibility and how such effects may translate into an *in vivo* setting (see **section 3.4**, **questions 3 and 4**).

The first section of results in this work studied solubility and dissolution rate. The second section connected solubility to permeation. This chapter will connect dissolution to solubility and solubility to permeation. Starting with solubility, the phase separation limit was assessed in presence of various excipients. Dialysis flux was used to complement the excipient selection based on phase separation limits. Two-step dissolution of the tosylate salt form in presence of selected excipients was performed to understand how fast the solubility limit can be achieved, related to the dissolution rate, including a stomach to intestine transition step. The impact of those excipients on bioaccessibility was further studied using the ultracentrifugation-flux combo assay. Finally, the *in vitro* to *in vivo* translation of bioaccessibility was investigated by correlating to *in vivo* exposures based on a pharmacokinetic study outcome in beagle dogs.

5.3.1 Phase separation limit in presence of excipients

The assessment of phase separation of naporafenib in $Buffer_{PBS}$ and $FaSSIF\text{-}V1_{PBS}$ with 1 mg/mL pre-dissolved excipient was studied and results are shown in **Figure 49**. The phase separation limit was not affected by Hydroxypropylcellulose (HPC), Hydroxypropylmethylcellulose (HPMC) nor Kollidon VA64 (VA64) and resembled the limit for the $Buffer_{PBS}$ and $FaSSIF\text{-}V1_{PBS}$ system in absence of excipients. In contrast to this, Eudragit EPO significantly increased the phase separation limit in the buffer system. In $FaSSIF\text{-}V1_{PBS}$, the limit was also increased but less than additive, suggesting non-synergistic effects between the polymer and the biorelevant components. Kolliphor RH40 (RH40) and sodium dodecyl sulfate (SDS) elevated the phase separation limit both in $Buffer_{PBS}$ and $FaSSIF\text{-}V1_{PBS}$ compared to without excipients. Interestingly, the limit appeared slightly lower with SDS in $FaSSIF\text{-}V1_{PBS}$ compared to SDS in $Buffer_{PBS}$.

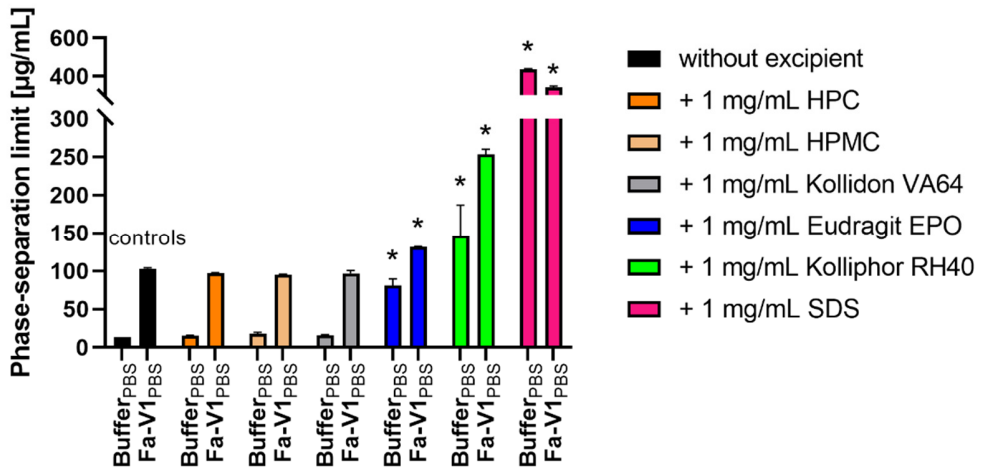

*Figure 49: Determination of apparent phase separation limits of naporafenib solution form (DMSO) by UV titration in FaSSIF-V1$_{PBS}$ and Buffer$_{PBS}$ with 1 mg/mL pre-dissolved excipient, respectively. Data in absence of excipients in FaSSIF-V1$_{PBS}$ and Buffer$_{PBS}$ already presented in **Figure 18** and included as controls. Data presented as mean +/- standard deviation of triplicates. Statistical significance ($\alpha = 0.05$) compared to Buffer$_{PBS}$ or FaSSIF-V1$_{PBS}$ as control respectively, is indicated by an asterisk (*) and was assessed using two separate one-way ANOVAs for each medium with post-hoc Dunnet's test for multiple comparison to the respective control medium in absence of excipients. Analysis was performed with statistics tools in GraphPad Prism Version 9.3.1. Data was provided by J. Schlauersbach.*

5.3.2 Excipient impact on dialysis flux

To evaluate for a potential benefit from the excipients on permeation, phase separation limits were complemented by dialysis flux. **Figure 50** shows dialysis flux in Buffer$_{PBS}$ and FaSSIF-V1$_{PBS}$ with 1 mg/mL pre-dissolved excipient under excess drug conditions. Flux in absence of excipients was included for reference. The values obtained were found to be in a similar range as in **Figure 36**, and about 100-fold lower than lipidic flux values. Overall, dialysis flux under excess drug conditions did not show much differences with respect to presence of excipients. It was speculated whether the presence of phase separated amorphous drug species may mask the effects of excipients on dialysis flux. This could be related to the low transport observed through this regenerated cellulose barrier in combination with relatively fast dissolution kinetics (r_{in}) of the phase separated drug to replenish permeated drug. The decision was made to re-evaluate the excipient impact on dialysis flux at 50% saturation, relative to the determined phase separation limit in the respective media (based on **Figure 49**). The results are shown in **Figure 51**. As expected, the flux was about half as under excess drug conditions and the excipients impact on dialysis mass transport was slightly more differentiated in absence of phase separated drug species.

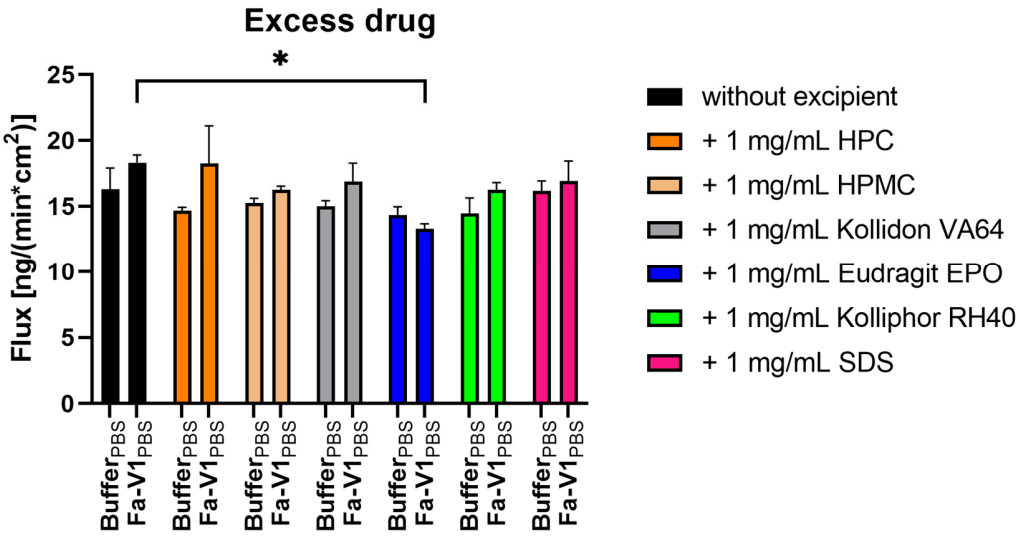

Figure 50: Flux of naporafenib solution form (DMSO) through regenerated cellulose size-exclusion (dialysis) membrane under excess drug (1 mg/mL) conditions in FaSSIF-V1$_{PBS}$ and Buffer$_{PBS}$ in presence of 1 mg/mL excipients, respectively. Data presented as mean +/- standard deviation of triplicates. Statistical significance (α = 0.05) compared to Buffer$_{PBS}$ or FaSSIF-V1$_{PBS}$ as control, respectively, is indicated by an asterisk (*) and was assessed using two separate one-way ANOVAs for each medium with post-hoc Dunnet's test for multiple comparison to the respective control media in absence of excipients. Analysis was performed with statistics tools in GraphPad Prism Version 9.3.1. Data was provided by J. Schlauersbach.

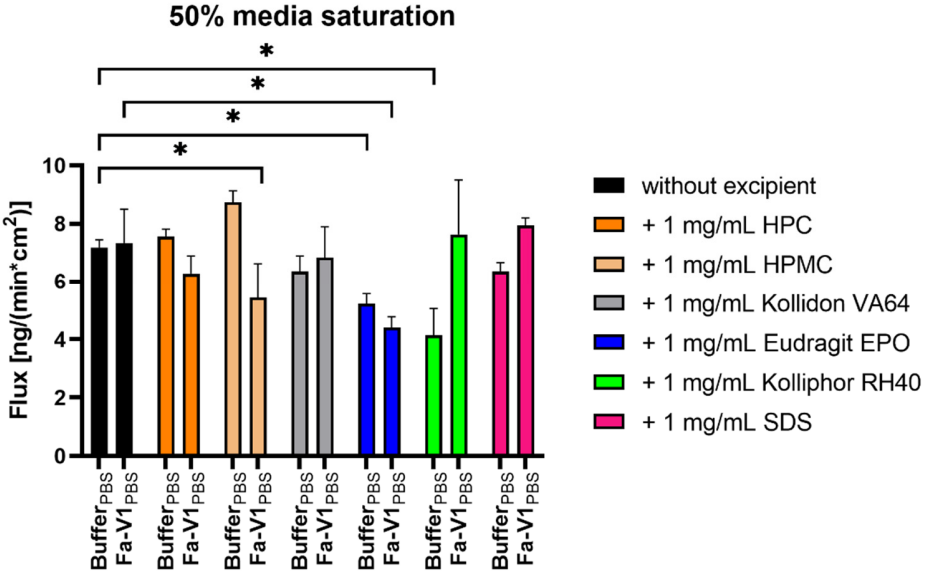

*Figure 51: Flux of naporafenib solution form (DMSO) through regenerated cellulose size-exclusion (dialysis) membrane at 50% of the respective phase separation limit (**Figure 49**) in FaSSIF-V1$_{PBS}$ and Buffer$_{PBS}$ in presence of excipients, respectively. Data presented as mean +/- standard deviation of triplicates. Statistical significance (α = 0.05) compared to Buffer$_{PBS}$ or FaSSIF-V1$_{PBS}$ as control, respectively, is indicated by an asterisk (*) and was assessed using two separate one-way ANOVAs for each medium with post-hoc Dunnet's test for multiple comparison to the respective control media in absence of excipients. Analysis was performed with statistics tools in GraphPad Prism Version 9.3.1. Data was provided by J. Schlauersbach.*

Most dialysis flux values were still very close to the control without excipients. A trend was observed for HPC, HPMC and Eudragit EPO that the flux was reduced in FaSSIF-V1$_{PBS}$ compared to Buffer$_{PBS}$. A slight opposite trend of increased flux in biorelevant media compared to Buffer$_{PBS}$ was seen for RH40 and SDS. Flux in presence of VA64 was about equal to without excipient. Interestingly, the pronounced impact of SDS on the phase separation limit (see **Figure 49**) did not materialize in terms of dialysis flux. In a similar way, the positive impact of Eudragit EPO on phase separation had just a slightly negative effect on dialysis flux, both at excess drug condition and 50% saturation. Flux with RH40 was only reduced in Buffer$_{PBS}$ at 50% saturation and else about equal compared to the absence of excipients. As the low dialysis flux values were not substantially altered through excipient presence, further statistical interpretation can be neglected.

5.3.3 Nuclear magnetic resonance spectroscopy with selected excipients

To shine light on discrepancies found between the impact of excipients on dissolved drug concentrations and the availability for permeation, ^{1}H-NMR was used to investigate molecular interactions in such drug-excipient systems. **Figure 52** shows aromatic drug proton signals of naporafenib in Buffer$_{PBS}$ and FaSSIF-V1$_{PBS}$ in absence and presence of the excipients, HPC (representative for HPMC and VA64), EPO, and RH40 (assumed representative of SDS). In agreement with the impact on the phase separation limit and flux, HPC did not substantially alter the drug signals observed in NMR. In contrast, Eudragit EPO appeared to reduce/eliminate the aromatic drug proton signals. This may resolve the discrepancy between elevated drug in solution but slightly reduced dialysis flux. Reduced NMR signals may indicate that molecular mobility (tumbling) is negatively affected by a strong interaction in solution. This leads to the hypothesis that Eudragit EPO could form complexes in solution with naporafenib, thereby increasing the apparent phase separation limit but reducing the drug's availability to permeate. Kolliphor RH40 showed increased drug proton signals, in line with the effect on the phase separation limit.

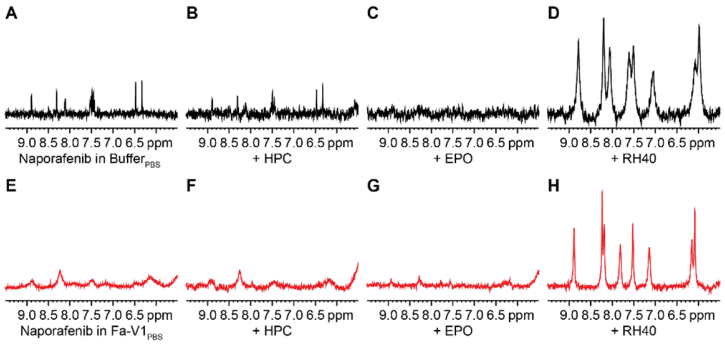

*Figure 52: Aromatic proton region of the ^{1}H-NMR spectra of naporafenib in Buffer$_{PBS}$ (A-D) and FaSSIF-V1$_{PBS}$ (E-H) in presence of 1 mg/mL excipients: Hydroxypropylcellulose (HPC, B,F), Eudragit EPO (EPO, C, G) and Kolliphor RH40 (RH40, D, H). Data in absence of excipients (A, E) already presented in **Figure 20** and included for reference. Scaling is equal among the spectra. Figure provided by J. Schlauersbach.*

5.3.4 Two-step dissolution with selected excipients

The excipient selection based on phase separation limits and dialysis flux was narrowed down to a few selected cases for further investigation. HPC was selected as potential precipitation inhibitor, not disturbing the biorelevant media system nor altering the molecular mobility of the drug to a large degree, based on ^{1}H-NMR. Biorelevant components were considered highly relevant to the solution behavior of naporafenib based on previous sections. Eudragit EPO was included as it was capable to increase dissolved amount of naporafenib, potentially even stabilize the drug regarding form conversion but with suspected negative impact on permeation. Kolliphor RH40 was of interest because of its ability to provide an environment for drug solubilization, potentially even larger compared to Eudragit EPO in both Buffer$_{PBS}$ and FaSSIF-V1$_{PBS}$. SDS was not selected due to a suspected non-synergistic interaction with the SIF components based on **Figure 49**. In other words, HPC was considered a non-SIF interacting excipient and reference, while RH40 was considered cooperative with respect to biorelevant media components. Eudragit EPO was included to verify the hypothesis that complexation may increase dissolved drug concentrations but in turn reduce bioaccessibility.

Since a crucial process after drug liberation from the formulation is dissolution, a two-step dissolution assay was performed with the tosylate form of naporafenib in absence and presence of selected excipients. Obviously, the solution form (via DMSO stock solution) was considered not suitable to assess the effect of excipients on dissolution rate. **Figure 53** shows the concentration-time profile of the two-step dissolution assay with the dashed line indicating the FaSSGF to FaSSIF-V1$_{PBS}$ transition step.

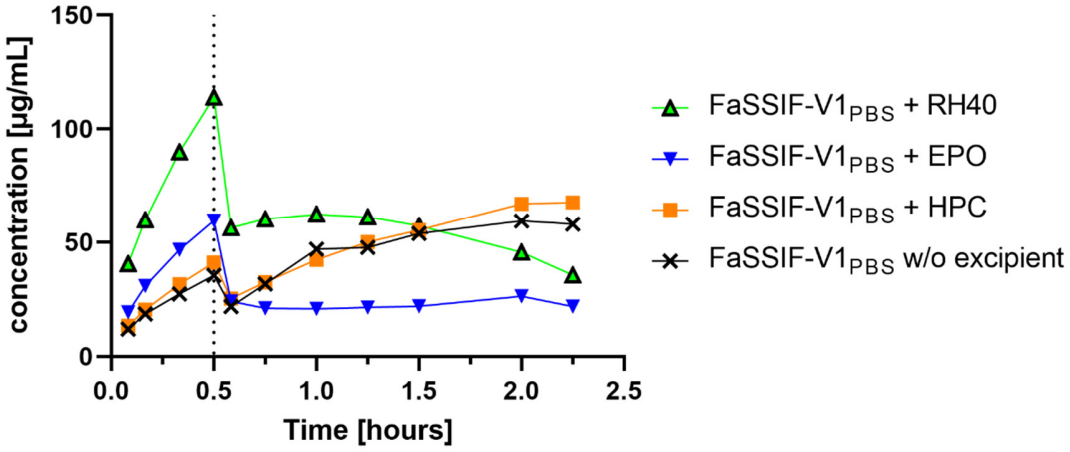

Figure 53: Two-step dissolution profile of naporafenib tosylate salt form in absence and presence of 1 mg/mL pre-dissolved excipients. The dotted line at 0.5 hours indicates the FaSSGF to FaSSIF-V1$_{PBS}$ transition step. Data points were artificially connected and presented as average of duplicates. Data was provided by S. Juanes.

Kolliphor RH40 increased the dissolution rate compared to without excipient in the gastric phase but showed a transient concentration plateau after the media switch with declining concentrations over time in FaSSIF-V1$_{PBS}$. Eudragit EPO also slightly elevated the dissolution rate in the gastric phase compared to no excipient but caused a large drop in dissolved drug concentrations in FaSSIF-V1$_{PBS}$, resulting in concentrations lower than expected from the phase separation assessment. The concentration levels achieved were even lower compared to FaSSIF-V1$_{PBS}$ without excipients, indicating that the polymer affected the colloidal systems from the biorelevant medium. The addition of Hydroxypropylcellulose resulted in a similar concentration-time profile as in absence of excipients.

5.3.5 Influence of excipients on bioaccessibility

To assess the effect of selected excipients on the bioaccessiblity of naporafenib, the ultracentrifugation-flux combo experiment was performed with the lipidic membrane as permeation barrier. **Figure 54** shows the concentration-time profile in the donor and acceptor compartment for FaSSIF-V1$_{PBS}$ and Buffer$_{PBS}$, each with 1 mg/mL pre-dissolved HPC and compares it to the condition without excipient. Buffer$_{PBS}$ in absence of excipients was not tested here due to expected fast form conversion from amorphous to crystalline, associated with desupersaturation (see **Figure 17**).

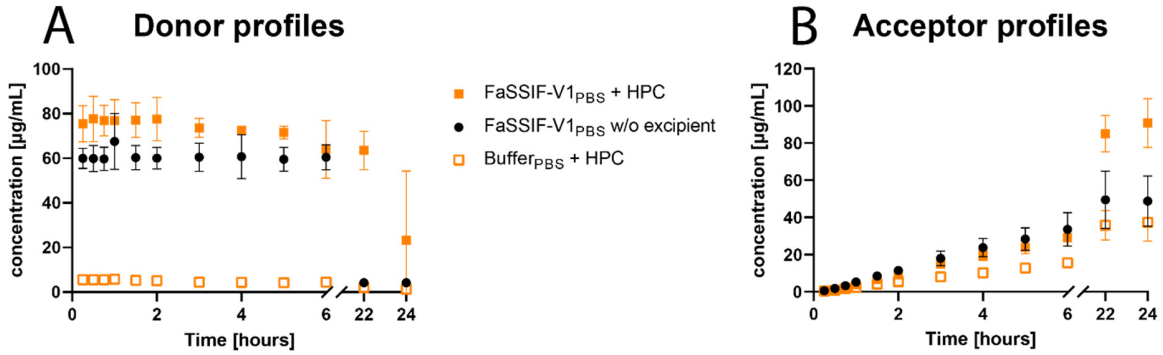

*Figure 54: Concentration-time profiles of excess naporafenib in A) FaSSIF-V1$_{PBS}$ and Buffer$_{PBS}$ with pre-dissolved 1 mg/mL HPC, respectively in the donor and B) resulting mass transport as cumulative concentrations in acceptor sink buffer in the acceptor compartment. Nominal donor input was 1 mg/mL drug via solution form (DMSO) considered excess drug conditions. Data provided as mean +/- standard deviation of quadruplicates. Data in FaSSIF-V1$_{PBS}$ without excipients already presented in **Figure 37** and included for reference. Error bars are in some cases smaller than symbols.*

Donor concentrations were found to be very low in the buffer system supplemented with HPC while concentrations in FaSSIF-V1$_{PBS}$ with or without HPC were comparable. This large difference in concentration (> 5-fold) between the buffer and biorelevant media systems did not translate into large flux differences. Flux in FaSSIF-V1$_{PBS}$ was comparable with and without excipient, potentially slightly reduced in presence of HPC as will be discussed later. The buffer system showed roughly

half the flux. Noteworthy, the 22 and 24 hour acceptor concentrations appeared higher in presence of HPC with the underlying hypothesis that HPC may have delayed the form conversion of naporafenib and associated desupersaturation, resulting in more mass transfer over 24 hours.

Figure 55 provides the results from similar experiment but with Eudragit EPO as excipient. It can be clearly seen that this excipient does not affect the bioaccessibility of naporafenib to the same degree in $Buffer_{PBS}$ as in FaSSIF-V1$_{PBS}$. In $Buffer_{PBS}$, dissolved drug concentrations in the donor were increasing over time until a sudden crash at about 3 hours. In contrast, EPO in FaSSIF-V1$_{PBS}$ showed very low dissolved amount of drug already from the beginning and most importantly, the concentrations were apparently lower than in FaSSIF-V1$_{PBS}$ without excipient. This may hint towards incompatibility of this excipient with (some) biorelevant media components. Comparing to flux in absence of polymer, the flux from $Buffer_{PBS}$ + Eudragit EPO was lower, but more importantly the flux from Eudragit EPO in the biorelevant medium was the lowest.

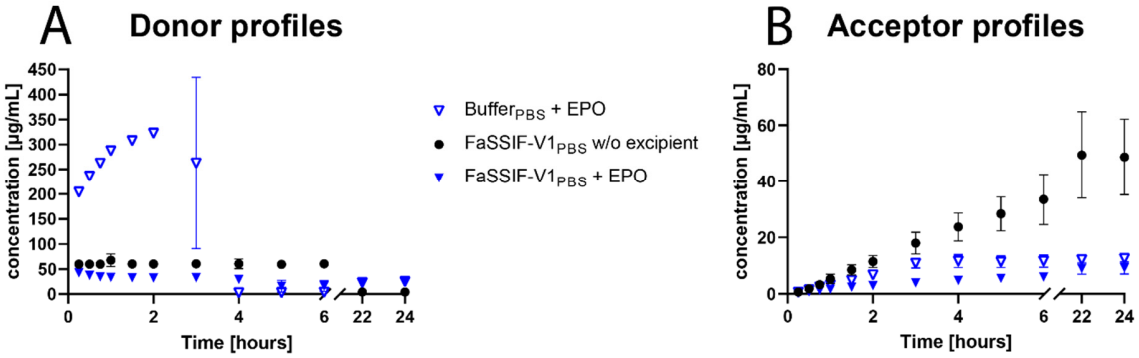

*Figure 55: Concentration-time profiles of excess naporafenib in A) FaSSIF-V1$_{PBS}$ and $Buffer_{PBS}$ with pre-dissolved 1 mg/mL Eudragit EPO, respectively in the donor and B) resulting mass transport as cumulative concentrations in acceptor sink buffer in the acceptor compartment. Nominal donor input was 1 mg/mL drug via solution form (DMSO) considered excess drug conditions. Data provided as mean +/- standard deviation of quadruplicates. Data in FaSSIF-V1$_{PBS}$ without excipients already presented in **Figure 37** and included for reference. Error bars are in some cases smaller than symbols.*

The third excipient explored in this setup was Kolliphor RH40 and results are provided in **Figure 56**. The donor profiles were quite similar in buffer and biorelevant media in presence of RH40 but different to the condition without excipient. In both systems containing RH40, after an elevated concentration peak, a sudden drop in dissolved drug was observed between 1 and 2 hours, potentially earlier in the $Buffer_{PBS}$ system. The cumulative acceptor concentrations were flattening around the same time. It can be speculated that the difference in acceptor concentrations between FaSSIF-V1$_{PBS}$ and $Buffer_{PBS}$ with RH40 may be attributed to a time difference when form conversion and desupersaturation occured. Whether the increased donor concentrations at the beginning resulted in initially higher flux compared to FaSSIF-V1$_{PBS}$ without excipient will be discussed later in this section.

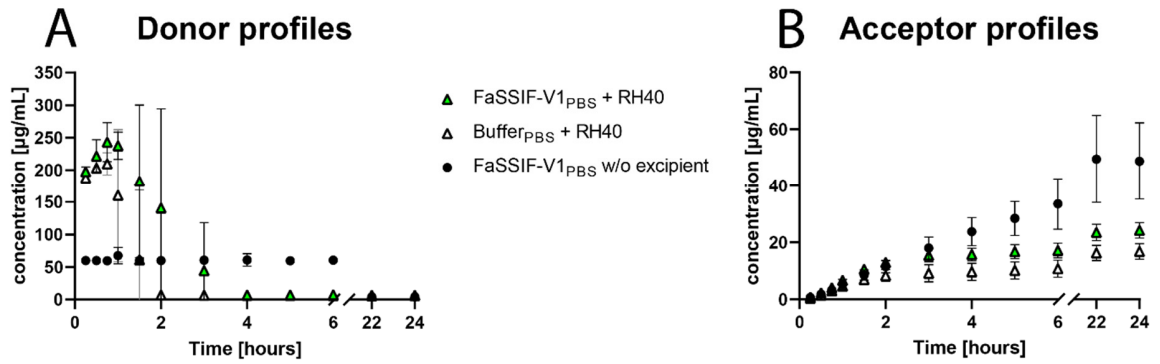

*Figure 56: Concentration-time profiles of excess naporafenib in A) FaSSIF-V1$_{PBS}$ and Buffer$_{PBS}$ with pre-dissolved 1 mg/mL Kolliphor RH40, respectively in the donor and B) resulting mass transport as cumulative concentrations in acceptor sink buffer in the acceptor compartment. Nominal donor input was 1 mg/mL drug via solution form (DMSO) considered excess drug conditions. Data provided as mean +/- standard deviation of quadruplicates. Data in FaSSIF-V1$_{PBS}$ without excipients already presented in **Figure 37** and included for reference. Error bars are in some cases smaller than symbols.*

The ultracentrifugation-flux combo data for FaSSIF-V1$_{PBS}$ with Hydroxypropylcellulose (**Figure 54**), Eudragit EPO (**Figure 55**) and Kolliphor RH40 (**Figure 56**) are shown in **Figure 57**. Some issues with the ultracentrifugation equipment were encountered and the affected data are marked in grey and should not be interpreted. The amount of molecularly dissolved drug in FaSSIF-V1$_{PBS}$ with HPC as well as EPO were surprisingly robust and comparable to previously obtained values of about 10 µg/mL at early time points. Furthermore, the 24 hour values for free drug were found slightly elevated in presence of EPO. The values measured in presence of RH40 at early time points (t=0 and t=1h) were found increased compared to the expectation up to about 30 µg/mL.

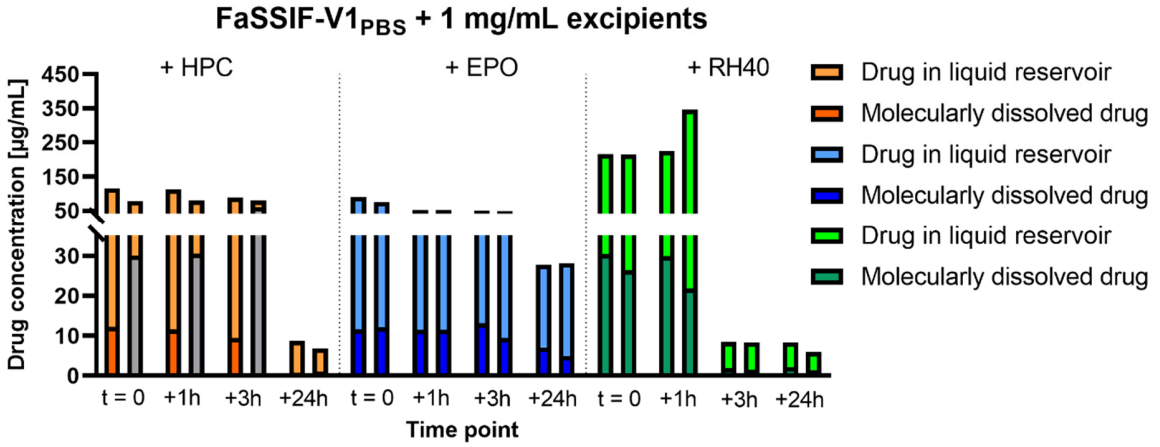

*Figure 57: Ultracentrifugation-flux combo data for excess naporafenib in FaSSIF-V1$_{PBS}$ + 1 mg/mL pre-dissolved excipients. Data presented as bar plots over time (relative to the flux experiment, **Figure 54**, **Figure 55** and **Figure 56**), differentiating between molecularly dissolved drug and drug in liquid reservoir. Liquid reservoir calculated from total apparently dissolved drug measured after filtration minus molecularly dissolved drug estimated by ultracentrifugation. Data presented as individual replicates. Grey bars indicate issues with the experimental protocol.*

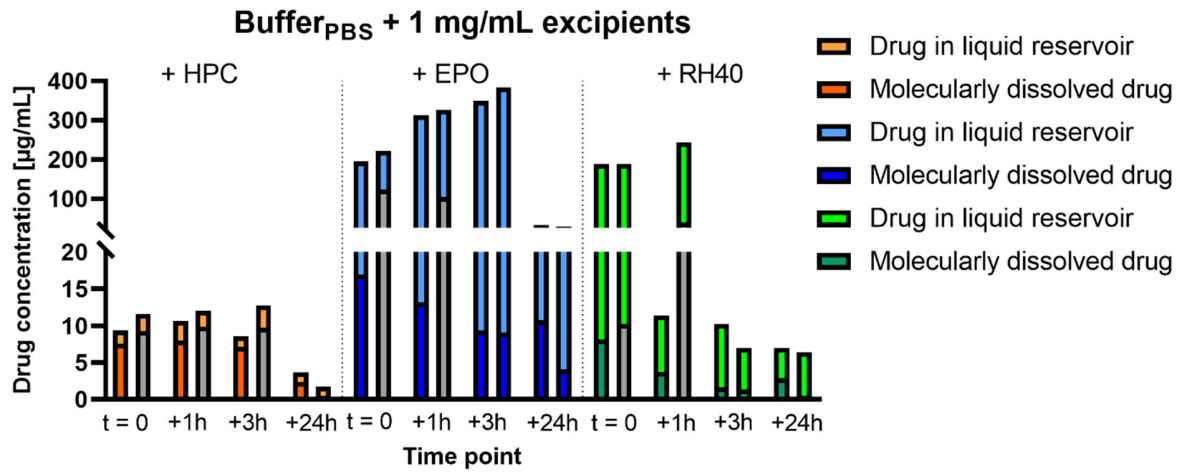

*Figure 58: Ultracentrifugation-flux combo data for excess naporafenib in Buffer$_{PBS}$ + 1 mg/mL pre-dissolved excipients. Data presented as bar plots over time (relative to the flux experiment, **Figure 54**, **Figure 55** and **Figure 56**), differentiating between molecularly dissolved drug and drug in liquid reservoir. Liquid reservoir calculated from total apparently dissolved drug measured after filtration minus molecularly dissolved drug estimated by ultracentrifugation. Data presented as individual replicates. Grey bars indicate issues with the experimental protocol.*

Excipients may also form colloidal structures or aggregates on their own based on DLS. The ultracentrifugation-flux combo data for the Buffer$_{PBS}$ system in presence of HPC, EPO and RH40 are shown in **Figure 58**. The difference between the amount measured after filtration and after ultracentrifugation either reflects drug that was associated to some sort of soluble aggregate that could be separated by ultracentrifugation or may also reflect unspecific binding loss to the materials involved in the ultracentrifugation protocol. The difference was reported as drug in liquid reservoir but such effects could not be differentiated. The obtained results, therefore, have to be interpreted with caution. Buffer$_{PBS}$ + HPC was found to result in very similar values after filtration and ultracentrifugation which were only slightly lower than from the FaSSIF-V1$_{PBS}$ + HPC system. Eudragit EPO showed more variable values, possibly due to the dynamic concentration-time profile observed in the donor. The amount apparently dissolved drug (free + liquid reservoir) increased until 3 hours and then declined, but with comparably high residual dissolved drug at 24 hours. In agreement with **Figure 57**, molecularly dissolved drug at 24 hours indicated that the form has not fully converted into the crystalline monohydrate form. In presence of Kolliphor RH40, the amount of freely dissolved drug was determined in a similar range as in the Buffer$_{PBS}$ + HPC system but were less consistent and a faster decline over time could be suspected.

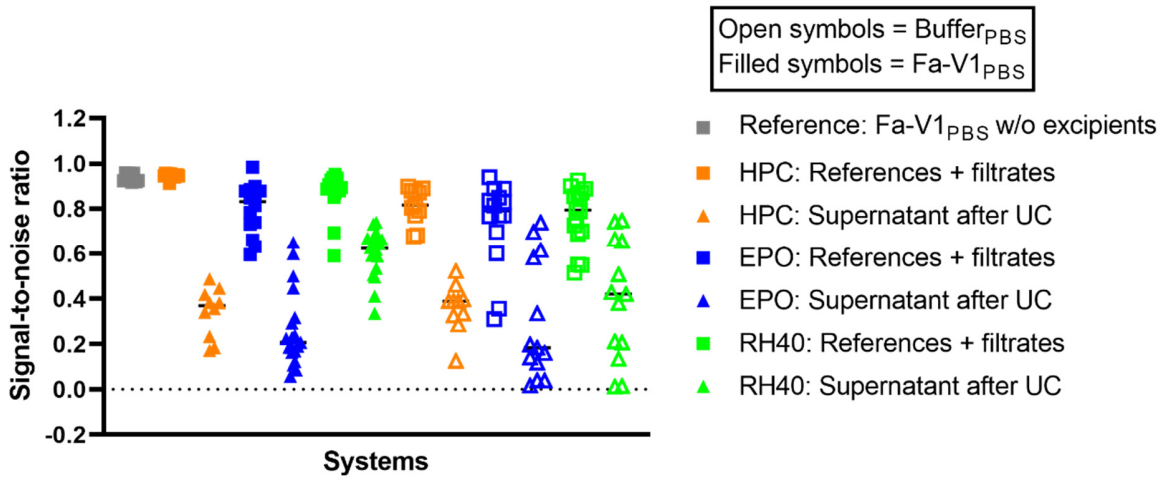

Figure 59: DLS scatter plot of signal-to-noise ratios of naporafenib in FaSSIF-V1$_{PBS}$ and Buffer$_{PBS}$ in presence of various excipients, divided into references and filtrates before ultracentrifugation (media before drug addition and filtrates after drug addition) and supernatants measured after ultracentrifugation treatment for both, the amorphous and crystalline systems (not differentiated). Data presented as individual measurements.

DLS signal-to-noise ratios measured in the supernatants after ultracentrifugation of the Buffer$_{PBS}$ and FaSSIF-V1$_{PBS}$ systems containing excipients are depicted in **Figure 59**. Biased values due to vacuum issues encountered with the ultracentrifugation were excluded. A high and reproducable signal-to-noise ratio was observed for FaSSIF-V1$_{PBS}$ without excipients and with 1 mg/mL HPC. The ratio was slightly reduced and/or more variable when Eudragit EPO or Kolliphor RH40 were dissolved in FaSSIF-V1$_{PBS}$. All excipients showed slightly more variable signal-to-noise ratios in the Buffer$_{PBS}$ system which would be expected based on the overall lower amount of light scattered in absence of biorelevant media colloids. It can be seen that the supernatants for both, the FaSSIF-V1$_{PBS}$ and Buffer$_{PBS}$ system in presence of those excipients show larger variations in comparison to without excipients, see **Figure 34** and **Figure 47**. The separation efficiency was similarly weak as for the FeSSIF-V1$_{PBS}$ system and, therefore, confidence to remove all colloidal structures affecting drug concentrations of naporafenib by ultracentrifugation was low. Despite the fact that the concentrations measured in supernatants were largely in range of expectation, no claim should be made that those values represent only moleculary dissolved drug.

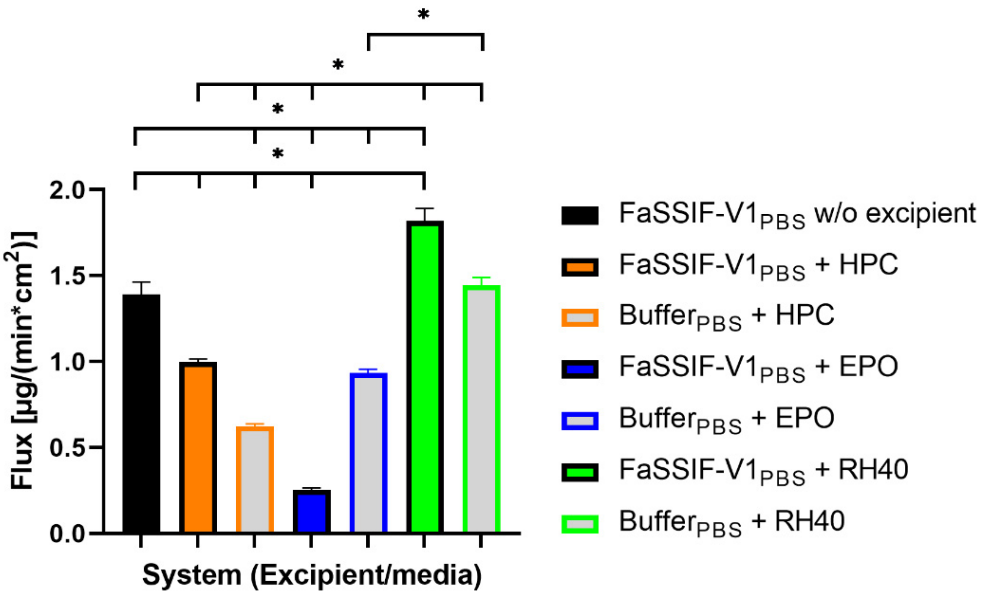

*Figure 60: Overview of surface-normalized flux of naporafenib in FaSSIF-V1$_{PBS}$ and Buffer$_{PBS}$ with 1 mg/mL pre-dissolved excipients, respectively. Slopes derived from **Figure 54**, **Figure 55** and **Figure 56**. Data in FaSSIF-V1$_{PBS}$ without excipient already presented in **Figure 43** and included as control. Data provided as mean +/- standard deviation of quadruplicates. Statistical significance (α = 0.05) was assessed using a one-way ANOVA with post-hoc Tuckey's test for multiple comparison and is indicated by an asterisk (*). Analysis performed with GraphPad Prism Version 9.3.1.*

Derived surface-normalized flux values are visualized in **Figure 60** and tabulated in **Table 11**. Flux in FaSSIF-V1$_{PBS}$ without excipients was already shown in **section 5.2** and was included for reference. All values were generated at 100 rpm stirring speed under excess drug condition, i.e. 1 mg/mL drug equivalent. The flux slopes were derived as stated in the materials and methods section based on the donor profile and subsequently normalized for liquid volumes and membrane surface area. Flux in presence of HPC was reduced in both, the FaSSIF-V1$_{PBS}$ and Buffer$_{PBS}$ system compared to without excipient. The lowest flux was observed for Eudragit EPO in FaSSIF-V1$_{PBS}$ while the flux from Buffer$_{PBS}$ + EPO was higher and comparable to the flux from FaSSIF-V1$_{PBS}$ + HPC. Interestingly, Buffer$_{PBS}$ supplemented with Kolliphor RH40 resulted in a similar flux as when buffer was supplemented with biorelevant media components (fasted state). The highest flux was observed in FaSSIF-V1$_{PBS}$ + RH40 but this flux rapidly declined after roughly 1 hour, in line with the decay of dissolved drug concentrations in the donor compartment. The reduced flux with HPC was not suspected to be related to dissolved donor concentrations but rather effects on unstirred water layer diffusion, viscosity-related. Bile components contained in FaSSIF-V1$_{PBS}$ showed a positive contribution in presence of HPC on permeation. Increased flux in presence of Kolliphor RH40 could be attributed to possible formation of mixed SIF-excipient colloids which increased apparently dissolved drug and may have served as "shuttles" across the unstirred water layer resulting in more drug being delivered directly to the membrane surface. It was not possible

to answer whether separate Kolliphor RH40 colloids co-exist alongside biorelevant media structures or whether mixed supramolecular aggregates were formed. Also, a direct interaction between those colloids and the membrane could not be exluded, e.g. direct delivery of drug from the colloidal environment into the membrane. Due to the impaired confidence of colloid separation using ultracentrifugation based on DLS, it was not possible to verify an increased amount of molecularly dissolved drug in the case of FaSSIF-V1$_{PBS}$ + RH40 that could enhance the flux. Furthermore, no indications based on dialysis flux supporting this view were observed, see **Figure 50** and **Figure 51**. The substantial reduction of flux in the FaSSIF-V1$_{PBS}$ + Eudragit EPO system (**Figure 55**) was in great contrast with the ultracentrifugation-flux combo data (**Figure 57**) showing comparable amounts of molecularly dissolved drug as in presence of HPC or in absence of excipients. Due to already discussed uncertainties in free drug values, no further interpretations should be made. In addition, the higher donor concentrations in the Buffer$_{PBS}$ + EPO system observed within the first 2 hours did still result in a lower flux compared to without excipients. Together with NMR insights, the observations from dialysis flux and phase separation limit determination, the hypothesis is made that this excipient seems to be able to stabilize large amounts of naporafenib in solution via the formation of soluble drug-excipient complexes, but in turn reduces the drug's availability to permeate, i.e. bioaccessibility. Similar observations were made with other basic drugs and this polymer, confirming a discrepancy between *in vitro* solubilization and *in vivo* exposures (142). It was of great interest to verify potential effects *in vivo*, for example, a sustained release mechanism and/or stabilization of the amorphous drug form. It was decided to test HPC, EPO and RH40 as representative excipients *in vivo*.

*Table 11: Table format of **Figure 60** including R^2 values for the linear fit of the cumulative acceptor concentrations based on the donor profiles. Flux slope provided as mean with standard deviation in brackets of quadruplicates.*

System (Media, excipient)	Flux slope [µg/(min*cm^2)]	R^2
FaSSIF-V1$_{PBS}$ + Eudragit EPO	0.25 (0.01)	0.9275
Buffer$_{PBS}$ + Hydroxypropylcellulose	0.62 (0.01)	0.9823
Buffer$_{PBS}$ + Eudragit EPO	0.93 (0.02)	0.9862
FaSSIF-V1$_{PBS}$ + Hydroxypropylcellulose	1.00 (0.02)	0.9876
Buffer$_{PBS}$ + Kolliphor RH40	1.44 (0.05)	0.9852
FaSSIF-V1$_{PBS}$ + Kolliphor RH40	1.82 (0.07)	0.9697

The inclusion of excipients required to control experimental parameters such as final pH at the end of experiments or confirming final drug form by XRPD, similar as was done in the first section of results regarding form selection. An overview is provided in **Table 12**. It can be seen that pH was slightly increased when using the basic polymer Eudragit EPO. Generally, the crystalline monohydrate form was detectable at the end of the experiments, under all conditions. However, it has to be noted that some drying processes could not be excluded between residual solids retrieval, preparation of the XRPD holder and the effective measurement. It was also not possible to quantify relative amounts of amorphous and crystalline material. Whenever crystalline peaks corresponding to the monohydrate form were detected, they are reported as such. If the sample showed very poor crystalline peaks it was stated as traces of crystalline monohydrate.

*Table 12: Overview of experimental control parameter (**Figure 54-Figure 58**) pH and final drug form at the end of the experiments. XRPD analysis based on references provided in **Figure 15**. Only three XRPD replicates were available for Eudragit EPO and Kolliphor RH40 in FaSSIF-V1$_{PBS}$ due to preparation issues.*

Experimental control	**1 mg/mL Naporafenib in FaSSIF-V1$_{PBS}$ + 1 mg/mL excipient pre-dissolved**			**1 mg/mL Naporafenib in Buffer$_{PBS}$ + 1 mg/mL excipient pre-dissolved**		
Excipient	**HPC**	**Eudragit EPO**	**Kolliphor RH40**	**HPC**	**Eudragit EPO**	**Kolliphor RH40**
Final pH	6.53 6.54 6.60 6.52	6.85 6.87 6.98 6.97	6.48 6.48 6.57 6.57	6.54 6.54 6.62 6.66	6.92 6.93 6.93 6.93	6.50 6.45 6.55 6.57
Final form (by XRPD)	Monohydrate and amorphous	Traces of Monohydrate and amorphous	Monohydrate	Monohydrate and amorphous	Monohydrate and amorphous	Monohydrate and amorphous

The appearance of residual solids retrieved from the donor compartments at the end of the experiment with Eudragit EPO and Kolliphor RH40 in FaSSIF-V1$_{PBS}$ is exemplified in **Figure 61**. The drug phases appeared substantially different. A “chewing gum-like” phase was observed in presence of EPO, while with RH40 crystalline drug phases were clearly visible. This impression complements the XRPD results provided in **Table 12** and indicate that the majority of solids with Eudragit EPO were still amorphous at the end of the experiment. The presence of crystalline monohydrate, or traces thereof, in FaSSIF-V1$_{PBS}$ + EPO measured with XRPD could reflect partial recrystallization due to a drying process on the surface of those phases. This phase-behavior in presence of Eudragit EPO was consistent between replicates.

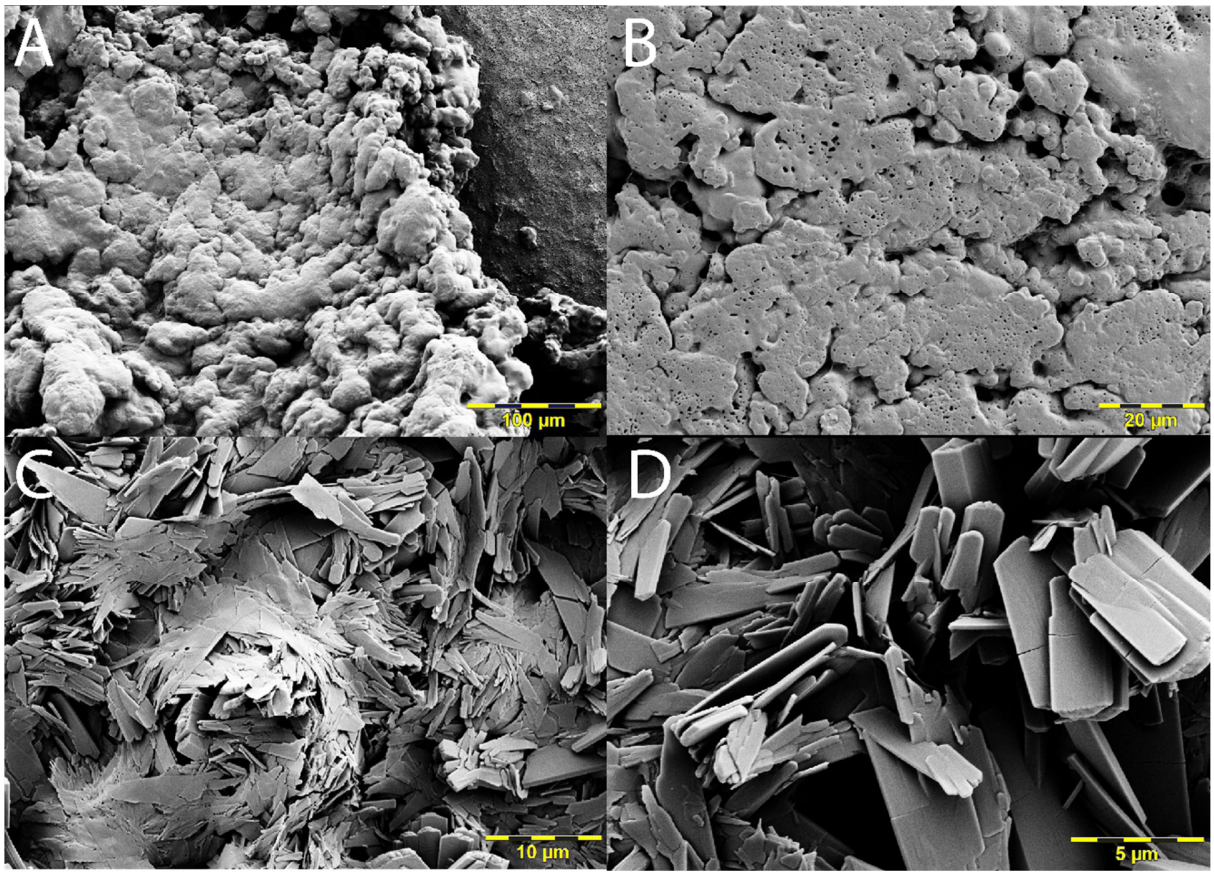

Figure 61: Scanning electron microscopy of residual naporafenib solids retrieved from the donor compartment at the end of the ultracentrifugation-flux combo experiment for Eudragit EPO (A, B) and Kolliphor RH40 (C, D) in FaSSIF-V1$_{PBS}$, respectively. Images were provided by M. Dehlinger.

The unspecific binding loss to the filter materials was also determined for FaSSIF-V1$_{PBS}$ and Buffer$_{PBS}$ systems in presence of excipients and is given in **Table 13**. Consistently, the loss to syringe filters was less than the loss to the centrifugal filters, in line with previous observations and likely due to differences in liquid volumes. Overall, the binding loss was found comparable to the condition without excipients in FaSSIF-V1$_{PBS}$ with up to about 30% (compare to **Table 6**). Surprisingly, a very pronounced material loss was observed for the Buffer$_{PBS}$ + HPC system during the kinetic concentration plateau with > 70% measured binding loss to the centrifugal filters.

The calculated free fractions are reported in **Table 14** for completeness but were not further interpreted due to the impaired confidence regarding the separation efficiency (see **Figure 59**) and ultracentrifugation issues for some runs. In addition, the dynamic behavior observed in presence of Kolliphor RH40 and Eudragit EPO make mechanistic interpretations even more difficult.

*Table 13: Overview of the unspecific binding loss determined during the ultracentrifugation-flux combo experiment by re-filtering a filtrate of known concentration through either 0.45 µm PTFE syringe filters or 0.45 µm PVDF centrifugal filters using identical volumes to the initial filtration. Loss of drug concentration required to substantiate discrepancies between donor concentration-time profiles (**Figure 54, Figure 55** and **Figure 56**) and apparently dissolved drug levels from the ultracentrifugation-flux combo data (**Figure 57** and **Figure 58**). Unspecific binding loss shown as individual replicates as percentage of the initial drug concentration in the filtrate.*

Unspecific binding loss	**1 mg/mL Naporafenib in FaSSIF-V1$_{PBS}$ + 1 mg/mL excipient pre-dissolved**			**1 mg/mL Naporafenib in Buffer$_{PBS}$ + 1 mg/mL excipient pre-dissolved**		
Excipient	**HPC**	**Eudragit EPO**	**Kolliphor RH40**	**HPC**	**Eudragit EPO**	**Kolliphor RH40**
Syringe filter, t=0	7.0% 1.9%	9.8% 8.1%	- 7.1%	6.0% 5.0%	0.7% 11.7%	1.0% 5.8%
Centrifugal filter, t=0	20.2% 22.3%	16.2% 28.8%	14.7% 16.9%	77.4% 71.7%	13.9% 19.3%	15.0% 13.5%
Centrifugal filter, t=1h	13.6% 22.3%	37.6% 34.6%	15.6% 32.7%	73.7% 71.7%	7.2% 8.2%	8.2% 12.6%
Centrifugal filter, t=3h	11.7% 24.1%	34.1% 34.5%	9.3% 7.5%	71.1% 75.4%	11.2% 10.7%	38.2% 8.8%
Centrifugal filter, t=24h	8.3% 10.7/11.6%	2.1% 2.9/1.6%	12.1% 8.0/11.1%	66.3% 65.7/32.3%	4.0/3.2% 7.5/5.8%	28.4/9.3% 9.4/11.1%

*Table 14: Overview of the free fraction calculated as molecularly dissolved drug measured in the supernatant after ultracentrifugation divided by apparently dissolved drug measured after filtration. The ratio is visually reflected in **Figure 57** and **Figure 58**. Data provided as individual replicates.*

Free fraction (free/total)	**1 mg/mL Naporafenib in FaSSIF-V1$_{PBS}$ + 1 mg/mL excipient pre-dissolved**			**1 mg/mL Naporafenib in Buffer$_{PBS}$ + 1 mg/mL excipient pre-dissolved**		
	HPC	**Eudragit EPO**	**Kolliphor RH40**	**HPC**	**Eudragit EPO**	**Kolliphor RH40**
t=0	0.12 ~~0.38~~[a]	0.13 0.16	0.14 0.12	0.81 ~~0.81~~[a]	0.09 ~~0.56~~[a]	0.04 ~~0.05~~[a]
t=1h	0.10 ~~0.38~~[a]	0.22 0.22	0.13 0.06	0.75 ~~0.82~~[a]	0.04 ~~0.32~~[a]	0.33 ~~0.16~~[a]
t=3h	0.11 ~~0.74~~[a]	0.26 0.19	0.23 0.18	0.84 ~~0.76~~[a]	0.03 0.02	0.16 0.21
t=24h	0.08 0.14/0.14	0.26 0.17/0.18	0.26 0.24/0.23	0.82 0.27/0.37	0.31/0.35 0.17/0.12	0.40/0.42 0.08/0.07

[a]: vacuum issues with ultracentrifugation

5.3.6 Verification of bioaccessibility in a dog pharmacokinetic study

The understanding of how excipients manipulated bioaccessibility *in vitro* was translated into an *in vivo* pharmacokinetic study setting. Three arms involving the tosylate salt form suspended in a citrate-phosphate buffer at pH 2.6 with pre-dissolved excipients Eudragit EPO, Hydroxypropylcellulose and Kolliphor RH40 administered via oral gavage were compared to each other at a 30 mg/kg dose in beagle dogs with n=6. The *in vitro* mass transport (acceptor profiles) and the plasma concentration-time profiles observed *in vivo* are shown in **Figure 62**. First and foremost, it was observed that the trajectory of the plasma profile had a very similar shape between the HPC and the EPO arm, which is in agreement with the acceptor profiles obtained *in vitro*. The RH40 study arm showed a different course with a more rapid increase in plasma concentration, which was in line with a more sudden increase in acceptor concentrations compared to the FaSSIF-V1$_{PBS}$ + HPC system.

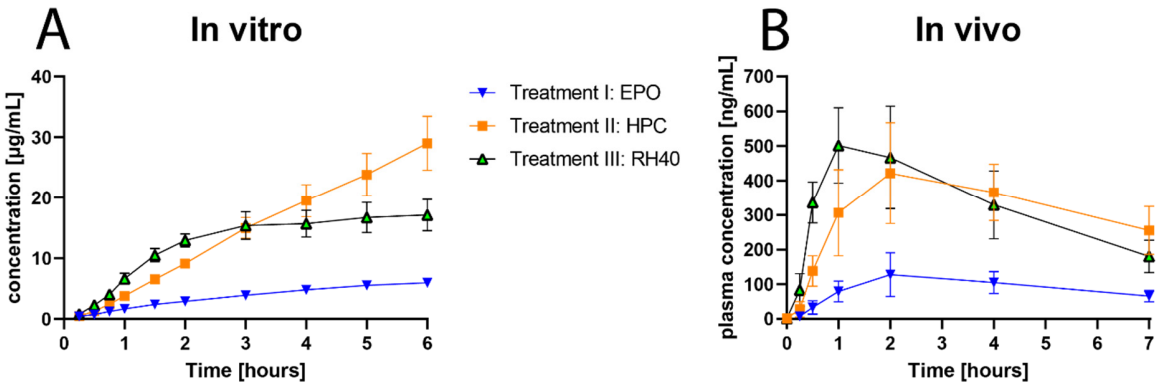

*Figure 62: Relation between A) In vitro drug mass transport across biomimetic barriers and B) observed in vivo plasma concentration-time profiles of three treatments. The in vitro data were generated from 1 mg/mL naporafenib solution form (DMSO) in FaSSIF-V1$_{PBS}$ containing 1 mg/mL pre-dissolved excipients in the donor (already presented in **Figure 54-Figure 56**) and the in vivo administration was performed using 30 mg/kg tosylate salt form suspended in pH 2.6 citrate-phosphate buffer with 10 mg/mL pre-dissolved excipients in beagle dogs. Data points were artifically connected and presented as mean +/- standard deviation of quadruplicates (in vitro) and of n=6 (in vivo).*

Establishing a quantitative relationship was attempted by correlating the drug mass transport rate obtained *in vitro* from the biomimetic flux study to an estimate of *in vivo* absorption rate (see **Equation 17**). As long as the plasma concentration-time profile is dominated by absorption, the absorption rate can be estimated in a simplified way according to a change in the mass of drug absorbed ($m_{absorption}$) over time, proportional to the change in plasma concentration (c_{plasma}) times plasma volume:

$$\frac{dm_{absorption}}{dt} \propto V \frac{dc_{plasma}}{dt} \qquad \text{(Equation 17)}$$

It can be taken from **Figure 62** that the greatest *in vivo* change is the steepest slope during the initial phase, however, quantifiable only between two points. For this reason, it is more practical to use the interval from t=0 to the time point of the maximum plasma concentration, leading to Cmax/Tmax as concentration gradient. The respective correlation with *in-vitro* flux is provided in **Figure 63** in terms of dose normalization, i.e. Cmax/Dose/Tmax. The correlation quality is strikingly high. Comparing to an approach of only considering Cmax (or Cmax/Dose), it becomes evident that the time interval is relevant as for example the maximum concentration in the RH40 arm is attained in much shorter time compared to the HPC and EPO arms. Consequently, the shown correlation with Cmax/Dose is inferior. An approach to correlate flux (slope) with AUC is not meaningful considering physical principles. Possibly, comparing AUCs of *in vitro* and *in vivo* concentration profiles could be attempted, however, confounded by other physiological processes such as distribution, metabolism and elimination. Furthermore, time selection for calculation of AUC specifically *in vitro* is challenging. Beyond the herein used simplified approach (of relating mass transport rates) more elaborate approaches such as deconvoluting the absorption coefficients from the plasma concentration-time profile can be performed if desired (18).

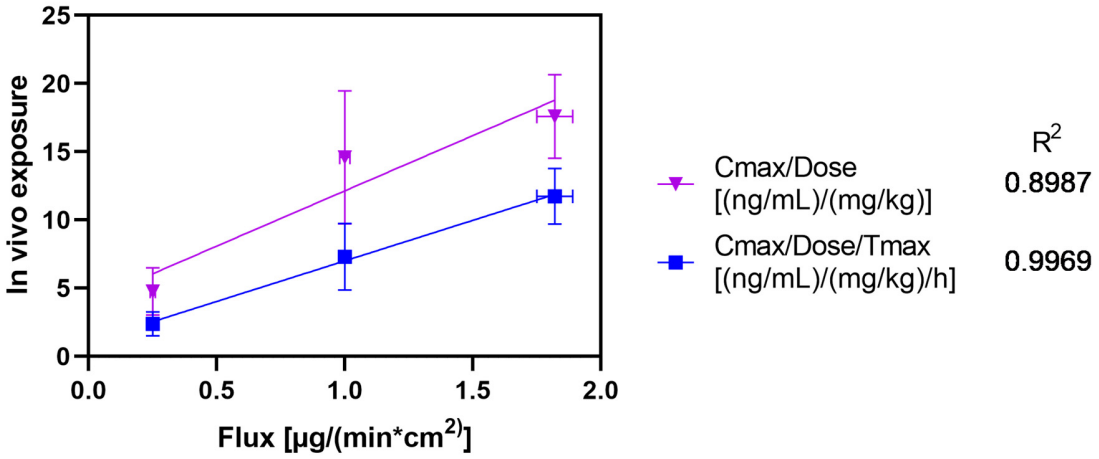

*Figure 63: Correlation between in vitro bioaccessibility measured as flux across biomimetic barriers and in vivo dose-normalized exposures measured as Cmax or Cmax/Tmax (surrogate of absorption rate). Flux slopes taken from **Table 11.** Pharmacokinetic parameters from the in vivo study were provided by Covance. Linear regression was performed using GraphPad Prism Version 9.3.1.*

5.3.7 Context to the bioaccessibility concept

The understanding of how excipients can alter bioaccessibility *in vitro* (see **section 3.4**) was approached by evaluating the impact of excipients on solubility or the more relevant amorphous solubility limit in the case of naporafenib. The impact on the apparent crystalline solubility was considered less relevant and was not assessed but could have been scientifically meaningful in case a non-supersaturating formulation concept was in scope. The link between increased dissolved drug concentrations and a potential benefit in terms of mass transport was attempted using dialysis flux, complemented by NMR insights. This allowed to limit the excipient selection to special cases, i.e. Hydroxypropylcelluose as reference excipient and Eudragit EPO and Kolliphor RH40 as extremes. HPC was considered non-interfering with the biorelevant media system while EPO and RH40 were found to particularly interact with biorelevant media according to (123).

As required next step, the impact of excipients on the dissolution rate was evaluated using the two-step dissolution assay, incorporating a gastric-to-intestinal media transition step. Subsequently, bioaccessibility of naporafenib was asssessed in presence of those excipients by translating apparently dissolved drug concentrations into a permeation gradient using the biomimetic flux setup. Due to the experimental protocol, potential impact from drug dissolution out of a solid delivery system for example was eliminated by equilibrating DMSO dissolved drug with excipient in relevant media for 30 minutes before entering into the flux setup. The kinetic process of drug dissolution up to the solubility limit (here phase separation limit) and the translation of apparently dissolved drug (solubility) into a driving force for permeation using flux were assessed separately and not in the same setup. The connection was attempted via solubility according to the bioaccessibility concept.

Based on the assumption of a 300 mg dose in about 300 mL of available liquid volume in the GIT of the dog (143), less than 10% of the dose is expected to dissolve (assuming FaSSIF-V1$_{PBS}$ representative for the dog situation), i.e. most of the dose would enter the intestinal region undissolved. Furthermore, one would expect that the pH 2.6 vehicle in combination with the gastric pH brings sufficient drug in solution so that the apparent solubility in the intestine is exceeded after the gastrointestinal transfer. The applied non-sink conditions (0.5-1 mg/mL naporafenib) for the *in vitro* studies such as the two-step dissolution assay but also flux studies appear therefore justified. However it would have been interesting to assess how residual tosylate salt (with diluted pH 2.6 citrate phosphate buffer) dissolves under intestinal conditions, even if the effect of the excipients on the dissolution rate are expected to correlate with their effect on apparent solubility. Dialysis flux performed at 50% media saturation was considered valuable to deconvolute the impact of phase separated drug species from the excipient impact but not considered relevant to the *in vivo*

study condition. For improved interpretability and direct comparison of assays, the lipidic flux assay might have been performed additionally at 50% media saturation as well.

Justified criticism may include that the membrane integrity was not verified, related to both, clogging and disintegration issues. Exploratory use of high permeability marker molecules impaired conclusion since the excipients were suspected to impact flux of the markers as well. Furthermore, the use of a different drug form *in vitro* (solution form) versus *in vivo* (tosylate salt) and the uncertainty of human FaSSIF versions to adequately represent the dog intestinal situation were additional factors that can be challenged. Dog FaSSIF was not used due to increased compositional complexity and inability to separate colloids by ultracentrifugation similar to FeSSIF-$V1_{PBS}$ (data not shown).

The ultracentrifugation-flux combo assay did provide very strong insights into the drug-excipient-biorelevant media interplay and was able to provide a mechanistic interpretation of *in vivo* observations. The assay was able to quantify the impact of excipients on bioaccessibility in presence of phase separated drug species, which were considered *in vivo* relevant due to dose/volume considerations. The results obtained support the relevance of bioaccessibility for the oral bioavailability of naporafenib and provide mechanistic guidance for the formulation scientist.

5.4 Opportunities for drug formulation development

Several learnings were made based on the *in vivo* study read out and *in vitro* findings presented in the previous section (see **section 3.4**, **question 5**). Improving apparently dissolved amount of drug via inclusion of Kolliphor RH40 has temporarily boosted the liquid reservoir while effects on freely dissolved drug remained unclear. As a consequence of an increased liquid reservoir, r_{in} related to dissolution was also found increased. On the other hand, the dissolved drug concentrations likely reached a critical limit, thereby promoting the driving force for form conversion from amorphous to crystalline and associated desupersaturation. Once the most stable crystalline form is present, the effective concentration level is so low that absorption / permeation may become minimal. The risk of increasing the liquid reservoir and boosting r_{in} as driver for absorption is associated with an increased likelihood of crystallization and desupersaturation, related to r_{out} as inhibitor for absorption. Hydroxypropylcellulose on the other hand did not impact the liquid reservoir and was mainly expected to inhibit r_{out} to achieve more sustained absorption. Finally, Eudragit EPO was likely impacting the biorelevant media system which was found relevant to the solution behavior of naporafenib. While the polymer may have stabilized the solid reservoir in amorphous form and caused increased dissolved drug concentrations even after long time (24 hours), a possible liquid-state interaction was suspected that reduced the bioaccessibility of dissolved naporafenib.

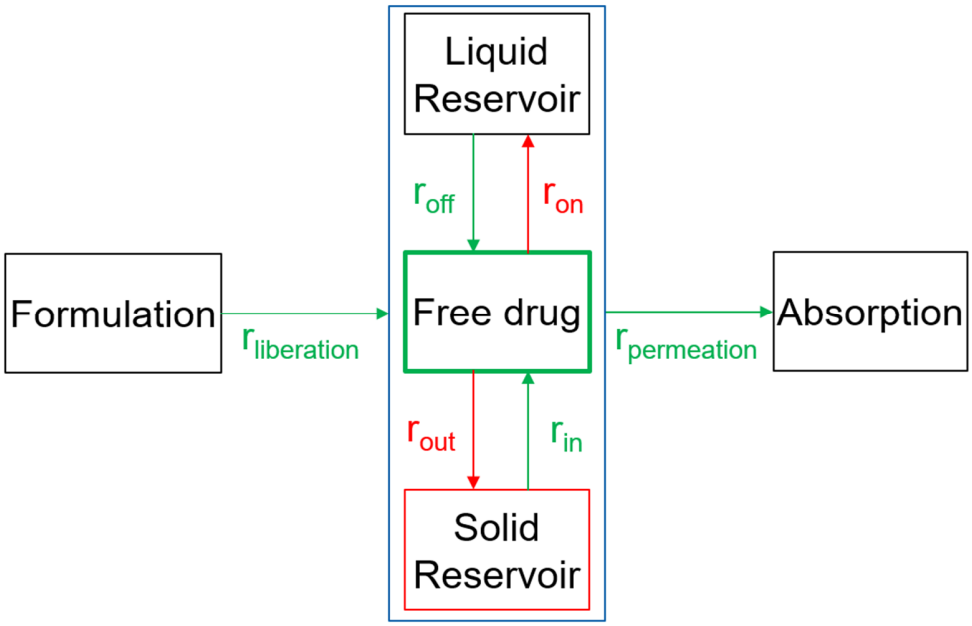

Figure 64: Illustration of the bioaccesibility concept for discussion about driving and inhibiting factors of absorption as guidance for the formulation scientist.

5.4.1 Risk mitigation through improving dissolution rate and delaying precipitation

The initial dissolution in the acidic stomach compartment was expected to have little effects on absorption as long as the amount dissolved approached the phase separation limit after the gastric-to-intestine transition. The higher phase separation limit in acidic environment compared to more neutral pH 6.5 conditions support this assumption. Following dose per volume considerations, the dissolution of undissolved drug material in the intestine may constitute a rate-limiting process to replenish absorbed drug. Revisiting the drug form differentation activities, the tosylate salt form supplemented with HPC was compared to an amorphous solid dispersion based on HPMC in a single-step dissolution assay in FaSSIF-V1$_{PBS}$, see **Figure 65**. HPC and HPMC are both expected not to influence the phase separation limit based on **Figure 49**. It was observed that within the given time, the amorphous form (as ASD) reached higher dissolved drug concentrations than the tosylate form with HPC. Already after five minutes of dissolution, the ASD showed about 30 µg/mL dissolved pure naporafenib while the tosylate + HPC required about 30 minutes to reach the same concentration level. With increasing media saturation, the dissolution rate is expected to decline according to the Noyes-Whitney equation (**Equation 9**). The decline in dissolution rate seen for the ASD in **Figure 65,** can be understood since the dissolved drug concentration attained the phase separation limit of Naporafenib in FaSSIF-V1$_{PBS}$. The tosylate salt showed substantially slower dissolution kinetics, possible reasons could be lower surface area among other factors.

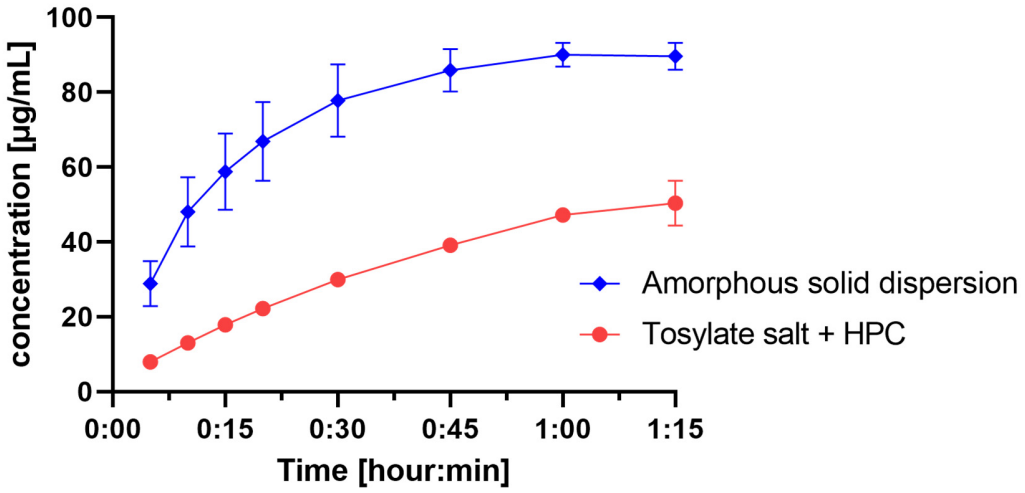

Figure 65: Single-step dissolution profile of naporafenib formulations in FaSSIF-V1$_{PBS}$ comparing amorphous solid dispersion against tosylate salt + 1 mg/mL pre-dissolved HPC. Data presented as mean +/- standard deviation of triplicates. Error bars are in some cases smaller than symbols. Data was provided by L. Toelle.

Form conversion of naporafenib to crystalline monohydrate has to be considered an absorption risk. In presence of this crystalline solid reservoir, very low drug concentrations below 1 µg/mL are expected to be molecularly dissolved, thereby limiting the driving force for absorption to a large degree. The amorphous solid dispersion not only incorporates the amorphous form of naporafenib but also HPMC as polymer which may delay precipitation similar to HPC. The ASD was equilibrated in the biorelevant media landscape used for form differentation to confirm a potentially beneficial "spring-parachute effect", see **section 2.4.3**. The concentration-time profiles are shown in **Figure 66** and illustrate a kinetic concentration plateau maintained for a minimum of 2 hours in all media. An *in vivo* benefit from sustained supersaturation, related to the "spring-parachute effect" of the ASD can be expected along with a benefit from an increased dissolution rate compared to the salt form.

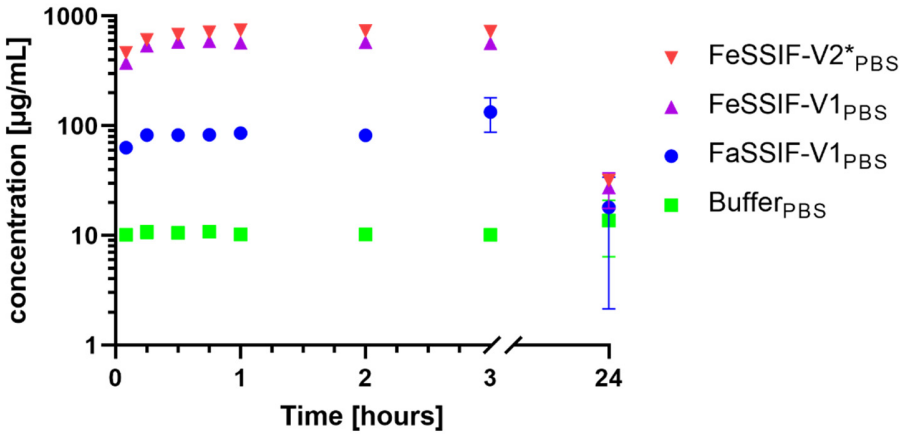

Figure 66: Equilibration monitored over time of naporafenib amorphous solid dispersion at 1 mg/mL nominal pure drug concentration in selected biorelevant media. Concentration data referring to pure drug in solution presented as mean of triplicates +/- standard deviation in semi-log plot. Error bars are in most cases smaller than symbols.

5.4.2 Addressing the solubility resistance by increasing amount of drug in solution

Since the inclusion of Kolliphor RH40 resulted in a faster increase of the plasma concentration-time profile, it was of interest to bring as much drug as possible into solution through a microemulsion approach. A microemulsion composed of Kolliphor RH40 and other constituents was compared to other formulation principles such as the tosylate + Hydroxypropylcellulose and the amorphous solid dispersion based on HPMC in a two-step dissolution assay, shown in **Figure 67**. The ASD was tested in form of a hot-melt extrudate (granules) and additionally as film-coated tablet (FCT). No difference was observed, supporting that the particle dissolution process is rate-limiting and not the drug liberation process ($r_{liberation}$) related to wetting, disintegration and dispersion of particles from e.g. the tablet matrix. Consistent with the single-step dissolution results

(**Figure 65**), the tosylate + HPC dissolved slower than the ASD, both in gastric and intestinal situation. In case of the microemulsion the drug stayed dissolved in the gastric phase (around 1 mg/mL) but concentration declined rapidly after switching to intestinal phase. After roughly 2 hours the dissolved concentrations from the microemulsion were below the ASD and tosylate + HPC. The reader is pointed towards the logarithmic ordinate in **Figure 67**.

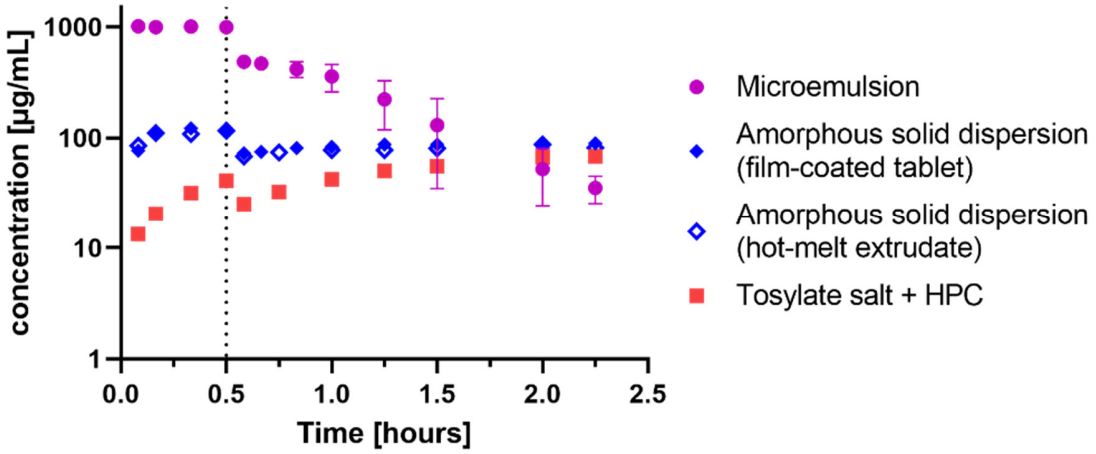

*Figure 67: Two-step dissolution profile of naporafenib formulations at 1 mg/mL nominal pure drug concentration.The dotted line at 0.5 hours indicates the FaSSGF to FaSSIF-V1$_{PBS}$ transition step. Data presented as average of duplicates for ASD HME and tosylate + HPC and as mean +/- standard deviation of triplicates for ME and ASD FCT. Error bars are in some cases smaller than symbols. Data for tosylate salt + HPC already presented in **Figure 53**. Data was provided by N. Stehle (ASD FCT), S. Juanes (ASD HME and tosylate salt + HPC) and P. Halbeisen (ME).*

5.4.3 Formulation-dependent bioaccessibility

The amorphous solid dispersion and tosylate salt + HPC approach were assessed in the ultracentrifugation-flux combo assay to verify whether the determined dissolution rate difference would translate into a flux difference *in vitro*. The intial dissolution phase was less of interest but rather the dissolution of the residual solid reservoir to replenish permeated drug during the course of permeation. To analyze this, an equal dose of 1 mg/mL pure drug was pre-equilibrated for 30 minutes before the suspensions were inserted into the donor compartment. This was performed in Buffer$_{PBS}$ as well as in FaSSIF-V1$_{PBS}$ to additionally explore the impact of the biorelevant liquid reservoir on bioaccessibility. Furthermore, an exploratory two-step protocol was performed to check for a potential impact of the initial dissolution period and resulting amount of generated phase separated drug after gastric to intestinal transfer on flux. The donor and acceptor concentration-time profiles are shown in **Figure 68**. As expected, above one order of magnitude differences in dissolved donor concentrations were observed between Buffer$_{PBS}$ and FaSSIF-V1$_{PBS}$. The flux difference, however, was only about 50% between those systems. More importantly, the flux was about equal between the ASD and the salt + excipient approach.

Consequently, in this setup, it was therefore not possible to detect differences in bioaccessibility related to dissolution rate differences. Noteworthy, the donor concentrations at 22 and 24 hours indicated that the involved solids likely have not fully converted from amorphous to crystalline state. The residual concentration levels are higher than expected from a desupersaturated crystalline monohydrate system. Both HPC and HPMC may therefore exhibit a similar “parachute” functionality, stabilizing the amorphous form and high concentrations of molecularly dissolved drug for a longer period of time.

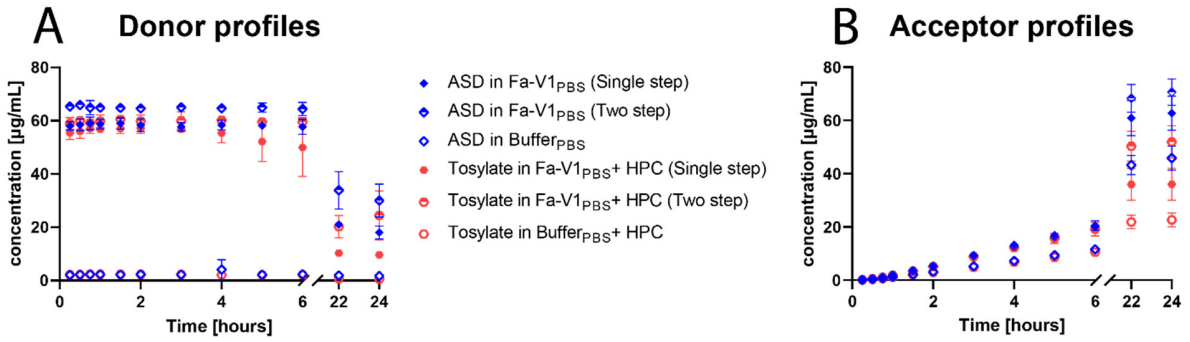

Figure 68: Concentration-time profiles of naporafenib in A) FaSSIF-V1$_{PBS}$ single-step and two-step and Buffer$_{PBS}$ as amorphous solid dispersion or tosylate salt form + 1 mg/mL pre-dissolved HPC in the donor and B) resulting mass transport as cumulative concentrations in acceptor sink buffer in the acceptor compartment. Nominal donor input was 1 mg/mL drug considered excess drug conditions. Data provided as mean +/- standard deviation of quadruplicates. Error bars are in some cases smaller than symbols.

The ultracentrifugation-flux combo data are shown in **Figure 69** for Buffer$_{PBS}$ and single-step FaSSIF-V1$_{PBS}$ system and in **Figure 70** for the two-step FaSSIF-V1$_{PBS}$ system. Tosylate salt + HPC system showed slightly lower concentrations at earlier time points, likely related to the dissolution rate difference. Freely dissolved drug values were overall in an expected range with slightly lower values in Buffer$_{PBS}$ compared to FaSSIF-V1$_{PBS}$.

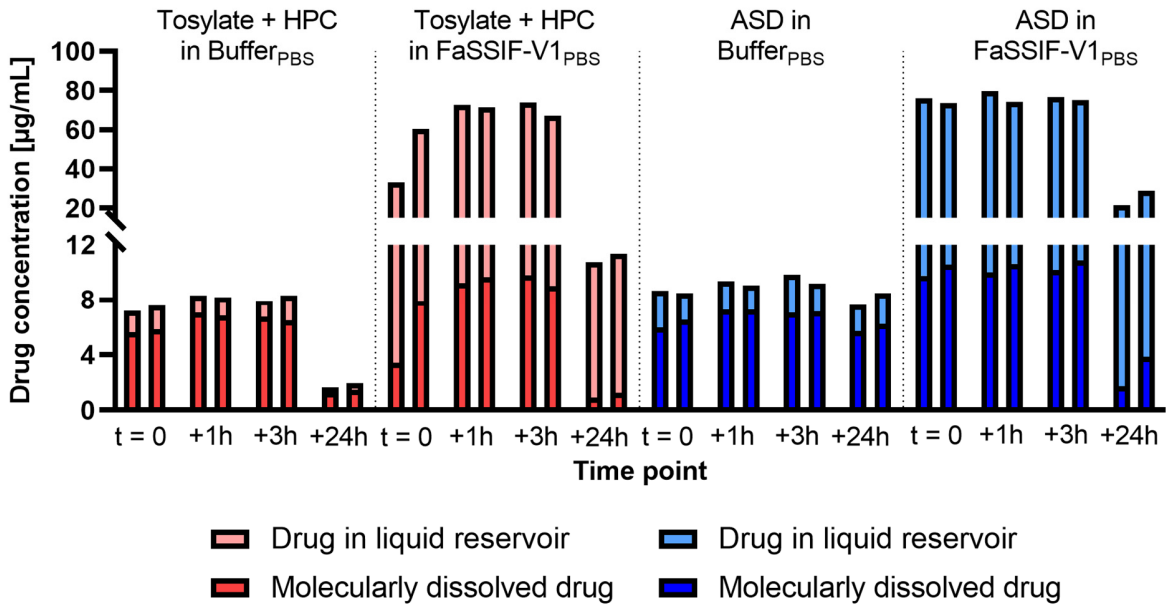

*Figure 69: Ultracentrifugation-flux combo data of excess naporafenib in Buffer$_{PBS}$ and single-step FaSSIF-V1$_{PBS}$. Data presented as bar plots over time (relative to the flux experiment, **Figure 68**), differentiating between molecularly dissolved drug and drug in liquid reservoir. Liquid reservoir calculated from total apparently dissolved drug measured after filtration minus molecularly dissolved drug estimated by ultracentrifugation. Data presented as individual replicates.*

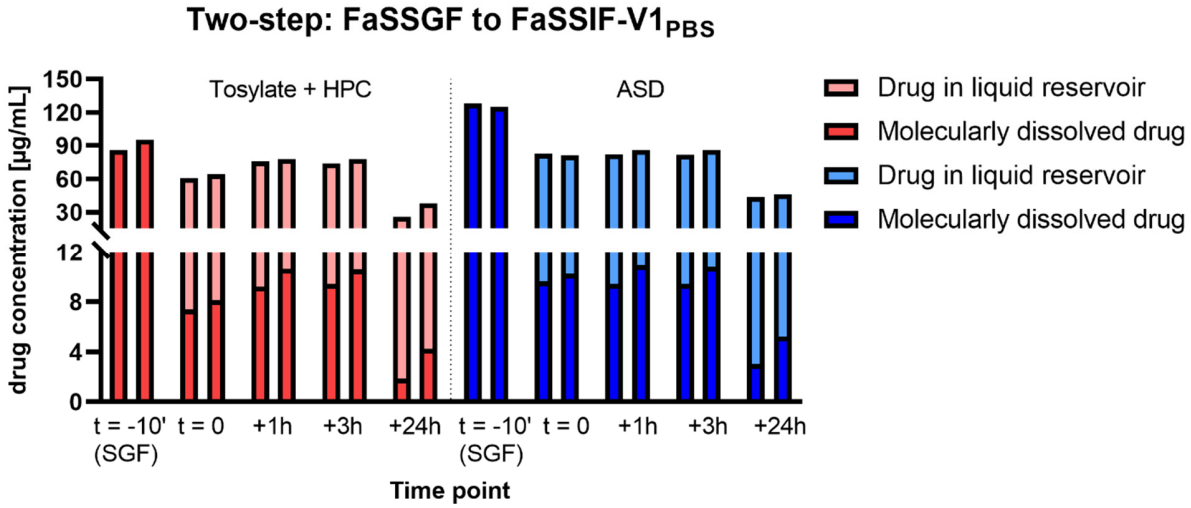

*Figure 70: Ultracentrifugation-flux combo data of excess naporafenib in two-step FaSSIF-V1$_{PBS}$. Data presented as bar plots over time (relative to the flux experiment, **Figure 68**), differentiating between molecularly dissolved drug and drug in liquid reservoir. Liquid reservoir calculated from total apparently dissolved drug measured after filtration minus molecularly dissolved drug estimated by ultracentrifugation. Data presented as individual replicates.*

The amount freely dissolved drug in FaSSGF was measured through filtration and was assumed to be only molecularly dissolved due to the absence of colloidal structures. A slight difference of dissolved drug between the ASD and the tosylate salt form + HPC further supported the previously observed dissolution rate difference. Important to note is that the differences were not observed at later time points, neither in the donor profiles (**Figure 68**) nor in the ultracentrifugation-flux combo data. This observation points towards a "traffic jam" in the donor compartment related to a low rate of drug permeation whereas dissolution was able to "catch up". In this case, the dissolution rate was considered as not rate-limiting while the permeation was. Accordingly, no large differences were observed for the FaSSIF-V1$_{PBS}$ systems between single-step (**Figure 69**) and two-step approach (**Figure 70**).

The surface-normalized flux values, representing naporafenib bioaccessibility from the involved formulations, are visualized in **Figure 71** and tabulated in **Table 15**. Interestingly, the observed flux was lower with the solid powder formulations than from the solution form of naporafenib (DMSO). This may be caused by the amount of phase separated drug species generated via solution form in contrast to the solid powder formulation approaches. Under the assumption that the amount of molecularly dissolved drug and drug in liquid reservoir would be similar, limited by the aqueous solubility and media components, the difference in bioaccessibility was attributed to differences in solid reservoir bioaccessibilities. This may include effects on UWL diffusion ("particle drifting") but also on the kinetics how fast permeated drug can be replenished (r_{in} in the bioaccessiblity concept).

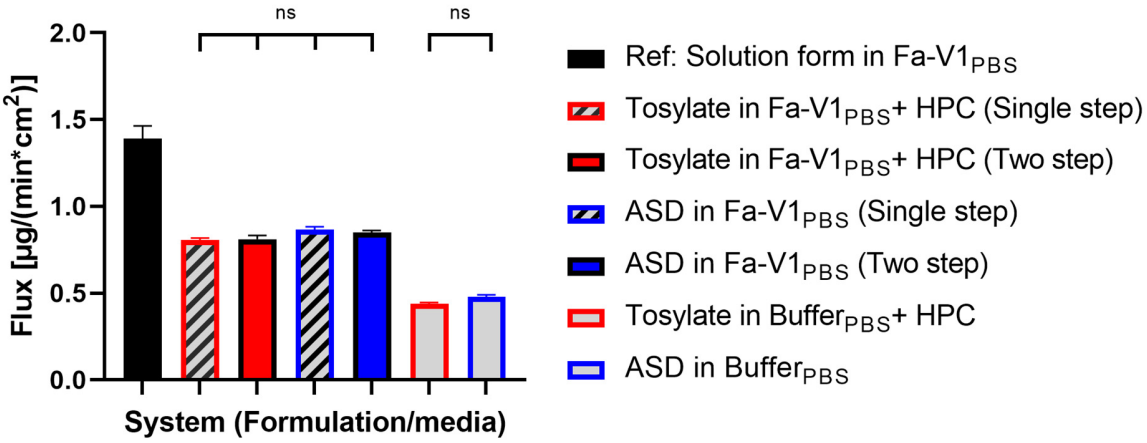

*Figure 71: Overview of surface-normalized flux for tosylate salt + 1 mg/mL pre-dissolved HPC or amorphous solid dispersion in single-step and two-step FaSSIF-V1$_{PBS}$ and Buffer$_{PBS}$. Data in FaSSIF-V1$_{PBS}$ without excipient already presented in **Figure 43** and included for reference. Slopes were derived from **Figure 68** using linear regression. Data provided as mean +/- standard deviation of quadruplicates. Statistical significance (α = 0.05) was evaluated using a one-way ANOVA with post-hoc Tuckey's test for multiple comparison. Exceptionally, only not signifcant (ns) comparisons are marked to facilitate interpretation. Analysis performed with GraphPad Prism Version 9.3.1.*

Flux from the amorphous solid dispersion was practically indistinguishable from tosylate salt + HPC flux in all media. The assumption was made that HPMC can be considered equivalent to HPC and both would impact the bioaccessibility to the same degree. It was not possible to translate dissolution rate differences into flux differences in this setup. This hints towards a limitation of the setup to adequately mimic the dynamic interplay between the dissolution and permeation process, which could be different *in vivo* and specifically relevant for poorly water-soluble drugs at high doses.

*Table 15: Table format of **Figure 71** including R^2 values for the linear fit of the cumulative acceptor concentrations based on the donor profiles. Flux slope provided as mean with standard deviation in brackets of quadruplicates.*

System (Formulation, medium)	Flux slope [µg/(min*cm²)]	R2
Tosylate salt in $Buffer_{PBS}$ + HPC	0.44 (0.01)	0.9912
Amorphous solid dispersion in $Buffer_{PBS}$	0.48 (0.01)	0.9764
Tosylate salt in FaSSIF-$V1_{PBS}$ + HPC (Single-step dissolution-flux)	0.81 (0.01)	0.9910
Tosylate salt in FaSSIF-$V1_{PBS}$ + HPC (Two-step dissolution-flux)	0.81 (0.02)	0.9726
Amorphous solid dispersion in FaSSIF-$V1_{PBS}$ (Two-step dissolution-flux)	0.85 (0.01)	0.9938)
Amorphous solid dispersion in FaSSIF-$V1_{PBS}$ (Single-step dissolution-flux)	0.87 (0.02)	0.9865

DLS signal-to-noise ratios for the studied formulations are shown in **Figure 72**. The reference media as well as the filtrates containing apparently dissolved drug resulted in very robust signal-to-noise ratios in FaSSIF-$V1_{PBS}$ but more variable ratios in $Buffer_{PBS}$. A lot of colloid separations using ultracentrifugation resulted in low signal-to-noise ratios between close to zero and 0.4. However, some spreading of values was detected, reaching also values around 0.5 and higher. The confidence to state absence of colloidal structures impacting aqueous concentrations of naporafenib is lower compared to the study with pure biorelevant media but higher than for the excipient studies. Considering **Figure 25** and the obtained results shown in **Figure 69** and **Figure 70**, it seems safe to say that despite detection of residual colloidal structures in the supernatants, they did not appear to have pronounced effects on the measured drug concentrations.

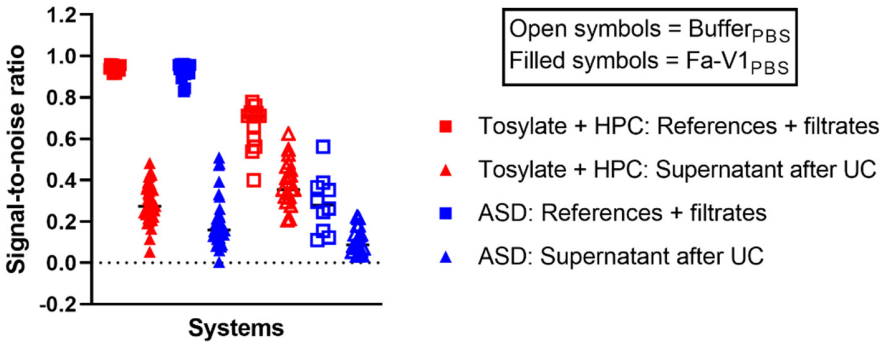

Figure 72: DLS scatter plot of signal-to-noise ratios of naporafenib in FaSSIF-V1$_{PBS}$ and Buffer$_{PBS}$, divided into references and filtrates before ultracentrifugation (media before drug addition and filtrates after drug addition) and supernatants measured after ultracentrifugation treatment for both, the amorphous and crystalline systems (not differentiated). Data presented as individual measurements.

The experimental control parameters final pH and final solid form by XRPD are summarized in **Table 16** for the ultracentrifugation-flux combo experiments with naporafenib formulations. The pH was more or less constant for all conditions, eventually slightly reduced in presence of the tosylate salt. The final forms, identified by XRPD at the end of the experiments, were primarly amorphous with traces of crystalline monohydrate for the ASD and co-existing tosylate salt and crystalline monohydrate in the case of tosylate form + HPC systems. Interestingly, in absence of HPC, no residual tosylate form was detected in early drug equilibration over time studies (see **Table 2**) independent of the media.

*Table 16: Overview of experimental control parameters (**Figure 68-Figure 70**) pH and final drug form at the end of the experiments. XRPD analysis based on references provided in **Figure 15**. Data provided as individual replicates.*

Experimental control	**Tosylate salt + HPC pre-dissolved**			**Amorphous Solid Dispersion**		
Medium	**Phosphate buffer pH 6.5**	**Single-step FaSSIF-V1**	**Two-step FaSSIF-V1**	**Phosphate buffer pH 6.5**	**Single-step FaSSIF-V1**	**Two-step FaSSIF-V1**
Final pH	6.37 6.32 6.36 6.38	6.44 6.46 6.30 6.32	6.37 6.38 6.42 6.41	6.44 6.43 6.43 6.42	6.54 6.55 6.42 6.42	6.46 6.46 6.48 6.47
Final form (by XRPD)	Monohydrate and tosylate	Monohydrate and tosylate	Monohydrate and tosylate	Amorphous	Traces of monohydrate and amorphous	Traces of monohydrate and amorphous

The unspecific binding losses for the systems containing naporafenib formulations are listed in **Table 17** and they allow to interpret the discrepancy of dissolved drug concentrations between the donor compartments in **Figure 68** and apparently dissolved drug amounts in **Figure 69** and **Figure 70**. A striking loss was detected for both formulations in the $Buffer_{PBS}$ system with values between 70-80%. This was consistent with the unspecific binding loss measured in $Buffer_{PBS}$ + HPC when adding the solution form of naporafenib. Most other values for the FaSSIF-$V1_{PBS}$ system were found between 20-25%. There was no apparent difference between the tosylate salt + HPC and the amorphous solid dispersion systems.

The calculated free fractions, defined as moleculary dissolved divided by total apparently dissolved drug, are shown in **Table 18**. The values in FaSSIF-$V1_{PBS}$ show good reproducibility between t=0 and t=3h for both formulations and are in agreement with free fractions obtained for the amorphous systems in **Table 4**. Also, a trend of lower fractions towards t=24h was detected for most systems. The values in $Buffer_{PBS}$ showed up to 30% reduction after ultracentrifugation which may either be unspecific loss of drug or loss with separated residual excipient colloids.

*Table 17: Overview of the unspecific binding loss determined during the ultracentrifugation-flux combo experiment by re-filtering a filtrate of known concentration through either 0.45 µm PTFE syringe filters or 0.45 µm PVDF centrifugal filters using identical volumes to the initial filtration. Loss of drug concentration required to substantiate discrepancies between donor concentration-time profiles (**Figure 68**) and apparently dissolved drug levels from the ultracentrifugation-flux combo data (**Figure 69** and **Figure 70**). Unspecific binding loss shown as individual replicates as percentage of the initial drug concentration in the filtrate.*

Unspecific binding loss	**Tosylate salt + HPC pre-dissolved**			**Amorphous Solid Dispersion**		
Medium	**Phosphate buffer pH 6.5**	**Single-step FaSSIF-V1**	**Two-step FaSSIF-V1**	**Phosphate buffer pH 6.5**	**Single-step FaSSIF-V1**	**Two-step FaSSIF-V1**
Syringe filter, t=0	10.7% 8.8%	0.5% 1.1%	- -	6.3% 9.2%	1.6% 4.8%	- -
Centrifugal filter, t=0	69.2% 77.4%	13.5% 16.9%	9.3% 17.3%	79.3% 78.6%	22.4% 24.1%	14.1% 24.1%
Centrifugal filter, t=1h	78.8% 77.6%	22.0% 22.2%	23.7% 22.9%	81.8% 77.7%	24.1% 25.8%	25.1% 21.7%
Centrifugal filter, t=3h	74.2% 77.8%	23.1% 20.2%	22.9% 22.5%	77.2% 78.7%	21.3% 23.3%	24.1% 26.1%
Centrifugal filter, t=24h	69.3/69.5% 66.2/69.4%	6.4/8.6% 12.1/8.2%	9.7/13.0% 16.0/13.2%	76.0/80.1% 78.7/78.0%	8.6/7.8% 16.1/13.1%	15.5/15.4% 14.3/12.6%

*Table 18: Overview of the free fraction calculated as molecularly dissolved drug measured in the supernatant after ultracentrifugation divided by apparently dissolved drug measured after filtration. The ratio is visually reflected in **Figure 69** and **Figure 70**. Data provided as individual replicates.*

Free fraction (free/total)	**Tosylate salt + HPC pre-dissolved**			**Amorphous Solid Dispersion**		
Medium	**Phosphate buffer pH 6.5**	**Single-step FaSSIF-V1**	**Two-step FaSSIF-V1**	**Phosphate buffer pH 6.5**	**Single-step FaSSIF-V1**	**Two-step FaSSIF-V1**
t=0	0.78 0.77	0.10 0.13	0.10 0.10	0.69 0.77	0.13 0.14	0.09 0.10
t=1h	0.85 0.83	0.13 0.14	0.12 0.14	0.78 0.80	0.13 0.14	0.11 0.13
t=3h	0.85 0.78	0.13 0.13	0.13 0.14	0.72 0.77	0.13 0.14	0.12 0.13
t=24h	0.77/0.80 0.77/0.77	0.08/0.08 0.11/0.10	0.07/0.07 0.11/0.11	0.76/0.75 0.72/0.75	0.07/0.09 0.13/0.14	0.07/0.06 0.11/0.11

5.4.4 Comparison of conventional and enabled formulations in a dog PK study

From the first three arms of the pharmacokinetic study in beagle dogs, involving tosylate salt suspensions, important learnings for possible formulation optimization were derived. Adressing the identified oral absorption risks resulted in an amorphous solid dispersion (ASD) and microemulsion (ME) formulation. The comparison of drug exposure from those “enabled formulations”, defined as involvement of amorphous drug or a lipid-based approach, to the conventional crystalline approaches supplemented with excipients is shown in **Figure 73** and pharmakokinetic parameters are listed in **Table 19** further below.

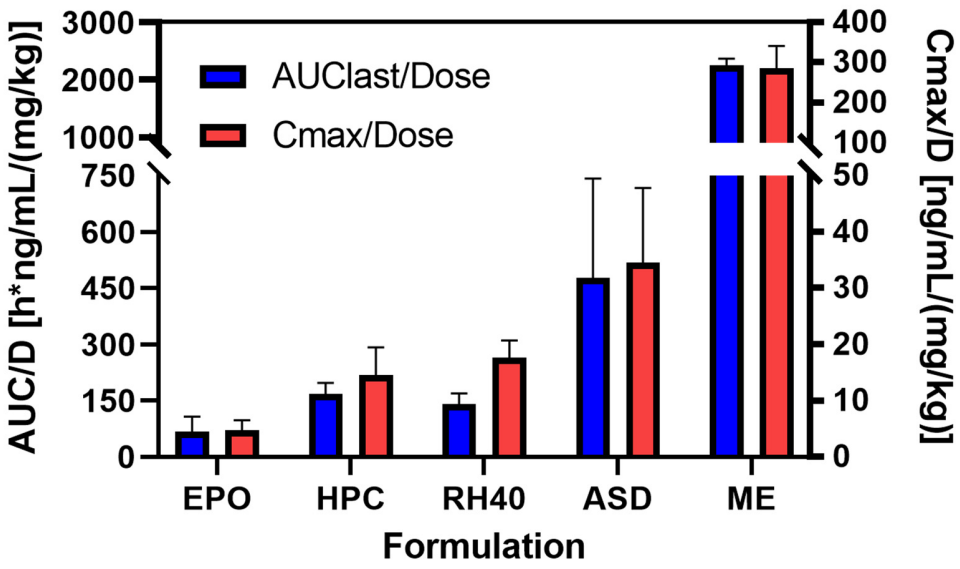

Figure 73: In vivo pharmacokinetic study in beagle dogs with five formulation arms at 30 mg/mL pure drug equivalent: Naporafenib tosylate salt administered as pH 2.6 citrate-phosphate buffer suspension with three different excipients (Eudragit EPO, Hydroxypropylcellulose (HPC) and Kolliphor RH40) and naporafenib amorphous solid dispersion (ASD) and microemulsion (ME) flushed with the same pH 2.6 buffer. Data provided as mean +/- standard deviation of n=6. The pharmacokinetic parameters were provided by Covance.

The results show that both, the ASD and the ME approach provided higher drug exposure regarding Cmax and AUC of the plasma concentration-time profile. The highest plasma concentration is about two-fold higher with the ASD compared to the tosylate salt form with either HPC or RH40. The microemulsion provided almost an 8-fold increase in Cmax compared to the ASD. Therefore, improving dissolution rate and delaying precipitation with the ASD approach resulted in an increased exposure but could be further elevated providing drug in solubilized form such as with the microemulsion strategy. Relevant absorption rate-limitations consist therefore of the dissolution rate, comparing e.g. tosylate salt with HPC to HPMC based ASD (**Figure 65** and **Figure 67**), and a limitation of the driving force for permeation by apparent solubility differences, comparing e.g. the ASD to the ME (**Figure 67**). The microemulsion exposure was presumably limited by the concentration controlled permeation rate which was initially maximized but declined during the course of desupersaturation, related to precipitation and monohydrate conversion of the drug. The hypothesis for arm I to III was that, despite possible differences in dissolution rate, the absorption rate was controlled by different effective concentrations related to excipients involved. The relative differences in driving force for permeation could be quantified by comparing the *in vitro* flux, i.e. relative bioaccessibility of a high dose of naporafenib in presence of excipients.

Table 19: Pharmacokinetic parameters from the dog study involving five arms of naporafenib formulations administed at a 30 mg/kg dose using a pH 2.6 citrate-phosphate buffer. Dose-normalized exposure provided as maximal concentration in the blood (Cmax/Dose) and area-under-the-curve of the plasma concentration-time profiles (AUC/Dose) +/- standard deviations. The time at which the maximum concentration in the blood was observed (Tmax) is provided as median with range in brackets.

Naporafenib exposure in beagle dogs	**Arm I Tosylate salt + EPO**	**Arm II Tosylate salt + HPC**	**Arm III Tosylate salt + RH40**	**Arm IV Amorphous solid dispersion**	**Arm V Microemulsion**
Cmax/D (ng/mL)/ (mg/kg)	4.77 +/- 1.73	14.6 +/- 4.88	17.6 +/- 3.07	34.5 +/- 13.3	286 +/- 55.4
AUClast/D (h*ng/mL)/ (mg/kg)	68.3 +/- 39.8	167 +/- 30.0	140 +/- 29.4	476 +/- 266	2250 +/- 119
Tmax (hours)	2.0 (2.0-24)	2.0 (1.0-4.0)	1.5 (0.5-2.0)	2.0 (2.0-4.0)	1.0 (1.0-1.0)

An overview of measured drug mass transport rates for both dissolution and permeation processes is provided in **Table 20**. It can be clearly seen that dissolution and permeation rates obtained were affected by experimental setup parameters such as surface-to-volume ratio but also resistance layer (membrane) in case of flux studies. The hydrophilic regenerated cellulose membrane as barrier formed a layer possessing much higher resistance for permeation compared to the lipophilic phospholipid-impregnated barrier in the specific case of naporafenib. This has implications regarding assay sensitivity to detect differences, for example, chances to detect an impact of different dissolution rates in the dialysis flux setup are minimal. However, an increased permeation rate of about 100-fold in the lipidic flux setup was still insufficient to differentiate the tosylate form + HPC from the amorphous solid dispersion. For the time being, it is recommended to split the process investigations: 1) Investigate the dissolution process up to reaching the solubility limit, i.e. phase separation limit in case of “high energy forms” such as amorphous drug or salt form, 2) translate solubility into an effective permeation gradient using flux as a measure for relative bioaccessibility. Direct coupling of dissolution with permeation was not possible in the given *in vitro* setups and would require further research, e.g. in the direction of surface-to-volume contraints or permeation barrier properties (resistances).

*Table 20: Overview of drug mass transport rates derived from flux and dissolution assays performed in this work: Dialysis flux (**Figure 35** and **Figure 36**), intrinsic dissolution rate (**Figure 19**), lipidic flux (**Figure 46** and **Figure 71**) and single-step dissolution (**Figure 65**). Assay specific parameters, dimensions and conditions such as surface area (A), volume (V) and surface-to-volume ratio (A/V), stirring speed in rotations per minute (rpm) as well as the drug form and nominal input are provided. The mass transports were surface- and volume-normalized whenever applicable and are reported as mean with standard deviations in brackets.*

Mass transport assay	Assay dimensions and parameter	Assay conditions (Drug form / dose)	Surface-normalized mass transport in µg/(min*cm²)	Volume-normalized mass transport in µg/(min*mL)
Dialysis flux	A: 1.77 cm^2 V: 10 mL A/V: 0.177 cm^{-1} Stirring: 500 rpm	0.2 mg/mL and ~ 1 mg/mL **Solution form** (DMSO)	**0.017** (0.0004)	**0.003** (0.0001)
Intrinsic dissolution rate	A: 0.07 cm^2 V: 20 mL A/V: 0.0035 cm^{-1} Stirring: 4800 rpm	**Tosylate salt form**	**9.64** (1.00)	**0.034** (0.004)
		Amorphous form	**15.17** (1.06)	**0.053** (0.004)
		ASD	**18.01** (4.78)	**0.063** (0.017)
Lipidic flux	A: 1.54 cm^2 V: 22 mL A/V: 0.07 cm^{-1} Stirring: 100/400 rpm	1 mg/mL **Tosylate + HPC** (single-step)	**0.81** (0.01)	**0.057** (0.001)
		1 mg/mL **ASD** (single-step)	**0.87** (0.02)	**0.061** (0.001)
		1 mg/mL **Solution form** (100 rpm)	**1.39** (0.07)	**0.097** (0.005)
		1 mg/mL **Solution form** (400 rpm)	**1.81** (0.03)	**0.127** (0.002)
Single-step dissolution	A: unknown V: 500 mL A/V: unknown Stirring: 75 rpm	0.5 mg/mL **Tosylate + HPC**	-	**0.998** (0.018) (30 min point)
		0.5 mg/mL **ASD**	-	**5.781** (1.215) (5 min point)

5.4.5 Context to the bioaccessibility concept

Based on the *in vivo* study read out from the tosylate salt + excipient arms, rational optimization of formulation principles resulted in an amorphous solid dispersion (ASD) approach and a microemulsion (ME) approach (relate to **section 3.4**). The HPMC-based ASD showed improved dissolution rate in a single-step assay in FaSSIF-V1$_{PBS}$ compared to the tosylate salt form supplemented with HPC. Therefore, the assumption of different bioaccessibilities resulting from the amorphous or tosylate salt solid reservoir species, related to r_{in} in the bioaccessibility concept, appeared valid. Nevertheless, this dissolution rate difference did not translate into a flux difference in the µFlux™ setup, resulting in equal *in vitro* bioaccessibility. Strikingly, the *in vivo* exposure of the ASD was about 2-fold compared to the salt with excipient despite equal flux *in vitro*. Those findings alongside **Table 20,** substantiate the hypothesis that the kinetic relationship between r_{in} and $r_{permeation}$ in the bioaccessibility concept cannot be assessed *in vitro* in a biorepresentative manner. However, some estimations can be made based on available literature regarding surface-

to-volume differences between the *in vitro* and *in vivo* situation. Based on geometrical considerations of the human intestine, a range of surface-to-volume ratios from 1 to 14 cm^{-1} is proposed depending on the percent compression of the intestine compared to the assumption of a perfect cylinder (144). Sugano proposed 2.3 cm^{-1} based on an equation relating human jejunal effective permeation rate to the fraction absorbed to estimate the surface-to-volume ratio (145). Another approach estimated 1.9 +/- 1.4 cm^{-1} by taking literature values of the absorption rate coefficient for passively absorbed drugs and dividing them through their estimated human jejunal permeation rate based on a molecular descriptor model (146). The drugs were required to have a complete permeation-limited absorption and a minimum of 90% absorbed. Inspired by the mathematical scaling approach to relate *in vitro* partitioning to *in vivo* absorption reported by Mudie et al. in 2012 (144), it could be attempted to scale the observed *in vitro* flux for the tosylate salt form supplemented with HPC to possible *in vivo* dimensions. Comparing volume-normalized mass transport rates, it can be shown that an equivalence of the dissolution and permeation rates can be achieved if the μFlux™ setup would incorporate a surface-to-volume ratio of about 1.3 cm^{-1}. Beyond that value, the rate-limitation would be shifted from solubility- or permeability-limited to dissolution rate-limited absorption. This may explain why the ASD could not be differentiated from the tosylate salt form *in vitro* but a further increase in exposure was observed *in vivo*. Why the exposures did not differ by a factor of 5, as proposed by the estimated early dissolution rate difference, might be explained by the fact that the overall resistance is a combination of the individual contributions from permeation and dissolution. The assumption of similar intestinal surface-to-volume ratio for the dog as for the human situation as well as the GIT-PAMPA membrane being representative for the cellular membrane in the intestine needs to be appreciated.

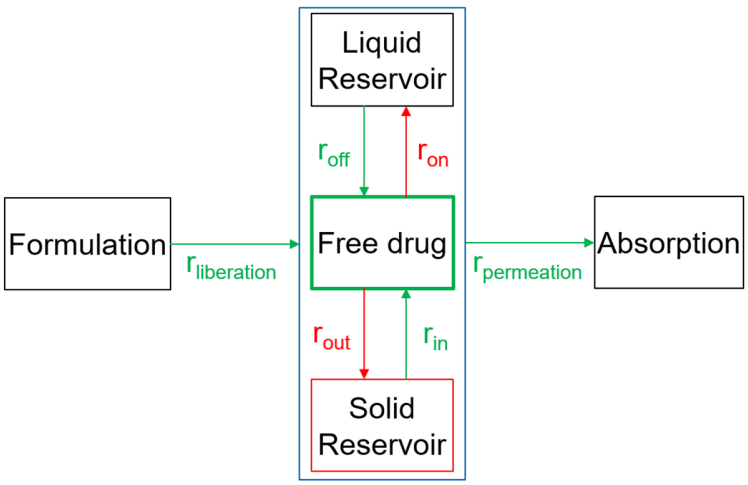

Figure 74: The bioaccessibility concept to illustrate and discuss the interplay between the drug dissolution process (r_{in}) and the permeation/absorption process ($r_{permeation}$) differing between in vitro and in vivo dimensions.

6. Concluding discussion

6.1 Review of problem statement

Identifying and overcoming oral absorption rate-limitations of poorly water-soluble drug substances is crucial for a safe and efficacious treatment. Mechanistic understanding is required to enable rational drug formulation development, saving time and money through first time right decisions. An exact analytical solution to project the fraction absorbed for general cases has not yet been discovered and is one of the main quests of theoretical biopharmaceutics today (90). The bioaccessibility concept and associated *in vitro* methodology presented in this work are conceptually nothing entirely new but more of a “connecting dots” and simplification approach. The proposed guidance illustrates how absorption rate-limitations can be estimated and addresssed *in vitro* and how this may translate into *in vivo* exposures (dogs) based on a single case study with the poorly water-soluble model compound naporafenib.

The problem from a pharmaceutical development perspective can be summarized by the apparent disconnect between solubility and permeability, typically assessed under non-identical conditions. During drug formulation development of poorly water-soluble molecules, the majority of investigations focuses on solubility and dissolution rate, which is partially justified by the fact that absorption for those unformulated drug molecules is often limited by dissolution rate and/or solubility. However, the dose as well as the drug form and formulation components may shift rate-limitations, as exemplified in the introduction. It could be misleading to believe that simply double the amount of drug in solution (e.g. though solubilization) would enable double the driving force for absorption. It was exemplified in this work why this may not be always true, i.e. apparent solubility not corresponding to effective driving force, specifically for poorly water-soluble drugs. Dependencies are for example, the dose, the relevant mass transport rate-limitation(s) and drug species contributing to permeation, i.e. bioaccessibility. A potential discrepancy between *in silico* model predictions (prospective) and observed exposures *in vivo* may arise from pairing apparently dissolved amount of drug with the permeability coefficient for the neat drug substance molecule. The fact that the true solubility is an intrinsic parameter and cannot be changed for a specific drug form is often ignored but appears crucial for the concept of freely dissolved drug as key driving force for absorption. Furthermore, it was recognized already in 1982 that micelle-solubilized drugs may show increased apparent solubility but decreased apparent permeability (106). This may have implications not only on the currently available *in silico* models but also for example on how to use classification systems such as the BCS or DCS. Typically, dose-numbers are calculated by dividing the dose by the apparent solubility in order to indicate how much liquid volume would be

required to dissolve the dose and therefore, whether a solubility-limited absorption has to be addressed. But which solubility, related to media selection, to use for this calculation/estimation? It was illustrated in this work that using either the apparent solubility of naporafenib in FaSSIF-V1 or (modified) FaSSIF-V2 may change the dose number by over a factor of 2. It is important to consider that the simulated intestinal fluids (SIFs) do not contain all components contained *in vivo* and even if, they are trying to represent an average condition rather than an upper and lower limit. This may pose a remaining risk when working with apparent solubilities measured in SIFs compared to human intestinal fluids, while being aware of real life variability (refer to **Figure 9**).

There is currently no agreement on which biorelevant media is the most appropriate for estimating the *in vivo* relevant solubility to calculate a dose number. And importantly, effects of solubilizing additives such as bile micelles that are encountered by every orally administered drug on permeability are rarely considered in the classification systems. Effective permeability is usually derived from the conversion of cellular permeabilities measured in absence of bile and/or formulation components. The assay is typically conducted at lower concentrations than estimated by the pharmaceutical dose per *in vivo* volume considerations, i.e. typically excess drug conditions for poorly water-soluble drugs where high doses are required for the treatment. Such limits of using cellullar assays to derive permeability can be addressed with artificial biomimetic membranes that are able to withstand pharmaceutically relevant drug concentrations and the presence of various excipients and biorelevant components. The open question remains how biorepresentative those artificial barriers are and what they are lacking in terms of *in vivo* relevant absorption resistances, e.g. such as the mucus layer. While permeation across artificial barriers is easier to interpret, it lacks of transport mechanisms and/or other absorption routes such as the paracellular pathway that may be included in cellular assays that likely remain more biorepresentative. In that sense, the use of artificial barriers is considered specifically beneficial for formulation development and optimization (what we can influence) but less suitable for absorption predictions if there is uncertainty about uptake mechanisms.

Another important aspect that is often inadequately addressed is the interaction of excipients with the endogenous bile-related transport system. As soon as the drug appears “bile-sensitive”, i.e. bile components are affecting apparent solubility and/or permeability, an interaction between the excipient and the bile system could indirectly affect the drug. Such interactions can be synergistic but also antagonistic. Examples are available in literature (123, 147) which support the findings of this work. Specifically for poorly water-soluble drug candidates, the selection of suitable excipients should include considerations about the API-bile-excipient interplay.

This work contributed to re-connect solubility with permeability under identical conditions *in vitro* (one assay) and illustrates limitations of available concepts and methodologies. The bioaccessibility concept has the potential to serve as future basis for classification systems of formulations while incorporating the API-bile-excipient interplay. The understanding of rate-limitations and relative effects on bioaccessibility can be further used for relative oral absorption predictions based on passive transcellular diffusion as major uptake mechanism. As long as the rate-limitation is matched between *in vitro* and *in vivo*, relative performance evaluations should be possible and an *in vitro-in vivo* relationships can be established.

A major milestone regarding the physicochemical basis of the absorption process was Fick's law published in 1855 about mass transport based on diffusion (52). The application of this law for pharmaceutical purposes is hampered by the presence of various drug species and potential rate-limitations of an oral absorption process. In 1960, a fantastic article was published in the field of skin permeation (percutaneous absorption from creams and ointments) by T. Higuchi that already contained most important considerations for applying Fick's law to better understand absorption processes (148). First and foremost, he found that instead of concentration, the thermodynamic activity is dictating the rate of the process. In the context of skin permeation the thermodynamic activity of the drug in the formulation vehicle was correlating with the mass transport observed. Furthermore, he differentiated between rate-limitations (skin barrier penetration or drug release from vehicle), routes of penetration (transepidermal or transfollicular) and dose/solubility conditions ("infinite dose" when applied as suspension or finite dose when applied as emulsion). This knowledge can be translated to the oral drug absorption situation where the drug activity in the gastrointestinal tract needs to be considered driving absorption. The rate-limitations need to incorporate the relevant kinetic processes of drug liberation, dissolution and permeation through relevant resistance layers, the route of absorption should differentiate between uptake mechanisms (transcellular, paracellular or active transport as examples) and the dose/solubility considerations can be integrated with the dose number approach. Due to the uncertainity of available *in vivo* volumes (e.g. fluid pockets), it is generally recommended to evaluate finite as well as infinite dose conditions *in vitro*. It was not attempted to calculate thermodynamic activities in this work but to use relative bioaccesibilities instead as obtained by *in vitro* flux setups. Kunst and Lee reported that the thermodynamic activity is proportional to the degree of saturation (149). Good linear correlation was observed in this work between the media degree of saturation (related to phase separation limit) and the mass transport observed for both, dialysis and lipidic flux setups. This is in good agreement with a variety of recent literature stating that the flux increases linearly up to the point of phase separation limit and that above this limit, phase separated drug may serve

as reservoir to replenish permeated drug while flux cannot be further increased linearly (150-153). For a drug formulator, it is essential to understand the impact of additives (e.g. excipients or biorelevant components) on membrane flux, which is basically impossible solely based on apparent concentrations. Unique insights into apparently dissolved drug concentrations were gained within this work by differentiating between solubilization and supersaturation in absence and presence of additives. In contrast to other work performed in this research area (139, 154), it was attempted to directly measure the amount of freely dissolved drug, as separated by ultracentrifugation, alongside flux measurements to link the presence of drug species to the observed mass transport for more mechanistic understanding.

A fascinating and related method to enable permeability measurements of poorly water-soluble drugs under solubilizing conditions, called the reciprocal permeability approach, was proposed by Katneni, Charman and Porter in 2006 (155). The difference to this work was the focus on surfactant concentration-dependent species generation and their impact on flux, in contrast to the drug concentration-dependency focus of this work. Generally, solubility limitations of BCS II and IV molecules pose problems to adequately determine their permeability, e.g. using cell-based assays. This is also a possible reason why such assays are typically performed at very low concentrations. The approach was two-fold but both aimed to measure permeability in presence of solubilizing agents and then correct for their presence to derive the intrinsic permeability in absence of solubilization. The first approach requires an estimation of the micellar association constant, for example based on equilibrium solubility or equilibrium dialysis studies which then allow to correct the observed apparent permeability measured at a given surfactant concentration to the intrinsic permeability. Those micellar association constants, however, can be quite inaccurate in case the uptake into micellar structures is not linear e.g. concentration-dependent (not constant) or in case the overall concentrations are very low (analytical constraints). Furthermore, such approaches are considered time-consuming and require relatively large amounts of material. The second approach eliminates the requirement of knowing the micellar association constant upfront. The apparent permeability ($P_{app,\ uncorrected}$) is measured under various surfactant concentrations (at least three above the critical micellar concentration) and then plotted reciprocally against amount of surfactant used. In order for this to work, one needs to know the amount of surfactants present in micellar form, hence knowledge about the critical micellar concentration. With that, the intrinsic apparent permeability can be obtained from extrapolation to the situation of zero surfactant and the micellar association constant can be derived from the slope. The results obtained with the reciprocal permeability approach were considered superior to

the use of separately determined micellar assocation constants. For more information, the reader is referred to the publication itself (155).

In frame of this work, time was insufficient to combine this approach with the work performed, e.g. in the form of a “reciprocal bioaccessibility approach”. Measurement of bioaccessibility (flux) in dependency of drug concentration (dose) and presence of additives (excipients or biorelevant components) at various concentration levels alongside direct measurement of what is freely dissolved by ultracentrifugation could provide unique mechanistic understanding of the concentration-dependent interplay between the drug, the excipient and the media components and resulting effect on the rate-limitations of drug mass transport.

A major persisting problem from a physiological/biopharmaceutical perspective is the intra- and interindividual variability, and furthermore, differences among pre-clinical species relative to the human situation (156, 157). Not only the gastrointestinal fluid compositions are of concern but also differences in physiology. For example differences in gastrointestinal motility due to a disease-state of a patient may affect the transit time of the drug through the GIT and can have an impact on drug absorption, specifically if the absorption window is narrow. Therefore, it is no surprise that 1) specific patient populations, 2) regional differences along the gastrointestinal tract, 3) advanced formulations and 4) food-drug interactions are considered key future research areas in the field of oral drug absorption (17).

Within this work, a systematic approach was followed by creating a biorelevant media landscape where only one parameter was changed at a time. This is in contrast to the commercially proposed media composition where for example a FaSSIF to FeSSIF difference does not allow to conclude whether it is rather driven by pH or biorelevant media components. The goal was to provide a clear strategy forward, avoiding to try and mimic the “average situation” but more aiming to identify what are the relevant components for a specific drug and to include them for further *in vitro* work. It was found that about 0.5 mM phospholipids can double the apparently dissolved concentration of naporafenib. Considering the compositional variability of phospholipids in humans in the fasted state (see **Figure 9** in the introduction), one may suspect that this variation of several mM phospholipids contributes to the overall variability observed in terms of absorption. On the other hand, it was shown in this work that such increased apparently dissolved drug concentrations do not necessarly translate into permeation differences *in vitro*. Confirmation *in vivo* would be desired but such studies are basically impossible to conduct. It is therefore of great interest to understand and evaluate potential physiological/biopharmaceutical risks in terms of exposures upfront during development. Generally, it is considered advantageous to keep the complexity of media

compositions at a minimum and to tailor the investigations according to project needs. For example, a non-ionizable compound does not necessarily need to be studied at various pH levels. Another example would be a highly lipophilic molecule where the inclusion of bile- and food-derived lipids may play a huge role. Overall, it is recommended to integrate biorelevant components into development activities for drug form and excipient selection. This is in line with the recommendation from experts (112). Future work may therefore be directed towards an *in vitro* screen of possible components present *in vivo* in order to identify what is relevant for a specific drug molecule. This may also serve as a tool to flag potential biopharmaceutical risks before *in vivo* studies are conducted. The inspiration came from a publication titled topography of simulated intestinal equilibrium solubility (158) which could be extented to flux/bioaccessibility.

6.2 Review of the bioaccessibility concept and *in vitro* guidance

The starting point for the guidance was the selection of a drug candidate for development with poor aqueous solubility, hence a BCS II or IV drug. The applicability and usefulness for BCS I and III but also IV drugs needs to be further investigated. Several potential model drugs were initially screened. Naporafenib as BCS II drug was selected as a model compound due to its low water solubility, sensitivity towards bile components and aqueous behavior related to supersaturation and form conversion. The first important question was which drug form to choose for further development. An essential first characterization was performed by equilibration in aqueous environment, monitored over time. It is recommended to use biorelevant media for improved form differentiation of poorly water-soluble drugs by apparent solubility. Learning that the kinetic concentration plateau of the high energy drug forms (amorphous, tosylate salt and solution form) was consistently achieved, an orthogonal method to detect phase separation of drug species was employed and found extremely useful to screen more conditions in a relatively short amount of time (121). Specifically for weak bases, gastric and intestinal pH values should be targeted. The amorphous and tosylate salt form should have been equilibrated in FaSSGF or 0.01 M HCl and monitored over time as well but was omited due to later dissolution experiments involving those forms. For form selection, apparent solubility appeared sufficient in this case but it needs to be remembered that within this work, important factors such as stability and processability were not considered. There is little to no benefit if the successfully delivered molecule is not active at its target site or when the manufacturing cannot be scaled up to commercial scale to reach a lot of patients. Intrinsic dissolution rate and nuclear magnetic resonance spectroscopy (NMR) were useful additions but not essential investigations for form selection. The first understanding of the bioaccessibility concept was gained, namely the relationship of the solid reservoir with the liquid phase, i.e. apparently dissolved drug.

The second question of interest dealt with factors that influence the bioaccessibility of naporafenib. Based on learnings from the form selection investigations, biorelevant media components were found to largely impact the aqueous concentration-time profiles. A novel method was explored to separate biorelevant media colloids containing solubilized drug from molecularly dissolved drug by ultracentrifugation. This allowed to understand the dose- and media-dependent formation of drug species. The presence of drug species was subsequently linked to drug mass transport using dialysis and lipidic flux experiments to obtain more mechanistic understanding on what factors are affecting the bioaccessibility in those setups. The barriers were found to form different resistances for naporafenib to permeate, which needs to be considered when comparing the two assays. However, the degree of saturation of the media linked to the saturation of molecularly dissolved drug, was found to be the main driver of permeation in both flux assays. This was further supported by direct measurements of molecularly dissolved drug in some systems. The main factor affecting bioaccessibility was considered the dose up to the point of media saturation where phase separations occurs. Below media saturation, distribution of drug between the liquid reservior (e.g. mixed micelles) and the aqueous phase reduce the amount of freely dissolved drug and reduce the driving force for permeation. The liquid reservoir therefore is considered a limiting factor of bioaccessibility below media saturation but may still offer higher bioaccessibility compared to undissolved crystalline solids. A drug formulator should in any case try to avoid using excess amounts of solubilizers and needs to assess whether endogenous components in the gastrointestinal tract are expected to exhibit extensive solubilization *in vivo*, relative to the dose administered. Limitations of mass transport *in vitro* were further explored by adjusting the hydrodynamics condition through an increase in stirring speed. The unstirred water layer was found a relevant resistance layer for the permeation of naporafenib under excess drug conditions. This is in line with theoretical considerations of the expected absorption rate-limitation of a supersaturating delivery system of a BCS II compound (86, 88). In reality, it is very likely that the mucus layer poses an even greater resistance to permeation. A drug formulator should also consider small drug species (e.g. drug solubilized in small micelles or drug nanoparticles) as additional promoter of bioaccessibility through shuttling mechanisms of drug through the unstirred water layer to the actual membrane surface. It is very unclear whether direct interactions between the epithelial membrane and the solid and/or liquid reservoir are possible and needs further investigations. The role of mucus also needs to be further explored. In order to identify factors affecting bioaccessibility, it may be sufficient to measure flux. However, parallel characterization of drug species present may provide valuable insights into why apparent concentrations in the donor may not be reflected in the

acceptor compartment. The section aimed to connect the learnings from the previous section about apparent solubility to the driving force for permeation via drug species differentiation into molecularly dissolved drug, drug in liquid reservoir and drug in solid reservoir. All undissolved drug species are included in the solid reservoir.

The third question was about how excipients can further manipulate bioaccessibility. The first screening investigation was characterizing the effects of excipients on the phase separation limit. This allowed to estimate excipient functionalities and categorize them into inert excipients and excipients with an effect on e.g. solubility or bile interaction. An increase in the phase separation limit indicates a solubilizing functionality of the excipient, i.e. providing a hydrophobic environment for the drug. A decrease in the limit may indicate that the excipient has an effect on the existing liquid reservoir (as for example in the case of simulated bile systems) or effects on the solid reservoir. As we have seen within this work, an increase in the apparent phase separation limit does not necessarly translate into a benefit for bioaccessibility. Both, nuclear magnetic resonance spectroscopy and dialysis flux were useful tools to complement the phase separation assessment and to flag potentially misleading hits. Once the excipient effects on apparent solubility were understood, the kinetic process towards this situation, namely liberation and dissolution rate, and the kinetic process from that situation, namely diffusion and permeation, were assessed separately. A connection between the dissolution assay and the flux investigation was done via apparent solubility, as illustrated in the bioaccessibility concept. The differentiation of drug species in presence of excipients was not sufficiently working. It would be required to make dilution series with the excipients of interest and determine the effect on apparent solubility in parallel to dynamic light scattering measurements in order to establish suitable parameters to claim robust removal of solubilized drug species. Orthogonal characterization of drug species is useful to understand bioaccessibilty, but not essential. The outcomes of the lipidic flux experiments were able to reflect the *in vivo* exposures observed in dogs by mimicking absorption in the intestine in presence of excipients and phase separated drug species. The phase separation limit was considered misleading in the case of Eudragit EPO but was in line with Hydroxypropylcellulose and Kolliphor RH40. Dialysis flux to some extent and more the NMR observations were allowing to flag Eudragit EPO as likely non-favorable excipient. The two-step dissolution assay was qualitatively in agreement with the *in vivo* exposures in the intestinal phase. However, due to the administered dose, the use of an acidic pH vehicle, the expected *in vivo* solubility at the absorption site and the assumption that the excipients mainly affected the dissolution rate indirectly via apparent solubility increase, the initial dissolution rate was not considered the major differentiating factor among the three tosylate salt suspensions with

excipients. When the dissolution rate is affected by excipients via liquid reservoir and not the solid reservoir, it was assumed that the increase in the rate of dissolution was proportional to the apparent solubility (phase separation limit) increase in presence of this excipient. This might not be valid in case sub-processes such as wetting or disintegration are rate-limiting the dissolution. Furthermore, it may be expected that the amount of freely dissolved drug during the course of dissolution in presence of solubilizing excipients will be equal among excipients and proportional to the respective media saturation. Expressing the dissolution rate as degree of media saturation over time might yield equal curves if no other mechanisms (e.g. wetting) play a role. The translation of apparent concentrations expected at the site of absorption (small intestine) into a driving force for permeation, hence bioaccessibility, was considered most adequate to correlate with *in vivo* performances of tosylate salt – excipient suspensions. This answered the question how *in vitro* bioaccessibility translated into *in vivo* exposures in those specific cases.

Based on the dog PK study read out, the most important question then was how the identified/suspected oral absorption risks or limitations can be further addressed using rational formulation development. Due to *in vitro* findings with Eudragit EPO and *in vivo* confirmation, one should be careful using that excipient, specifically related to bile compatibility and possible drug-excipient complex formation in solution with reduced bioaccessibility. With Kolliphor RH40 as solubilizing excipient, the initial absorption phase was likely accelerated but suspected to have rapidly declined afterwards due to drug form conversion to crystalline monohydrate. With Hydroxypropylcellulose, the apparent solubility and bile system should have remained untouched, while mainly preventing form conversion / desupersaturation. Two possible ways of improving the absorption of naporafenib are offered here, which likely need to be balanced. One may increase the apparent solubility (related to phase separation limit) using solubilizing excipients, expected to increase the initial rate of dissolution but might also promote form conversion / desupersaturation. The other option was to inhibit form conversion by inclusion of a “parachute functionality” with HPC. A potential gain from an optimized spring effect using the amorphous form compared to the salt form was also investigated. This translated into a microemulsion (ME) formulation to increase the amount of drug in solution (apparently dissolved) and into an amorphous solid dispersion (ASD) approach to increase dissolution rate through the solid reservoir and delay form conversion through a crystallization inhibitor. Both “enabling” approaches resulted in higher exposures compared to the conventional approaches, i.e. tosylate salt suspension study arms. This could not be predicted by *in vitro* bioaccessibility, illustrating very important limitations of the proposed tools. While it is feasible to identify possible opportunities for the drug formulator to manipulate bioaccessibility to increase exposure, it is currently not possible to understand at which point the rate-limitations are shifting and another

aspect of the formulation needs to be optimized. A nice example was provided within this work showing that both, dissolution and permeation are important processes related to oral drug absorption, but those processes cannot be connected *in vitro* in a biorepresentative manner with the given setups. For example, the missing surface area for permeation in available flux setups compared to the *in vivo* available intestinal surface area does not allow to evaluate differences in kinetics of the solid reservoirs to replenish permeated drug via dissolution. No difference was found *in vitro* between the amorphous and tosylate salt solid reservoirs while *in vivo* there was a substantial difference in exposure. Since both HPC and HPMC were found not to affect the phase separation limit, it appears valid to suspect the dissolution rate as differentiating factor between the tosylate salt suspension + HPC and the ASD. The microemulsion was also evaluated in a MacroFlux assay internally but yielded the same flux slope as the ASD despite much more drug in solution in the donor compartment (data not shown). Highlighting those assay limitations is considered highly valuable for the scientific community, pharmaceutical development but also the regulatory authorities.

6.3 Learnings for drug formulation development

In a nutshell, the key assumption for drug formulation scientists is that aside from stability and processability aspects, optimization of *in vitro* drug mass transport of poorly water-soluble drugs based on passive diffusion through a biorepresentative barrier is sufficient to guide formulation development. Other mechanisms for drug absorption can hardly be influenced in a targeted manner with the formulation. The challenge of this task is formed by the selection of biorepresentative conditions such as the gastro-intestinal transfer step, dose per volume considerations, assay scale limitations (surface-to-volume ratio), selection of a biorepresentative barrier and the inclusion of relevant endogenous components. For the moment, the dissolution and permeation processes cannot be adequately connected within a simple single assay and need to be evaluated separately. Therefore, the flux assay should be viewed complementary to the rather well established dissolution assays. The main limitations of bioaccessibility amenable to manipulation by the formulation scientist are presented below.

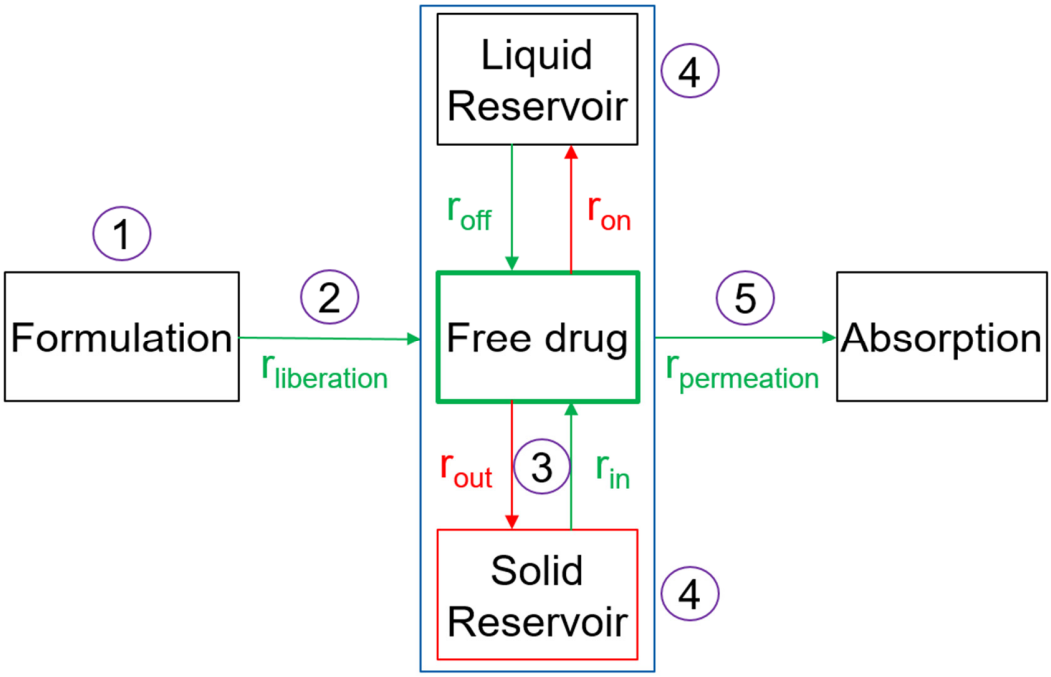

Figure 75: The bioaccessibility concept and associated absorption rate-limitations amenable to manipulation by the formulation scientist.

1) **Dose-limited**: Increase dose and test if dose-linearity is observed, e.g. for *in vitro* dissolution and flux and/or *in vivo* exposures
2) **Liberation rate-limited**: Increase $r_{liberation}$ by optimizing the release of drug from the dosage form. Ensure adequate wetting, water penetration and disintegration, dispersion. Can be evaluated with disintegration (or dissolution) tests.
3) **Dissolution rate-limited**: Increase r_{in} (dissolution) directly through exchange of the solid reservoir (e.g. cocrystal, salt or amorphous form) or reduction in particle size (increase in surface-area for dissolution). Increase r_{in} indirectly through an increase in apparent solubility (liquid reservoir) using solubilizing additives. Decrease r_{out} (precipitation/form conversion) by including precipitation/crystallization inhibitors. Optimize "spring-parachute effect". Can be evaluated based on dissolution assays or equillibration over time experiments.
4) **Solubility-limited**: Differentiate between solid or liquid reservoir-limited. Increase F_{BAC}.
    a. **Solid reservoir-limited**: Promote solid reservoir with higher bioaccessibility, e.g. use of salt or amorphous forms, avoid crystallization into most stable forms. Main option to affect molecularly dissolved amount of drug and limited by the apparent phase separation limit (typically amorphous solubility). Needs to be evaluated with flux assays and supported by monitoring drug forms present by XRPD.

b. **Liquid reservoir-limited**: Use solubilizing additives to bring more drug in a dissolved state (apparently dissolved) while not affecting freely dissolved drug above saturation. Solubilization is beneficial if r_{in} is considered a higher resistance to permeation than r_{off}, which is typically the case for poorly water-soluble drugs. If r_{off} is a higher resistance than $r_{permeation}$, a potential decrease in bioaccessibility through solubilization needs to be appreciated. If the dose is lower than the apparent solubility (freely dissolved drug and liquid reservoir), a dose-limited case is present and reduced bioaccessibility is observed due to the liquid reservoir. Needs to be evaluated with flux assays below and above media saturation.

5) **Permeability-limited**: Increase $r_{permeation}$ via effective permeability P_{eff}. Further differentiate resistance layers of permeation, i.e. unstirred water layer (UWL), mucus layer or epithelial membrane. Options are limited depending on the major resistance layer.
    a. **UWL-limited**: Increase permeability through the unstirred water layer (P_{UWL}) via effective diffusion coefficient (D_{eff}) related to fraction of drug in e.g. micelles (f_m) or drug in form of colloidal nanoparticles (f_c) and their hydrodynamic diameter.
    b. **Mucus layer-limited**: Out of scope for this work
    c. **Epithelial membrane-limited**: Out of scope for this work

For the permeability-limited, mucus and epithelial membrane-limited cases, some options are discussed in literature such as mucoadhesive strategies or the so called “permeation enhancers”. However, modification of the mucus or epithelial membrane should be approached with caution due to uncertainties regarding safety. Application of extensive amounts of surfactants for example may yield high exposures in permeability-limited cases, however, at what cost?

In conclusion, the processes involved in oral drug absorption should be considered as resistances. Every single resistance will influence the overall resistance, however to different degrees. The proposed strategy for formulation scientists is to try and identify the largest resistances and to address them *in vitro* first using dissolution and flux assays, with subsequent confirmation *in vivo* due to limitations of the proposed tools. Specific attention has to be paid to possible shifts in the absorption rate-limitation. From the *in vivo* confirmation, one may then further optimize the formulation in case the observations can be explained conceptually sound. If his is not the case, one has to identify the underlying root cause of the discrepancy, e.g. whether it is due to other uptake mechanisms with involvement of active transport processes etc. This work concludes therefore that mechanistic understanding regarding absorption is a must have to enable rational formulation development. For example, if drug species promoting bioaccessibility are identified, the formulation should target to generate those species, eventually already providing drug in the

form of those species. The microemulsion approach would be one case where drug was provided primarly as solubilized drug species. Potentially, such mechanistic understanding can in some cases improve the often lacking confidence regarding the translation to humans from readouts from preclinical/animal studies, see **Figure 76**. More generally, the proposed bioaccessibility concept and *in vitro* methodology is in alignement with the recently proposed absorption-driven drug formulation or flux-based formulation development concept showcasing the use of flux throughout early development phases (159).

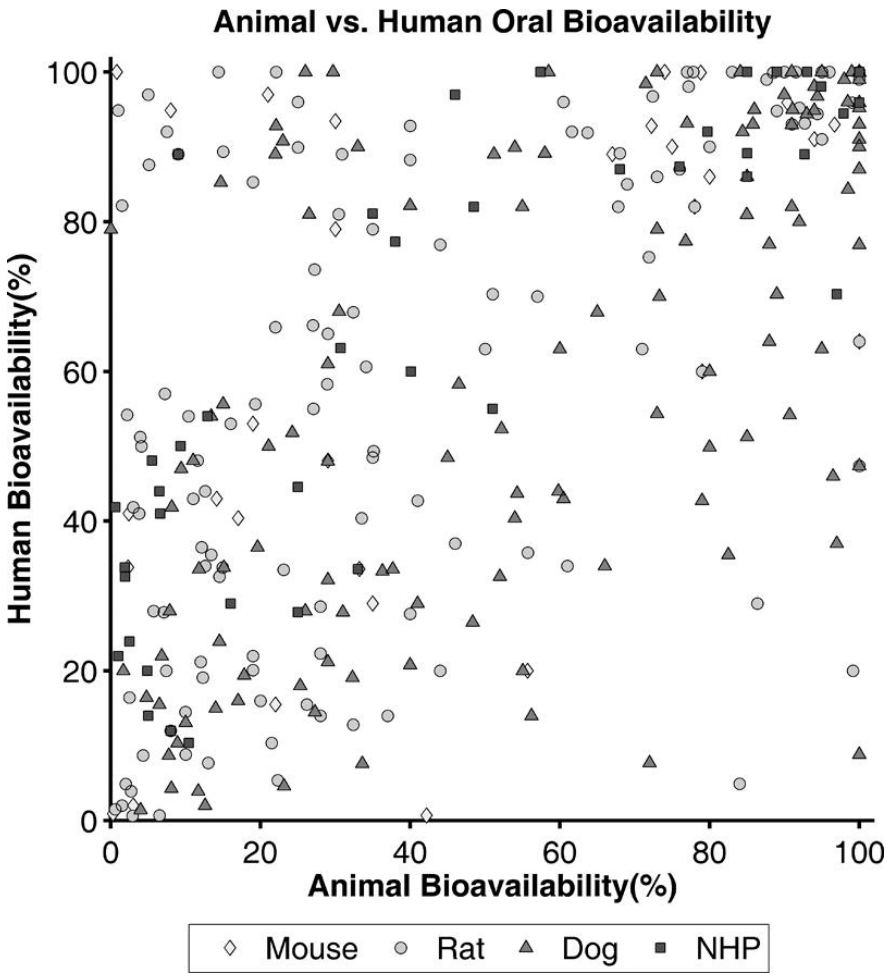

Figure 76: Correlation between bioavailability observed in humans and preclinical species: mouse, rat, dog and non-human primates (NHP). Adopted from open access article: European Journal of Pharmaceutical Sciences, Animal versus human oral drug bioavailability: do they correlate? Musther et al. (116). Copyright 2013 Elsevier B.V.

7. Outlook

A major limitation of using flux for either formulation development but also relative performance predictions is the uncertainty of matching the *in vivo* rate-limitations *in vitro*. Future work should therefore target ways to integrate specific *in vivo* conditions into a representative *in vitro* setup. Primary focus should receive the barrier and its resistance properties as well as *in vitro* dimension (surface-to-volume) and assay conditions (media selection, stirring). It may well be that this can never be fully achieved due to the anatomical and physiological complexity of the gastrointestinal tract. A possible work around could be to use existing *in silico* models which already contain several compartments along the GIT and extend them by an "*in vitro* compartment" reflecting specific equipment dimensions and conditions. The differences can then be used to scale the *in vitro* findings to the *in vivo* situation but much more work is required to enable this. Generally, an updated mechanistic absorption model is currently missing. While individual processes can be described mathematically, a general solution involving all relevant processes is not yet available. Typically, a lot of assumptions and only one dominating rate-limitation are applied to express a specific case mathematically, similar as for the physicochemical basic equations of the oral drug absorption process. Some steps are taken in the right direction by balancing individual factors as performed by Sugano and Tereda. They expressed the absorption rate as function of the dissolution rate and permeation rate, while a weighting between dissolution and permeation was approached using the dose number (90). A global mathematical solution, however, should incorporate the most recent knowledge about driving factors of oral absorption and remove the ideology that apparently dissolved drug can be used as surrogate to estimate the driving force for absorption, specifically in the case of poorly water-soluble drugs. Ideally, any efforts incorporate possible confounders including drug stability in the gastrointestinal environment or other absorption routes alongside previously mentioned mechanisms such as metabolism, clearance etc. One may also think about additional areas for example lipidic digestion, which appear intuitively relevant considering the natural function of the bile system.

In a blue sky scenario, establishing an updated mechanistic absorption model could pave the path for digital drug development and may open the doors for simulating a "formulation space". Currently, we cannot evaluate whether a further increase in dissolution rate or apparent solubility provides an additional benefit for exposure or whether the absorption rate-limitation has already shifted, e.g. from dissolution rate/solubility-limited to permeability-limited. There may be a great benefit for the interface between pharmaceutical industries and the regulatory authoritites related to a new potential fundament for biowaivers/bioequivalence studies, improved *in vitro-in vivo* correlations and the next generation of more mechanistic PBPK models. Eventually an updated

“formulation classification system” (FCS) may emerge, incorporating the concept of drug species and the understanding of the dose-dependent drug-exipient-bile interplay. In the end, we hopefully all would like to bring a direct benefit to patients, while ensuring safety and efficacy.

8. Summary

Poor and variable oral bioavailability is of major concern regarding safety and efficacy for the treatment of patients with poorly water-soluble drugs (PWSDs). The problem statement of this work involves a pharmaceutical development perspective, the physicochemical basis of the absorption process and physiological/biopharmaceutical aspects. A methodology was developed to attempt closing the gap between drug liberation and dissolution and the appearance of drug in the blood. Considering what is out of control from a formulation development perspective, a clear differentiation between bioavailability and bioaccessibility was necessary. Focusing on the absorption process for formulation development, bioaccessibility of a model drug was measured by means of flux across artificial biomimetic membranes. Such setups can be considered to reasonably mimic relevant oral absorption resistances *in vitro* in terms of diffusion through an unstirred water layer (UWL) and a lipidic barrier. Mechanistic understanding of the driving force for permeation was gained by differentiating drug species and subsequently linking them to the observed transfer rates using a bioaccessibility concept. The three key species that need to be differentiated are molecularly dissolved drug, drug associated in solution with other components (liquid reservoir) and undissolved drug (solid reservoir). A guidance for rational formulation development of PWSDs is proposed based on naporafenib, a BCS II model active pharmaceutical ingredient (API) with poor aqueous solubility and high permeability. The guidance is exemplified using the five question from **section 3.4** for drug formulation scientists.

Once a drug candidate with poor aqueous solubility is selected, the first question to be addressed is which drug substance form to select. Form selection should typically balance stability and processability (technology) with biopharmaceutical aspects, while here, considerations were limited to the suitability to achieve adequate exposures *in vivo* (biopharmacy). Forms were first distinguished using X-ray powder diffraction (XRPD), single-crystal structures (crystalline forms only) and scanning electron microscopy (SEM) for morphology. Identified relevant forms of naporafenib were: a monohydrate, an anhydrate, a tosylate salt, an amorphous form and a solution form (dissolved drug in DMSO). Differentiation based on apparent solubility was performed monitoring drug equilibration over time in various aqueous environments including biorelevant components. The assay was conducted over 24 hours to account for possible form conversions as identified by XRPD. Phase separation limits were assessed in an extented media landscape and linked to the amorphous “solubility”. Insights were complemented by nuclear magnetic resonance spectroscopy (NMR) and intrinsic dissolution rates (IDR) of selected forms. No differentiation of species measured as apparently dissolved drug was performed in this section. Irrespective of employing the tosylate salt, the amorphous or solution form, the same kinetic

concentration plateau was observed before conversion to crystalline monohydrate occured, associated with a sudden drop in dissolved drug concentrations (desupersaturation). Phase separation limits detected by orthogonal techniques were in acceptable agreement with those concentration plateaus. The tosylate salt and the amorphous form were chosen as suitable drug form candidates based on apparent solubility in biorelevant media. To note, low concentrations in aqueous buffer systems hampered robust form differentiation. Intrinsic dissolution rates were considered insufficient to select one form over the other, in line with theoretical expectation from the previously obtained similar kinetic concentration plateau. Overall, biorelevant media components substantially affected the concentration-time profiles of naporafenib and NMR signals were found to correlate with the amount of apparently dissolved drug in those systems. Based on the awareness of (mixed) micelles and vesicles that may form in such biorelevant media systems, it was of great interest to identify how much drug is associated to such colloidal structures (liquid reservoir) and how such intermolecular liquid-state interactions may affect the permeation of drug across an absorption barrier.

The driving force for permeation cannot be easily derived from apparently dissolved drug concentrations, as stated by experts in the field and supported by various recent literature. This is primarly attributed to the presence of multiple drug species. The important second question in the guidance dealt with identification of factors impacting bioacessibility with special emphasis on drug species differentiation. Drug contained in solubilizing entities (such as mixed micelles/vesicles) was separated from molecularly dissolved drug with ultracentrifugation by spinning at very high speed (1’019’000 g) for one hour. The separation efficiency was evaluated based on a signal-to-noise ratio from dynamic light scattering measurements of the supernatant. To the best of knowledge, this is the first time a successful separation of solubilized drug from molecularly dissolved drug was reported involving stable (crystalline) and metastable (amorphous) PWSD-simulated bile systems. After the study of dose-dependent drug species generation in two selected biorelevant media, their presence was linked to flux in an exploratory ultracentrifugation-flux combo experiment. Bearing in mind important concepts to enhance oral absorption of PWSD such as the “spring-parachute” and the “particle drifting” concept, differentiation between solubilization and supersaturation, hence solubilized and free drug, was considered key for the mechanistic understanding of bioaccessibility. Such understanding would be prerequisite to rationally manipulate the oral drug absorption process through formulation development. Despite beyond two-fold differences in the amount of apparently dissolved drug, flux was equal between two selected biorelevant media systems under excess drug conditions. This could be rationalized by an equal amount of molecularly dissolved drug measured after ultracentrifugation. It was shown

that the saturation of freely dissolved drug occurs at the phase separation limit in the respective media and that up to that point, a linear relationship between flux and media saturation exists. Above that point, only minor effects on flux were observed which is in line with literature. Performing ultracentrifugation-flux combo experiments at various dose levels at, above and below the phase separation limit enabled to understand the impact of drug species on flux. The context of those results to the first section supports the importance of the solid reservoir in relation to the amount of moleculary dissolved drug. The amount of freely dissolved drug in solution is dictated by the solid reservoir, related to solubility as intrinsic property. Addition of solubilizing components, as contained in biorelevant media or formulations, will primarly affect the liquid reservoir but does not per se increase the amount of molecularly dissolved drug and hence the main driving force for permeation. However, drug in reservoirs, that is drug either in the form of phase separated species or associated to colloids, may facilitate fast replenishment of permeated drug and therefore keep the amount of molecularly dissolved drug high throughout the transfer process. Those findings need to be considered when applying the “spring-parachute” concept for absorption predictions or for guidance of formulation development. Furthermore, limitations of *in vitro* drug mass transport were illustrated based on experiments at 100 and 400 rpm stirring speed which were understood to modify the involved UWL. The experiments demonstrated that different colloidal species, having an order of magnitude difference in hydrodynamic radius, impacted the UWL diffusive transport. It could be concluded that media saturation, reservoir effects as well as diffusing drug species alongside molecularly dissolved drug through the UWL were main factors impacting bioaccessibility of naporafenib.

The third question evolved around possibilities to manipulate bioaccessibility using excipients. The purpose was to understand if and how excipients modify generated drug species. If there is an interaction with the drug or biorelevant media components, the point at which phase separation occurs may be modified. A solubilizing functionality of an excipient would bring more drug in solution (increase of phase separation limit) but also drug complexation may result. Hydroxypropylcellulose (HPC), Hydroxypropylmethylcellulose (HPMC) and Kollidon VA64 (VA64) were found to be inert excipients, i.e. no change in the limit and therefore not affecting the simulated bile system. Eudragit EPO (EPO) and Kolliphor RH40 (RH40) both significantly increased the phase separation limit in buffer and biorelevant media compared to without excipients, respectively. Sodium dodecyl sulfate (SDS) also elevated the phase separation limit, seemingly slightly more for the buffer than the biorelevant system. Such behavior may indicate an interaction between the micelles formed by SDS and the biorelevant components. Apparent solubilization effects of excipients were complemented with flux through dialysis membranes and

NMR. Flux through dialysis membranes under excess drug conditions showed almost no differentiation between excipients and also very similar mass transport rates between buffer and biorelevant media. To evaluate for potential masking effects of amorphous phase separated drug species on excipients effects, flux experiments were repeated at 50% media saturation with no phase separated drug present. Also in that situation, rather poor differentiation between excipients was observed. Some slight reduction in dialysis flux for the specific case of EPO was creating discrepancy with respect to an increase in the phase separation limit. NMR investigations revealed reduced aromatic drug proton signals which were interpreted as reduced molecular mobility of the drug, despite an increase in the total amount of drug in solution. This likely means that EPO is solubilizing the drug by complexation, thereby reducing its bioaccessibility. NMR signals with HPC and RH40 were in line with the observed impact on the phase separation limit, i.e. no change and increase, respectively. Noteworthy, flux through dialysis membranes was about 100-fold lower compared to lipidic (biomimetic) membranes, thereby reducing the sensitivity to detect excipient/media effects on bioaccessibility. Three representative excipients were selected for further investigations *in vitro* using separate dissolution assay and the ultracentrifugation-flux combo experiment. HPC was representing the inert excipients, not affecting the bile system nor the drug's molecular mobility but with potential to act as crystallization inhibitor. EPO was included due to its ability to stabilize large amounts of drug in solution and potential to also stabilize the amorphous form of the drug, but with suspected negative impact on bioaccessibility. RH40 was selected based on its solubilizing properties for naporafenib and suspected synergistic action with the simulated bile system. Noteworthy, the separation efficiency by ultracentrifugation was considered insufficient with excipients compared to the sole biorelevant media, based on dynamic light scattering. The relevance of the API-bile-excipient interplay for excipient selection was already reported, for example in Schlauersbach et al. 2020 (122) and was confirmed in this work. Specifically, HPC and RH40 allowed higher flux in biorelevant media compared to the buffer system. On the contrary, EPO generated higher flux of naporafenib in aqueous buffer, hinting towards an incompatibility of EPO with simulated bile components.

The fourth question was subsequently approached for those specific cases to assess, how *in vitro* bioaccessibility translates into *in vivo* exposures. Three naporafenib tosylate salt suspensions based on a pH 2.6 citrate-phosphate buffer with EPO, HPC or RH40 as excipients were administered to beagle dogs at 30 mg/kg dose. Relative bioaccessibilities in presence of those three excipients evaluated through *in vitro* flux using excess drug (solution form) could be well correlated with suitable output parameters of the pharmacokinetic study. Specifically, the correlation with the parameter Cmax/Dose/Tmax as surrogate for the rate of absorption was

striking, i.e. $R^2 > 0.99$. This is physically sound as both the absorption rate *in vivo* and the permeation rate *in vitro* reflect mass transfer over time and area, i.e. flux. Thus, quantitating bioaccessibility in terms of flux was found biopredictive. This was probably facilitated by the situation that only one parameter, i.e. the excipient type, was changed for the *in vitro* and *in vivo* explorations. It is worth to note that the correlation of flux based bioaccessibility with absorption could be achieved simply employing DMSO dissolved drug added to FaSSIF-V1$_{PBS}$ with pre-dissolved excipients. Consequently, the pharmacokinetic study results verified the *in vitro* elaborated understanding of how bioaccessibility can be manipulated using excipients, in this case their impact on effective concentrations providing the gradient for permeation.

The fifth question was about how to mitigate identified oral absorption risks or limitations using rational formulation development. A potential dissolution rate-limitation and form conversion/desupersaturation risk was addressed with an amorphous solid dispersion (ASD) formulation. A suspected solubility-limitation was tackled with a microemulsion (ME) formulation. The ME and the ASD formulations were assessed in a two-step dissolution assay. Different dissolution, and for the ME desupersaturation, rates were observed and could be compared to the tosylate salt + HPC case. On top, the ASD was tested and compared to the tosylate salt + HPC case in separate dissolution (single-step) and ultracentrifugation-flux combo experiments. Interestingly, flux based bioaccessibility between tosylate salt + HPC and ASD was equal and the dissolution rate differences observed in other setups did not materialize. An overview of absolute mass transport rates measured *in vitro* for the various dissolution and flux assays indicates discrepancies at the order of magnitudes, i.e. flux transport rates significantly lower than dissolution rates. Consequently, the impact of dissolution rate on bioaccessibility of naporafenib was hidden when using the μFlux^{TM} / lipidic membrane (GIT-PAMPA) setup from Pion Inc. Ltd. This poses a challenge regarding *in vitro* to *in vivo* translation of both, dissolution and flux data and their inevitable interplay. Additional arms of the pharmacokinetic study in dogs revealed substantially increased exposures for the ASD and even more for the ME formulation. This would be in line with findings from the two-step dissolution assay, i.e. the absorption rate was limited by the rates of ASD dissolution and ME desupersaturation, respectively. Considering the three tosylate arms, dissolution rate could have been comparable or played a minor role while the effective concentrations driving permeation were altered by the involved excipients .

It can be concluded that *in vitro* permeation setups may not sufficiently reflect the dynamic interplay between the dissolution and the permeation process happening *in vivo*, e.g. due to surface-to-volume differences. However, and as demonstrated, the necessity to connect dissolution, solubility and permeation remains unchanged. For the time being, it is recommended

to assess dissolution and permeation separately and connect them via apparent solubility as illustrated with the bioaccessibility concept. The understanding of the evolution and dynamic interplay of drug species with their properties and effects on bioaccessibility is key for rational development of BCS II and likely also BCS IV drugs, given a reasonable dose. Such mechanistic understanding may also help to improve *in silico* modeling of absorption to allow for better predictions in the near future. This work follows recent literature trends related to a paradigm shift on how to develop poorly water-soluble drugs such as the absorption-driven drug formulation (ADDF) concept published by Kadar et al. in 2022. While previously the goal was to bring as much drug as possible into solution, the new trend is to target delivering as much drug as possible over a biorepresentative barrier.

9. Zusammenfassung

Eine geringe und variable orale Bioverfügbarkeit gibt Anlass zu grosser Besorgnis hinsichtlich Sicherheit und Wirksamkeit einer Behandlung von Patienten mit schwer wasserlöslichen Arzneimitteln. Die Fragestellung dieser Arbeit bezieht sich auf die pharmazeutische Entwicklungsperspektive, die physikalisch-chemischen Grundlagen des Absorptionsprozesses und physiologisch/biopharmazeutische Aspekte. Es wurde eine Methodik entwickelt, um die Lücke zwischen Wirkstofffreisetzung und -auflösung und dem Erscheinen des Wirkstoffes im Blut zu schliessen. Angesichts dessen, was aus Sicht der Formulierungsentwicklung nicht beeinflusst werden kann, war eine klare Unterscheidung zwischen Bioverfügbarkeit und Biozugänglichkeit notwendig. Mit Fokus auf den Absorptionsprozess wurde die Biozugänglichkeit eines Modellwirkstoffes mittels Massentransportexperimente durch künstliche biomimetische Membranen gemessen. Es kann davon ausgegangen werden, dass solche Anordnungen relevante orale Absorptionswiderstände hinsichtlich der Diffusion durch eine ungerührte Wasserschicht und eine Lipidbarriere *in vitro* nachahmen. Durch die Differenzierung der Wirkstoffspezies und die anschliessende Verknüpfung mit den beobachteten Transportraten mittels eines Biozugänglichkeitskonzepts wurde ein mechanistisches Verständnis der treibenden Kraft für die Permeation gewonnen. Die drei Schlüsselspezies, die unterschieden werden müssen, sind molekular gelöste Substanz, in Lösung mit anderen Bestandteilen assoziierte Substanz (flüssiges Reservoir) und ungelöste Substanz (festes Reservoir). Es wird ein Leitfaden für die rationale Formulierung von schlecht wasserlöslichen Substanzen vorgeschlagen, welcher auf Naporafenib basiert, einem pharmazeutischen Wirkstoff aus der BCS Klasse II mit geringer Wasserlöslichkeit und hoher Permeabilität. Der Leitfaden wird anhand der fünf Fragen aus **Abschnitt 3.4** veranschaulicht.

Sobald ein Wirkstoffkandidat mit schlechter Wasserlöslichkeit ausgewählt ist, stellt sich zunächst die erste Frage, welche Wirkstoffform ausgewählt werden soll. Bei der Wahl der Form sollte in der Regel Stabilität und Prozessierbarkeit (Technologie) mit biopharmazeutischen Aspekten abgewogen werden, während hier die Überlegungen auf die Eignung zur Erzielung adäquater Expositionen *in vivo* (Biopharmazie) beschränkt wurden. Die Unterscheidung der Formen erfolgte zunächst mittels Röntgenbeugungsanalyse, Einkristallstrukturen (nur kristalline Formen) und Rasterelektronenmikroskopie (REM) für die Morphologie. Relevante Formen von Naporafenib waren: ein Monohydrat, ein Anhydrat, ein Tosylatsalz, eine amorphe Form und eine Lösungsform (in DMSO gelöste Substanz). Es wurde eine Differenzierung basierend auf der scheinbaren Löslichkeit durchgeführt, durch die Überwachung des Löslichkeitsgleichgewicht über die Zeit in verschiedenen wässrigen Umgebungen einschliesslich biorelevanter Komponenten. Die Analyse

wurde über 24 Stunden durchgeführt, um mögliche Formkonvertierungen zu berücksichtigen, die durch Röntgenbeugungsanalyse identifiziert wurden. Phasentrenngrenzen wurden in erweiterten Umgebungen untersucht und mit der amorphen “Löslichkeit” verknüpft. Die Erkenntnisse wurden durch Kernspinresonanzspektroskopie und intrinsische Auflösesraten ausgewählter Formen ergänzt. In dieser Sektion wurde keine Differenzierung der Wirkstoffspezies vorgenommen, die als scheinbar gelöste Substanz gemessen wurde. Unabhängig von der Verwendung des Tosylatsalzes, der amorphen oder gelösten Form, wurde das gleiche kinetische Konzentrationsplateau beobachtet, vor der Konvertierung zu kristallinem Monohydrat, welche mit einem plötzlichen Abfall der gelösten Wirkstoffkonzentrationen (Übersättigung) verbunden ist. Die durch orthogonale Verfahren ermittelten Phasentrenngrenzen lagen in akzeptabler Übereinstimmung mit diesen Konzentrationsplateaus. Das Tosylatsalz und die amorphe Form wurden aufgrund der scheinbaren Löslichkeit in biorelevanten Medien als geeignete Wirkstoffkandidaten ausgewählt. Niedrige Konzentrationen in wässrigen Puffersystemen erschwerten eine robuste Formdifferenzierung. Die intrinsischen Auflösegeschwindigkeiten wurden als unzureichend erachtet um eine Form der anderen vorzuziehen. Dies entsprach der theoretischen Erwartung aus den zuvor beobachteten, vergleichbaren, kinetischen Konzentrationsplateaus. Insgesamt beeinflussten biorelevante Medienkomponenten die Konzentrations-Zeit-Profile von Naporafenib wesentlich und die Kernspinresonanzspektroskopie-Signale korrelierten mit der Menge des anscheinend gelösten Wirkstoffs in diesen Systemen. Basierend auf den Erkenntnissen über (gemischte) Mizellen und Vesikel, die sich in solchen biorelevanten Mediensystemen bilden können, war es von grossem Interesse, herauszufinden, wie viel Wirkstoff mit solchen kolloidalen Strukturen (flüssiges Reservoir) assoziiert ist und wie solche intermolekularen Wechselwirkungen in Lösung die Permeation des Wirkstoffs über eine Absorptionsbarriere beeinflussen können.

Die treibende Kraft für die Permeation lässt sich aus scheinbar gelösten Wirkstoffkonzentrationen nicht ohne weiteres ableiten, wie Experten auf diesem Gebiet behaupten und was durch verschiedene, aktuelle Literatur unterstützt wird. Dies wird in erster Linie auf das Vorhandensein mehrerer Wirkstoffspezies zurückgeführt. Die wichtige, zweite Frage des Leitfadens betraf die Identifikation von Faktoren, die die Biozugänglichkeit beeinflussen, mit besonderem Schwerpunkt auf der Differenzierung von Wirkstoffspezies. Der Wirkstoff, welcher in solubilisierenden Kolloiden (z.B. gemischte Mizellen/Vesikel) enhalten ist, wurde durch Ultrazentrifugation bei sehr hoher Geschwindigkeit (1’019’000 g) während einer Stunde von molekular gelöstem Wirkstoff getrennt. Die Abtrenneffizienz wurde anhand des Signal-Rausch-Verhältnisses aus dynamischen Lichtstreumessungen des Überstands bewertet. Dies ist nach bestem Wissen das erste Mal, dass

eine erfolgreiche Trennung von solubilisiertem und molekular gelöstem Wirkstoff in stabilen (kristallinen) und metastabilen (amorphen) simulierten Gallensystemen nachgewiesen wurde. Nach der Untersuchung der dosisabhängigen Generierung von Wirkstoffsspezies in zwei ausgewählten biorelevanten Medien wurde deren Präsenz mit der Transportrate in einem explorativen Ultrazentrifugation-Flux-Kombinationsexperiment verknüpft. Unter Berücksichtigung wichtiger Konzepte zur Verbesserung der oralen Absorption von schlecht wasserlöslichen Substanzen wie dem “Feder-Fallschirm”- (“Spring-Parachute”) und dem “Teilchen-Strömungs”-Konzept (“Particle Drifting”) wurde die Unterscheidung zwischen Solubilisierung und Übersättigung, also solubilisiertem und freiem Wirkstoff, als Schlüssel für das mechanistische Verständnis der Biozugänglichkeit angesehen. Ein solches Verständnis ist die Voraussetzung für eine rationale Manipulation des oralen Absorptionssprozesses bei der Formulierungsentwicklung. Trotz mehr als zweifachem Unterschied in der Menge an scheinbar gelöstem Wirkstoff war der Massentransport zwischen zwei ausgewählten biorelevanten Mediensystemen unter überschüssigen Wirkstoffbedingungen gleich. Dies konnte durch eine gleich grosse Menge an molekular gelöstem Wirkstoff, gemessen nach Ultrazentrifugation, rationalisiert werden. Es konnte gezeigt werden, dass die Sättigung von frei gelöstem Wirkstoff an der Phasentrenngrenze in den jeweiligen Medien stattfindet und dass bis zu diesem Zeitpunkt eine lineare Beziehung zwischen Massentransport und Mediensättigung besteht. Oberhalb dieses Punktes wurden nur geringfügige Auswirkungen auf den Transport beobachtet, was mit der Literatur übereinstimmt. Die Durchführung von Ultrazentrifugation-Flux-Kombinationsexperimenten mit unterschiedlichen Dosierungen bei, oberhalb und unterhalb der Phasentrennungsgrenze ermöglichte es, den Einfluss von Wirkstoffspezies auf den Transport zu verstehen. Diese Ergebnisse, im Kontext des ersten Abschnittes, unterstreichen die Bedeutung des festen Reservoirs im Verhältnis zur Menge der molekular gelösten Substanz. Die Menge an frei gelöster Substanz in Lösung wird durch das feste Reservoir bestimmt, welches mit der Löslichkeit als intrinsische Eigenschaft im Zusammenhang steht. Die Zugabe von solubilisierenden Komponenten, wie sie in biorelevanten Medien oder Formulierungen enthalten sind, wirkt sich primär auf das flüssige Reservoir aus, erhöht aber nicht per se die Menge des molekular gelösten Wirkstoffs und damit die Hauptantriebskraft der Permeation. Jedoch kann die Substanz in den Reservoirs, d.h. Wirkstoff entweder in Form von phasengetrennten Spezies oder assoziiert mit Kolloiden, eine schnelle Wiederauffüllung der abtransportieren Substanz erleichtern und folglich die Menge an molekular gelöstem Wirkstoff während des Transferprozesses hoch halten. Diese Erkenntnisse müssen bei der Anwendung des «Feder-Fallschirm»-Konzepts für Absorptionsvorhersagen oder bei der Formulierungentwicklung berücksichtigt werden. Darüber hinaus wurden die Grenzen des Massentransports anhand von Experimenten mit Rührgeschwindigkeit von 100 und 400

Umdrehungen pro Minute aufgezeigt, von denen angenommen wurde, dass sie die beteiligte ungerührte Wasserschicht modifizieren. Die Experimente zeigten, dass kolloidale Spezies mit unterschiedlichen, hydrodynamischen Radien von einer Grössenordnung, den ungerührten Wasserschicht-Diffusionstransport beeinflussten. Daraus konnte geschlossen werden, dass Mediensättigung, Reservoir-Effekte sowie die Diffusion von Wirkstoffspezies neben molekular gelöstem Wirkstoff durch die ungerührte Wasserschicht Hauptfaktoren waren, die die Biozugänglichkeit von Naporafenib beeinflussten.

Die dritte Frage bezog sich auf Möglichkeiten, die Biozugänglichkeit durch Hilfsstoffe zu manipulieren. Ziel war es zu verstehen, ob und wie Hilfsstoffe die generierten Wirkstoffspezies verändern. Wenn es eine Wechselwirkung mit dem Wirkstoff oder biorelevanten Medienkomponenten gibt, kann der Punkt, an dem die Phasentrennung stattfindet, verändert werden. Eine solubilisierende Funktionalität eines Hilfsstoffes bringt mehr Wirkstoff in Lösung (Erhöhung der Phasentrennungsgrenze), aber kann auch in Wirkstoffkomplexierung resultieren. Es wurde festgestellt, dass Hydroxypropylcellulose (HPC), Hydroxypropylmethylcellulose (HPMC) und Kollidon VA64 (VA64) inerte Hilfsstoffe sind, d.h. keine Veränderung der Phasentrenngrenze bewirken und daher keine Auswirkungen auf das simulierte Gallensystem haben. Eudragit EPO (EPO) und Kolliphor RH40 (RH40) erhöhten beide die Phasentrenngrenze in Puffer- und biorelevanten Medien signifikant im Vergleich zu ohne Hilfsstoffe. Natriumdodecylsulfat (SDS) erhöhte ebenfalls die Phasentrennungsgrenze, scheinbar etwas stärker für den Puffer als für das biorelevante System. Ein solches Verhalten kann auf eine Wechselwirkung zwischen den durch SDS gebildeten Mizellen und den biorelevanten Bestandteilen hinweisen. Die scheinbaren Solubilisierungseffekte der Hilfsstoffe wurden durch Massentransportexperimente durch Dialysemembranen und Kernspinresonanzspektroskopie ergänzt. Beim Transport durch Dialysemembranen unter überschüssigen Wirkstoff Bedingungen zeigte sich fast keine Differenzierung zwischen den Hilfsstoffen und sehr ähnliche Massentransportraten zwischen Puffer und biorelevanten Medien. Um mögliche Maskierungseffekte von amorphem, phasengetrenntem Wirkstoff auf die Wirkung von Hilfsstoffen zu untersuchen, wurden Transportexperimente bei 50% Mediensättigung ohne phasengetrennte Wirkstoffspezies wiederholt. Auch in dieser Situation wurde eine recht schwache Differenzierung zwischen den Hilfsstoffen beobachtet. Eine geringfügige Verringerung des Transports für den spezifischen Fall des EPO führte zu einer Diskrepanz hinsichtlich einer Erhöhung der Phasentrenngrenze. Kernspinresonanz-Untersuchungen ergaben reduzierte aromatische Wirkstoffprotonensignale, die als verringerte, molekulare Mobilität des Wirkstoffs interpretiert wurden, obwohl die Gesamtmenge des Wirkstoffs in Lösung zunahm. Dies bedeutet wahrscheinlich, dass EPO mit

dem Wirkstoff komplexiert und damit seine Biozugänglichkeit verringert. Kernspinresonanz-Signale mit HPC und RH40 entsprachen dem beobachteten Einfluss auf die Phasentrenngrenze, d.h. keine Veränderung bzw. Zunahme. Bemerkenswert ist, dass der Transport durch Dialysemembranen im Vergleich zur lipidischen (biomimetischen) Membranen etwa 100-mal geringer war, wodurch die Empfindlichkeit verringert wurde, Hilfsstoffe/Medienwirkungen auf die Biozugänglichkeit zu erkennen. Drei repräsentative Hilfsstoffe wurden für weitere Untersuchungen *in vitro*, sprich für separate Auflöseversuche und Ultrazentrifugations-Flux-Kombinationsexperimente verwendet. HPC repräsentierte die inerten Hilfsstoffe, die weder das Gallensystem noch die molekulare Mobilität des Wirkstoffes beeinträchtigten, aber das Potenzial hat als Kristallisationsinhibitor zu wirken. EPO wurde wegen seiner Fähigkeit, grosse Mengen des Wirkstoffs in Lösung zu stabilisieren, und wegen seines Potenzials, auch die amorphe Form des Wirkstoffs zu stabilisieren, miteinbezogen. RH40 wurde aufgrund seinen solubilisierenden Eigenschaften für Naporafenib und seiner vermuteten synergistischen Wirkung mit dem simulierten Gallensystem ausgewählt. Erwähnenswert ist, dass die Abtrennleistung durch Ultrazentrifugation mit Hilfsstoffen im Vergleich zu den alleinigen biorelevanten Medien, basierend auf dynamischer Lichtstreuung, als unzureichend angesehen wurde. Die Relevanz des Wirkstoff-Hilfstoff-Galle-Wechselspiels für die Hilfsstoffauswahl wurde bereits z.B. in Schlauersbach et al. (123) berichtet und in dieser Arbeit bestätigt. Spezifisch ermöglichten HPC und RH40 einen höheren Fluss in biorelevanten Medien im Vergleich zum Puffersystem. Im Gegenteil dazu erzeugte EPO einen höheren Transport von Naporafenib im wässrigen Puffer, was auf eine Inkompatibilität von EPO mit simulierten Gallenkomponenten hindeutet.

Anschliessend wurde die vierte Frage für diese spezifischen Fälle evaluiert, wie sich die Biozugänglichkeit *in vitro* auf die Exposition *in vivo* auswirkt. Drei Naporafenib-Tosylat-Salzsuspensionen, basierend auf einem Citrat-Phosphat-Puffer mit pH-Wert von 2,6 mit EPO, HPC oder RH40 als Hilfsstoffe, wurden mit einer Dosis von 30 mg/kg an Beagle-Hunden verabreicht. Die relativen Biozugänglichkeiten in Anwesenheit dieser drei Hilfsstoffe, die mittels Massentransport im Labor unter Verwendung von überschüssigem Wirkstoff (Lösungsform) gemessen wurden, konnten mit geeigneten pharmakokinetischen Parametern der Studie gut korreliert werden. Insbesondere war die Korrelation mit dem Parameter maximale Konzentration im Blut/Dosis/Zeit, bei welcher die maximale Konzentration gemessen wurde (Cmax/Dose/Tmax), als Annäherung für die Absorptionsrate auffallend, d.h. $R^2 > 0,99$. Dies ist physikalisch sinnvoll, da sowohl die Absorptionsrate *in vivo* als auch die Permeationsrate *in vitro* den Stofftransport über Zeit und Fläche, d.h. den Fluss, widerspiegeln. Daher wurde die Quantifizierung der Biozugänglichkeit in Form des Stofftransportes als biopredikativ befunden. Möglicherweise wurde

dies dadurch erleichtert, dass nur ein Parameter, nämlich der Hilfsstoff, für die *in vitro* und *in vivo* Untersuchungen geändert wurde. Es ist erwähnenswert, dass die Korrelation zwischen flussbasierter Biozugänglichkeit und Absorption erreicht werden konnte, einfach durch die Verwendung der Lösungsform des Wirkstoffes (in DMSO gelöst) hinzugefügt auf ein biorelevantes Medium (FaSSIF-V1$_{PBS}$) mit vorgelösten Hilfsstoffen. Folglich bestätigten die pharmakokinetischen Studienergebnisse das *in vitro* ausgearbeitete Verständnis, wie die Biozugänglichkeit durch Hilfsstoffe manipuliert werden kann, in diesem Fall deren Einfluss auf die effektiven Konzentrationen, die den Gradienten für die Permeation bilden.

Die fünfte Frage handelte davon, wie identifizierte Risiken oder Einschränkungen der oralen Absorption durch rationale Formulierungsentwicklung gemindert werden können. Eine mögliche Auflöserate-limitierung und Formkonvertierungs-/Entsättigungsrisiko wurde mit einer amorphen Feststoffdispersion (amorphous solid dispersion, ASD) adressiert. Eine vermutete Löslichkeitslimitierung wurde mit einer Mikroemulsion-Formulierung (ME) angegangen. Die Mikroemulsion- und amorphe Feststoffdispersions-Formulierungen wurden in einem zweistufigen Auflösetest bewertet. Unterschiedliche Auflöse- und für die Mikroemulsion Entsättungsraten wurden beobachtet und konnten mit dem Tosylatsalz + HPC-Fall verglichen werden. Darüber hinaus wurde die amorphe Feststoffdispersion und der Tosylat-Salz + HPC-Fall in separaten Auflösetest (einstufig) und Ultrazentrifugations-Flux-Kombinationsexperimente verglichen. Interessanterweise war die flussbasierte Biozugänglichkeit zwischen Tosylatsalz + HPC und amorpher Feststoffdispersion gleich und der beobachtete Unterschied der Auflösegeschwindigkeiten trat nicht auf. Ein Überblick über die *in vitro* gemessenen, absoluten Massentransportraten für die verschiedenen Auflöse- und Transportexperimente weist auf Diskrepanzen einer Grössenordnung hin d.h. Stofftransportraten, die deutlich unter den Auflöseraten liegen. Folglich wurde der Einfluss der Auflöserate auf die Biozugänglichkeit von Naporafenib bei Verwendung des μFlux^{TM} / Lipidmembran (GIT-PAMPA)-Setups von Pion Inc. Ltd. verborgen. Dies stellt eine Herausforderung hinsichtlich der Übersetzung von *in vitro* zu *in vivo* Situation dar für sowohl Auflösegeschwindigkeiten als auch Stofftransportraten und deren unvermeidliches Wechselspiel. Zusätzliche Arme der pharmakokinetischen Studie an Hunden zeigten deutlich erhöhte Expositionen für die amorphe Feststoffdispersion und noch stärker für die Mikroemulsions- Formulierung. Dies scheint mit den Ergebnissen des zweistufigen Auflösetests übereinzustimmen, d.h. die Absorptionsrate wurde durch die Auflöserate der amorphen Feststoffdispersion bzw. der Entsättigungsrate der Mikroemulsion begrenzt. Betrachtet man die drei Tosylatsalz Studienarme, so könnte die Auflöserate vergleichbar gewesen sein oder

eine untergeordnete Rolle gespielt haben, während die effektiven Konzentrationen, die die Permeation antreiben, durch die beteiligten Hilfsstoffe verändert wurden.

Daraus kann geschlossen werden, dass Stofftransport-Anordnungen *in vitro* das dynamische Wechselspiel zwischen Auflöse- und Permeationsprozess *in vivo*, z.B. aufgrund von Oberflächen/Volumen-Unterschiede, nicht ausreichend widerspiegeln. Die Notwendigkeit, Auflösung, Löslichkeit und Permeation miteinander in Verbindung zu bringen, bleibt jedoch unverändert. Vorerst empfiehlt es sich, Auflösung und Permeation getrennt zu bewerten und über die scheinbare Löslichkeit zu verbinden, wie das Biozugänglichkeitskonzept veranschaulicht. Das Verständnis über die Entwicklung von Wirkstoffspezies und deren dynamischen Wechselspiels, mit ihren Eigenschaften und Auswirkungen auf die Biozugänglichkeit, ist entscheidend für die rationale Entwicklung von BCS Klasse II und wahrscheinlich auch BCS Klasse IV Substanzen, vorausgesetzt es wird eine vernünftige Dosierung benötigt. Ein solches mechanistisches Verständnis kann auch dazu beitragen, die *in silico* Modellierung der Absorption zu verbessern, um in naher Zukunft bessere Vorhersagen zu ermöglichen. Diese Arbeit folgt aktuellen Literaturtrends im Zusammenhang mit einem Paradigmenwechsel bei der Entwicklung schlecht wasserlöslicher Medikamente wie dem von Kadar et al. im Jahr 2022 veröffentlichten Absorptions-getriebene Wirkstoffformulier-Konzept (ADDF, Absorption-Driven Drug Formulation). Während bisher das Ziel darin bestand, so viel Wirkstoff wie möglich in Lösung zu bringen, geht der neue Trend dahin, so viel Wirkstoff wie möglich über eine biorepräsentative Barriere zu liefern.

10. Work contribution

This work was performed in collaboration between Novartis Pharma AG, Basel and the university of Würzburg, Germany and contains data adopted from others. The single crystal structure illustrations were provided by Dr. B. Dittrich from the former API modelling group, Novartis Basel (**Figure 13**). Scanning electron microscopy (SEM) was performed in collaboration with M. Dehlinger from the Analytical Material Sciences team, Novartis Basel (**Figure 13**, **Figure 14** and **Figure 61**). J. Schlauersbach from the university of Würzburg performed the phase separation limit experiments (**Figure 18**, **Figure 49**), the intrinsic dissolution rate assessment (**Figure 19**), nuclear magnetic resonance spectroscopy (**Figure 20**, **Figure 21** and **Figure 52**) and dialysis flux experiments (**Figure 35**, **Figure 36**, **Figure 50** and **Figure 51**). Cryogenic-transmissive electron microscopy (Cryo-TEM) was performed in collaboration with C. Be from the Chemical, Biology and Therapeutics department, Novartis Basel (**Figure 23**, **Figure 24** and **Figure 28**). Liquid cell-transmissive electron microscopy (LC-TEM) was performed in collaboration with Dr. A. Gomez-Perez and J. Gonzáles-Casablanca from the external company NanoMEGAS SPRL, Brussels, Belgium under confidentiality (**Figure 23**, **Figure 24**, **Figure 29** and **Figure 30**). The dissolution assays were executed by the analytical research and development team, Novartis Basel. The two-step dissolution assay was performed by S. Juanes (**Figure 53** and **Figure 67**), N.Stehle (**Figure 67**) and P. Halbeisen (**Figure 67**). The single-step dissolution assay was performed by L.Toelle (**Figure 65**). The 5 arm pharmacokinetic study of naporafenib formulations in beagle dogs was conducted by Covance and sponsored by Novartis. The plasma concentration-time profile and pharmacokinetic parameters were received and used without modification (**Figure 62**, **Figure 63**, **Figure 73** and **Table 19**). Chromatography support was received from the Open Access Analytics team (F. Schneider, D. Schmid, J. Capece), Novartis Basel, Switzerland and Cambridge, USA.

11. Acknowledgements

First and foremost, I would like to thank Prof. Dr. Dr. L. Meinel for the opportunity to do my doctorate at the University of Würzburg and for his guidance and advices received over the past years. I would also like to thank J. Schlauersbach for the scientific discussion and valuable contributions to this thesis. The scientific foundation laid by my predecessors Dr. T. Widmer and Dr. M. Reggane from Novartis and Dr. J. Wiest from the university of Würzburg is worth mentioning as well, thank you all. I am specifically grateful to Dr. C. Harlacher and Dr. B. Galli who contributed as mentors to my scientific and personal development. The above mentioned people have taught me a lot, for example how to balance scientific exploration and thoroughness with pragmatism and bringing value to the organization. The word “simplicity” and associated attitude will continue to influence and shape my future development.

I would like thank my line managers at Novartis, Dr. F. Schaefer, Dr. D. Hook and Dr. H. de Waard for integrating me into their teams, for their support and allowing me to perform this thesis at Novartis, in collaboration with the university of Würzburg.

Special thanks is also directed towards people who contributed to this work, either directly by performing experiments and analysis, or indirectly by having fruitful discussion and sharing their experience and perspectives with me. The Open Access Analytics team, Basel receives specific attention for their outstanding support by measuring several thousand samples of mine throughout these years. I also appreciate and would like to highlight the support received from NanoMEGAS, the Analytical Research and Development team, the Material Sciences team, the Chemical, Biology and Therapeutics team, the Chemical and Pharmaceutical Profiling team, the Oral Early Phase team and our internal Flux Working Group, lead by Dr. S. Dodd and spanning across the globe. Thank you all sincerely for your contributions!

Further major appreciation goes to T. Hoeltkemeier from Novartis and Dr. M. Kaszuba and team from Malvern Panalytical related to pushing the boundaries of dynamic light scattering.

A special acknowledgement of my gratidude is directed towards Pion Inc., and more specifically towards Dr. Konstantin Tsinman, who unfortunately passed away during the course of my thesis. He was willing to take the time to get myself kick-started into this scientific field. I am unbelievably sad that I am not able to show him my work. I am herewith dedicating this work to him.

In Memoriam dear Konstanin

Last but not least, incredible thanks go to my love, Fiona Koch, to my family and to my friends both in private and professional environment for caring about my well-being all along the line.

12. Poster, presentations and publications

Poster presented at Global innovation day 2019, technical research and development (TRD), Novartis Basel: Novel ways to study drug-colloid interactions in simulated intestinal fluids.

Poster presented at Doktorandentagung 2022, Germany, virtual participation: Biorelevant media colloids and their contribution towards oral drug absorption – Bioaccessibility.

Presentation at the innovation spotlight 2021, pharmaceutical development (PHAD), Novartis Basel: Biopharmaceutical context of poorly water-soluble drugs.

Presentation at the ADME Science and Innovation Forum 2021, Novartis Institute for BioMedical Research (NIBR), Basel: Biopharmaceutical context of poorly water-soluble drugs

Publication: Co-author in Schlauersbach et al. 2022 (manuscript in preparation), Harnessing bile for drug absorption through rational excipient selection.

Publication: Co-author in Dodd et al. 2022 (manuscript in preparation), Application of in vitro absorption experiments for the prediction of food effects of the clinical formulations of nine BCS II/IV drugs.

Publication: Co-author in Dittrich et al. 2022 (manuscript submitted), Energy partitioning of pharmaceutical cocrystal structures.

13. List of tables and figures

14. Permissions

Figure 1: License by Oxford University Press with number 5327571002096 of reference (7).

Figure 4: License by Springer Nature with number 5327571420656 of reference (39).

Figure 5: License by ACS publications/CCC RightsLinks (open access article) of reference (23).

Figure 6: License by Elsevier with number 5327580137957 of reference (82).

Figure 7: License by Elsevier with number 5327580315888 of reference (90).

Figure 8: License by Elsevier with number 5327580479660 of reference (115).

Figure 9: License by Elsevier with number 5327580640019 of reference (117).

Figure 76: Open Access article, no license required of reference (116)

15. Bibliography

1. Schanker LS. On the mechanism of absorption of drugs from the gastrointestinal tract. J Med Pharm Chem. 1960;2:343-59. doi: 10.1021/jm50011a001.
2. Wagner JG. Biopharmaceutics: absorption aspects. J Pharm Sci. 1961;50:359-87. doi: 10.1002/jps.2600500502.
3. Welling PG. Influence of food and diet on gastrointestinal drug absorption: a review. J Pharmacokinet Biopharm. 1977;5(4):291-334. doi: 10.1007_BF01061694.
4. Vertzoni M, Augustijns P, Grimm M, Koziolek M, Lemmens G, Parrott N, et al. Impact of regional differences along the gastrointestinal tract of healthy adults on oral drug absorption: An UNGAP review. Eur J Pharm Sci. 2019;134:153-75. doi: 10.1016/j.ejps.2019.04.013.
5. Vinarov Z, Abdallah M, Agundez JAG, Allegaert K, Basit AW, Braeckmans M, et al. Impact of gastrointestinal tract variability on oral drug absorption and pharmacokinetics: An UNGAP review. Eur J Pharm Sci. 2021;162:105812. doi: 10.1016/j.ejps.2021.105812.
6. Koziolek M, Alcaro S, Augustijns P, Basit AW, Grimm M, Hens B, et al. The mechanisms of pharmacokinetic food-drug interactions - A perspective from the UNGAP group. Eur J Pharm Sci. 2019;134:31-59. doi: 10.1016/j.ejps.2019.04.003.
7. O'Shea JP, Holm R, O'Driscoll CM, Griffin BT. Food for thought: formulating away the food effect - a PEARRL review. J Pharm Pharmacol. 2019;71(4):510-35. doi: 10.1111/jphp.12957.
8. Abrahamsson B, McAllister M, Augustijns P, Zane P, Butler J, Holm R, et al. Six years of progress in the oral biopharmaceutics area - A summary from the IMI OrBiTo project. Eur J Pharm Biopharm. 2020;152:236-47. doi: 10.1016/j.ejpb.2020.05.008.
9. Butler J, Hens B, Vertzoni M, Brouwers J, Berben P, Dressman J, et al. In vitro models for the prediction of in vivo performance of oral dosage forms: Recent progress from partnership through the IMI OrBiTo collaboration. Eur J Pharm Biopharm. 2019;136:70-83. doi: 10.1016/j.ejpb.2018.12.010.
10. Assessing the Effects of Food on Drugs in INDs and NDAs – Clinical Pharmacology Considerations. https://www.fda.gov/regulatory-information/search-fda-guidance-documents/assessing-effects-food-drugs-inds-and-ndas-clinical-pharmacology-considerations [03.10.2022].
11. Drugmakers, EMA Comment on FDA Guidance on Assessing Food Effects on Drugs. [03.10.2022]; Available from: https://www.raps.org/news-and-articles/news-articles/2019/4/drugmakers-ema-comment-on-fda-guidance-on-assessi.
12. Bai JPF, Burckart GJ, Mulberg AE. Literature Review of Gastrointestinal Physiology in the Elderly, in Pediatric Patients, and in Patients with Gastrointestinal Diseases. J Pharm Sci. 2016;105(2):476-83. doi: 10.1002/jps.24696.
13. Effinger A, O'Driscoll CM, McAllister M, Fotaki N. Impact of gastrointestinal disease states on oral drug absorption - implications for formulation design - a PEARRL review. J Pharm Pharmacol. 2019;71(4):674-98. doi: 10.1111/jphp.12928.
14. Stillhart C, Vucicevic K, Augustijns P, Basit AW, Batchelor H, Flanagan TR, et al. Impact of gastrointestinal physiology on drug absorption in special populations--An UNGAP review. Eur J Pharm Sci. 2020;147:105280. doi: 10.1016/j.ejps.2020.105280.
15. Muller PY, Milton MN. The determination and interpretation of the therapeutic index in drug development. Nat Rev Drug Discov. 2012;11(10):751-61. doi: 10.1038/nrd3801.
16. Finkel R, Clark MA, Cubeddu LX. Pharmacology: Lippincott Williams & Wilkins; 2009.
17. Vinarov Z, Abrahamsson B, Artursson P, Batchelor H, Berben P, Bernkop-Schnurch A, et al. Current challenges and future perspectives in oral absorption research: An opinion of the UNGAP network. Adv Drug Deliv Rev. 2021;171:289-331. doi: 10.1016/j.addr.2021.02.001.
18. Beyer C. Biopharmazie, Theorie und Praxis der Pharmakokinetik. Hrsg. von J. Meier, H. Rettig und H. Hess, 473 S., geb., G. Thieme Verlag, Stuttgart, DM 210,—. Pharmazie in Unserer Zeit. 1981;10(6):189-. doi: 10.1002/pauz.19810100607.

19. Pentafragka C, Symillides M, McAllister M, Dressman J, Vertzoni M, Reppas C. The impact of food intake on the luminal environment and performance of oral drug products with a view to in vitro and in silico simulations: a PEARRL review. J Pharm Pharmacol. 2018. doi: 10.1111/jphp.12999.
20. Tenconi LT, Buniva G, Beretta E, Pagani V. Influence of food intake on the absorption of diftalone in man. Int J Clin Pharmacol Biopharm. 1977;15(10):485-91.
21. Sasaki M, Aoyama T, Sugawara M, Takekuma Y. Influence of gastrointestinal activity on the absorption of nilotinib. Drug Metab Pharmacokinet. 2020;35(1):102-10. doi: 10.1016/j.dmpk.2019.08.006.
22. Klumpp L, Leigh M, Dressman J. Dissolution behavior of various drugs in different FaSSIF versions. Eur J Pharm Sci. 2020;142:105138. doi: 10.1016/j.ejps.2019.105138.
23. Arce FA, Setiawan N, Campbell HR, Lu X, Nethercott MJ, Bummer P, et al. Toward Developing Discriminating Dissolution Methods for Formulations Containing Nanoparticulates in Solution: The Impact of Particle Drift and Drug Activity in Solution. Mol Pharm. 2020;17(11):4125-40. doi: 10.1021/acs.molpharmaceut.0c00599.
24. Gibaldi M, Feldman S. Mechanisms of surfactant effects on drug absorption. J Pharm Sci. 1970;59(5):579-89. doi: 10.1002/jps.2600590502.
25. Augustijns P, Vertzoni M, Reppas C, Langguth P, Lennernas H, Abrahamsson B, et al. Unraveling the behavior of oral drug products inside the human gastrointestinal tract using the aspiration technique: History, methodology and applications. Eur J Pharm Sci. 2020;155:105517. doi: 10.1016/j.ejps.2020.105517.
26. Galia E, Nicolaides E, Horter D, Lobenberg R, Reppas C, Dressman JB. Evaluation of various dissolution media for predicting in vivo performance of class I and II drugs. Pharm Res-Dordr. 1998;15(5):698-705. doi: Doi 10.1023/A:1011910801212.
27. Dressman JB, Amidon GL, Reppas C, Shah VP. Dissolution testing as a prognostic tool for oral drug absorption: Immediate release dosage forms. Pharm Res-Dordr. 1998;15(1):11-22. doi: Doi 10.1023/A:1011984216775.
28. Fuchs A, Dressman JB. Composition and physicochemical properties of fasted-state human duodenal and jejunal fluid: a critical evaluation of the available data. J Pharm Sci. 2014;103(11):3398-411. doi: 10.1002/jps.24183.
29. Jantratid E, Janssen N, Reppas C, Dressman JB. Dissolution media simulating conditions in the proximal human gastrointestinal tract: an update. Pharm Res. 2008;25(7):1663-76. doi: 10.1007/s11095-008-9569-4.
30. Fuchs A, Leigh M, Kloefer B, Dressman JB. Advances in the design of fasted state simulating intestinal fluids: FaSSIF-V3. Eur J Pharm Biopharm. 2015;94:229-40. doi: 10.1016/j.ejpb.2015.05.015.
31. Suarez-Sharp S, Lindahl A, Heimbach T, Rostami-Hodjegan A, Bolger MB, Ray Chaudhuri S, et al. Translational Modeling Strategies for Orally Administered Drug Products: Academic, Industrial and Regulatory Perspectives. Pharm Res. 2020;37(6):95. doi: 10.1007/s11095-020-02814-y.
32. Riethorst D, Baatsen P, Remijn C, Mitra A, Tack J, Brouwers J, et al. An In-Depth View into Human Intestinal Fluid Colloids: Intersubject Variability in Relation to Composition. Mol Pharm. 2016;13(10):3484-93. doi: 10.1021/acs.molpharmaceut.6b00496.
33. Lloyd RS, Hingle MI, Bloomer JC, Charles SJ, Butler JM, Paul A, et al. Negative Food Effect of Danirixin: Use of PBPK Modelling to Explore the Effect of Formulation and Meal Type on Clinical PK. Pharm Res. 2020;37(12):233. doi: 10.1007/s11095-020-02948-z.
34. Semple KT, Doick KJ, Jones KC, Burauel P, Craven A, Harms H. Defining bioavailability and bioaccessibility of contaminated soil and sediment is complicated. Environ Sci Technol. 2004;38(12):228A-31A. doi: 10.1021/es040548w.
35. Fernandez-Garcia E, Carvajal-Lerida I, Perez-Galvez A. In vitro bioaccessibility assessment as a prediction tool of nutritional efficiency. Nutr Res. 2009;29(11):751-60. doi: 10.1016/j.nutres.2009.09.016.

36. Pentafragka C, Tomaszewska I, Bellmann S, Minekus M, Schilderink R, Vertzoni M, et al. In Vitro Simulation of the Environment in the Upper Gastrointestinal Lumen After Drug Administration in the Fed State Using the TIM-1 System and Comparison With Luminal Data in Adults. J Pharm Sci. 2022;111(1):197-205. doi: 10.1016/j.xphs.2021.10.010.
37. Ruby MV, Davis A, Schoof R, Eberle S, Sellstone CM. Estimation of Lead and Arsenic Bioavailability Using a Physiologically Based Extraction Test. Environmental Science & Technology. 1996;30(2):422-30. doi: 10.1021/es950057z.
38. Intawongse M, Dean JR. In-vitro testing for assessing oral bioaccessibility of trace metals in soil and food samples. TrAC Trends in Analytical Chemistry. 2006;25(9):876-86. doi: 10.1016/j.trac.2006.03.010.
39. van de Waterbeemd H, Gifford E. ADMET in silico modelling: towards prediction paradise? Nat Rev Drug Discov. 2003;2(3):192-204. doi: 10.1038/nrd1032.
40. Waise TMZ, Dranse HJ, Lam TKT. The metabolic role of vagal afferent innervation. Nat Rev Gastroenterol Hepatol. 2018;15(10):625-36. doi: 10.1038/s41575-018-0062-1.
41. Clark JA, Coopersmith CM. Intestinal crosstalk: a new paradigm for understanding the gut as the "motor" of critical illness. Shock. 2007;28(4):384-93. doi: 10.1097/shk.0b013e31805569df.
42. Gold V. The IUPAC Compendium of Chemical Terminology2019.
43. Ilevbare GA, Taylor LS. Liquid–Liquid Phase Separation in Highly Supersaturated Aqueous Solutions of Poorly Water-Soluble Drugs: Implications for Solubility Enhancing Formulations. Crystal Growth & Design. 2013;13(4):1497-509. doi: 10.1021/cg301679h.
44. Bergstrom CAS, Larsson P. Computational prediction of drug solubility in water-based systems: Qualitative and quantitative approaches used in the current drug discovery and development setting. Int J Pharm. 2018;540(1-2):185-93. doi: 10.1016/j.ijpharm.2018.01.044.
45. Jain N, Yalkowsky SH. Estimation of the aqueous solubility I: Application to organic nonelectrolytes. J Pharm Sci-Us. 2001;90(2):234-52. doi: 10.1002/1520-6017(200102)90:2<234::Aid-Jps14>3.0.Co;2-V.
46. Ran Y, Yalkowsky SH. Prediction of drug solubility by the general solubility equation (GSE). J Chem Inf Comput Sci. 2001;41(2):354-7. doi: 10.1021/ci000338c.
47. Stella VJ, Nti-Addae KW. Prodrug strategies to overcome poor water solubility. Adv Drug Deliv Rev. 2007;59(7):677-94. doi: 10.1016/j.addr.2007.05.013.
48. Bergstrom CA, Wassvik CM, Johansson K, Hubatsch I. Poorly soluble marketed drugs display solvation limited solubility. J Med Chem. 2007;50(23):5858-62. doi: 10.1021/jm0706416.
49. Williams HD, Trevaskis NL, Charman SA, Shanker RM, Charman WN, Pouton CW, et al. Strategies to address low drug solubility in discovery and development. Pharmacol Rev. 2013;65(1):315-499. doi: 10.1124/pr.112.005660.
50. Koehl NJ, Holm R, Kuentz M, Griffin BT. New Insights into Using Lipid Based Suspensions for 'Brick Dust' Molecules: Case Study of Nilotinib. Pharm Res. 2019;36(4):56. doi: 10.1007/s11095-019-2590-y.
51. Hasselbalch KA. Die Berechnung der Wasserstoffzahl des Blutes aus der freien und gebundenen Kohlensäure desselben, und die Sauerstoffbindung des Blutes als Funktion der Wasserstoffzahl: Julius Springer; 1916.
52. Fick A. Ueber Diffusion. Annalen der Physik und Chemie. 1855;170(1):59-86. doi: 10.1002/andp.18551700105.
53. Einstein A. Über die von der molekularkinetischen Theorie der Wärme geforderte Bewegung von in ruhenden Flüssigkeiten suspendierten Teilchen. Annalen der Physik. 1905;322(8):549-60. doi: 10.1002/andp.19053220806.
54. Siepmann J, Siepmann F. Mathematical modeling of drug dissolution. Int J Pharm. 2013;453(1):12-24. doi: 10.1016/j.ijpharm.2013.04.044.
55. Lenz J, Bunjes H, Kwade A, Juhnke M. An improved method for the simultaneous determination of water uptake and swelling of tablets. Int J Pharm. 2021;595:120229. doi: 10.1016/j.ijpharm.2021.120229.

56. Lenz J, Fuest F, Finke JH, Bunjes H, Kwade A, Juhnke M. Tablet Disintegration and Dispersion under In Vivo-like Hydrodynamic Conditions. Pharmaceutics. 2022;14(1). doi: 10.3390/pharmaceutics14010208.
57. Noyes AA, Whitney WR. The Rate of Solution of Solid Substances in Their Own Solutions. Journal of the American Chemical Society. 1897;19(12):930-4. doi: 10.1021/ja02086a003.
58. Nernst W. Theorie der Reaktionsgeschwindigkeit in heterogenen Systemen. Zeitschrift für Physikalische Chemie. 1904;47U(1):52-5. doi: 10.1515/zpch-1904-4704.
59. Brunner E. Reaktionsgeschwindigkeit in heterogenen Systemen. Zeitschrift für Physikalische Chemie. 1904;47U(1):56-102. doi: 10.1515/zpch-1904-4705.
60. Balk A, Wiest J, Widmer T, Galli B, Holzgrabe U, Meinel L. Transformation of acidic poorly water soluble drugs into ionic liquids. Eur J Pharm Biopharm. 2015;94:73-82. doi: 10.1016/j.ejpb.2015.04.034.
61. Reggane M, Wiest J, Saedtler M, Harlacher C, Gutmann M, Zottnick SH, et al. Bioinspired co-crystals of Imatinib providing enhanced kinetic solubility. Eur J Pharm Biopharm. 2018;128:290-9. doi: 10.1016/j.ejpb.2018.05.012.
62. Sugano K, Kansy M, Artursson P, Avdeef A, Bendels S, Di L, et al. Coexistence of passive and carrier-mediated processes in drug transport. Nat Rev Drug Discov. 2010;9(8):597-614. doi: 10.1038/nrd3187.
63. Avdeef A, Kansy M, Bendels S, Tsinman K. Absorption-excipient-pH classification gradient maps: sparingly soluble drugs and the pH partition hypothesis. Eur J Pharm Sci. 2008;33(1):29-41. doi: 10.1016/j.ejps.2007.09.009.
64. Camenisch G, Alsenz J, van de Waterbeemd H, Folkers G. Estimation of permeability by passive diffusion through Caco-2 cell monolayers using the drugs' lipophilicity and molecular weight. European Journal of Pharmaceutical Sciences. 1998;6(4):313-9. doi: 10.1016/s0928-0987(97)10019-7.
65. Volpe DA. Advances in cell-based permeability assays to screen drugs for intestinal absorption. Expert Opin Drug Discov. 2020:1-11. doi: 10.1080/17460441.2020.1735347.
66. Dressman JB, Amidon GL, Fleisher D. Absorption potential: estimating the fraction absorbed for orally administered compounds. J Pharm Sci. 1985;74(5):588-9. doi: 10.1002/jps.2600740523.
67. Amidon GL, Lennernas H, Shah VP, Crison JR. A theoretical basis for a biopharmaceutic drug classification: the correlation of in vitro drug product dissolution and in vivo bioavailability. Pharm Res. 1995;12(3):413-20. doi: 10.1023/a:1016212804288.
68. M9 Biopharmaceutics Classification System Based Biowaivers: Guidance for Industry. 2021 [03.10.2022]; Available from: https://www.fda.gov/media/148472/download.
69. Butler JM, Dressman JB. The developability classification system: application of biopharmaceutics concepts to formulation development. J Pharm Sci. 2010;99(12):4940-54. doi: 10.1002/jps.22217.
70. Yu LX. An integrated model for determining causes of poor oral drug absorption. Pharm Res. 1999;16(12):1883-7. doi: 10.1023/a:1018911728161.
71. Sugano K. Introduction to computational oral absorption simulation. Expert Opin Drug Metab Toxicol. 2009;5(3):259-93. doi: 10.1517/17425250902835506.
72. Sugano K, Kataoka M, Mathews Cda C, Yamashita S. Prediction of food effect by bile micelles on oral drug absorption considering free fraction in intestinal fluid. Eur J Pharm Sci. 2010;40(2):118-24. doi: 10.1016/j.ejps.2010.03.011.
73. Sugano K. Fraction of a dose absorbed estimation for structurally diverse low solubility compounds. Int J Pharm. 2011;405(1-2):79-89. doi: 10.1016/j.ijpharm.2010.11.049.
74. Travell J. The influence of the hydrogen ion concentration on the absorption of alkaloids from the stomach. Journal of Pharmacology and Experimental Therapeutics. 1940;69:21-33.
75. Jacobs MH. Some Aspects of Cell Permeability to Weak Electrolytes. Cold Spring Harbor Symposia on Quantitative Biology. 1940;8(0):30-9. doi: 10.1101/sqb.1940.008.01.005.

76. Shore PA, Brodie BB, Hogben CA. The gastric secretion of drugs: a pH partition hypothesis. J Pharmacol Exp Ther. 1957;119(3):361-9.
77. Hogben CA, Tocco DJ, Brodie BB, Schanker LS. On the mechanism of intestinal absorption of drugs. J Pharmacol Exp Ther. 1959;125(4):275-82.
78. Lucas ML, Schneider W, Haberich FJ, Blair JA. Direct measurement by pH-microelectrode of the pH microclimate in rat proximal jejunum. Proc R Soc Lond B Biol Sci. 1975;192(1106):39-48. doi: 10.1098/rspb.1975.0150.
79. Hogerle ML, Winne D. Drug absorption by the rat jejunum perfused in situ. Dissociation from the pH-partition theory and role of microclimate-pH and unstirred layer. Naunyn Schmiedebergs Arch Pharmacol. 1983;322(4):249-55. doi: 10.1007/BF00508339.
80. Sakata T, von Engelhardt W. Mucin layer in the large intestine. Ann Rech Vet. 1979;10(2-3):485-7.
81. Rechkemmer G. Transport of weak electrolytes. The Gastrointestional System, Intestinal Absorption and Secretion. 1991:371-88.
82. Brouwers J, Brewster ME, Augustijns P. Supersaturating drug delivery systems: the answer to solubility-limited oral bioavailability? J Pharm Sci. 2009;98(8):2549-72. doi: 10.1002/jps.21650.
83. Williams HD, Trevaskis NL, Yeap YY, Anby MU, Pouton CW, Porter CJ. Lipid-based formulations and drug supersaturation: harnessing the unique benefits of the lipid digestion/absorption pathway. Pharm Res. 2013;30(12):2976-92. doi: 10.1007/s11095-013-1126-0.
84. Sugano K. Computational oral absorption simulation for low-solubility compounds. Chem Biodivers. 2009;6(11):2014-29. doi: 10.1002/cbdv.200900101.
85. Sugano K. Computational oral absorption simulation of free base drugs. Int J Pharm. 2010;398(1-2):73-82. doi: 10.1016/j.ijpharm.2010.07.027.
86. Sugano K. Estimation of effective intestinal membrane permeability considering bile micelle solubilisation. Int J Pharm. 2009;368(1-2):116-22. doi: 10.1016/j.ijpharm.2008.10.001.
87. Stewart AM, Grass ME, Mudie DM, Morgen MM, Friesen DT, Vodak DT. Development of a Biorelevant, Material-Sparing Membrane Flux Test for Rapid Screening of Bioavailability-Enhancing Drug Product Formulations. Mol Pharm. 2017;14(6):2032-46. doi: 10.1021/acs.molpharmaceut.7b00121.
88. Stewart AM, Grass ME, Brodeur TJ, Goodwin AK, Morgen MM, Friesen DT, et al. Impact of Drug-Rich Colloids of Itraconazole and HPMCAS on Membrane Flux in Vitro and Oral Bioavailability in Rats. Mol Pharm. 2017;14(7):2437-49. doi: 10.1021/acs.molpharmaceut.7b00338.
89. Stewart AM, Grass ME. Practical Approach to Modeling the Impact of Amorphous Drug Nanoparticles on the Oral Absorption of Poorly Soluble Drugs. Mol Pharm. 2020;17(1):180-9. doi: 10.1021/acs.molpharmaceut.9b00889.
90. Sugano K, Terada K. Rate- and Extent-Limiting Factors of Oral Drug Absorption: Theory and Applications. J Pharm Sci. 2015;104(9):2777-88. doi: 10.1002/jps.24391.
91. Bevernage J, Brouwers J, Clarysse S, Vertzoni M, Tack J, Annaert P, et al. Drug supersaturation in simulated and human intestinal fluids representing different nutritional states. J Pharm Sci. 2010;99(11):4525-34. doi: 10.1002/jps.22154.
92. Peeters J, Neeskens P, Tollenaere JP, Van Remoortere P, Brewster ME. Characterization of the interaction of 2-hydroxypropyl-beta-cyclodextrin with itraconazole at pH 2, 4, and 7. J Pharm Sci. 2002;91(6):1414-22. doi: 10.1002/jps.10126.
93. Van Peer A, Woestenborghs R, Heykants J, Gasparini R, Gauwenbergh G. The effects of food and dose on the oral systemic availability of itraconazole in healthy subjects. Eur J Clin Pharmacol. 1989;36(4):423-6. doi: 10.1007/BF00558308.
94. Barone JA, Moskovitz BL, Guarnieri J, Hassell AE, Colaizzi JL, Bierman RH, et al. Food interaction and steady-state pharmacokinetics of itraconazole oral solution in healthy volunteers. Pharmacotherapy. 1998;18(2):295-301. doi: 10.1002/j.1875-9114.1998.tb03856.x.

95. Borbas E, Kadar S, Tsinman K, Tsinman O, Csicsak D, Takacs-Novak K, et al. Prediction of Bioequivalence and Food Effect Using Flux- and Solubility-Based Methods. Mol Pharm. 2019;16(10):4121-30. doi: 10.1021/acs.molpharmaceut.9b00406.
96. Brouwers J, Geboers S, Mols R, Tack J, Augustijns P. Gastrointestinal behavior of itraconazole in humans - Part 1: Supersaturation from a solid dispersion and a cyclodextrin-based solution. Int J Pharm. 2017;525(1):211-7. doi: 10.1016/j.ijpharm.2017.04.029.
97. Heinz A, Gordon KC, McGoverin CM, Rades T, Strachan CJ. Understanding the solid-state forms of fenofibrate--a spectroscopic and computational study. Eur J Pharm Biopharm. 2009;71(1):100-8. doi: 10.1016/j.ejpb.2008.05.030.
98. Hens B, Brouwers J, Corsetti M, Augustijns P. Gastrointestinal behavior of nano- and microsized fenofibrate: In vivo evaluation in man and in vitro simulation by assessment of the permeation potential. Eur J Pharm Sci. 2015;77:40-7. doi: 10.1016/j.ejps.2015.05.023.
99. Szmulewitz RZ, Ratain MJ. Playing Russian roulette with tyrosine kinase inhibitors. Clin Pharmacol Ther. 2013;93(3):242-4. doi: 10.1038/clpt.2012.245.
100. Peng B, Lloyd P, Schran H. Clinical pharmacokinetics of imatinib. Clin Pharmacokinet. 2005;44(9):879-94. doi: 10.2165/00003088-200544090-00001.
101. Reckmann A, Fischer T, Peng B, editors. Effect of food on STI571 Glivec pharmacokinetics and bioavailability. Proc Am Soc Clin Oncol; 2001.
102. Tian X, Zhang H, Heimbach T, He H, Buchbinder A, Aghoghovbia M, et al. Clinical Pharmacokinetic and Pharmacodynamic Overview of Nilotinib, a Selective Tyrosine Kinase Inhibitor. J Clin Pharmacol. 2018;58(12):1533-40. doi: 10.1002/jcph.1312.
103. Xia B, Heimbach T, He H, Lin TH. Nilotinib preclinical pharmacokinetics and practical application toward clinical projections of oral absorption and systemic availability. Biopharm Drug Dispos. 2012;33(9):536-49. doi: 10.1002/bdd.1821.
104. Tanaka C, Yin OQ, Sethuraman V, Smith T, Wang X, Grouss K, et al. Clinical pharmacokinetics of the BCR-ABL tyrosine kinase inhibitor nilotinib. Clin Pharmacol Ther. 2010;87(2):197-203. doi: 10.1038/clpt.2009.208.
105. FDA approves asciminib for Philadelphia chromosome-positive chronic myeloid leukemia. [03.10.2022]; Available from: https://www.fda.gov/drugs/resources-information-approved-drugs/fda-approves-asciminib-philadelphia-chromosome-positive-chronic-myeloid-leukemia.
106. Schoepfer J, Jahnke W, Berellini G, Buonamici S, Cotesta S, Cowan-Jacob SW, et al. Discovery of Asciminib (ABL001), an Allosteric Inhibitor of the Tyrosine Kinase Activity of BCR-ABL1. J Med Chem. 2018;61(18):8120-35. doi: 10.1021/acs.jmedchem.8b01040.
107. Hoch M, Zack J, Quinlan M, Huth F, Forte S, Dodd S, et al. Pharmacokinetics of Asciminib When Taken With Imatinib or With Food. Clin Pharmacol Drug Dev. 2022;11(2):207-19. doi: 10.1002/cpdd.1019.
108. Menssen HD, Quinlan M, Kemp C, Tian X. Relative Bioavailability and Food Effect Evaluation for 2 Tablet Formulations of Asciminib in a 2-Arm, Crossover, Randomized, Open-Label Study in Healthy Volunteers. Clin Pharmacol Drug Dev. 2019;8(3):385-94. doi: 10.1002/cpdd.602.
109. Dodd S, Grandeury A, Rousaki E, Suffert E. Crystalline form of N-[4-(Chlorodifluoromethoxy)phenyl]-6-[(3R)-3-hydroxypyrrolidin-1-yl]-5-(1H-pyrazol-5-yl)pyridine-3-carboxamide. WO2020/230099 A1, 19.11.2020.
110. Loftsson T, Brewster ME. Pharmaceutical applications of cyclodextrins: basic science and product development. J Pharm Pharmacol. 2010;62(11):1607-21. doi: 10.1111/j.2042-7158.2010.01030.x.
111. Amidon GE, Higuchi WI, Ho NF. Theoretical and experimental studies of transport of micelle-solubilized solutes. J Pharm Sci. 1982;71(1):77-84. doi: 10.1002/jps.2600710120.
112. Boyd BJ, Bergstrom CAS, Vinarov Z, Kuentz M, Brouwers J, Augustijns P, et al. Successful oral delivery of poorly water-soluble drugs both depends on the intraluminal behavior of drugs and of appropriate advanced drug delivery systems. Eur J Pharm Sci. 2019;137:104967. doi: 10.1016/j.ejps.2019.104967.

113. Borbas E, Sinko B, Tsinman O, Tsinman K, Kiserdei E, Demuth B, et al. Investigation and Mathematical Description of the Real Driving Force of Passive Transport of Drug Molecules from Supersaturated Solutions. Mol Pharm. 2016;13(11):3816-26. doi: 10.1021/acs.molpharmaceut.6b00613.
114. Elkhabaz A, Moseson DE, Brouwers J, Augustijns P, Taylor LS. Interplay of Supersaturation and Solubilization: Lack of Correlation between Concentration-Based Supersaturation Measurements and Membrane Transport Rates in Simulated and Aspirated Human Fluids. Mol Pharm. 2019. doi: 10.1021/acs.molpharmaceut.9b00956.
115. Buckley ST, Frank KJ, Fricker G, Brandl M. Biopharmaceutical classification of poorly soluble drugs with respect to "enabling formulations". Eur J Pharm Sci. 2013;50(1):8-16. doi: 10.1016/j.ejps.2013.04.002.
116. Musther H, Olivares-Morales A, Hatley OJ, Liu B, Rostami Hodjegan A. Animal versus human oral drug bioavailability: do they correlate? Eur J Pharm Sci. 2014;57:280-91. doi: 10.1016/j.ejps.2013.08.018.
117. Riethorst D, Mols R, Duchateau G, Tack J, Brouwers J, Augustijns P. Characterization of Human Duodenal Fluids in Fasted and Fed State Conditions. J Pharm Sci. 2016;105(2):673-81. doi: 10.1002/jps.24603.
118. Vertzoni M, Markopoulos C, Symillides M, Goumas C, Imanidis G, Reppas C. Luminal lipid phases after administration of a triglyceride solution of danazol in the fed state and their contribution to the flux of danazol across Caco-2 cell monolayers. Mol Pharm. 2012;9(5):1189-98. doi: 10.1021/mp200479f.
119. Mann J, Dressman J, Rosenblatt K, Ashworth L, Muenster U, Frank K, et al. Validation of Dissolution Testing with Biorelevant Media: An OrBiTo Study. Mol Pharm. 2017;14(12):4192-201. doi: 10.1021/acs.molpharmaceut.7b00198.
120. Klumpp L, Nagasekar K, McCullough O, Seybert A, Ashtikar M, Dressman J. Stability of Biorelevant Media Under Various Storage Conditions. Dissolution Technologies. 2019;26(2):6-18. doi: 10.14227/dt260219p6.
121. Almeida e Sousa L, Reutzel-Edens SM, Stephenson GA, Taylor LS. Assessment of the amorphous "solubility" of a group of diverse drugs using new experimental and theoretical approaches. Mol Pharm. 2015;12(2):484-95. doi: 10.1021/mp500571m.
122. Gravestock T, Box K, Comer J, Frake E, Judge S, Ruiz R. The " dissolution" method: a low volume, in vitro apparatus for assessing the dissolution/precipitation behaviour of an active pharmaceutical ingredient under biorelevant conditions. Anal Methods. 2011;3(3):560-7. doi: 10.1039/c0ay00434k.
123. Schlauersbach J, Hanio S, Lenz B, Vemulapalli SPB, Griesinger C, Poppler AC, et al. Leveraging bile solubilization of poorly water-soluble drugs by rational polymer selection. J Control Release. 2020;330:36-48. doi: 10.1016/j.jconrel.2020.12.016.
124. ISO22412:2017. [03.10.2022]; Available from: https://www.iso.org/standard/65410.html.
125. Schätzel K, Drewel M, Stimac S. Photon Correlation Measurements at Large Lag Times: Improving Statistical Accuracy. Journal of Modern Optics. 2007;35(4):711-8. doi: 10.1080/09500348814550731.
126. Wiest J, Saedtler M, Bottcher B, Grune M, Reggane M, Galli B, et al. Geometrical and Structural Dynamics of Imatinib within Biorelevant Colloids. Mol Pharm. 2018. doi: 10.1021/acs.molpharmaceut.8b00469.
127. Endres S, Karaev E, Hanio S, Schlauersbach J, Kraft C, Rasmussen T, et al. Concentration and composition dependent aggregation of Pluronic- and Poly-(2-oxazolin)-Efavirenz formulations in biorelevant media. J Colloid Interface Sci. 2022;606(Pt 2):1179-92. doi: 10.1016/j.jcis.2021.08.040.
128. Ross FM. Liquid Cell Electron Microscopy2016.
129. de Jonge N, Ross FM. Electron microscopy of specimens in liquid. Nat Nanotechnol. 2011;6(11):695-704. doi: 10.1038/nnano.2011.161.

130. Monaco KA, Delach S, Yuan J, Mishina Y, Fordjour P, Labrot E, et al. LXH254, a Potent and Selective ARAF-Sparing Inhibitor of BRAF and CRAF for the Treatment of MAPK-Driven Tumors. Clin Cancer Res. 2021;27(7):2061-73. doi: 10.1158/1078-0432.CCR-20-2563.
131. Saxena V, Panicucci R, Joshi Y, Garad S. Developability assessment in pharmaceutical industry: An integrated group approach for selecting developable candidates. J Pharm Sci. 2009;98(6):1962-79. doi: 10.1002/jps.21592.
132. Ramurthy S, Taft BR, Aversa RJ, Barsanti PA, Burger MT, Lou Y, et al. Design and Discovery of N-(3-(2-(2-Hydroxyethoxy)-6-morpholinopyridin-4-yl)-4-methylphenyl)-2-(trifluorom ethyl)isonicotinamide, a Selective, Efficacious, and Well-Tolerated RAF Inhibitor Targeting RAS Mutant Cancers: The Path to the Clinic. J Med Chem. 2019. doi: 10.1021/acs.jmedchem.9b00161.
133. Sheldrick GM. A short history of SHELX. Acta Crystallogr A. 2008;64(Pt 1):112-22. doi: 10.1107/S0108767307043930.
134. Hubschle CB, Sheldrick GM, Dittrich B. ShelXle: a Qt graphical user interface for SHELXL. J Appl Crystallogr. 2011;44(Pt 6):1281-4. doi: 10.1107/S0021889811043202.
135. DOC-M86-EXX229 APEX3 Software User Manual. [03.10.2022]; Available from: https://xray.uky.edu/Resources/manuals/Apex3-manual.pdf.
136. Kuentz M, Bergstrom CAS. Synergistic Computational Modeling Approaches as Team Players in the Game of Solubility Predictions. J Pharm Sci. 2021;110(1):22-34. doi: 10.1016/j.xphs.2020.10.068.
137. Meyerhoffer SM, McGown LB. Critical micelle concentration behavior of sodium taurocholate in water. Langmuir. 1990;6(1):187-91. doi: 10.1021/la00091a030.
138. Carey MC. Micelle Formation by Bile Salts. Archives of Internal Medicine. 1972;130(4):506. doi: 10.1001/archinte.1972.03650040040005.
139. Raina SA, Zhang GG, Alonzo DE, Wu J, Zhu D, Catron ND, et al. Impact of Solubilizing Additives on Supersaturation and Membrane Transport of Drugs. Pharm Res. 2015;32(10):3350-64. doi: 10.1007/s11095-015-1712-4.
140. Hanio S, Schlauersbach J, Lenz B, Spiegel F, Bockmann RA, Schweins R, et al. Drug-Induced Dynamics of Bile Colloids. Langmuir. 2021;37(8):2543-51. doi: 10.1021/acs.langmuir.0c02282.
141. Galipeau K, Socki M, Socia A, Harmon PA. Incomplete Loading of Sodium Lauryl Sulfate and Fasted State Simulated Intestinal Fluid Micelles Within the Diffusion Layers of Dispersed Drug Particles During Dissolution. J Pharm Sci. 2018;107(1):156-69. doi: 10.1016/j.xphs.2017.06.006.
142. Saal W, Wyttenbach N, Alsenz J, Kuentz M. Interactions of dimethylaminoethyl methacrylate copolymer with non-acidic drugs demonstrated high solubilization in vitro and pronounced sustained release in vivo. Eur J Pharm Biopharm. 2018;125:68-75. doi: 10.1016/j.ejpb.2018.01.006.
143. Martinez M. Applying the biopharmaceutics classification system to veterinary pharmaceutical products Part II. Physiological considerations. Advanced Drug Delivery Reviews. 2002;54(6):825-50. doi: 10.1016/s0169-409x(02)00071-6.
144. Mudie DM, Shi Y, Ping H, Gao P, Amidon GL, Amidon GE. Mechanistic analysis of solute transport in an in vitro physiological two-phase dissolution apparatus. Biopharm Drug Dispos. 2012;33(7):378-402. doi: 10.1002/bdd.1803.
145. Sugano K. Theoretical investigation of passive intestinal membrane permeability using Monte Carlo method to generate drug-like molecule population. Int J Pharm. 2009;373(1-2):55-61. doi: 10.1016/j.ijpharm.2009.02.002.
146. Winiwarter S, Ax F, Lennernäs H, Hallberg A, Pettersson C, Karlén A. Hydrogen bonding descriptors in the prediction of human in vivo intestinal permeability. Journal of Molecular Graphics and Modelling. 2003;21(4):273-87. doi: 10.1016/s1093-3263(02)00163-8.
147. Clulow AJ, Barber B, Salim M, Ryan T, Boyd BJ. Synergistic and antagonistic effects of non-ionic surfactants with bile salt + phospholipid mixed micelles on the solubility of poorly water-soluble drugs. Int J Pharm. 2020;588:119762. doi: 10.1016/j.ijpharm.2020.119762.

148. Higuchi T. Physical Chemical analysis of Percutaneous Absorption Process from Creams and Ointments. J Soc Cosmet Chem. 1960;11:85-97.
149. Kunst A, Lee G. Release and Skin Permeation of Scopolamine From Thin Polymer Films in Relation to Thermodynamic Activity. J Pharm Sci. 2016;105(4):1496-500. doi: 10.1016/j.xphs.2016.02.004.
150. Raina SA, Zhang GGZ, Alonzo DE, Wu J, Zhu D, Catron ND, et al. Enhancements and limits in drug membrane transport using supersaturated solutions of poorly water soluble drugs. J Pharm Sci. 2014;103(9):2736-48. doi: 10.1002/jps.23826.
151. Indulkar AS, Gao Y, Raina SA, Zhang GG, Taylor LS. Exploiting the Phenomenon of Liquid-Liquid Phase Separation for Enhanced and Sustained Membrane Transport of a Poorly Water-Soluble Drug. Mol Pharm. 2016;13(6):2059-69. doi: 10.1021/acs.molpharmaceut.6b00202.
152. Wilson V, Lou X, Osterling DJ, Stolarik DF, Jenkins G, Gao W, et al. Relationship between amorphous solid dispersion in vivo absorption and in vitro dissolution: phase behavior during dissolution, speciation, and membrane mass transport. J Control Release. 2018;292:172-82. doi: 10.1016/j.jconrel.2018.11.003.
153. Hate SS, Mosquera-Giraldo LI, Taylor LS. A Mechanistic Study of Drug Mass Transport from Supersaturated Solutions Across PAMPA Membranes. J Pharm Sci. 2021. doi: 10.1016/j.xphs.2021.07.003.
154. Indulkar AS, Mo H, Gao Y, Raina SA, Zhang GGZ, Taylor LS. Impact of Micellar Surfactant on Supersaturation and Insight into Solubilization Mechanisms in Supersaturated Solutions of Atazanavir. Pharm Res. 2017;34(6):1276-95. doi: 10.1007/s11095-017-2144-0.
155. Katneni K, Charman SA, Porter CJ. Permeability assessment of poorly water-soluble compounds under solubilizing conditions: the reciprocal permeability approach. J Pharm Sci. 2006;95(10):2170-85. doi: 10.1002/jps.20687.
156. Sjogren E, Abrahamsson B, Augustijns P, Becker D, Bolger MB, Brewster M, et al. In vivo methods for drug absorption - comparative physiologies, model selection, correlations with in vitro methods (IVIVC), and applications for formulation/API/excipient characterization including food effects. Eur J Pharm Sci. 2014;57:99-151. doi: 10.1016/j.ejps.2014.02.010.
157. Hatton GB, Yadav V, Basit AW, Merchant HA. Animal Farm: Considerations in Animal Gastrointestinal Physiology and Relevance to Drug Delivery in Humans. J Pharm Sci. 2015;104(9):2747-76. doi: 10.1002/jps.24365.
158. Dunn C, Perrier J, Khadra I, Wilson CG, Halbert GW. Topography of Simulated Intestinal Equilibrium Solubility. Mol Pharm. 2019;16(5):1890-905. doi: 10.1021/acs.molpharmaceut.8b01238.
159. Kadar S, Tozser P, Nagy B, Farkas A, Nagy ZK, Tsinman O, et al. Flux-Based Formulation Development-A Proof of Concept Study. AAPS J. 2022;24(1):22. doi: 10.1208/s12248-021-00668-9.